Leg 209 Preliminary Report

Drilling Mantle Peridotite along the Mid-Atlantic Ridge from 14° to 16°N

6 May 2003–6 July 2003

Shipboard Scientific Party

Ocean Drilling Program
Texas A&M University
1000 Discovery Drive
College Station TX 77845-9547
USA

October 2003

PUBLISHER'S NOTES

This report was prepared from shipboard files by scientists who participated in the cruise. The report was assembled under time constraints and does not contain all works and findings that will appear in the *Initial Reports* of the ODP *Proceedings*. Reference to the whole or to part of this report should be made as follows:

Shipboard Scientific Party, 2003. Leg 209 Preliminary Report. *ODP Prelim. Rpt.,* 109 [Online]. Available from World Wide Web: <http://www-odp.tamu.edu/publications/prelim/209_prel/209PREL.PDF>. [Cited YYYY-MM-DD]

Distribution: Electronic copies of this series may be obtained from the Ocean Drilling Program's World Wide Web site at http://www-odp.tamu.edu/publications.

This publication was prepared by the Ocean Drilling Program, Texas A&M University, as an account of work performed under the international Ocean Drilling Program, which is managed by Joint Oceanographic Institutions, Inc., under contract with the National Science Foundation. Funding for the program is provided by the following agencies:

Australia/Canada/Chinese Taipei/Korea Consortium for Ocean Drilling
Deutsche Forschungsgemeinschaft (Federal Republic of Germany)
Institut National des Sciences de l'Univers–Centre National de la Recherche Scientifique (INSU-CNRS; France)
Ocean Research Institute of the University of Tokyo (Japan)
National Science Foundation (United States)
Natural Environment Research Council (United Kingdom)
European Science Foundation Consortium for Ocean Drilling (Belgium, Denmark, Finland, Iceland, Ireland, Italy, The Netherlands, Norway, Spain, Sweden, and Switzerland)
Marine High-Technology Bureau of the State Science and Technology Commission of the People's Republic of China

DISCLAIMER

The following scientists and personnel were aboard the JOIDES Resolution for Leg 209 of the Ocean Drilling Program:

SHIPBOARD SCIENTIFIC PARTY

Peter B. Kelemen
Co-Chief Scientist
Department of Geology and Geophysics
Woods Hole Oceanographic Institution
Woods Hole MA 02543
USA
Work: (508) 289-2956
Fax: (508) 457-2183
peterk@whoi.edu

Eiichi Kikawa
Co-Chief Scientist
Deep Sea Research Department
Japan Marine Science and Technology Center
2-15 Natsushima-cho
Yokosuka 237-0061
Japan
Work: (81) 46-867-9340
Fax: (81) 46-867-9315
kikawa@jamstec.go.jp

D. Jay Miller
Staff Scientist
Ocean Drilling Program
Texas A&M University
1000 Discovery Drive
College Station TX 77845-9547
USA
Work: (979) 845-2197
Fax: (979) 845-0876
miller@odpemail.tamu.edu

Natsue Abe
Petrologist
Deep Sea Research Department
Japan Marine Science and Technology Center
2-15 Natsushima-cho
Yokosuka 237-0061
Japan
Work: (81) 46-867-9329
Fax: (81) 46-867-9315
abenatsu@jamstec.go.jp

Wolfgang Bach
Petrologist
Marine Chemistry and Geochemistry
Woods Hole Oceanographic Institution
360 Woods Hole Road
MS #8
Woods Hole MA 02543
USA
Work: (508) 289-2523
Fax: (508) 457-2183
wbach@whoi.edu

Richard L. Carlson
Physical Properties Specialist
Department of Geology and Geophysics
Texas A&M University
College Station TX 77843-3115
USA
Work: (979) 845-1398
Fax: (979) 845-6162
carlson@geo.tamu.edu

John F. Casey
Petrologist
Department of Geosciences
University of Houston
4800 Calhoun Road, SR1 Building
Houston TX 77204-5503
USA
Work: (713) 743-3390
Fax: (713) 748-7906
jfcasey@uh.edu

Lynne M. Chambers
Petrologist
NERC Isotope Geosciences Laboratory
British Geological Survey
Kingsley Dunham Centre, Keyworth
Nottingham, Nottinghamshire NG12 5GG
United Kingdom
Work: (44) 115 936 3134
Fax: (44) 115 936 3302
lmch@bgs.ac.uk

Michael Cheadle
Petrologist
Department of Geology and Geophysics
University of Wyoming
Laramie WY 82071
USA
Work: (307) 766-3206
Fax: (307) 766-6679
cheadle@uwyo.edu

Anna Cipriani
Petrologist
Lamont-Doherty Earth Observatory
Columbia University
PO Box 1000, 61 Route 9W
Palisades NY 10964
USA
Work: (845) 365 8905
Fax: (845) 365-8155
anka@ldeo.columbia.edu

Henry J.B. Dick
Petrologist
Department of Geology and Geophysics
Woods Hole Oceanographic Institution
MS #8, McLean Laboratory
Woods Hole MA 02543
USA
Work: (508) 289-2590
Fax: (508) 457-2196
hdick@whoi.edu

Ulrich Faul
Petrologist
Research School of Earth Sciences
The Australian National University
Canberra ACT 0200
Australia
Work: (61) 2 6125 8846
Fax: (61) 2 6125 5989
uli.faul@anu.edu.au

Miguel Garces
Paleomagnetist
Stratigraphy, Paleontology, and Marine Geosciences
Universitat de Barcelona
Campus de Pedralbes
08018 Barcelona
Spain
Work: (34) 93 409 5410
Fax: (34) 93 411 0012
garces@natura.geo.ub.es

Carlos Garrido
Petrologist
Departamento de Mineralogia y Petrologia
Universidad de Granada
Facultad de Ciencias, Fuentenuva s/n
18002 Granada
Spain
Work: (34) 958 240473
Fax: (34) 958 243368
carlosg@ugr.es

Jeffrey S. Gee
Paloemagnetist
Scripps Institution of Oceanography
University of California, San Diego
Geosciences Research Division - 0220
La Jolla CA 92093-0220
USA
Work: (858) 534-4707
Fax: (858) 534-0784
jsgee@ucsd.edu

Marguerite M. Godard
Petrologist
Laboratoire de Tectonophysique
Université Montpellier II
Case Courrier 49
Place Eugéne Bataillon
34095 Montpellier Cedex 5
France
Work: (33) 467-14-39-37
Fax: (33) 467-14-36-03
margot@dstu.univ-montp2.fr

David W. Graham
Petrologist
College of Oceanic and Atmospheric Sciences
Oregon State University
Oceanography Administration Building 104
Corvallis OR 97331-5503
USA
Work: (541) 737-4140
Fax: (541) 737-2064
dgraham@coas.oregonstate.edu

Dale W. Griffin
Microbiologist
Coastal and Marine Division
U.S. Geological Survey
600 4th Street South
St. Petersburg FL 33701
USA
Work: (727) 803-8747, ext 3113
Fax: (727) 803-2032
dgriffin@usgs.gov

Jason Harvey
Petrologist
Department of Earth Sciences
The Open University
Walton Hall
Milton Keynes MK7 6AA
United Kingdom
Work: (44) 1908 655947
Fax: (44) 1908 655151
j.harvey@open.ac.uk

Benoit Ildefonse
Physical Properties Specialist
Laboratoire de Tectonophysique
ISTEEM
Université Montpellier 2, CC49
34095 Montpellier
France
Work: (33) 4-67-14-38-18
Fax: (33) 4-67-14-36-03
benoit@dstu.univ-montp2.fr

Gerardo J. Iturrino
Logging Staff Scientist
Borehole Research Group
Lamont-Doherty Earth Observatory
Columbia University
PO Box 1000, 61 Route 9W
Palisades NY 10964
USA
Work: (846) 365-8656
Fax: (846) 365-3182
iturrino@ldeo.columbia.edu

Jennifer Josef
Microbiologist
Marine Geology
Oregon State University
104 Ocean Administration Building
Corvallis OR 97333
Work: (541) 737-2594
Fax: (541) 737-2064
jjosef@coas.oregonstate.edu

William P. Meurer
Petrologist
Department of Geosciences
University of Houston
312 Science and Research Building 1
Houston TX 77204-5007
USA
Work: (713) 743-0214
Fax: (713) 748-7906
wpmeurer@mail.uh.edu

Holger Paulick
Petrologist
Mineralogisch-Petrologisches Institut
Universität Bonn
Poppelsdorfer Schloss
53115 Bonn
Germany
Work: (49) 228-73 6816
Fax: (49) 228-73 2763
hoger.paulick@uni-bonn.de

Martin Rosner
Petrologist
Department of Inorganic and Isotope Geochemistry
GeoForschungsZentrum Potsdam
Telegrafenberg B122
14473 Potsdam
Germany
Work: (49) 331-288-1422
Fax: (49) 331-288-1474
rosner@gfz-potsdam.de

Timothy Schroeder
Petrologist
Department of Geology and Geophysics
University of Wyoming
PO Box 3006
Laramie WY 82071
USA

Present address:
Environmental Earth Sciences Department
Eastern Connecticut State University
83 Wyndham Street
Willimantic CT 06226
USA
Work: (860) 423-1364
schroedert@easternct.edu

Monique Seyler
Petrologist
Laboratoire de Geosciences Marine
Institut de Physique du Globe de Paris
4 Place Jussieu
75252 Paris Cedex 05
France
Work: (33) 1 44 275190
Fax: (33) 3 20 43 39 11 or 1 44 27 39 11
seyler@ipgp.jussieu.fr

Eiichi Takazawa
Petrologist
Department of Geology, Faculty of Science
Niigata University
2-8050
Ikarashi, Niigata 950-2181
Japan
Work: (81) 25-262-6114
Fax: (81) 25-262-6114
takazawa@geo.sc.niigata-u.ac.jp

Stefan Mrozewski
Schlumberger Drilling and Measurements
135 Rousseau Road
Youngsville LA 70592
USA
Work: (337) 837-9803
Fax: (337) 837-0460
smrozewski@youngsville.oilfield.slb.com

TRANSOCEAN OFFICIALS

Tom Hardy
Master of the Drilling Vessel
Overseas Drilling Ltd.
707 Texas Avenue South, Suite 213D
College Station TX 77840-1917
USA

Wayne Malone
Drilling Superintendent
Overseas Drilling Ltd.
707 Texas Avenue South, Suite 213D
College Station TX 77840-1917
USA

ODP SHIPBOARD PERSONNEL AND TECHNICAL REPRESENTATIVES

Lisa Brandt
Marine Laboratory Specialist (Chemistry)

Lisa Crowder
Marine Laboratory Specialist (Underway Geophysics)

Roy Davis
Laboratory Officer

Randy Gjesvold
Marine Electronics Specialist

Dennis Graham
Marine Laboratory Specialist (Chemistry)

Ted Gustafson
Marine Laboratory Specialist (Downhole Tools/ Thin Sections)

Margaret Hastedt
Marine Computer Specialist

Scott Herman
Marine Laboratory Specialist (Paleomagnetism)

Michiko Hitchcox
Marine Laboratory Specialist (Yeoperson)

Eric Jackson
Marine Laboratory Specialist (X-Ray)

Michael Meiring
Marine Electronics Specialist

Erik Moortgat
Marine Computer Specialist

Stefan Mrozewski
LWD Logging Engineer (Anadrill)

Robert Olivas
Marine Laboratory Specialist (Core Lab)

Chieh Peng
Assistant Laboratory Officer/Storekeeper

Cyndi Prince
Marine Laboratory Specialist (Photographer)

Mads Radsted
Marine Laboratory Specialist (Physical Properties)

Michael Storms
Operations Manager

Kerry Swain
Schlumberger Logging Engineer

Paula Weiss
Marine Laboratory Specialist (Curation)

ABSTRACT

Leg 209 was devoted to drilling mantle peridotites and associated gabbroic rocks along the Mid-Atlantic Ridge from 14° to 16°N. This area was identified at the 1996 Workshop on Oceanic Lithosphere and Scientific Drilling into the 21st Century (OL Workshop) as the ideal region for drilling of a strike line of short holes to sample the upper mantle in a magma-starved portion of a slow-spreading ridge (spreading rate = ~25 km/m.y.). In this area, igneous crust is locally absent and the structure and composition of the mantle can be determined at sites more than ~100 km apart along strike.

A central paradigm of Ridge Interdisciplinary Global Experiments (RIDGE) studies is the hypothesis that mantle flow, or melt extraction, or both, are focused in three dimensions toward the centers of magmatic ridge segments, at least at slow-spreading ridges such as the Mid-Atlantic Ridge. This hypothesis has essentially reached the status of accepted theory, but it has never been subject to a direct test. A strike line of oriented mantle peridotite samples extending for a significant distance within magmatic segments offers the possibility of directly testing this hypothesis. Continued dredging and submersible studies cannot provide the spatial information required to make such a test.

The primary aim of drilling was to characterize the spatial variation of mantle deformation patterns, residual peridotite composition, melt migration features, plutonic rocks, and hydrothermal alteration along axis. Hypotheses for focused solid or liquid upwelling beneath ridge segments make specific predictions regarding the spatial variation of mantle lineation or the distribution of melt migration features. These predictions were directly tested by drilling. We discovered that penetrative mantle deformation fabrics are weak at every site where mantle peridotite was sampled from 14°43′N to 15°39′N. Instead, at all of these sites, deformation was localized along high-temperature shear zones and later brittle faults. Intact blocks of peridotite with high-temperature, protogranular fabrics were preserved between these zones of localized deformation and underwent substantial tectonic rotation, perhaps as much as 90° around horizontal, ride-parallel rotation axes in some places.

At most sites, drilling recovered substantial proportions of gabbroic rocks intrusive into mantle peridotite. Some of these rocks have mineral assemblages that are probably indicative of crystallization at depths of 12 to 20 km beneath the Mid-Atlantic Ridge. Localized deformation at several of these sites occurred preferentially within contact zones between peridotite and these gabbroic intrusions. Abundant gabbroic intrusions were found close to the 15°20′ Fracture Zone, at Site 1271, and far from the fracture zone at Sites 1270, 1268, and 1275. Conversely, some holes intersected very little gabbroic material; these were at Site 1272, very close to the fracture zone, and Site 1274, far from the fracture zone. Thus, there is little evidence from the results of this leg for focusing of melt distribution away from the fracture zone and toward the centers of volcanically active ridge segments.

Three new hypotheses may account for our observations:

1. Shallow mantle peridotites beneath the Mid-Atlantic Ridge in this region do not undergo penetrative deformation during “corner flow” associated with plate spreading. Instead, they rise passively until they reach the base of the thermal boundary layer at depths of 15 to 20 km below this slow-spreading ridge. There, they cool and become incorporated into the lithosphere. Subsequently, corner flow and ridge extension are accommodated along localized ductile shear zones which gradually evolve into brittle faults at shallower depths and lower temperatures. As some faults rotated to shallow dips and could no longer accommodate extension, new ones formed. Crosscutting generations of faults rotated nearly undeformed blocks of peridotite and associated gabbroic intrusions, with total rotations probably >60° or even 90° in some cases.

2. Textures in the relatively undeformed peridotite blocks suggest that many residual peridotites interacted with melts migrating by diffuse porous flow along grain boundaries at the base of the thermal boundary layer. In most peridotites, our qualitative observations of textures suggest that igneous spinel and pyroxene crystallized within a matrix of residual mantle olivine and orthopyroxene. More extensive crystallization of intergranular melt at slightly lower temperatures formed impregnated peridotites and hybrid troctolites, particularly abundant at Sites 1271 and 1275. Based on our limited sampling, it seems that focusing of melt transport into dunite conduits with sharp contacts against residual mantle peridotites, common in some ophiolites and perhaps beneath fast-spreading ridges, was not a very important process in the region we investigated. Instead, melts probably were in equilibrium with mantle peridotite up to the base of the thermal boundary layer, after which they probably ascended in brittle cracks.
3. We wonder if the "amagmatic" region between 14°40′ and 15°40′N along the Mid-Atlantic Ridge is truly "magma starved" as has often been proposed or whether, instead, the relative lack of lava and gabbroic crust is offset by a relatively high proportion of gabbroic intrusions into peridotite, distributed over 15 to 20 km depth. In this view, many melts may crystallize 100% below the seafloor, with no magma rising to form lava flows. In keeping with this hypothesis, gabbroic rocks, particularly those at Site 1275, the top of Mt. Mike at 15°44′N, ~25 km west of the ridge axis, are generally very evolved. They cannot represent the refractory, primitive cumulates required to complement compositional variation in mid-ocean-ridge basalts, and instead must represent the crystal products of very evolved melts that rarely erupt. This may be heresy, but we wonder if, for example, gravity data for the Mid-Atlantic Ridge might be reconciled with such a theory, given that the widely distributed gabbroic rocks in such a lithospheric structure would generally be farther from the seafloor and therefore would have a smaller gravity signal than a thick gabbroic layer concentrated near the surface.

Very different hydrothermal alteration styles were observed at different Sites. In Hole 1268A, talc was particularly abundant in metaperidotites, accompanied by a dramatic metasomatic decrease in the (Mg + Fe)/Si ratio. Elsewhere, brucite was a prominent part of the alteration assemblage in peridotites, and rocks retain high (Mg + Fe)/Si. Gabbroic intrusions appear to have an important local control on serpentinization reactions in peridotite. Carbonate alteration of peridotites in some locales seems to be correlated with a metasomatic influx of calcium and may also substantially affect the trace element budget of serpentinites in some cases.

INTRODUCTION

Site Survey Data and Other Geological Background

The Mid-Atlantic Ridge near the 15°20′ Fracture Zone has been the focus of a long-term cooperative French-American and allied Russian research program. During the summer of 1998 the area was visited by a Japanese/American team, funded in part as a site survey for the Ocean Drilling Program (ODP). In addition to identifying many suitable drill sites, these cruises identified many suitable drill sites and completed shipboard bathymetric, gravity, and magnetics surveys (Fig. F1).

In addition to nearly continuous outcrops of mantle peridotite on both walls of the rift valley for at least 100 km from 14°40′ to 15°40′N (Fig. F2), significant features of the area include:

1. Large "gravity bulls-eyes," concentric negative residual Bouger and mantle Bouger gravity anomalies, centered at ~14° and 16°N (Fig. F1);
2. A regional chemical anomaly with "hotspot" characteristics centered at ~14°N (Fig. F3);
3. "Megamullion" structures, interpreted to be long-lived low-angle faults exposed on the seafloor over regions of ~100 km² (e.g., 46°54′W, 15°44′N) (Fig. F2); and
4. At least three areas with high methane signatures in the water column, including one active hydrothermal field within mantle peridotites.

Seismic Studies

In June 1997, a seismic refraction experiment was carried out north of the 15°20′ Fracture Zone from the *Ewing,* led by John Collins of Woods Hole Oceanographic Institute (WHOI). Using NOBEL (Near Ocean Bottom Explosives Launcher), refraction profiles were shot over areas previously mapped using the submersible *Nautile*. Source and receiver were on the seafloor for determination of seismic velocity structure at length scales of 10 to 100 m instead of 100 m to 1 km with conventional surveys. NOBEL profiles were taken at 15°37′N on (1) an ultramafic outcrop, (2) a gabbro/wehrlite outcrop, and (3) basalt, to determine whether seismic velocities can be used to map the extent of gabbro and peridotite emplaced at or near the seafloor. In addition, a 100-km-long conventional refraction profile was shot along the median valley of the Mid-Atlantic Ridge north of the 15°20′ Fracture Zone. Results show anomalous seismic structure in the crust with pronounced gradients in velocity rather than the layered structure typical for fast-spreading ridges (Fig. F4). This type of seismic structure is typical for slow-spreading ridges near fracture zones (R. Detrick, pers. comm., 1998).

Submersible Studies

Many possible drill sites were identified during the Faranaut cruise with the French *Nautile* submersible in 1992 (e.g., Cannat et al., 1995, 1997b). In 1998, the joint Japan Marine Science and Technology Center (JAMSTEC)/WHOI MODE 98, Leg 1 cruise with the Japanese *Shinkai* 6500 submersible completed the survey for possible drill sites. A summary of lithologic observations from dredging and diving is shown in Figure F2, and a summary of drill sites is shown in Figure F5. In addition, it is worthy of note that extensive exposures of moderate- to low-angle fault surfaces underlain by peridotite were observed on the seafloor, particularly at Sites 1275 and 1270 (Fig. F5).

Shipboard Geophysics

Although the 1992 Faranaut cruise included shipboard bathymetric, gravity, and magnetics surveys, the quality of the gravity and magnetics data was less than optimal. The 1998 MODE 98, Leg 1 cruise conducted additional surveys. The combined Faranaut and MODE 98 survey coverage is illustrated in Figure F2 (Cannat et al., 1995, 1997b; Casey et al., 1998; Kelemen et al., 1998b; Matsumoto et al., 1998; Escartin and Cannat, 1999; Fujiwara et al., 2003). For the purposes of this report, the most important result is the identification of large "gravity bulls-eyes," concentric negative residual Bouger and mantle Bouger gravity anomalies, centered at ~14° and 16°N (Fig. F1). These gravity lows correspond to areas with well-organized seafloor magnetic anomalies and ridge-parallel abyssal hill topography, whereas the relative gravity highs correspond to known areas with outcrops of serpentinized peridotites along the ridge axis and to areas with poorly organized seafloor magnetic anomalies and chaotic topography. Also note that the negative gravity anomaly at 14°N is about twice as large as that at 16°N, in keeping with geochemical indications that the 14°N area resembles a "hotspot."

The gravity lows have been interpreted as centers of magmatic segments where there is accretion of thick igneous crust, whereas the gravity highs on the periphery of these magmatic segments were thought to be magma starved. This idea was central to our drilling plan because it provides a potential explanation for the extensive outcrops of peridotite along the Mid-Atlantic Ridge between 14°40′ and 15°40′N, but it has never been tested. This region was ideal for testing hypotheses that explain focused crustal accretion, or at least focused volcanic activity in regions with low gravity, along magmatic segments.

Geochemical Background

Extensive analytical work has been done on samples recovered by dredging in the 14° to 16°N region along the Mid-Atlantic Ridge (Bonatti et al., 1992; Bougault et al., 1988, 1990; Casey, 1997; Casey et al., 1992, 1994, 1995; Dick and Kelemen, 1992; Dosso et al., 1991; Peyve et al., 1988; Silantyev et al., 1996; Sobolev et al., 1992a, 1992b, 1992c; Staudacher et al., 1989; Xia et al., 1991, 1992; C. Xia et al., unpubl. data). This work reveals that the mantle source of basalts south of the 15°20′ Fracture Zone is geochemically "enriched," similar to the source of hotspot-related mid-ocean-ridge basalts (MORB) elsewhere along the Mid-Atlantic Ridge (Fig. F3). Perhaps related to this is the observation that mantle peridotites seem to have undergone unusually high degrees of melting (mantle olivines have molar Mg/(Mg+Fe) up to 0.92, and spinels have molar Cr/(Cr+Al) up to 0.7, forming the depleted end-members for peridotites recovered from mid-ocean ridges (Fig. F6). North of the fracture zone, however, basalts and peridotites sampled by dredging and submersible have compositions typical for the Mid-Atlantic Ridge away from hotspots (Fig. F3).

MANTLE UPWELLING, MELT TRANSPORT, AND IGNEOUS CRUSTAL ACCRETION

Focused Crustal Accretion at Slow-Spreading Ridges

A central paradigm of RIDGE studies is the hypothesis that mantle flow, or melt extraction, or both, are focused in three dimensions toward the centers of magmatic ridge segments, at least at slow-spreading ridges such as the Mid-Atlantic Ridge. This is based on:

1. Observations from ophiolites, with emphasis on the Oman ophiolite (Ceuleneer, 1991; Ceuleneer et al., 1988; Ceuleneer and Rabinowicz, 1992; Jousselin et al., 1998; Nicolas and Boudier, 1995; Nicolas and Rabinowicz, 1984; Nicolas and Violette, 1982);
2. The theory that partially molten mantle may be subject to diapirism via Rayleigh Taylor instabilities (Barnouin-Jha et al., 1997; Buck and Su, 1989; Crane, 1985; Jha et al., 1994; Parmentier and Phipps Morgan, 1990; Rabinowicz et al., 1984, 1987; Schouten et al., 1985; Sparks and Parmentier, 1993; Sparks et al., 1993; Su and Buck, 1993; Whitehead et al., 1984);
3. The observation that peridotites are commonly dredged near fracture zones along slow-spreading ridges but not near ridge segment centers (Dick, 1989; Whitehead et al., 1984); and
4. Gravity and seismic studies of the Mid-Atlantic Ridge suggesting thick crust near segment centers and thin crust at segment ends (e.g., Barclay et al., 1998; Kuo and Forsyth, 1988; Lin et al., 1990; Tolstoy et al., 1992; Tucholke et al., 1997).

In addition to a possible role for mantle diapirism, various workers have proposed that melt transport may be focused in two or three dimensions, on the basis of theoretical work and field observations (e.g., Aharonov et al., 1995; Kelemen et al., 1995a, 1995b, 2000; Magde et al., 1997; Phipps Morgan, 1987; Sparks and Parmentier, 1991, 1994; Spiegelman, 1993; Spiegelman and McKenzie, 1987). Such focused melt extraction could operate, with or without focused flow of the upwelling mantle, to produce the observed focusing of crustal accretion toward the center of magmatic ridge segments.

The idea that focused mantle upwelling at the centers of magmatic ridge segments occurs only beneath slow-spreading ridges was formulated by Marc Parmentier and his students (e.g., Lin and Phipps Morgan, 1992; Parmentier and Phipps Morgan, 1990; Turcotte and Phipps Morgan, 1992) and is supported by seismic results from the recent Mantle Electromagnetic and Tomography (MELT) experiment along the fast-spreading southern East Pacific Rise, in which no focused mantle upwelling was detected (e.g., Forsyth et al., 1998; MELT Team, 1998; Toomey et al., 1998). However, recent observations from Oman and the fast-spreading northern East Pacific Rise have called this into question (e.g., Barth and Mutter, 1996; Dunn and Toomey, 1997; Nicolas et al., 1996). Nevertheless, most investigators agree that slow-spreading ridges such as the Mid-Atlantic Ridge represent the best place to test general hypotheses for the mechanism(s) of three-dimensional (3-D) focusing of crustal accretion.

Really Focused, Sort of Focused, Unfocused, Blurry: Terms For Mantle Upwelling

In the literature describing theories of three-dimensionally focused mantle upwelling, the terms "focused" and "3-D" receive different definitions from different authors. Thus, Parmentier and Phipps Morgan (1990), who first presented the now-famous "phase diagram" for two-dimensional (2-D) vs. 3-D mantle upwelling as a function of spreading rate and mantle viscosity, chose a detailed example that is indeed 3-D but that does not correspond well to observations of diapirs in the mantle section of the Oman ophiolite. In Parmentier and Phipps Morgan's example, the region of mantle upwelling at, for example, 40 km depth is ~200 km wide in a ridge-parallel section and widens upward; near the top it is almost as wide as their 300-km ridge segment. Along-ridge transport of upwelling mantle occurs gradually over the upper 60 km of the upwelling region. In contrast, the interpretation of Jousselin et al. (1998), loosely based on observations from Oman, is that "at any depth above 50 km there is no vertical flow outside the narrow zone of subridge upwelling." They take the zone of upwelling to be cylindrical, with a diameter of ~10 km. Furthermore, in their interpretation, all corner flow (ridge parallel and ridge perpendicular) occurs in the upper 500 m of the upwelling region. More than one-half of the shallow mantle in their 25-km-long ridge

segments is fed by horizontal flow in this 500-m-thick layer just below the base of the lithosphere. Such narrow pipes of upwelling mantle may be consistent with the physical models of Buck and Su (1989; Su and Buck, 1993), which show very sharp focusing of mantle flow. Such features could conceivably have escaped seismic detection in the recent MELT experiment. However, if this is the geometry of mantle upwelling, then the amount of ridge-parallel, horizontal transport of mantle material must be very large.

In the ensuing discussion, we take the Jousselin et al. geometry as the end-member example of 3-D focused mantle flow and passive corner flow to be the end-member example of 2-D mantle flow with no focusing. The Jousselin et al. scenario may seem extreme at first, but it does provide a clear description of an upwelling geometry that could produce a variation in igneous crustal thickness from ~10 km at a segment center to ~0 km near the segment ends, as interpreted on the basis of geological and geophysical observations in the 14° to 16°N region of the Mid-Atlantic Ridge. These observations are typical of the first-order features of slow-spreading ridges, which are thought to reflect three-dimensionally focused magmatic accretion.

In contrast, available 3-D physical models of diapric mantle upwelling beneath ridges cannot account for these observations because the upwelling is not sufficiently tightly focused. As stated by Barnouin-Jha et al. (1997), "short wavelength segmentation of slow-spreading centers requires some process not included in our models of mantle flow." This missing process might be tightly focused upwelling, as in the schema of Jousselin et al., or focused melt migration.

Testing Hypotheses for the Mechanism(s) of Focused Crustal Accretion

Despite the difficulties with 3-D physical models (outlined above in **"Really Focused, Sort of Focused, Unfocused, Blurry: Terms for Mantle Upwelling"**), the hypothesis that mantle flow, or melt extraction, or both, are focused in three dimensions toward centers of magmatic segments at slow-spreading ridges has essentially reached the status of accepted theory. However, these ideas have never been subject to a direct test. A strike line of oriented mantle peridotite samples extending for a significant distance within such magmatic segments offers the possibility of directly testing hypotheses for focused crustal accretion.

The primary aim of drilling in the 14° to 16°N area along the Mid-Atlantic Ridge was to characterize the spatial variation of mantle deformation patterns, residual peridotite composition, melt migration features, and hydrothermal alteration along axis. Published hypotheses for focused solid or liquid upwelling beneath ridge segments make specific predictions regarding the spatial variation of mantle lineation or the distribution of melt migration features.

Interpretation of Ductile Flow Fabrics in Mantle Peridotites

Models of focused solid upwelling require ridge-parallel, subhorizontal flow of residual mantle peridotites from segment centers to segment ends (Fig. F6A) (Barnouin-Jha et al., 1997; Buck and Su, 1989; Crane, 1985; Jha et al., 1994; Parmentier and Phipps Morgan, 1990; Rabinowicz et al., 1984, 1987; Schouten et al., 1985; Sparks and Parmentier, 1993; Sparks et al., 1993; Su and Buck, 1993; Whitehead et al., 1984). Futhermore, because focused mantle upwelling must be faster than plate spreading, these models predict zones of substantial shear strain at the top of the upwelling "fountain" of mantle peridotite, through which all the upwelling solid material must pass. These theories are substantiated to some extent by patterns of mantle flow inferred from ductile fabrics in residual peridotites in the Oman ophiolite (Fig. F6B) (Ceuleneer, 1991; Ceuleneer et al., 1988; Ceuleneer and Rabinowicz, 1992; Jousselin et al., 1998; Nicolas and Boudier, 1995; Nicolas and Rabinowicz, 1984; Nicolas and Violette, 1982), although as already noted in **"Really Focused, Sort of Focused, Unfocused, Blurry: Terms for Mantle Upwelling,"**

the scale of focused upwelling in Oman (~10 km) is different from that in current 3-D models of mantle diapirism (~100 km). In Oman and other ophiolite massifs, mantle flow direction can be determined by measurement of spinel shape fabrics (lineation at high strain is parallel to ductile flow), measurement of the orientation of olivine crystal shape fabrics relative to subgrain boundaries (subgrain boundaries are oblique to the long sides of elongate crystals, indicating the sense of shear), and measurement of olivine crystal lattice preferred orientation (olivine a-axes are aligned parallel to ductile flow directions at high strain).

Cores from a series of drill holes in mantle peridotites along a slow-spreading ridge axis can, in principle, be used to test the prediction that shallow ductile flow of residual mantle at the ends of segments is ridge parallel and subhorizontal. There are two problems with this approach: (1) the core must be restored to a geographical reference frame and (2) tectonic rotations of the peridotite that postdate ductile flow must be considered before the orientation of ductile fabrics can be interpreted in terms of large-scale mantle flow. Work on cores of partially serpentinized mantle peridotite from the East Pacific (Boudier et al., 1996) and the Atlantic (Ceuleneer and Cannat, 1997) has shown that they can be reoriented into the geographical reference frame using remanent magnetization, provided that tectonic rotations were minor or that their effects can be removed (Hurst et al., 1997; Kelso et al., 1996; Kikawa et al., 1996; Lawrence et al., 1997; Richter et al., 1996).

There are several assumptions involved in the reorientation process, namely

1. The remanence in individual samples accurately records the geomagnetic field direction (there is little magnetic anisotropy);
2. The average remanence in a given hole or at a given site reflects the time-averaged field direction (magnetization is slow enough that paleosecular variation is averaged;
3. The type of remanence and the timing of remanence acquisition must be known (the remanence need not be primary, so that, for example, a late viscous remanence would be adequate for geographic reorientation
4. The polarity of the remanence must be known; and
5. Independent constraints on the rotation axis—if any—must be available.

It is not clear whether all these assumptions are actually valid in all previous studies that attempted reorientation of core from ODP drilling, but all of them are implicit in the reorientation process.

It is noteworthy that there are two distinct types of reorientation studies. In the first, one simply reorients all the remanence directions to a common azimuth to look at the clustering of the structural features. For convenience, this common azimuth may be chosen as 360° or 180°, depending on the polarity of the remanence. During drilling, individual core pieces are rotated to different extents around a near-vertical axis, and this process restores them all to a common orientation, presuming that all had a common remanence azimuth prior to drilling. This process may also be interpreted as crudely placing structural features in a geographical reference frame. However, this interpretation is only valid if the remanence is a relatively recent one (e.g., as at ODP Site 920) or if the amount of rotation is sufficiently small or about an axis such that little change in declination has occurred.

A second reorientation process is needed when the amount of remanence deviation from the expected dipole direction is large, or if rotations occurred about axes that will substantially change both the inclination and declination of the remanence (as is generally the case). This reorientation requires selecting a plausible rotation axis (on geological grounds) and calculating the amount of deviation in both inclination and declination. For specific examples of this type of process, with a quantification of the

effect of different rotation axes on both the declination and inclination of the remanence direction, see the "Paleomagnetism" sections in the "**Site 1268**" and "**Site 1270**" summaries below.

After "undoing" tectonic rotations prior to drilling, the improved declination can, in principle, be used for the common azimuth in reorientation to yield something closer to a geographical reference frame. One could go further and undo the full rotation of the remanence vector to provide the attitude of structural features at the acquisition.

Where the magnetic inclination in the core after horizontal rotation is not parallel to the inferred magnetic inclination at the time of lithospheric formation, tectonic rotations may be inferred and then "removed." However, an important caveat is that the remanent magnetization in partially serpentinized peridotites is hosted in magnetite that is produced during serpentinization, so tectonic rotations of the peridotite prior to serpentinization cannot be detected.

Accounting fully for possible tectonic rotations of exposed mantle peridotite is a daunting prospect, but there was hope for a definitive result for the following reasons. Tectonic rotations resulting from normal faults are likely to occur mainly around axes parallel to the ridge axis. Thus, subhorizontal, ridge-parallel flow lineation is likely to be affected very little, if at all. Furthermore, rotations are likely to be away from the ridge axis, increasing the angle between lineations and the ridge axis. Thus, if ridge-parallel lineations had been consistently observed, this could have been taken as good evidence that shallow ductile flow of the mantle was parallel to the ridge. In the best case, observation of systematically varying ductile flow lineations in mantle peridotites, ranging from nearly ridge-perpendicular lineation near segment centers to ridge-parallel lineations near segment ends would have constituted evidence that focused mantle upwelling did occur near segment centers.

Interpretation of Chemical Variation in Mantle Peridotites

Models of focused crustal accretion predict different patterns of mantle depletion due to melt extraction as a function of distance from magmatic segment centers. For strongly focused 3-D mantle flow, there should be no variation in the degree of mantle depletion along axis, since all of the shallow mantle peridotites originate within a narrow, pipelike upwelling zone. For purely passive corner flow, with no other factors considered, again there should be no variation in depletion along axis. However, when passive flow is coupled with cooling of the ends of ridge segments against a fracture zone wall, then the degree of melting is predicted to decrease along axis away from segment centers. This has been termed the "transform edge effect" (Ghose et al., 1996; Langmuir and Bender, 1984; Magde et al., 1997; Phipps Morgan and Forsyth, 1988). Provided that melt extraction is equally efficient throughout the melting region, this variation in melt production should be observed in shallow mantle samples. If partial crystallization of melt migrating into conductively cooled mantle lithosphere occurs, forming "impregnated peridotites" (e.g., Ceuleneer et al., 1988; Ceuleneer and Rabinowicz, 1992; Dick, 1989; Elthon et al., 1992; Seyler and Bonatti, 1997), then this should occur primarily near fracture zones, enhancing the chemical signal of the transform edge effect in mantle peridotites. Furthermore, impregnated peridotites often preserve structural relationships indicative of the nature of melt migration. Impregnated peridotite samples from the western ridge/transform intersection (RTI) of the Kane Fracture Zone (Ishizuka et al., 1995) show evidence for migration of melts into localized ductile shear zones, suggesting that melt migration extended into the active transform fault.

In general, geochemists have searched for the transform edge effect in lavas, which is complicated by the difficulties of seeing through variations in crustal differentiation processes and mantle source composition. Detailed analysis of our suite of peridotite samples, collected from a two ridge segments at

various distances from a fracture zone, will provide an independent evaluation of the presence and importance of the transform edge effect.

Interpretation of Melt Transport Features in Mantle Peridotites

Models of focused melt migration toward ridge segment centers predict various different spatial distributions and orientations of melt transport features. Before discussing the various predictions, we will introduce some of the melt transport features that can be recognized in mantle peridotite samples. For reviews of the literature on these features, please see papers by Nicolas (1986, 1990) and Kelemen et al. (1995a, 1997a). Melt transport features include the following:

1. Dunites are rocks composed almost entirely of the mineral olivine, with minor spinel; pyroxene generally forms <1% of these rocks. Dunites occur in tabular to cylindrical bodies in ophiolite peridotites. Few, if any, are tabular dikes filled entirely with magmatic olivine. Instead, most or all form by dissolution of pyroxene and crystallization of a smaller amount of olivine in olivine-saturated melt migrating by porous flow. Some have an origin entirely via focused porous flow, either in dissolution channels or within ductile shear zones, whereas others form in porous reaction zones around cracks. The relative importance of entirely porous- vs. fracture-related origins for dunites is controversial, but is not crucial to this report. The main point to be made here is that dunites commonly form in the region of adiabatic mantle upwelling beneath spreading ridges, though they also form within the region of transition between adiabatic upwelling and conductively cooled lithosphere.
2. Pyroxenite and gabbro mantle dikes are highly elongate, generally parallel-sided features that almost certainly form as fracture-filling magmatic rocks. Their compositions, where they have been studied in detail, are indicative of crystal fractionation from magma that was cooling within conductive "lithosphere." However, this is debated, and Nicolas and coworkers have interpreted them to be representative of melt-filled fractures that form within the adiabatically upwelling mantle.
3. Large gabbroic plutons, perhaps generally with high aspect ratios but distinguished from dikes by having horizontal extents of tens to thousands of meters, may intrude mantle peridotite. These are abundant in the "crust–mantle transition zone" of the Oman ophiolite (Boudier and Nicolas, 1995; Boudier et al., 1996; Kelemen et al., 1997b; Korenega and Kelemen, 1997), where they are interpreted as "ponds" of melt accumulated beneath a permeability barrier created by the onset of crystallization from cooling magma entering the thermal boundary layer (Kelemen and Aharonov, 1998). At slow-spreading ridges, such plutons might form at much greater depth, perhaps as deep as 20 km, since thermal models and metrological data suggest that the thermal boundary layer is that thick at half-spreading rates of ~10 mm/yr (Sleep, 1975; Reid and Jackson, 1981; Braun et al., 2000; Michael and Chase, 1987; Meurer et al., 2001; Grove et al., 1992; C. Xia et al., unpubl. data).

We now consider predictions of spatial distribution and orientation of melt migration features, with an emphasis on dunites formed within the adiabatically upwelling mantle. Most models predict that such dunites are transposed into a subhorizontal orientation in the shallow mantle, at least by 2-D corner flow and perhaps also by 3-D diapiric flow. (Dunites that are not subhorizontal may have formed in the region of transition from adiabatically upwelling mantle to conductively cooled lithosphere).

1. If melt migration and crustal accretion are focused mainly because of diapirism, as proposed by Nicolas (1990), then no systematic variation in dunite abundance along the ridge axis is predicted. Futhermore, if melt-filled fractures form within mantle diapirs and these are represented by mantle dikes (Nicolas, 1990), then mantle dikes may be nearly vertical near segment centers and progressively transposed into a horizontal orientation toward segment ends.
2. If melt migration and crustal accretion are focused mainly because of melt migration beneath permeability barriers parallel to the base of the lithosphere, as proposed by Sparks and coworkers (Magde et al., 1997; Sparks and Parmentier, 1991, 1994) and Spiegelman (1993), then dunites should be shallowest (and most commonly sampled by drilling) near the centers of segments.
3. If melt migration and crustal accretion are focused mainly as a result of coalescing porous flow within the upwelling mantle, as proposed by Phipps Morgan (1987), Spiegelman and McKenzie (1987), Kelemen and coworkers (Aharonov et al., 1995; Kelemen et al., 1995a, 1995b, 2000), and Daines, Zimmerman, and Kohlstedt (Daines and Kohlstedt, 1997; Kohlstedt and Zimmerman, 1996), then dunite abundance in the shallow mantle should increase toward segment centers. Thus if porous flow mechanisms predominate in producing focused crustal accretion, then dunite abundance should increase toward segment centers, whereas if diapiric upwelling is the predominant reason for focused crustal accretion, then dunite abundance should be relatively constant along axis.

On a smaller scale, the detailed size/frequency and spatial distribution statistics of a large number of dunite veins in outcrops of mantle peridotite can be used as indicators of the geometry of melt extraction conduits (Kelemen et al., 2000; Braun and Kelemen, 2002). Dunites in mantle outcrops in the Ingalls and Oman ophiolites show a negative power-law relationship between size and abundance, with many small dunites and only a few large ones. This is consistent with the hypothesis that dunites form an interconnected channel network in which many small conduits feed a few large ones. The systematics of the spatial distribution can be used to distinguish between dunites that originate as reaction zones around cracks and dunites that form entirely as a result of porous flow mechanisms.

MANTLE TEMPERATURE AND COMPOSITION

Along the Mid-Atlantic Ridge near Iceland and the Azores, major element indices of the degree of mantle melting (Na/Mg in lavas and pyroxene content in peridotites) suggest an unusually high degree of melting, if one assumes constant source composition. In contrast, trace element indices (high La/Sm and K/Ti) from the same regions, interpreted in the same way, indicate a small degree of melting. This apparent paradox is easily resolved; the mantle source composition is not constant along the ridge (e.g., Schilling, 1973). This is borne out by radiogenic isotope ratios, which indicate a long-term enrichment in incompatible elements (such as La and K) in the mantle source where the degree of melting is large (e.g., Hart et al., 1973). Enriched areas with apparent high degrees of melting areas have been interpreted as "hotspots" in accord with the notion that high temperature and chemical enrichment are correlated in the mantle. However, because this correlation between temperature and enrichment is poorly understood and may vary from place to place, there is debate over their relative importance in controlling igneous crustal thickness, crustal composition, axial depth, and geoid height.

Work in the 14° to 16°N region provides constraints for deconvolving the effects of temperature and composition on mantle melting. There is a substantial gradient over 150 km along the ridge, from geochemically "normal" MORB in the north (moderately high Na/Mg and low La/Sm) to strongly

"enriched" MORB in the south (low Na/Mg and high La/Sm) (Fig. F3), and there appears to be a large gradient in crustal thickness, based on interpretation of gravity data, increasing away from the fracture zone. One hypothesis holds that "enriched" basalts are derived by partial melting of veins that compose a few percent of the volume of the source region. The volumetric proportion of veins in peridotite drill core, and future isotope measurements on these veins, will place constraints on the original proportion and composition of these veins prior to decompression melting.

HYDROTHERMAL ALTERATION OF PERIDOTITE

Another goal of drilling was characterization of hydrothermal alteration of mantle peridotite and plutonic rocks to quantify chemical changes at a variety of temperatures. Systematic geochemical studies of samples with different extents and types of alteration will be necessary to discriminate between major and trace element features retained from igneous processes vs. those that are dominantly imposed during open system alteration. It is now recognized that a large proportion of slow-spreading lithosphere is composed of serpentinized peridotite, which is eventually subducted, but the composition of this geochemical reservoir is poorly characterized and understood. As for melt transport veins, discussed above in "**Interpretation of Melt Transport Features in Mantle Peridotites,**" continuous core was used for detailed studies of the size/frequency and spatial distribution statistics of alteration veins. Postcruise analysis of these data will provide important information on the mechanisms of vein formation and fluid transport (e.g., Kelemen et al., 2000; Magde et al., 1995).

GABBRO PLUTONS IN PERIDOTITE

A variety of recent observations on slow-spreading ridges, including the Mid-Atlantic Ridge, suggests that the crust in these settings is a complicated mixture of gabbroic plutons and partially serpentinized peridotite (review in Cannat, 1996). Mantle peridotite is known to crop out along both flanks of the Mid-Atlantic Ridge from at least 14°40′ to 15°40′N (Fig. F2). In some cases, lava flows lie directly over mantle peridotite without intervening gabbroic "lower crust." Thus this region has been interpreted as "magma starved," an end-member compared to the "robust" East Pacific Rise.

Surprisingly, seismic surveys of regions of slow-spreading ridges with abundant peridotite outcrops generally yield significant crustal thicknesses, if crust is defined as material with a seismic *P*-wave velocity of <8 km/s. This is true, for example, for the Mid-Atlantic Ridge just north of the 15°20′ Fracture Zone, within the Leg 209 drilling area (Fig. F4) (Detrick and Collins, pers. comm., 1998). In general, seismic data have been used to determine an average crustal thickness of 6 to 7 km for oceanic crust formed far from mantle hotspots, independent of spreading rate (e.g., White et al., 1992). This paradox represents a first-order problem in studies of the global ridge system.

If possible, it will be very important to develop a geophysical technique for distinguishing between partially serpentinized peridotite and plutonic gabbroic rocks, even where these have the same seismic velocity and density (e.g., Christensen and Salisbury, 1975; Miller and Christensen, 1997). Obtaining extensive drill core of altered mantle peridotite from well below the surface weathering horizon in the 15°N area, together with prior geophysical characterization of this area and downhole logging, was a first step in resolving this problem. Physical properties of the samples measured in the laboratory (remanent magnetization, density, seismic velocities and attenuation, and electrical conductivity) can be compared with geophysical data in order to calibrate the large-scale surface techniques used worldwide. As postcruise data become available, a combination of lithologic observations on core and geophysical

measurements made at true seismic wavelengths will be used to seek out features in the geophysical signals that are characteristic of partially serpentinized peridotite and truly measurable in the field.

NATURE AND SOURCE OF MAGNETIZATION IN SERPENTINIZED PERIDOTITES

Although serpentinized peridotite may compose a significant proportion of slow-spreading lithosphere, extending up to the seafloor, regional geophysical surveys show a systematic alternation of normally and reversely magnetized seafloor correlated with crustal age, just as in fast-spreading volcanic Pacific crust. Although we did not focus on this problem during Leg 209, we obtained substantial data on the magnetic properties of serpentinized peridotite, which will aid in interpretation of magnetic data for crust formed at slow-spreading ridges.

SITE SUMMARIES

Site 1268

Site 1268 was located along the track of the *Shinkai* 6500 submersible Dive 427 from 1998, which recovered samples of peridotite, pyroxenite, and gabbro from a series of steep outcrops separated by flat, sedimented seafloor along the western flank of the rift valley. The specific drill site was in flat terrain upslope and west of a steep scarp from which samples of dunite and peridotite with a gabbroic dike or vein were recovered during the dive survey. Recovery averaged ~53%, with 79% recovery from Cores 209-1268A-12R through 20R.

Proportions of Igneous Rocks

The igneous and residual mantle protoliths of recovered core were harzburgite, dunite, gabbro, gabbronorite, and minor pyroxenite (Fig. F7). Gabbro, gabbronorite, and pyroxenite are intrusive into the peridotite and become increasingly common toward the bottom of the hole. About 63% of the Hole 1268A core is composed of harzburgite, 11% is dunite, and gabbroic rocks compose ~26%. Strikingly, the proportion of peridotite (harzburgite + dunite) to gabbroic rocks is the same as the proportion of gabbro to peridotite (6 peridotites/2 gabbros) collected during *Shinkai* Dive 427, and the proportion of peridotite to gabbro in all dredge and dive samples along the Mid-Atlantic Ridge south of the 15°20′ Fracture Zone to 14°40′N (~77 peridotites/~25 gabbros, based on the compilation presented in the Leg 209 *Scientific Prospectus,* data in Fujiwara et al., 2003, and references cited therein).

In some regions, the seismic structure of "crust" beneath slow-spreading ridges exhibits a *P*-wave velocity gradient from values <4 km/s in the upper kilometer to values near 8 km/s at 7 km depth (e.g., Canales et al., 2000; Detrick and Purdy, 1980; Detrick et al., 1993). This is in contrast to nearly constant lower crustal *P*-wave velocities of ~7 km/s with a sharp increase to ~8 km/s at 7 km depth in seismic profiles from the Pacific (e.g., Vera et al., 1990; compilation by White et al., 1992; see also Fig. F4E). The velocity gradient beneath some slow-spreading ridges is often interpreted to indicate that the "crust" is composed mainly of serpentinized mantle peridotite with proportions of serpentine and/or open cracks decreasing from the seafloor to ~7 km depth. However, the *P*-wave velocities we measured on altered gabbros from Hole 1268A during Leg 209 range from 3.7 to 5 km/s, very similar to those for serpentinite. Thus, gabbroic intrusions could compose 25% or more of the seismic crust in this region.

It is interesting to speculate on the depth of emplacement of the gabbroic rocks into peridotite at Site 1268. Abundant gabbroic intrusions into peridotite have been sampled by dredging along the Mid-Atlantic Ridge, in particular in the 14° to 16°N area (e.g., Cannat, 1996; Cannat et al., 1992, 1997a, 1997b; Cannat and Casey, 1995). Some of these record high-temperature plastic deformation (~600°C or more), leading Cannat and coworkers to propose that some intrusions are emplaced, solidified, and cooled at depths of 15 km or more. Our onboard compilation of *P*-wave velocities for the "upper mantle" in oceanic plates at depths of 7 km or more shows a large range (from 7.6 to >8.4 km/s) (Fig. F8), even for near-axis regions.

The observed range of *P*-wave velocities in oceanic plates at depths of 7 km or more may arise, in part, from differences in temperature and degree of alteration as well as from variable experimental methods and uncertainties in the data. However, the range of velocities could also be due in part to the presence of variable proportions of gabbroic intrusions within mantle peridotite. If unaltered, crack-free, cold, olivine-rich peridotites in the shallow mantle beneath slow-spreading ridges have *P*-wave velocities of 8.1 km/s and gabbroic rocks under the same conditions have *P*-wave velocities of ~7.2–7.3 km/s (e.g., Behn and Kelemen, in press; Hacker et al., 2003; Korenaga et al., 2000, 2002), then the presence of 25% gabbro within 75% residual mantle harzburgite at depths of 7–20 km would yield a *P*-wave velocity of 7.9 km/s, well within the observational range of "mantle" velocities beneath oceanic crust in general and slow-spreading mid-ocean ridges in particular.

Highly Depleted Mantle Peridotites

With very few exceptions, peridotites from Site 1268 are 100% altered to a mixture of serpentine and talc (Figs. F9, F10). However, geochemical analyses of these peridotites show exceptionally low concentrations of nominally "immobile" incompatible elements such as Al, Sc, and V. For example, Al_2O_3 concentrations in Site 1268 peridotites are <1 wt% (average = 0.6 wt%), whereas Al_2O_3 in peridotites from Site 920 along the Mid-Atlantic Ridge at 23°20′N ranges from 1 to 2 wt% (Casey, 1997). If these values have not been modified by hydrothermal metasomatism, then the peridotites from Site 1268 are among the most depleted residual mantle peridotites yet obtained from the mid-ocean ridges.

Molar $MgO/(MgO+FeO_{total})$, or Mg#, of the peridotites varies from ~88% to 94%. This includes the normal range of whole-rock Mg# in residual mantle peridotites from mid-ocean ridges (~89%–92%; average = ~90%–91%) (e.g., Dick, 1989), but values <89% and >92% may be indicative of metasomatic changes in Fe/Mg during hydrothermal alteration.

Petrogenesis of Intrusive Gabbronorites

Most of the gabbroic rocks, in two thick sequences toward the bottom of the hole, were probably gabbronorites, based on the presence of relict clinopyroxene together with texturally distinct, altered orthopyroxene. (Orthopyroxene is completely replaced by talc in all samples). Because the pyroxenes have undergone substantial alteration and metasomatism, interpretation of their whole-rock compositions in terms of igneous petrogenesis is highly uncertain. Nevertheless, some aspects of their bulk composition are intriguing from an igneous perspective.

The gabbronorites from Hole 1268A are unusually primitive. Molar Mg# is 75%–83% in the large gabbbronorite bodies near the base of the hole. In contrast, gabbronorites from East Pacific Rise, Mid-Atlantic Ridge, and Southwest Indian Ridge crust at ODP Sites 735, 894, and 923,respectively, are comparatively evolved, with whole-rock and orthopyroxene Mg# < 72% (e.g., Cannat et al., 1997a; Casey,

1997; Dick et al., 1991, 2002; Natland and Dick, 1996). Such evolved crustal gabbronorites must form by nearly complete crystallization of orthopyroxene-normative basalts because MORB lavas very rarely contain orthopyroxene crystals and phase equilibria confirm that primitive and normal MORB are not saturated in orthopyroxene at crustal pressures.

Primitive gabbbronorites are found in the crustal section of the northern massifs in the Oman ophiolite. For example, the lower crustal section of the Fizh massif has abundant orthopyroxene-rich, primitive cumulates, including pyroxenites (websterites) as well as gabbronorites (orthopyroxene Mg# = 80%–90%) (e.g., Smewing, 1981). We interpret the presence of high-Mg# orthopyroxene in the plutonic section of the northern Oman massifs to indicate an important role for crystallization of primitive andesite, with a higher SiO_2 content than MORB, at crustal depths in these massifs.

In the southern Oman ophiolite massifs (Samail and Wadi Tayin), orthopyroxene is essentially absent from the lower crustal section (e.g., Pallister and Hopson, 1981), but undeformed, primitive orthopyroxene-bearing cumulates (Mg# = 80%–93%) form small, isolated intrusions and dikes in the mantle section (e.g., Amri et al., 1996; Benoit et al., 1996; Kelemen et al., 1997b), cutting ductile fabrics in surrounding peridotite. These gabbronorite and websterite intrusions into the mantle section have been attributed to crystallization of late, hydrous, incompatible element–depleted, primitive andesite magmas in the uppermost mantle. Such magmas could have formed by partial melting of depleted, serpentinized, shallow mantle peridotite at a mid-ocean ridge (Benoit et al., 1996) or by fluid-fluxed melting above a subduction zone during the initial stages of ophiolite obduction (Kelemen et al., 1997b). These melts must have been rare compared to the MORB-like basalts that formed crustal gabbros, dikes, and lavas in the southern Oman ophiolite massifs.

If the relatively high Mg#s of the Hole 1268A gabbronorites are indeed representative of their primary igneous composition, they would be distinct from evolved gabbronorites previously recovered from mid-ocean ridges and relatively similar to primitive gabbronorites that intrude the mantle section of the Oman ophiolite. Thus, it is possible that primitive gabbronorite cumulates crystallized from depleted hydrous magmas formed by hydrous partial melting of shallow, already depleted, hydrothermally altered peridotite, as has been proposed for the Oman gabbronorites (Benoit et al., 1996). If this occurred, it would give rise to relatively SiO_2-rich melts. Indeed, primitive glasses (Mg# > 60%) from the 14° to 16°N region of the Mid-Atlantic Ridge (Melson et al., 1977; C. Xia et al., unpubl. data) extend to >52 wt% SiO_2. These are among the most SiO_2-rich primitive glasses that have been recovered from the mid-ocean ridges (Fig. F11).

An alternative hypothesis is that the relatively primitive gabbronorites from Hole 1268A crystallized at depths corresponding to pressures of 0.4 to 1 GPa, where orthopyroxene forms relatively early during crystallization of primitive MORB. This idea is consistent with the hypothesis that some Mid-Atlantic Ridge lava suites lie along a liquid line of descent, indicative of crystal fractionation at 0.4–0.8 GPa (Grove et al., 1992; Michael and Chase, 1987; Meurer et al., 2001). C. Xia et al. (unpubl. data) showed that lavas from the Mid-Atlantic Ridge from 14°N to the 15°20′ Fracture Zone fall along a liquid line of descent for crystallization of MORB at ~0.6 GPa. Thus, magmas beneath the Mid-Atlantic Ridge in this region begin to conductively cool and crystallize at a depth of ~20 km. This inference is consistent with slow magma transport into the base of a conductive boundary layer with a thickness of 20 km, as predicted by thermal models of slow-spreading ridges (e.g., Braun et al., 2000; Reid and Jackson, 1981; Shen and Forsyth, 1995; Sleep, 1975). However, by itself, crystal fractionation at 0.6 GPa would not explain the relatively SiO_2-rich nature of some lavas from this region.

An intermediate hypothesis is that magmas entering a thick thermal boundary layer begin to cool, crystallize, and interact with surrounding mantle peridotite at 0.4–1 GPa in a process of "combined assimilation and fractional crystallization" (DePaolo, 1981; Gaetani et al., 1995; Kelemen, 1986, 1990; Kelemen et al., 1997a, 1997b). This process would give rise to relatively incompatible element–enriched, primitive basaltic andesites or andesites that were saturated in orthopyroxene at low to moderate pressure. In **"Site 1275,"** we calculate olivine–orthopyroxene–clinopyroxene–plagioclase saturation pressures for lavas from 14°14′ to 16°N in order to constrain the likely pressures of gabbronorite crystallization in this region. For primitive lavas (Mg# > 60%, in equilibrium with pyroxene having an Mg# > 75%), saturation pressures range from ~0.4 to ~0.9 GPa (average = 0.54 GPa).

To summarize, if they record their igneous Mg#s, the Hole 1268A gabbronorites are the most primitive gabbronorites yet recovered from a mid-ocean ridge. As such, they probably record cooling and partial crystallization of ascending MORB near the base of the thermal boundary layer beneath the Mid-Atlantic Ridge (perhaps at 15–25 km), followed by tectonic uplift and unroofing at the seafloor together with host peridotites. This is an exciting hypothesis. However, since these rocks have undergone compositional changes during hydrothermal alteration, it may be that their Mg#s increased during metasomatism and are not representative of the original igneous values. Postcruise, electron probe analyses of Mg# in unaltered clinopyroxene will provide additional constraints on the igneous composition of these rocks.

Hydrothermal Alteration, Metamorphism, and Metasomatism

Hydrous alteration of peridotites to serpentine and talc is substantial in most peridotites from Hole 1268A. In a very unusual paragenesis, talc replaces serpentine in a distinct metamorphic event that occurred after complete serpentinization (Fig. F12). Serpentinization and later replacement of serpentine by talc occurred at temperatures <400°C under static conditions in most of the core. However, there are a few cataclastic shear zones with syn- and post-kinematic talc and serpentine. Talc alteration is most pronounced near contacts with gabbroic intrusions. Gabbros were also altered under static conditions, with pyroxenes pseudomorphed mainly by talc and chlorite and plagioclase pseudomorphed mainly by chlorite and quartz. Some gabbros show 100% replacement of pyroxene by talc pseudomorphs. Fresh plagioclase and clinopyroxene are increasingly well preserved toward the bottom of the hole.

In addition to the unusual replacement of serpentine by talc, the alteration of Hole 1268A peridotites and gabbronorites was accompanied by remarkably extensive metasomatism. Talc-altered peridotites with pseudomorphic textures that unambiguously indicate a harzburgite protolith have whole-rock compositions corresponding to the stoichiometric composition of talc itself (Fig. F13), indicating large amounts of SiO_2 gain and/or MgO + FeO loss. This compositional change is similar to but more extensive than metasomatism of peridotites during seafloor weathering documented by Snow and Dick (1995). In fact, the normative orthopyroxene contents of all the altered peridotites in Hole 1268A, including talc-free serpentinites, are generally >30 wt%, in contrast to the 20–25 wt% generally observed in fresher residual mantle harzburgites (e.g., Cannat et al., 1995; Dick, 1989; Dick et al., 1984). Therefore, we infer that even serpentinites without talc alteration have undergone SiO_2 addition or MgO + FeO loss. Transforming a harzburgite with an Mg# of 90% and 20 wt% orthopyroxene (SiO_2 = ~44 wt%) to a rock with the composition of talc (SiO_2 = ~66 wt%) by SiO_2 addition requires adding ~40 wt% SiO_2 to the original rock mass. Performing the same transformation by removing MgO and FeO from the harzburgite (MgO = ~46 wt% and FeO = ~9 wt%) to form talc with the same Mg# requires removal of 30 wt% of the MgO and FeO from the original rock, corresponding to removal of 16% of the original rock mass. This is in addition to possible removal of Al_2O_3, Cr_2O_3, CaO, Na_2O, and other oxides, which together total 0.4–3

wt% of the altered peridotites from Hole 1268A (average = 1.2 wt%). Conversion of a multicomponent polymineralic rock to a monomineralic rock during metasomatism is typical of "blackwall" reaction zones composed of pure talc and pure chlorite that form between peridotite and relatively silicic wallrocks in metamorphic belts (e.g., Chidester, 1962; Hanford, 1982; Thompson, 1959).

Whole-rock compositions of altered gabbronorites also show dramatic metasomatic effects, with low CaO and high MgO + FeO in the most altered rocks (Fig. F14). The compositions of the most altered rocks approach those of talc + chorite + quartz mixtures. These minerals are abundant in the alteration assemblage. Again, the style of metasomatism and the mineral assemblages involved recall the formation of metasomatic "blackwall" between peridotite and felsic wallrock. In settings other than blackwall reaction zones, relative CaO loss from gabbroic rocks in contact with serpentinized peridotites is unusual, as serpentinization of host peridotite produces Ca-rich fluids that commonly react with gabbroic rocks to form metasomatic calc-silicate assemblages known as rodingites. However, in Hole 1268A, both peridotites and gabbronorites apparently lost CaO. Although we hypothesize that hydrothermal alteration of the gabbros produced the fluids that added SiO_2 to the talc-altered peridotites, there is no obvious sign of SiO_2 loss from the altered gabbronorites.

As discussed in more detail in "**Structural Geology**" below, it is important to add that hydrothermal alteration and metasomatism of both peridotite and gabbro occurred at low temperature (<400°C) after intrusion of gabbro into relatively hot peridotite (>600°C) and after ductile deformation of both gabbro and peridotite. Thus, although the gabbroic rocks may have acted as the source of SiO_2 during silica enrichment of peridotites, the intrusion of the gabbro did not cause the hydrothermal alteration and metasomatism of Site 1268 peridotites.

Structural Geology

Intrusion of gabbroic rocks into peridotite probably occurred while the peridotite was at high temperature (>600°C). This inference is based on two observations, neither of which is definitive. First, the presence of coarse-grained gabbronorite crosscutting peridotite in a contact preserved in Section 209-1268A-21R-1 (Fig. F15) suggests but does not prove that the contact was at high temperature during intrusion. Second, mylonite zones are present at depths of 15, ~48–53, 65, 76–79, and 88–89 meters below seafloor (mbsf). The largest two are within zones of abundant millimeter- to centimeter-scale gabbroic veins or dikes in peridotite, termed magmatic breccias. The mylonites record crystal-plastic deformation under granulite facies conditions at temperatures >600°C and probably >900°C.

Deformation intensity in both gabbro and peridotite varied substantially over length scales of <1 m throughout the hole, with protogranular, porphyroclastic, and mylonitic textures in peridotites and undeformed to mylonitic textures in gabbroic rocks. Strain was concentrated in and around the mylonite zones discussed in the previous paragraph and thus occurred mainly in zones of mixed gabbroic intrusions and peridotite.

Brittle deformation features are also common throughout the core. Cataclastic shear zones cutting peridotite and intrusive rocks are present at several depths. Fault gouge zones were recovered in core at depths at ~60, 65, and 80 mbsf. That two of the fault gouge zones are immediately beneath the mylonitic zones discussed in the previous two paragraphs is probably indicative of continued localization of deformation in these zones over a wide range of temperatures. Some brittle faults and shear zones show syn-kinematic serpentine and talc mineralization, demonstrating that deformation continued to temperatures less than ~300°C.

We used crosscutting relationships to reconstruct the following sequence of events for the core from Hole 1268A:

1. Partial melting of mantle peridotite together with formation of dunite bands and protogranular textures in residual harzburgite;
2. Cooling of peridotite at the base of the thermal boundary layer;
3. Intrusion of gabbroic veins and gabbronorite bodies while peridotites were still at high temperature;
4. Formation of high-temperature mylonite zones with associated ductile deformation in surrounding gabbroic and ultramafic rocks while temperatures were >600°C and probably >900°C [**N1**];
5. Cooling of peridotites and gabbroic rocks to <400°C;
6. Static, pervasive, nearly complete serpentinization of peridotites, perhaps with continued deformation in highly localized shear zones;
7. Static replacement of serpentine in peridotites and pyroxenes in gabbronorites by talc, with associated alteration of plagioclase to chlorite + quartz; and
8. Continued brittle deformation.

Paleomagnetic Data and Tectonics

Paleomagnetic data were collected on half cores and individual discrete samples. Some samples retained a stable remanent magnetization. Using these data, we rotated the measured orientations of foliations, faults, veins, and dikes in individual core pieces around a vertical axis, thereby restoring core pieces to a common orientation (assuming the remanent magnetization vector in all core pieces had a common azimuth prior to drilling). Rotation of brittle shear zones, faults, and cracks into a common magnetization orientation produces a systematic girdle of poles. Furthermore, rotation of crystal-plastic foliations into the same common magnetization orientation produces a fairly tight cluster of poles.

The average remanent inclination for 11 discrete samples from the gabbros is 15° (95% confidence interval [CI] = +7°/–8°), significantly shallower than the expected inclination of 28°. The average inclination of the peridotites calculated from 38 discrete samples is 40° (95% CI = +5°/–9°), significantly steeper than the expected value of 28°. The most reliable peridotite magnetizations (9 high-coercivity talc-altered samples) have an average inclination of 36° (95% CI = +12°/–14°).

One possible explanation for the statistically significant difference between the expected and observed inclinations in the gabbroic rocks is that they cooled quickly through their dominant unblocking temperature range (~500°–570°C) and therefore do not average secular variation. If so, they may record an inclination that does not correspond to that expected from a geocentric axial dipole. However, the observed range of inclinations in discrete samples (6°–36°) is larger than would be expected solely from orientation errors. Also, as explained above, geologic evidence (high-temperature contacts between gabbro and peridotite and high-temperature ductile fabrics cutting some gabbros) suggests that wallrocks were at temperatures greater than ~600°C during gabbroic intrusion, higher than the upper thermal stability limits for serpentine and talc at lithospheric pressures. Thermal modeling and inferences from igneous petrology both suggest that the conductive boundary layer beneath slow-spreading ridges in general, and the 14° to 16°N region in particular, is ~20 km thick. Therefore, cooling of the gabbroic rocks through the Curie temperature by conduction coupled with tectonic uplift to the seafloor was probably slow. For these reasons, we infer that the magnetization directions from the gabbros likely represent some degree of time averaging.

A second possible explanation for the statistically significant difference between the expected and observed inclinations in the gabbroic rocks is that tilting of the gabbroic rocks occurred after cooling and blocking of the remanence. If so, the magnetization of the peridotites must have occurred later, during alteration that postdated some of this tilting. In the following paragraphs we outline the quantitative implications of this hypothesis. It should be emphasized, however, that this is simply a forward model.

With additional assumptions, paleomagnetic inclination data may be used to infer the direction and magnitude of tectonic rotations that may have occurred between the time the sample recorded remanent magnetization and the present. Restoration of the core to its pretilt attitude has no unique solution. Unless other independent information on core orientation is available, the uncertain azimuth of cores precludes an estimation of the strike and plunge of the rotation axis along which tilting was produced. If the rotation axis is assumed to be horizontal, the azimuth of this axis dictates the amount of rotation required to rotate an original inclination of 28° to produce an observed inclination of 15°. Figure F16 illustrates this point. If a horizontal rotation axis strikes 000°, the required rotation is ~60°. Alternatively, if a horizontal rotation axis strikes 270°, the required rotation is only 13°.

Some constraints can be derived from seafloor topography and inferences about the processes that produce it. The stepwise alternation of steep, east-facing slopes and nearly horizontal benches along the western flank of the Mid-Atlantic Ridge is generally interpreted to result from the presence of numerous tilted normal fault blocks. Back-tilting of fault blocks on the west side of the rift valley in the region around Site 1268 is probably top-to-the-west (counterclockwise around a northeast-striking axis). In this region, the east-facing slopes strike ~020°, parallel to the strike of the rift valley. We infer that tilting was produced by counterclockwise rotation of normal fault blocks along an approximately rift-parallel axis. For a horizontal rotation axis striking 020°, ~90° of counterclockwise rotation is required to change an original inclination of 28° to the observed average inclination of 15° in gabbros from Hole 1268A.

The differences between magnetic inclination in the gabbros (~15°) and the peridotites (~36°) require that the two lithologies record different amounts of rotation. The inclinations in the peridotite are not statistically different from the expected inclination of 28° at 95% CI. Thus, one option is that gabbroic rocks were rotated prior to magnetization of the peridotites.

However, the average inclinations are 40° for all the peridotites and 36° for the more reliable data from talc-altered peridotites. The relatively steep average inclinations in the peridotites can be explained as the result of smaller counterclockwise rotations around a horizontal axis striking 020° because small counterclockwise rotations around this axis produce a steepening of the magnetic inclination (Fig. F16). This hypothesis is consistent with relatively early magnetization of the gabbroic rocks during cooling through their discrete blocking temperature range (~500°–570°C) and later magnetization of the peridotites during magnetite crystallization accompanying serpentinization at ~300°C. In this scenario, counterclockwise rotation of the Site 1268 section around a horizontal axis striking 020° began before magnetization of the gabbroic rocks and continued after magnetization of the peridotites [**N2**].

An additional uncertainty in inferring the amount of tilting is introduced by the unknown plunge of the rotation axis. Figure F17 illustrates this problem. For a rotation axis with a fixed azimuth of 020°, if the plunge were 10° along 020°, ~120° of counterclockwise rotation would be required to change an original inclination of 28° to the observed average inclination of the gabbroic rocks of 15°. Conversely, if the plunge were 10° along 200°, ~80° of counterclockwise rotation would be required for the same change in inclination [**N3**].

In summary, if the hypothesis outlined here is correct, the gabbroic rocks in Hole 1268A underwent a large amount of counterclockwise rotation (~60°–90°) around a nearly horizontal, rift-parallel axis after acquisition of the magnetic remanence. The magnetic remanence in the gabbroic rocks was probably

acquired when they passed through their dominant blocking temperature at >500°C. The peridotites record only ~30° of this rotation.

This is a potentially important result because it is consistent with the independent hypothesis that the large fault planes forming the top surfaces of oceanic core complexes rotate from steep normal faults at depth to a subhorizontal attitude as they reach the seafloor. However, the rotations we infer from the paleomagnetic data are larger than the rotations predicted in most models of oceanic core complex formation. Finally, it must be emphasized again that this is a nonunique forward model, one of many which could potentially account for the observed paleomagnetic data, and that the model results are subject to the numerous uncertainties outlined in the previous paragraphs.

Microbiology

One sample of metaperidotite was taken from interval 209-1268A-2R-1, 38–47 cm, to characterize the microbial community inhabiting this environment. Aliquots of surface and bottom water were also sampled and prepared for deoxyribonucleic acid (DNA) analysis. Results of cultures and DNA analysis of rock and water samples will not be available for this report. Direct counts of microorganisms were performed on the seawater samples. Atmospheric dust and air samples were obtained, and both bacterial and viral growth were measured in these samples.

Site 1269

Although serpentinized peridotite and gabbro were sampled from nearby outcrops during precruise submersible dives, the only rocks recovered from three different hole locations at Site 1269 were basalts. Since the outcrops were too steep to be viable drilling targets, we chose to attempt to drill through the flat, lightly sedimented terraces above the outcrops and into the oceanic basement below. We interpret the low recovery of only basaltic rock and poor hole conditions at this site to indicate that the terrain between outcrops exposed by faulting is covered by basalt flows or talus.

The basalts recovered from Site 1269 are fresh and range from aphyric to slightly plagioclase-olivine phyric. Glomerocrysts of plagioclase and olivine are present but rare, and acicular plagioclase laths and quench clinopyroxene with minor amounts of fresh brown glass and skeletal opaque minerals make up the groundmass. The most striking characteristic of these basalts is their high vesicularity, commonly >15 vol% (Fig. F19).

MORB erupted deeper than 2500 m water depth typically has <2 vol% vesicles because of the high hydrostatic pressure (Moore et al., 1977). One exception is the 14° to 15°N section of the Mid-Atlantic Ridge where MORB with high volatile abundances and uncommon noble gas compositions has been recovered in dredge hauls (Staudacher et al., 1989; Sarda and Graham, 1990; Javoy and Pineau, 1991; Burnard et al., 1997; Moreira et al., 1998; Pineau et al., 1976).

Based on rare gas abundance, high CO_2, and vesicle size distribution analysis, high-vesicularity basalts previously recovered from 14° to 15°N have been interpreted to represent undegassed MORB magma (Sarda and Graham 1990). The basalts recovered from Site 1269 have the same high vesicularity, and analysis of images of the Site 1269 basalts yields similar trends in vesicle size distribution. However, a higher abundance of larger vesicles and a lack of intermediate-sized vesicles (possibly due to coalescence) in the Site 1269 basalts compared to previous studies may represent a more mature stage in the vesicle forming process in MORB.

Site 1270

Site 1270 was located along the track of *Shinkai* 6500 submersible Dive 425 from 4 July 1998, which recovered samples of peridotite and gabbro from nearly planar, striated outcrops along the eastern flank of the Mid-Atlantic Ridge. The slope of the outcrop surfaces was nearly constant throughout most of the dive, leading to the inference that the slope of the rift valley along the dive track represented a single, kilometer-scale fault surface. All holes at Site 1270 were begun in exposed outcrop surfaces. Recovery averaged ~20%, with 37% recovery over 46 m in Hole 1270B.

Hole 1270A was begun near the site of *Shinkai* 6500 sample 425-R007, a mylonitic peridotite taken from a planar fault surface. Poor drilling conditions, especially the intersection of a zone of unconsolidated fault gouge at 17 mbsf, caused us to abandon this hole. Hole 1270B was situated ~100 m upslope to the east, near another striated, planar outcrop observed during the *Shinkai* 6500 dive. This hole had better recovery but became unstable after 46 m of penetration and had to be abandoned. Hole 1270C was sited ~200 m upslope from Hole 1270B, in an outcrop ~20 m upslope from the top of a steep, 10- to 20-m-tall cliff, near the site of *Shinkai* 6500 sample 425-R008, a weathered harzburgite. The outcrop on and above the cliff is more weathered than those at Holes 1270A and 1270B. Poor drilling conditions caused us to abandon this hole after ~19 m. We inferred that a slope-parallel, low-angle fracture along the base of the nearby cliff might have interfered with circulation in the hole. Thus, we sited Hole 1270D in outcrop ~30 m farther upslope. Again, however, poor drilling conditions forced us to abandon this Hole after 57 m of penetration. Overall, fault gouge, altered shear zones, poor recovery, and/or anomalously rapid progress in drilling were encountered at 15–20 mbsf in each hole at Site 1270. Our impression is that the planar fault surfaces exposed on the seafloor are underlain by parallel brittle fault zones over the entire slope sampled by the *Shinkai* 6500 and our drilling program at this site.

Proportions of Igneous Rocks

The igneous and residual mantle protoliths of recovered core were harzburgite, dunite, gabbro, gabbronorite, and minor pyroxenite (Fig. F20). Gabbro, gabbronorite, and pyroxenite are intrusive into the peridotite in Holes 1270A, 1270C, and 1270D. Hole 1270B includes only a few small fragments of completely altered peridotite and no intrusive contacts, so it is not certain that the gabbroic rocks intrude peridotite. However, by analogy to relationships in Holes 1270A, 1270C, and 1270D and at Sites 1268, 1271, 1272, and 1274, we infer that the gabbros and gabbronorites in Hole 1270B were also intrusive into peridotite.

About 89% of the core from Hole 1270A (total depth = 27 mbsf) is composed of harzburgite, 5% is dunite, and gabbroic rocks compose ~4%, with the remainder being serpentinite and fault breccias with unknown protoliths. Core from Hole 1270B (total depth = 46 mbsf) is 98% gabbro and gabbronorite, with only 2% completely altered peridotite. Core from Hole 1270C (total depth = 19 mbsf) is 81% harzburgite, 17% dunite, 1% gabbroic dikes or veins, and 1% pyroxenite dikes or veins. Core from Hole 1270D (total depth = 57 mbsf) is composed of 91% harzburgite, 7% dunite, and 2% gabbroic dikes or veins.

The overall proportion of rock types in all the holes at Site 1270, weighted by length of recovered core, is ~41% harzburgite, 4% dunite, and 55% gabbro. Weighted by depth of penetration in each hole and using the proportions of rock types recovered in core in each hole, the proportion of lithologies is ~62% harzburgite, 6% dunite, and 32% gabbro and gabbronorite, similar to the proportion of gabbro to peridotite in Hole 1268A (63% harzburgite, 11% dunite, and 26% gabbronorite and gabbro), the proportion of lithologies (2 gabbros/6 peridotites) collected during *Shinkai* Dive 427, and the proportion of peridotite to gabbro in all dredge and dive samples along the Mid-Atlantic Ridge south of the 15°20′

Fracture Zone to 14°40′N (~77 peridotites/~25 gabbros, based on the compilation presented in the Leg 209 *Scientific Prospectus,* and references cited therein).

As discussed in "**Site 1268**" above, these data suggest that much of the seismic crust and even parts of the uppermost mantle may be composed of ~75% peridotite and 25% gabbroic rocks, with crack density and alteration in both lithologies decreasing with depth. However, shipboard measurements of seismic *P*-wave velocities for the fresh gabbroic rocks from Hole 1270B range from 4.6 to 5.8 km/s. These velocities are too high for these rocks to compose a substantial proportion of the seismic crust in this region at depths from <2 to 3 km. Instead, if gabbroic rocks compose a significant proportion of the shallow crust, they must be more altered or there must be a relatively large proportion of cracks compared to the samples from Hole 1270B whose *P*-wave velocities were measured on board.

Highly Depleted Mantle Peridotites

With some notable exceptions, peridotites from Site 1270 are 100% altered, mainly to serpentine. However, geochemical analyses of these peridotites show exceptionally low concentrations of nominally immobile incompatible elements such as Al, Sc, and V. For example, with the exception of a peridotite sample including a gabbroic dike or vein, Al_2O_3 concentrations in Site 1270 peridotites are <1 wt% (average = 0.6 wt%), whereas Al_2O_3 in peridotites from Site 920 along the Mid-Atlantic Ridge at 23°20′N ranges from 1 to 2 wt% (Casey, 1997). The average Al_2O_3 concentration in 7 peridotites from Site 1270 is the same as that determined for 20 peridotites from Site 1268. If these values have not been modified by hydrothermal metasomatism, then the peridotites from Sites 1268 and 1270 are among the most depleted residual mantle peridotites yet obtained from the mid-ocean ridges.

Molar Mg# of the peridotites from Site 1270 varies from 90.0% to 91.5%. This is a narrower range of Mg# than in Site 1268 peridotites (88%–94%) and lies within the normal range of whole-rock Mg# in residual mantle peridotites from mid-ocean ridges (~89%–92%; average = ~90%–91%) (e.g., Dick, 1989). By comparison, we infer that Mg#s <89% and >92% in Site 1268 peridotites are due to metasomatic changes in Fe/Mg during the extensive hydrothermal metasomatism at that site.

Petrogenesis of Intrusive Gabbronorites

Most of the gabbroic rocks in Hole 1270B are Fe-Ti oxide–bearing gabbronorites (Fig. F21) with substantial proportions of igneous plagioclase, clinopyroxene, orthopyroxene, and Fe-Ti oxide minerals preserved. The question arises, how much of the oxide is igneous? It has been proposed that some gabbronorites in the Haylayn massif of the Oman ophiolite were originally oxide-free olivine gabbros that were oxidized at near-solidus conditions via the reaction

$$6(Mg,Fe)_2SiO_4\ (\text{olivine}) + O_2 = 3(Mg,Fe)_2Si_2O_6\ (\text{pyroxene}) + 2Fe_3O_4\ (\text{magnetite}),$$

consuming olivine and forming orthopyroxene + magnetite (Boudier et al., 2000). The compositions of Hole 1270B gabbronorites lie within the volume olivine + plagioclase + pyroxene on most major element projections (e.g., Fig. F22). However, the gabbronorites are rich in TiO_2. Even if they are assumed to contain no ferric iron, and thus no magnetite, CIPW norms for these compositions yield 2–12 wt% Fe-Ti oxide in the form of normative ilmenite ($FeTiO_3$). In addition, the freshest, least deformed samples of oxide gabbronorite contain coarse discrete oxide and pyroxene crystals separated from each other by plagioclase, suggesting that both oxide and pyroxene crystallized directly from a melt. Thus, we infer that the magma(s) that crystallized the Hole 1270B gabbronorites were saturated in Fe-Ti oxide minerals.

Fe-Ti oxides also form interstitial crystals, even within deformed and recrystallized plagioclase. This suggests that the gabbronorites may have been partially molten and igneous Fe-Ti oxides may have continued to crystallize during high-temperature crystal-plastic deformation. However, interstitial textures can form during metamorphism as well as igneous crystallization. Thus, we view the hypothesis that melt was present during deformation of the gabbronorites as intriguing but uncertain.

Analyzed samples have Mg#s from 39% to 68%, similar to the range observed in gabbronorites from ODP Sites 735, 894, and 923 (e.g., Cannat et al., 1997a; Casey, 1997; Dick et al., 1991, 2002; Natland and Dick, 1996). Evolved crustal gabbronorites formed at pressures <0.3 GPa must form by nearly complete crystallization of orthopyroxene-normative basalts because MORB lavas very rarely contain orthopyroxene crystals and phase equilibria confirm that primitive and normal MORB are not saturated in orthopyroxene at 0.3 GPa or less. However, the coarse igneous textures and scarcity of optical zoning in plagioclase and pyroxene suggest that the rocks are "cumulates" formed by partial crystallization of a melt followed by extraction of the remaining liquid.

The inference that evolved melts were extracted after crystallization of Hole 1270B gabbronorites presents an interesting puzzle because no lavas with appropriate compositions have been found along the Mid-Atlantic Ridge from 14° to 16°N. We do not know the igneous Mg# of the pyroxenes in Hole 1270B gabbronorites because the samples contain substantial amounts of magnetite. Thus, the whole-rock Mg# must be substantially lower than the pyroxene Mg#. Also, postcrystallization Fe/Mg exchange between pyroxenes and oxides—plus possible oxidation reactions—may have modified the original igneous Mg#s. However, we can estimate that the clinopyroxenes have Mg#s of 70% or 75% in the Hole 1270B gabbronorites with the highest Mg# and lowest proportion of oxide minerals. Using an Fe/Mg pyroxene/liquid K_d of 0.23 (Sisson and Grove, 1993a, 1993b) and FeO/(FeO+Fe_2O_3) of 100–70 wt%, we can infer that liquids coexisting with these clinopyroxenes must have had an Mg# less than ~41%. In contrast, the lowest reported Mg# in glass from lavas dredged along the Mid-Atlantic Ridge from 14° to 16°N is 50%. Indeed, Mg#s <50% are rare along the entire Mid-Atlantic Ridge (Fig. F23). Thus, the final destination of evolved liquids beneath mid-ocean ridges, once they are extracted after crystallizing evolved gabbronorites, is not yet known.

Gabbroic veins intruding peridotite in Holes 1270A, 1270C, and 1270D are heavily altered and have been recrystallized during extensive ductile deformation. They include plagioclase and clinopyroxene, interpreted as igneous phases. Clinopyroxene is replaced by high-temperature pleochroic amphibole, which could be igneous or could be a high-temperature alteration product. Locally, the veins contain oxide minerals, zircon, and apatite (Fig. F24). Natural gamma emissions recorded on the multisensor track show high radioactivity in the intervals containing these veins. As might be expected from the mineral assemblages in the veins and their gamma ray emissions, the whole-rock composition of a peridotite containing one of these veins (interval 209-1270D-3R-1, 63–66 cm) is enriched in incompatible elements; for example, this sample contains 96 ppm zirconium. Thus, we infer that the melt parental to the veins was enriched in highly incompatible trace elements. Perhaps these veins crystallized from liquids extracted from evolved gabbronorites similar to those recovered from Hole 1270B.

Hydrothermal Alteration, Metamorphism, and Metasomatism

Most peridotites from Site 1270 are completely altered to serpentine with minor talc. As is typical for hydrated peridotites worldwide, most of the talc alteration was in early replacement of pyroxene, followed by serpentinization of olivine and remaining pyroxene. Serpentinization occurred at temperatures <400°C under static conditions in most of the core.

Although talc alteration is subdued in Site 1270 peridotites compared to Site 1268 peridotites, samples from both sites show a similar kind of metasomatism with enrichment in SiO_2 and/or loss of MgO + FeO. The normative orthopyroxene contents of all but two of the altered peridotites from Sites 1268 and 1270 are >30 wt% (Fig. F25), in contrast to the 20–25 wt% generally observed in fresher residual mantle harzburgites from mid-ocean ridges (e.g., Cannat et al., 1995; Dick, 1989; Dick et al., 1984). It is unlikely that MgO and FeO are geochemically similar in the hydrothermal alteration environment; variable proportions of FeO and MgO loss during hydrothermal alteration would probably modify the Mg#. In view of the fact that most peridotites from both Sites 1268 and 1270 have Mg#s within the normal range for abyssal peridotites (see above and the "**Site 1268**" summary), we infer that MgO and FeO were comparatively immobile during metasomatism and the high SiO_2 contents of peridotite samples from both sites are due mainly to SiO_2 enrichment.

An unexplained but consistent observation is that peridotites within a few centimeters of gabbroic veins in Holes 1270C and 1270D and peridotite inclusions within the veins are much less altered than peridotites elsewhere in this hole.

Gabbronorites and gabbros in Hole 1270B were extensively recrystallized during deformation but are relatively free of hydrous alteration phases. Given the extensive recrystallization of pyroxene and oxide phases during subsolidus or near-solidus high-temperature deformation, it is likely that these minerals approached chemical equilibrium. Both quartz and olivine are absent from these rocks, whereas ilmenite and Ti-bearing magnetite are common. Thus, metamorphic conditions during deformation must be bracketed by the reactions

$$2(Mg,Fe)_2SiO_4 \text{ (olivine)} + 2FeTiO_3 \text{ (ilmenite)} = 2Fe_2TiO_4 \text{ (ulvospinel in magnetite)} + (Mg,Fe)_2Si_2O_6 \text{ (pyroxene)}$$

and

$$Fe_2Si_2O_6 \text{ (ferrosilite in pyroxene)} + 2FeTiO_3 = 2Fe_2TiO_4 + SiO_2 \text{ (quartz)}.$$

Exsolution of ilmenite from titanomagnetite also constrains the temperature and oxygen fugacity. And in addition, two pyroxene thermometry will provide independent constraints on temperature. Thus, we are optimistic that the pressure and temperature conditions of high-temperature recrystallization and reequilibration can be quantified in these rocks.

Hydrothermal alteration of gabbros and gabbronorites in Hole 1270B is limited mainly to formation of chlorite-amphibole assemblages along pyroxene/plagioclase contacts. Brown hornblende of high-temperature metamorphic or low-temperature magmatic origin is associated with Fe-Ti oxides and locally replaces pyroxene along grain boundaries.

Gabbroic veins in Holes 1270C and 1270D are extensively altered, though they include fresh recrystallized plagioclase, pyroxene, and even olivine in mylonitic zones. Altered portions of veins include talc + serpentine + albite + tremolite ± chlorite ± brown amphibole. Brown amphibole replaces pyroxene within veins and along contacts between peridotite boudins and veins, but not within the boudins, suggesting that circulation of high-temperature fluids and/or hydrous melts was restricted almost entirely to the veins. Locally, a rodingite assemblage (Ca silicates including prehnite and hydrogrossular) replaces the veins.

Structural Geology

Intrusion of gabbroic rocks into peridotite occurred while the peridotite was at high temperature, >600°C and probably close to 900°C. This inference is based on the presence of coarse-grained relict igneous pyroxene in the veins and tiny anastomosing branches from igneous veins, the association of veins with high-temperature hornblende replacing pyroxene, and high-temperature deformation structures in mylonite zones within gabbroic veins.

Ductile deformation of the peridotites away from gabbroic veins was relatively subdued, with most samples preserving protogranular textures. Hole 1270A peridotites are an end-member in this regard, with protogranular to weakly porphyroclastic textures, very few magmatic veins, and little evidence anywhere in the core for ductile deformation under subsolidus conditions. This is particularly striking given the peridotite mylonite (*Shinkai* 6500 sample 425-R007) (Fig. F26) recovered from a planar outcrop surface just tens of meters away from the site of Hole 1270A.

In contrast, all of the gabbroic veins in Holes 1270C and 1270D were the locus of high-temperature mylonitic deformation. Additional deformation of peridotites surrounding these mylonitized veins is evident in the form of olivines with well-developed subgrain boundaries and bent pyroxene crystals, but the entire gradient from protogranular to mylonitic textures is present over a few millimeters and true mylonites were not developed in peridotites. This indicates that the gabbroic veins were much weaker than surrounding peridotites during deformation, either because they were partially molten during the onset of deformation or because they were hydrous while surrounding peridotites were dry or simply because gabbroic mineral assemblages had a lower viscosity than peridotites at the conditions of deformation.

High-temperature ductile deformation of the gabbroic rocks in Hole 1270B is extensive and irregularly distributed. The top of the hole had relatively poor recovery, perhaps due in part to ductile and brittle deformation features associated with the fault that formed the planar outcrop surface on which we started the hole. In any case, crystal-plastic deformation intensity in the top 10–15 m of the hole is relatively high. Below this depth, crystal-plastic deformation is concentrated in a second zone at 40–45 mbsf, underlain by less deformed gabbronorites. The intensity of ductile deformation of the gabbroic rocks appears to be correlated with the abundance of oxide minerals (Fig. F27). This is consistent with the tentative hypothesis, based on preliminary data, that there may be a correlation between deformation intensity and the proportion of oxide minerals in oceanic crustal gabbros from Holes 735B and 1105A from Atlantis Bank on the Southwest Indian Ridge, as has been cautiously proposed on a provisional basis (e.g., Dick et al., 1991, 2000, 2002; Natland and Dick, 2002; Natland et al., 1991; Niu et al., 2002; Ozawa et al., 1991; Pettigrew, Casey, Miller, et al., 1999).

The correlation between deformation intensity and magnetite proportion in Hole 1270B gabbronorites is poorly quantified and uncertain because of incomplete recovery, a lack of continuous measurements of oxide proportion (magnetic susceptibility is heavily weighted to ferromagnetic phases) in the recovered core [**N4**], a "nugget effect" resulting from coarse-grained, irregularly distributed oxide crystals, and the presence of anastomosing ductile shear zones, including less deformed lenses, leading to irregular variations in deformation intensity on the centimeter to decimeter scale. The apparent relationships in Figure F27 should provide an excellent starting point for postcruise research to test and fully quantify the hypothesis that there is a correlation between oxide proportion (measured in detail by image analysis of thin sections) and deformation intensity (quantified by, for example, grain size analysis of recrystallized plagioclase).

Brittle deformation features are relatively uncommon in the core, compared to Site 1268. However, there is a fault gouge zone—probably several meters thick—at ~17 mbsf in Hole 1270A and we encountered poor recovery and difficult drilling at this depth in the other holes at Site 1270 as well. We believe that this indicates the presence of large faults parallel to planar outcrop surfaces and to the overall slope that forms the eastern wall of the rift valley in this region.

Crosscutting relationships define the following sequence of events for the core from Site 1270:

1. Partial melting of mantle peridotite, together with formation of dunite bands and protogranular textures in residual harzburgite;
2. Cooling of peridotite at the base of the thermal boundary layer;
3. Intrusion of gabbroic veins and gabbronorite bodies while peridotites were still at high temperature;
4. Formation of high-temperature mylonite zones in gabbroic veins within peridotite in Holes 1270C and 1270D, perhaps with synchronous ductile deformation in gabbroic rocks in Hole 1270B, while temperatures were >600°C and probably >900°C;
5. Cooling of peridotites and gabbroic rocks to <400°C;
6. Static, pervasive, nearly complete serpentinization of peridotites; and
7. Continued brittle deformation in large fault zones, probably parallel to exposed fault surfaces in outcrops observed during *Shinkai* 6500 Dive 425 and to the entire slope of the eastern flank of the Mid-Atlantic rift valley in this region.

This is similar to the sequence of events inferred for Site 1268, except that mylonitic deformation at Site 1270 took place entirely within gabbroic rocks (within massive gabbros in Hole 1270B and within gabbroic veins in peridotite in Holes 1270C and 1270D), whereas at Site 1268 mylonitic deformation was concentrated in zones of mixed peridotite and gabbroic veins and affected both lithologies. Also, replacement of serpentine by talc was common at Site 1268 but rare or absent at Site 1270 and small brittle deformation features are relatively uncommon at Site 1270 compared to Site 1268.

Dips of crystal-plastic foliation planes in gabbros from Hole 1270B and in mylonitized gabbroic veins in Holes 1270C and 1270D dip at 30°–60° (average = ~45°). Thus, foliations in the core are significantly steeper than the striated planar outcrop surfaces with slopes of ~20° observed on the seafloor during *Shinkai* 6500 Dive 425 and during the camera surveys on this cruise. Also, we did not recover peridotite mylonites (matrix grain size < 10 µm) in core from Site 1270, despite the fact that *Shinkai* 6500 sample 425-R007 is a peridotite mylonite recovered from a striated outcrop surface just a few tens of meters from the site of Hole 1270A (Fig. F26). Thus, it is apparent that the faults represented by the striated outcrop surfaces are not related in a simple way to the coarser-grained, higher-temperature mylonitic shear zones observed in core from Site 1270. Instead, the fault surface that forms seafloor outcrops dipping ~20° to the west must cut the higher-temperature fabrics at an average angle >20°. In the following section, we argue that the high-temperature foliation in the core probably dips ~45° to the east and thus intersects the west-dipping fault(s) represented by outcrop surfaces at an angle of ~65°.

Paleomagnetic Data and Tectonics

Paleomagnetic data were collected on half cores and individual discrete samples. Some samples retain a stable remanent magnetization. Using these data, we rotated the measured orientations of foliations,

faults, veins, and dikes in individual core pieces around a vertical axis, thereby restoring core pieces to an orientation with a common azimuth for the remanent magnetization vector.

In the case of Site 1270, this procedure was complicated because of the low inclinations of the remanent magnetization. Mainly negative stable inclinations in gabbroic rocks from Hole 1270B (average = –14°; see below for details) suggest that these may have acquired their magnetization during a period of reversed polarity. Hole 1270B is 13–18 km from the rift axis, indicative of 1.0–1.4 m.y. of spreading at a half-rate of 12.8 km/m.y. (Fujiwara et al., 2003), so it could have formed and been magnetized during the Matuyama Reversed Chron. This is consistent with—but not required by—the sea-surface magnetic data presented by Fujiwara et al. (2003). Thus, the negative inclinations in Hole 1270B may indicate that the rocks were reversely magnetized. Based on this interpretation, rotation of structural features around a vertical axis into a common magnetic orientation—together with the assumption that tectonic rotations have not substantially modified the azimuth of the remanent magnetization vector—yields the result that high-temperature foliations in the gabbroic rocks from Hole 1270B dipped ~45° to the east when the remanent magnetization vector pointed south.

Some peridotites in Holes 1270C and 1270D retain a stable remanent magnetization. Inclinations of this magnetization are nearly horizontal (average = –3°; see below). Thus, the polarity of the Earth's magnetic field when these rocks acquired their magnetization is highly uncertain. Assuming that the peridotites were reversely magnetized like the gabbroic rocks in Hole 1270B yields the result that mylonite zones in gabbroic veins dipped ~45° to the west when the remanent magnetization vector pointed south, assuming that tectonic rotations have not substantially modified the azimuth of the remanent magnetization vector (Fig. F28A). Alternatively, assuming that both peridotites and gabbroic rocks were normally magnetized implies that the crystal-plastic foliation in the gabbroic rocks dipped to the west and the mylonite zones in the peridotites dipped to the east (Fig. F28B) when the remanent magnetization vector pointed south, again with the assumption that the azimuth of the remanent magnetization vector has not been modified by tectonic rotations.

Holes 1270C and 1270D are only a few hundred meters from Hole 1270B, and the deformation features in all three holes record similar conditions (localized deformation at ~900°C, possibly in partially molten rocks). Thus, the result that the fabrics have dips that differ by 90° seems problematic. An alternative is that the peridotites were magnetized during the Brunhes Normal Chron (or the Jaramillo, or even some older normal polarity chron). In this case, rotation of the high-temperature foliations in Holes 1270C and 1270D yields ~45° dips to the east, parallel to the high-temperature foliation in Hole 1270B (Fig. F28C). This scenario is similar to our interpretation of remanent magnetization in Hole 1268A, in which we inferred that gabbroic rocks acquired their magnetization during cooling of igneous magnetite through 500°–600°C, whereas peridotites acquired their magnetization significantly later as a result of metamorphic growth of magnetite during serpentinization at ~300°C.

The average remanent inclination for 10 discrete samples from the gabbroic rocks in Hole 1270B is –14° (95% CI = +10°/–10°), much shallower than the expected inclination of ±28°. The average inclination of 10 discrete samples of peridotite from Holes 1270C and 1270D is –3° (95% CI = +13°/–13°), which is also significantly shallower than the expected value of 28° but not significantly different from the inclinations in the gabbroic rocks of Hole 1270B.

One possible explanation for the statistically significant difference between the expected and observed inclinations in both gabbroic rocks and peridotites is that tilting occurred after cooling and blocking of the remanence. As discussed in "**Paleomagnetic Data and Tectonics**" in "Site 1268" above, with additional assumptions paleomagnetic inclination data may be used to infer the direction and magnitude of tectonic rotations that may have occurred between the time the sample recorded remanent

magnetization and the present. The stepwise alternation of steep rift-facing slopes and nearly horizontal benches along the flanks of the Mid-Atlantic Ridge is generally interpreted to result from the presence of tilted normal fault blocks. Back-tilting of fault blocks on the east side of the rift valley in the region around Site 1270 is probably top-to-the-east (clockwise around a northeast-striking axis). In this region, the west-facing slopes strike ~010°–020°, parallel to the strike of the rift valley. We infer that tilting may have been produced by clockwise rotation of normal fault blocks along an approximately rift-parallel axis. For a horizontal rotation axis striking 020° and assuming that the gabbroic rocks are reversely magnetized, ~35° of clockwise rotation is required to change an original inclination of –28° to the observed average inclination of –14° in reversely magnetized gabbros from Hole 1270B (Fig. F29). Similarly, if we adopt the interpretation that the peridotites are normally magnetized (Fig. F28C), the peridotites must have undergone ~60° of clockwise rotation to change an original inclination of +28° to the observed average inclination of –3°. Given the uncertainties in the data, both gabbro and peridotite inclinations can be explained, within error, using a model in which there was ~45°–50° of clockwise rotation around a horizontal axis striking 020° after both lithologies acquired their magnetization.

Alternatively, the differences between magnetic inclination in the gabbros (approximately –14°) and in the peridotites (approximately –3°) suggest that the two lithologies might record different amounts of rotation. If we adopt the interpretation in Figure F28B, in which both peridotites and gabbroic rocks are normally magnetized, we can explain this difference in the same manner as for Site 1268. For a horizontal rotation axis striking 020°, ~85° of clockwise rotation is required to change an original inclination of +28° to the observed average inclination of –14°. And, as already stated above, the peridotites must have undergone ~60° of clockwise rotation. In this scenario, clockwise rotation of the Site 1270 section around a horizontal axis striking 020° began before magnetization of the peridotites and continued after magnetization of the peridotites [**N5**].

An additional uncertainty in inferring the amount of tilting is introduced by the unknown plunge of the rotation axis. Figure F30 illustrates the effect of gently plunging rotation axes. For a rotation axis with a fixed azimuth of 020°, if the plunge were 10° along 020° and gabbroic rocks are normally magnetized, ~115° of clockwise rotation would be required to change an original inclination of 28° to the observed average inclination of the gabbroic rocks in Site 1270B of –14°. Conversely, if the plunge were 10° along 200°, ~75° of counterclockwise rotation would be required for the same change in inclination [**N6**].

In summary, if the hypothesis outlined here is correct, the gabbroic rocks in Hole 1270B underwent a large amount of clockwise rotation (~45°–100°) around a nearly horizontal, rift-parallel axis after acquisition of the magnetic remanence. The peridotites record only ~50°–65° of this rotation.

These results and hypotheses are similar to our interpretation of paleomagnetic and structural data from Site 1268. At Sites 1270 and 1268, the magnetic inclination data, together with the assumption that tectonic rotations occurred around rift-parallel, nearly horizontal rotation axes, require tectonic rotations of 35°–120°. Also, at both sites the peridotites may record smaller tectonic rotations than the gabbroic rocks, perhaps due to early magnetization of the gabbroic rocks compared to the peridotites.

It must be emphasized again that our tectonic interpretations of structural and magnetic data are nonunique, forward models, chosen from among many other models that could potentially account for the data. However, the low paleomagnetic inclinations at Sites 1268 and 1270 require large tectonic rotations and the presence of faults that do not consistently dip toward the rift valley.

Site 1271

Site 1271 is located along the track of Faranaut 15°N Dive 7 on the western flank of the Mid-Atlantic rift valley. The dive, using the *Nautile* submersible, recovered basaltic samples at water depths >3700 m and three samples of peridotite and two samples of gabbro higher on the rift valley walls. Hole 1271A was initiated on a smooth, sedimented slope uphill from gabbro sample FR07-10. After a relatively promising beginning, relatively high penetration rates and poor recovery from 13 to 28 mbsf suggested that we had encountered a near-surface fault zone, similar to those encountered at Site 1270. We continued to drill to 44.8 mbsf, but the hole was unstable and ultimately had to be abandoned. Recovery averaged ~13%. We then moved 74 m southwest and spudded Hole 1271B into a similar sedimented slope. Although drilling conditions were far from ideal, we were able to drill to a depth of 104 mbsf with 15% recovery. At this point, because of poor recovery combined with great lithologic diversity, we decided to log the hole, anticipating that density and resistivity contrasts in downhole data would help us to map the distribution of gabbroic intrusions and peridotite host rocks. However, even after the bit was released, it was very difficult to raise the drill string. Apparently, the hole collapsed as the pipe was withdrawn. The logging string encountered obstructions just a few meters below the base of the open pipe, ending operations at Site 1271.

Proportions of Igneous Rocks

The igneous and residual mantle protoliths of recovered core were dunite, harzburgite, troctolite, gabbro, minor gabbronorite, and a small but significant amount of chromitite in three 1- to 3-cm-thick lenses (Fig. F31). Gabbroic rocks are intrusive into the peridotite in Holes 1271A and 1271B (Fig. F32). The process of igneous intrusion was probably variable; brown amphibole gabbros apparently were injected into sharp-sided dikes, whereas olivine gabbros, troctolites, and impregnated peridotites apparently crystallized from melt migrating along peridotite grain boundaries.

Among igneous and mantle rocks, dunite is abundant in Holes 1271A (98%) and 1271B (56%), whereas harzburgite composes <1% of recovered samples from Hole 1271A and only 9% of the rocks from Hole 1271B. Brown amphibole gabbro composes <2% of the igneous and mantle material in Hole 1271A and 21% in Hole 1271B, whereas olivine gabbro and troctolite compose 14% of igneous and mantle rocks recovered from Hole 1271B. Weighting the proportions of rocks in Holes 1271A and 1271B by the length of each hole yields overall proportions of 68% dunite, 6.5% harzburgite, 15% brown amphibole gabbro, and 10% olivine gabbro and troctolite. Although the ratio of dunite to harzburgite at Site 1271 is much higher than that observed at Sites 1268 and 1270, the ratio of peridotite (75%) to gabbroic rocks (25%) at Site 1271 is remarkably similar to the proportions in Hole 1268 (74% peridotite/26% gabbroic rocks), in Hole 1270 (68% peridotite/32% gabbroic rocks), and recovered from dives and dredging along the Mid-Atlantic Ridge from 14° to 16°N (75.5% peridotite/24.5% gabbroic rocks).

Highly Depleted Mantle Peridotites

With some notable exceptions, peridotites from Site 1271 are 100% altered, mainly to serpentine and brucite. Many peridotites—both harzburgites and dunites—contain 1%–15% interstitial gabbroic material interpreted as the crystallization products of melt migrating through the peridotite along grain boundaries. However, despite this "impregnation," geochemical analyses of all but one of the Site 1271 peridotites show low concentrations of nominally immobile incompatible elements such as Al, Sc, and V. For example, the Al_2O_3 concentrations in all but one of the Site 1271 peridotites are <1 wt% (average = 0.9

wt%), whereas Al_2O_3 concentrations in peridotites from Site 920 on the Mid-Atlantic Ridge at 23°20′N range from 1 to 2 wt% (Casey, 1997). Thus, despite the presence of gabbroic impregnations, the average Al_2O_3 concentration in 8 peridotites from Site 1271 is low, though not as low as the average of 0.6 wt% Al_2O_3 in 7 peridotites from Site 1270 and 20 peridotites from Site 1268. If Al_2O_3 concentrations have not been modified by hydrothermal metasomatism, then the peridotites from Sites 1268, 1270, and 1271 are among the most depleted residual mantle peridotites yet obtained from the mid-ocean ridges.

Origin of Site 1271 Dunites

Molar Mg# of the peridotites from Site 1271 ranges from 85% to 89% in five dunites and from 90% to 92% in three harzburgites. Most of the Site 1271 dunite Mg#s are lower than Mg#s in most harzburgites from Sites 1268, 1270, and 1271 and below the normal range of whole-rock Mg# in residual mantle peridotites from mid-ocean ridges (~89%–92%; average = ~90%–91%) (e.g., Dick, 1989). The low Mg# in dunite could be due to metasomatic changes in Fe/Mg during the hydrothermal metasomatism, olivine crystal fractionation, or reaction of migrating melt with residual mantle peridotites.

Figure F33 shows that two dunites have bulk compositions very close to the composition of pure olivine. Other dunites lie along mixing lines between olivine and pyroxene, as do two of the harzburgites. Still other dunites, including a sample of impregnated dunite with 15% interstitial gabbroic material (probably composed of plagioclase and pyroxene ± hornblende, prior to alteration), show significant compositional shifts away from olivine-pyroxene mixing lines toward mixtures including plagioclase ± Cr-Al spinel ± igneous amphibole. Because of the compositional shifts resulting from the presence of interstitial gabbroic material in most peridotite samples from Site 1271, it is difficult to discern if the peridotites were also modified by subsolidus metasomatism. Nonetheless, there is no compelling evidence for SiO_2 gain or MgO loss from these samples, so we tentatively rule out metasomatic changes as the cause of the low Mg#s in Site 1271 dunites.

We now wish to distinguish between olivine crystal fractionation and melt-rock reaction as explanations for the composition of Site 1271 dunites. Figure F34 shows that Site 1271 dunites have Ni contents in olivine that are comparable to those in harzburgites from Sites 1268, 1270, and 1271, despite the fact that Site 1271 dunites have lower Mg#s than the harzburgites. Similar relationships are seen in dunites from the crust–mantle transition zone in the Oman ophiolite (Godard et al., 2000; Koga et al., 2001; Korenaga and Kelemen, 1997). Nearly constant concentrations of compatible elements accompanied by decreasing Mg# are the hallmark of dunites formed by reaction between relatively low Mg#, migrating melt, and residual mantle olivine (e.g., DePaolo, 1981; Kelemen, 1986; Kelemen et al., 1998a; Navon and Stolper, 1987). In contrast, olivine crystal fractionation leads to a steep decline in olivine Ni contents with decreasing Mg#, as seen in Figure F34. Therefore, we conclude that the Site 1271 dunites are the product of reaction between residual peridotite and migrating melts with relatively low Mg#. The low Mg# of the migrating melts probably indicates that they were undergoing gradual conductive cooling, with decreasing magma mass due to reaction and crystallization near the base of the thermal boundary layer beneath the Mid-Atlantic Ridge.

Chromitites from Mid-Ocean Ridges

To our knowledge, the three chromitites recovered at Site 1271 are the first to be sampled from the Mid-Atlantic Ridge. In fact, Site 1271 is only the second chromitite locality that has been found along any mid-ocean ridge, the first being near the East Pacific Rise at Hess Deep at ODP Site 895 (Arai and Matsukage,

1996). The recovery of chromitites at Site 1271 is an important result. The chromitite recovered from Hess Deep is a single, elongate, discontinuous train of chromite grains <1 cm wide. It resembles chromite "trails" observed in dunites worldwide almost as much as it resembles massive chromitites in ophiolites. In contrast, the Site 1271 chromitites are rounded rather than elongate, have sharp contacts with surrounding peridotite, and are clearly massive (Fig. F35).

It has been proposed that the formation of chromitite occurs only during subduction-related arc magmatism because the formation process requires hydrous magmas (Matveev and Ballhaus, 2002). Based on our results, confirming the Hess Deep observation, it is clear that chromitites are not restricted to arc magmatism. However, there is abundant high-temperature amphibole in core from Site 1271, some of which could be igneous. If the presence of amphibole is genetically related to the formation of chromitite at Site 1271, then Matveev and Ballhause (2002) may be correct in inferring that hydrous magmas are important in chromitite genesis.

Based on the observation of unusually high molar Cr/(Cr+Al), or Cr#, in spinels from harzburgite and dunite dredged from the Mid-Atlantic Ridge in the 14° to 16°N region (Bonatti et al., 1992; Dick and Kelemen, 1992; Sobolev et al., 1992b), together with the general observation that spinels in chromitites have higher Cr# than spinels in residual mantle peridotites (e.g., Dick and Bullen, 1984), we anticipate that the Cr#s in the Site 1271 chromitites will be the highest yet observed in spinel from mid-ocean ridges. High Cr#s would provide insight into the processes that form chromitite. In addition, such a result would change the interpretation of ophiolite provenance. It has been proposed that spinel Cr#s >60 are only found in mantle peridotites from subduction-related settings (e.g., Dick and Bullen, 1984), and high Cr#s have been cited as evidence that most ophiolites with high Cr# in mantle spinels do not form at normal mid-ocean ridges.

Petrogenesis of Intrusive Rocks

There appear to be two types of gabbroic rocks in core from Site 1271. Brown amphibole–bearing metagabbros (termed "BAG") with relicts of igneous plagioclase (and locally some relict clinopyroxene) always contain ~50% plagioclase and 50% mafic minerals in their igneous protolith (Fig. F36). Contacts of BAG with peridotite were not recovered, but its consistent phase proportions suggest that the BAG forms dikes with sharp contacts in peridotite. In contrast, olivine gabbros and troctolites (>15% plagioclase, pyroxene, amphibole, and alteration products derived from these phases) are gradational into host peridotites with 1%–15% interstitial gabbroic material. As a result, we interpret much of the olivine in olivine gabbros and troctolites as xenocrysts, derived from a partially disaggregated residual mantle protolith.

The origin of amphibole in the BAG is uncertain. Some of the amphibole is tremolite-actinolite, clearly metamorphic in origin, but other crystals appear to be idiomorphic brown hornblende and could be igneous (Figs. F36, F37). We analyzed a fragment of this amphibole obtained from a coarse-grained sample of the BAG. Its chemistry indicates that the amphibole is a hornblende solid solution composed of ~71 mol% tremolite-actinolite and ~29 mol% pargasite. In detail, the chemical analysis combined with stoichiometric constraints suggests that there is also ferric iron in a hastingsite component. If this amphibole formed by subsolidus reaction of igneous minerals with H_2O, it could have formed from olivine, pyroxene, and plagioclase via reactions such as

$$14H_2O + 6(Mg,Fe)_2SiO_4 + 15(Mg,Fe)_2Si_2O_6 + 24Ca(Mg,Fe)Si_2O_6 + 4CaAl_2Si_2O_8 + 4NaAlSi_3O_8 =$$
$$4NaCa_2(Mg,Fe)_4AlSi_6Al_2O_{22}(OH)_2 + 10Ca_2(Mg,Fe)_5Si_8O_{22}(OH)_2.$$

Alternatively, this type of amphibole could be igneous. However, the large proportion of tremolite-actinolite component in the solid solution suggests a relatively low, near-solidus temperature of crystallization.

A fragment of altered white material believed to be relict plagioclase and alteration products replacing plagioclase were analyzed separately, yielding a composition close to that of plagioclase with 81 mol% anorthite. However, the composition includes appreciable Mg, Fe, and Ti and 0.5 wt% K_2O, so the sample probably incorporates minerals other than plagioclase and plagioclase alteration products.

One BAG was analyzed for major and trace element contents. It has Mg# = 84, higher than that in any of the gabbroic rocks from Sites 1268 and 1270 (maximum = 83% at Site 1268). This Mg# is indicative of crystallization from a relatively primitive melt, close to Fe/Mg equilibrium with residual mantle peridotite. At the same time, the BAG has higher incompatible element concentrations than any gabbroic rocks from the previous sites. For example, the BAG has Y = 48 ppm and Zr = 123 ppm, compared with a maximum of Y = 17 ppm and Zr = 48 ppm in gabbroic rocks from Sites 1268 and 1270. Although the high Y and Zr contents may be due, in part, to the (possible) presence of igneous hornblende in the BAG, it is likely that the parental melt also had high Y and Zr contents. The combination of high Mg# together with high incompatible element concentrations in magmas is the signature of decreasing melt mass resulting from partial crystallization combined with buffering of the Mg# at high values from reaction of melt with residual mantle peridotite (e.g., DePaolo, 1981; Kelemen, 1986). Thus, we infer that the melt parental to the BAG was derived from a primary basalt but was modified by conductive cooling, partial crystallization, and reaction with peridotite wallrocks.

We also analyzed an olivine gabbro from Hole 1271B. It has Mg# = 67, rather low for a rock that is thought to include xenocrysts of mantle olivine. If our interpretation of these rocks as hybrids is correct, then this sample must have formed with a relatively high melt/rock ratio.

Hydrothermal Alteration, Metamorphism, and Metasomatism

Many peridotites from Site 1271 are completely altered to serpentine. Unlike the SiO_2-rich metaperidotites from Sites 1268 and 1270, the compositions of metaperidotites from Site 1271 are similar to the compositions of fresh dunites and harzburgites and thus do not require large metasomatic increases in Si/(Mg+Fe) during alteration (Fig. F33). Brucite is an important accessory phase in the background alteration of many peridotites from Site 1271. The presence of brucite probably reflects the olivine-rich, low Si/(Mg+Fe) dunite protoliths for most Site 1271 peridotites (see Fig. F33). Brucite is not stable in bulk compositions with molar Si/(Mg+Fe) greater than that in serpentine (0.67). Most peridotites from Sites 1268 and 1270 have Si/(Mg+Fe) greater than 0.67, consistent with observed low-temperature alteration to serpentine + talc rather than serpentine + brucite. Lack of pyroxene in dunite protoliths may have allowed fluid compositions to reach low aqueous Si activities and relatively high pH compared to fluid compositions during hydrothermal alteration of harzburgites at Sites 1268 and 1270. These fluid compositions favor formation of brucite + serpentine.

Spinel in many metaperidotites from Site 1271 is surrounded by chlorite. The chlorite could be a hydrothermal alteration product of plagioclase, with the implication that crystallization of melt, migrating along peridotite grain boundaries, formed plagioclase halos around spinel crystals. However, chlorite around spinel may also have formed via subsolidus reactions involving olivine, pyroxene, spinel, and fluid, such as

$$H_2O + (Mg,Fe)_2SiO_4 + (Mg,Fe)_2Si_2O_6 + (Mg,Fe)(Al,Cr)_2O_4 = (Mg,Fe)_5(Al,Cr)_2Si_3O_{10}(OH)_4.$$

Similar chlorite rims around spinel are common in amphibolite-grade metaperidotites worldwide, even in the absence of plagioclase.

A strikingly large proportion of impregnated peridotites from Site 1271 with 1%–15% interstitial gabbroic material contains fresh olivine and pyroxene. In this way, they resemble the relatively fresh peridotite along contacts with gabbroic veins in cores from Holes 1270C and 1270D. The presence of relict clinopyroxene and plagioclase may have buffered fluid compositions to low pH, inhibiting the formation of serpentine from adjacent olivine and orthopyroxene.

Interstitial gabbroic material in impregnated peridotites, olivine gabbros, and troctolites from Site 1271 includes a large proportion of high-temperature hornblendic amphibole. As for the amphibole in the brown amphibole gabbros, it is not clear whether any of the amphibole in these other lithologies is igneous. Sharp contacts between olivine and high-temperature amphibole in some samples suggest that at some point the two phases were in equilibrium. Sharp contacts between olivine and plagioclase in peridotites, olivine gabbros, and troctolites likewise suggest that olivine and plagioclase were in equilibrium, probably at igneous temperatures. However, spinel + chlorite(?) symplectites separate olivine from amphibole and olivine from plagioclase in other parts of the core.

In addition to the presence of high-temperature metamorphic or igneous amphibole, gabbroic rocks at Site 1271 underwent secondary alteration to tremolite-actinolite, talc, chlorite, sericite, metamorphic plagioclase, and, locally, quartz. In the brown amphibole gabbros, rutile intergrown with quartz appears to replace Fe-Ti oxides. The presence of rutile rather than sphene suggests that this replacement occurred under amphibolite rather than greenschist facies conditions.

Structural Geology

Enstatite in orthopyroxene-poor harzburgites and orthopyroxene-bearing dunites from Site 1271 has transitional protogranular to porphyroclastic textures. In some particularly intriguing examples, elongate porphyroclastic orthopyroxene crystals showing incipient recrystallization are rimmed by undeformed vermicular spinels. This texture suggests that high-temperature exsolution of spinel or formation of spinel during reaction of migrating melt with orthopyroxene postdated deformation in these rocks.

Lower-temperature, more localized deformation at Site 1271 occurred preferentially in gabbroic veins and surrounding peridotite wallrocks, as observed at Sites 1268 and 1270. Shear zones in Hole 1271B show a well-developed progression from granulite facies recrystallization of dunite and gabbroic rocks into porphyroclastic mylonites, through amphibolite facies replacement of deformed minerals with amphibole that was itself deformed, to formation of greenschist facies, chlorite-amphibole, and serpentine schists. High-temperature shear zones, although locally crosscut by later features, apparently continued to be the primary locus of deformation throughout most of the cooling history of the Site 1271 core to temperatures <300°C.

Fault gouge and fault breccia zones sampled at several depths appear to be parts of major faults with substantial brittle offsets.

Paleomagnetic Data and Tectonics

Paleomagnetic data were collected on half cores and individual discrete samples. Using these data, we rotated the measured orientations of foliations, faults, veins, and dikes in individual core pieces around a vertical axis, thereby restoring core pieces to an orientation with a common azimuth for the remanent magnetization vector.

In the case of Site 1271, split cores and discrete samples all have positive inclinations, indicating that the rocks are normally polarized. The average remanent inclination for 15 discrete samples is 25° (95% CI = +11°/–13°), and the mean inclination for archive-half cores is 29° (95% CI = +3°/–4°). These inclinations are statistically indistinguishable from the expected inclination of 28°, which is consistent with the hypothesis that no significant block rotation has affected the section sampled at Site 1271. This hypothesis is quite different from the tectonic history of Sites 1268 and 1270, where remanent magnetic inclinations also require substantial rotation of the section. Alternatively, large rotations may have coincidentally produced an inclination magnetization. For example, a 70° counterclockwise rotation about a horizontal axis along 020° would restore the inclination to 28°, and so would also be consistent with the inclination data.

Site 1272

Site 1272 is located along the track of Faranaut 15°N Dive 2 on the western flank of the Mid-Atlantic rift valley, near the summit of the inside corner high just south of the 15°20′ Fracture Zone. The Faranaut dive recovered 10 peridotite samples from 3399 to 2484 meters below sea level (mbsl), with samples of basaltic lava and diabase at 3143 and 2490 mbsl. The inside corner high, with two summits known informally as Mt. Bougault (15°4.63′N, 45°59.10′W) and Mt. Dmitriev (15°5.58′N, 45°58.49′W) has been extensively dredged and surveyed during submersible dives (Bougault et al., 1988, 1993; Cannat, 1993; Cannat et al., 1992, 1997b; Cannat and Casey, 1995; Dosso et al., 1993; Fujiwara et al., 2003), which recovered numerous samples of dunite, orthopyroxene-poor harzburgite, and basalt.

The camera survey for Site 1272 began at 2677 mbsl near the site of Faranaut 15°N sample FR-02-11 (2650 mbsl), where cliffs interspersed with sedimented slopes were observed during the dive. Cliffs, a few meters high, were also observed near the beginning of the camera survey, but the intervening slopes were steep and talus covered, so the camera survey preceded west-southwest and upslope along the dive track toward the site of sample FR-02-12 (2484 mbsl), also close to a cliff outcrop. A large cliff (~5 m high) along the camera survey track at ~2600 mbsl is topped by a relatively flat area covered by mixed talus and sediment. We proceeded to the west-southwest, searching for a talus-free area. However, at 15°5.6645′N, 44°58.3060′W (2567 mbsl) there was an abrupt change from talus-covered sediment to completely smooth sediment along a sharp line striking approximately northwest. We feared that this feature is the surface expression of a major fault, so we moved back downslope 30 m to a relatively flat area, which—despite the presence of talus on the surface—we chose as the site of Hole 1272A at 2571 mbsl. A push-in test with the drill string indicated that the sediment cover was only ~1 m thick.

During drilling, numerous faults, zones of poor recovery, and diverse lithologies were encountered in the top 55 m of the hole. Two of these, a fine-grained diabase or basalt flow and a medium-grained hypabyssal gabbro-diorite-diabase, were recovered over depth intervals of several meters. At the time, our favored interpretation was that we were drilling along the margin of a large dike or sill emplaced into weathered peridotite. However, in retrospect, it may be that the top portion of Hole 1272A was in a tectonic breccia (fault or landslide) with individual blocks exceeding 5 m in maximum dimension (based on the size of the cliff observed during the camera survey at ~2600 mbsf and ~50 m downslope from Hole 1272A and on the lengths of recovered intervals composed of homogeneous lithologies). In support of the hypothesis that the top 55 m of the hole sampled a tectonic breccia, a carbonate-cemented breccia recovered at ~23 mbsf, with clasts of serpentinized peridotite, appears to have formed on or near the seafloor.

Paleomagnetic data on samples from the upper 55 m of the hole yield variable remanent inclinations, which could indicate that this section is a tectonic breccia. However, measurements of inclination in the medium-grained intrusive rock between ~15 and 25 mbsf (termed "gabbro" in this report) are internally consistent and parallel to consistent measurements of inclination in homogeneous peridotites at depths of 55–131 mbsf. Highly variable inclinations in other lithologies could have arisen as a result of drilling through rubble that had fallen from higher in the hole. Thus, the magnetic data do not clearly indicate whether the section is a tectonic breccia or an intact block.

In any case, below a fault gouge zone at 55 mbsf, we drilled ~75 m of homogeneous, green, serpentinized mantle peridotite with consistent magnetic inclinations. From a tectonic perspective, we are confident that this lower part of the hole is intact and in place.

Proportions of Igneous Rocks

The igneous and residual mantle protoliths of core recovered from above 55 mbsf were dunite, harzburgite, aphanitic diabase or basalt, and medium-grained gabbro-diorite-diabase (Fig. F38). The uncertain tectonic situation in the upper part of Hole 1272A, discussed in the previous section, makes it difficult to be certain if the fine-grained basaltic rocks are lavas or dikes. Because the gabbro-diorite lithology may be part of a thick dike and because it includes miarolitic cavities indicative of shallow crystallization, some workers might call it a diabase. However, based on grain size and texture, we refer to this lithology as gabbro in this report. In addition to the igneous and mantle rocks, 0.3 m of carbonate-cemented tectonic breccia was recovered in this part of the hole. There were also intervals with low recovery and abundant fine-grained fault gouge.

Core recovered from below 55 mbsf consists of 93% harzburgite, 3.4% dunite, and 3.5% fine-grained mafic rocks. The fine-grained mafic rocks are generally within a few centimeters of the top of each cored interval and are interpreted as fragments of blocks from above 55 mbsf that fell to the bottom of the hole during core recovery. In addition, at ~90 mbsf there is a short interval of coarse-grained oxide gabbronorite. The downhole Formation MicroScanner (FMS) log suggests that this gabbronorite is far more resistive than the surrounding serpentinized peridotites and that it is ~1 m thick. The gabbronorite is very much unlike the quickly cooled diabase and miarolitic gabbro in the upper 55 m, and—given the presence of exsolution lamellae in pyroxene and evidence for high-temperature ductile deformation in this lithology—it must have cooled slowly.

Because the bottom 75 m of Hole 1272A is almost completely composed of harzburgite and lesser amounts of dunite (Fig. F39), it is very different from Sites 1268, 1270, and 1271 and from overall dredging statistics for the Mid-Atlantic Ridge from the 15°20′ Fracture Zone to 14°S. In each of these other data sets, the peridotite to gabbro proportions are ~75/25. The upper 55 m of Hole 1272A is so different from the lower 75 m that it may be potentially misleading to group them. However, if we combine the 2 m of medium-grained gabbro and the 3 m of peridotite recovered from the upper 55 m of Hole 1272A with the 28 m of peridotite from the lower 75 m, we obtain "average" proportions of 94% peridotite to 6% gabbroic rocks, still lower than at any previous site on this leg. Although our sample set is small, the overall lithologic proportions recovered in Hole 1272A are consistent with previous dive and dredging results, which yielded mainly peridotite and basalt with very little gabbro on Mts. Bougault and Dmitriev.

The proportion of dunite to harzburgite in Hole 1272A is ~4/96, lower than at any previous site on this leg. In contrast, the proportion of dunite to harzburgite at Sites 1268, 1270, and 1271 are 15/85, 10/90, and 90/10, respectively. The low proportion of dunite in Hole 1272A is somewhat surprising, since dunites compose ~50% of all previous dive and dredging samples from Mt. Dmitriev and Mt. Bougault (Bougault

et al., 1988, 1993; Cannat, 1993; Cannat et al., 1992, 1997b; Cannat and Casey, 1995; Dosso et al., 1993; Fujiwara et al., 2003). We infer that the low proportion of dunite/harzburgite in Hole 1272A and the high proportion of dunite at Site 1271 are not representative of the inside corner in this region. Instead, we believe that the distribution of dunites is not uniform on the scale of our drilling.

Highly Depleted Mantle Peridotites

Geochemical analyses of all Site 1272 peridotites show low concentrations of nominally immobile incompatible elements such as Al, Sc, and V. For example, the Al_2O_3 concentrations in Site 1272 peridotites range from 0.1 to 0.8 wt% (average = 0.6 wt%), whereas the Al_2O_3 concentrations in peridotites from Site 920 along the Mid-Atlantic Ridge at 23°20′N range from 1 to 2 wt% (Casey, 1997). Thus, the average Al_2O_3 concentration in 12 peridotites from Site 1272 is lower than at that Site 1271 (average = 0.9 wt%) and as low as the average of 0.6 wt% Al_2O_3 in 7 peridotites from Site 1270 and 20 peridotites from Site 1268. If Al_2O_3 concentrations have not been modified by hydrothermal metasomatism, then the peridotites from Sites 1268, 1270, 1271, and 1272 are among the most depleted residual mantle peridotites yet obtained from the mid-ocean ridges.

Petrogenesis of Plutonic Rocks

There are two types of gabbroic rocks in core from Hole 1272A. The more abundant type, found in the upper 55 m of the hole, are the miarolitic gabbros or diorites. These have textures and mineral assemblages indicative of rapid cooling. For example, they include both olivine and quartz. The miarolitic cavities indicate that they rapidly became saturated in fluid without efficient degassing on the scale of the core samples, which is more likely during rapid cooling at low pressure. In fact, they may have crystallized in the central part of a large dike rather than in a "magma chamber." As such, they could retain liquid compositions on the scale of the core samples rather than the compositions of cumulate minerals in equilibrium with a melt from which the remaining liquid was later extracted. Figure F40 shows that the compositions of two miarolitic gabbros and three diabase samples lie within the range of SiO_2 content, incompatible element concentrations (illustrated using Zr) and Mg# observed for Mid-Atlantic Ridge basalt glasses in general, and for glasses from the 14° to 16°N area in particular. Like glasses from the 14° to 16°N region, diabase and miarolitic gabbro have high SiO_2 and Zr at a given Mg#, compared to average glasses from the Mid-Atlantic Ridge. The medium-grained miarolitic gabbros have higher SiO_2 contents than the diabases, but (1) their SiO_2 contents are not outside the range observed in glasses and (2) high SiO_2 is not expected for cumulate plutonic rocks. Thus, all appear to be close to liquid compositions.

The other type of plutonic rock from Site 1272A is a single interval of gabbronorite at ~90 mbsf. This gabbronorite is texturally and mineralogically similar to gabbronorites sampled elsewhere during Leg 209, particularly in Hole 1270B. Oxide gabbronorites will be useful in postcruise research, as oxide-oxide relationships record temperature and oxygen fugacity during magmatic and/or metamorphic processes and oxide-silicate relationships can be used to constrain equilibration pressures.

Hydrothermal Alteration, Metamorphism, and Metasomatism

Many peridotites from Site 1272 are completely altered to serpentine plus brucite and/or talc. Unlike the SiO_2-rich metaperidotites from Sites 1268 and 1270, the compositions of most metaperidotites from Site 1272 are similar to the compositions of fresh dunites and harzburgites with 0%–25% orthopyroxene

and thus do not require large metasomatic increases in Si/(Mg+Fe) during alteration (Fig. F41). Probably as a result of the low Si/(Mg+Fe), brucite is an important accessory phase in the background alteration of many peridotites from Sites 1271 and 1272.

Two samples of metaperidotite from the upper 55 m of Hole 1272A contain carbonate-bearing alteration veins. The presence of these veins is reflected in the bulk rock compositions, which lie well off the SiO_2 to MgO + FeO mixing line in Figure F41 and show a positive correlation between CaO and CO_3. Addition of carbonate to these metaperidotites also led to high Sr concentrations. This type of metasomatism—which may be common in serpentinized peridotites worldwide—is discussed more extensively in "**Site 1274**" below.

Fault gouge and some serpentinized peridotites from Site 1272 include substantial proportions of iowaite, a magnesium hydroxide–ferric oxychloride, whose very fine grain size may contribute to the clayey appearance of the rocks. Iowaite has been previously reported in metaperidotites from the Iberian margin and the Izu-Bonin forearc. It may form in oxidizing conditions, where Fe^{3+} in the brucite structure is charge balanced by Cl^- in interlayers (Heling and Schwarz, 1992) or during alteration associated with transport of high-Cl brines (Gibson et al., 1996).

Alteration in harzburgite from Hole 1272A becomes less intense with increasing depth. Decreasing intensity in alteration is mirrored by a downhole increase in seismic velocity, density, and thermal conductivity and a concomitant decrease in porosity and magnetic susceptibility measured on core samples. For example, *P*-wave velocity increases from ~3 km/s between 60 and 80 mbsf to ~3.5 km/s between 110 and 130 mbsf. This gradient, ~0.01 km/s/m, is much steeper than gradients observed in seismic studies of the Mid-Atlantic Ridge between 15° and 16°N, which show a relatively gradual increase from 3 km/s near the seafloor to 4 km/s at ~1 km depth at 16°N and from 3.5 km/s near the seafloor to 5.5 km/s at 1 km depth at 15°37′N (0.001–0.002 km/s/m) (Collins and Detrick, pers. comm., 1998). Thus, the relatively steep gradient in serpentinization in samples from Hole 1272A, with related gradients in physical properties, must be a local feature, not representative of the regional alteration gradient.

Structural Geology

Orthopyroxene and clinopyroxene in Site 1272 harzburgites show mainly protogranular textures. As in Site 1271 harzburgites and orthopyroxene-bearing dunites, orthopyroxene crystals are intergrown with vermicular spinel. This intergrowth suggests that high-temperature exsolution of spinel or formation of spinel during reaction of migrating melt with orthopyroxene postdated deformation in these rocks. Leg 209 peridotites from Sites 1268, 1270, and 1272 are surprisingly undeformed, unlike typical porphyroclastic harzburgites from ophiolites. Mylonitic shear zones within and near gabbroic veins in peridotite and gabbroic rocks are common at Sites 1268, 1270, and 1271. In Hole 1272A, the relative scarcity of gabbroic rocks intruding the harzburgite section is accompanied by a lack of mylonitic shear zones. The sole exception, a small oxide gabbronorite, does show signs of crystal-plastic deformation at moderate temperature (between ~600° and 1000°C), but no mylonites were recovered. We infer that this block of peridotite may have been largely insulated from far-field stresses by shear zones with a spacing larger than the scale of the hole, or that continued brittle deformation along long-lasting shear zones converted high-temperature mylonites into fault gouge.

At least four fault gouge zones were sampled between 75 and 131 mbsf in Hole 1272A (Fig. F42). Predictably, recovery was poor in these zones and other fault gouge zones may have been present but not sampled. We tentatively infer the presence of 10 or more gouge zones from the FMS images generated during downhole logging. These gouge zones must be parts of major faults with substantial brittle offsets.

They generally strike parallel to the rift axis or have northwest strikes intermediate between the rift axis and the 15°20′ Fracture Zone, in keeping with the position of Site 1272 atop the inside corner high just south of the fracture zone. Dips inferred from the FMS image are both toward and away from the rift and transform valleys.

The fault gouge recovered from Hole 1272A was strikingly plastic when water saturated, as it was when it first came on board. This may be due to the presence of abundant clay, particularly iowaite, in the gouge. Laboratory experiments show that serpentine muds, like those in the Hole 1272A fault gouge, have low plastic yield strengths (Phipps and Billotti, 1992). Thus, fault zones containing serpentine mud could yield at low stresses and potentially creep aseismically. Additionally, since serpentine muds are much less dense than serpentinites and have yield strengths lower than salt, the muds could rise diapirically along faults, lubricating previously stronger structures. With this said, the fault gouge zones sampled in Hole 1272A clearly had a cataclastic origin because they contain angular serpentinite and gabbroic fragments. Alteration of gouge or serpentinite protoliths to clay may have been pre-, post-, or syn-kinematic, but there is no doubt that the faults record brittle failure and cataclasis as well as plastic deformation.

Paleomagnetic Data and Tectonics

Paleomagnetic data were collected on half cores and individual discrete samples. Using these data, we rotated the measured orientations of foliations, faults, veins, and dikes in individual core pieces around a vertical axis, thereby restoring core pieces to an orientation with a common azimuth for the remanent magnetization vector.

In the case of Site 1272, half-core measurements and discrete samples all have positive inclinations, indicating that the rocks probably were normally polarized. As noted above, the upper 55 m of Hole 1272A may have sampled a tectonic breccia, though this is uncertain. The average remanent inclination for 14 discrete samples of harzburgite from depths below 55 mbsf is 45.2° (95% CI = +5.4°/–6.7°), and the mean inclination for archive half cores is 42.7° (95% CI = +1.4°/–3.5°). (Two miarolitic gabbro samples from the upper 55 m of the core also have magnetic inclinations in this range.) These values are significantly higher than the expected inclination of 28°. These data suggest that block rotation has affected the section sampled at Site 1272, as also found for Sites 1268 and 1270, where remanent magnetic inclinations require substantial rotation of the section. For Sites 1268 and 1270, we inferred that rotation axes were probably near horizontal and parallel to the normal faults that form steep slopes along the rift valley. At Site 1272, near the eastern inside corner formed by the Mid-Atlantic Ridge and the 15°20′ Fracture Zone, the choice of a tectonically reasonable rotation axis is less clear. Increasing the inclination from 28° to ~44° requires a minimum of 16° of counterclockwise rotation around a horizontal rotation axis with an azimuth of 270° or larger rotations (clockwise or counterclockwise) around axes parallel to the trend of the fracture zone (~290°), the rift valley (~020°), or the northwest-striking foliation, veins, cracks, and faults observed in FMS images from Hole 1272A.

Site 1273

Site 1273 is the southernmost drilling target on our transect of sites north of the 15°20′N Fracture Zone. Video tapes from a precruise submersible survey revealed during *Faranaut* 15N Dive extensive steep east-facing scarps on the western wall of the Mid-Atlantic Ridge axial valley with virtually continuous exposure, and serpentinized peridotite was sampled from a water depth just below our intended drilling location. Based on our assessment of precruise survey information, we considered the outcrop at Site 1273 to be the most favorable for drilling of all our primary targets.

Unfortunately, as at Site 1269, unforeseeable complications resulted in premature abandonment of drilling at this site. Low recovery of predominantly basalt, albeit with three small fragments of serpentinized peridotite, and unstable hole conditions led us to the conclusion that as promising as the exposure of peridotite might have been, locations where drilling was possible (on flat, sedimented terraces above steep outcrops) were covered with talus shed from farther upslope and were thus unsuitable for deeper penetration.

Only a few pieces of the basalt recovered from Site 1273 exhibit even incipient seafloor weathering. For the most part the rocks are fresh. Several of the samples appear to be fragments of pillows, based on subtriangular morphology and the occurrence on piece edges of glassy rims and hyaloclastite. These basalts are aphyric with rare small (length < 5 mm) plagioclase phenocrysts. Unlike the basalts recovered from Site 1269, fragments of basalt recovered from Site 1273 are only slightly to moderately vesicular (maximum < 8 vol%) with a maximum vesicle size of 1.5 mm. In thin section, we can see that the groundmass of the Site 1273 basalts contains acicular plagioclase laths and quench-textured clinopyroxene, with minor amounts of fresh brown glass and skeletal opaque minerals.

A thin section from one of the small fragments of serpentinized peridotite recovered with basalt pieces from Hole 1273C is a completely altered protogranular harzurgite. Olivine in the harzburgite has been completely replaced by serpentine and brown clay, and orthopyroxene is altered to talc, serpentine, and minor chlorite and tremolite.

Site 1274

Site 1274 is located along the track of *Shinkai* 6500 Dive 416 on the western flank of the Mid-Atlantic rift valley at ~15°39′N. *Shinkai* 6500 Dive 416 recovered eight peridotite samples from 4434 to 3915 mbsl from weathered outcrops along a gentle slope. Concerned about the possibility that some of these outcrops are large landslide blocks, we chose a drill site near the uppermost peridotite outcrop observed during the dive (sample 416R008) on a relatively small flat spot in the midst of a relatively steep slope. Site 1274 is the northernmost of our transect of drill sites along the rift valley and is ~31 km north of the northwestern intersection of the Mid-Atlantic Ridge and the 15°20′ Fracture Zone. Drilling of Hole 1274A penetrated to a depth of 156 mbsf with a total recovery of 35 m of core. At this point, to continue drilling we would have had to place the bottom-hole assembly below seafloor. Because the core had been relatively uniform and drilling conditions were not optimal, we elected to move on to Site 1275. At this point, the pipe became stuck and could only be recovered after dropping the bit.

Proportions of Igneous Rocks

The igneous and residual mantle protoliths of recovered core at Site 1274 were 77% harzburgite, 20% dunite, and 3% gabbro [N7] (Fig. F43). In this way, Site 1274 is similar to the lower portion of Site 1272 and different from Sites 1268, 1270, and 1271, where we recovered ~75% peridotite and ~25% gabbro. The relative lack of gabbroic rocks at Site 1272 could have been viewed as indicating that plutons emplaced in mantle peridotite become rare as the 15°20′ Fracture Zone is approached [N8], in keeping with the idea that magma supply from the mantle is focused to the centers of slow-spreading ridge segments, with lateral transport of melt to segment ends in shallow dikes and lava flows (e.g., Dick, 1989). However, in view of the fact that Site 1274 is not located near a fracture zone or other obvious discontinuity in the Mid-Atlantic Ridge and sits on the flank of a Mantle Bouguer Anomaly low centered at ~16°N (Escartin and Cannat, 1999; Fujiwara et al., 2003), the relative lack of gabbroic rocks in Hole 1274A suggests that

gabbroic rocks are not homogeneously distributed in exposed mantle peridotites along the ridge at the scale of our drill, dredge, and submersible sampling.

The proportion of dunite to harzburgite in Hole 1274A is 21/79, much higher than at Site 1272 (4/96). The proportion of dunite to harzburgite at Sites 1268, 1270, and 1271 are 15/85, 10/90, and 90/10, respectively. We infer that dunite proportions are not uniform at the scale of our drilling, dredging, and submersible sampling.

Highly Depleted Mantle Peridotites

Geochemical analyses of all Site 1274 peridotites show low concentrations of nominally immobile incompatible elements such as Al, Sc, and V. For example, the Al_2O_3 concentrations in Site 1274 peridotites range from 0.2 to 0.9 wt% (average = 0.6 wt%), whereas Al_2O_3 concentrations in peridotites from Site 920 along the Mid-Atlantic Ridge at 23°20′N range from 1 to 2 wt% (Casey, 1997). Thus, the average Al_2O_3 concentration in 9 peridotites from Site 1274 is lower than at Site 1271 (average = 0.9 wt%) and as low as the average of 0.6 wt% Al_2O_3 in 12 peridotites from Site 1272, 7 peridotites from Site 1270, and 20 peridotites from Site 1268. If Al_2O_3 concentrations have not been modified by hydrothermal metasomatism, then the peridotites from Sites 1268, 1270, 1271, 1272, and 1274 are among the most depleted residual mantle peridotites yet obtained from the mid-ocean ridges. This result is not consistent with previous inferences, based on the composition of dredged peridotite samples, that the degree of depletion of mantle peridotites decreases from south to north across the 15°20′ Fracture Zone from 14°40′ to 15°40′N along the Mid-Atlantic Ridge. Instead, our data suggest that the mantle in this region is uniformly depleted, perhaps as the result of a prior melt depletion event.

Hole 1274A harzburgites include appreciable amounts of clinopyroxene and CaO, generally more than is observed at Sites 1268, 1270, 1271, and 1272. CaO contents of Hole 1274A peridotites are weakly correlated with Al_2O_3 contents, although these elements do not show correlated variation in peridotites from previous sites. The low CaO in peridotites from previous sites may be due, in part, to hydrothermal metasomatism with removal of Ca during serpentinization. Thus, it could be that the relatively high CaO contents of Hole 1274A harzburgites are representative of the original CaO contents of all harzburgites sampled during Leg 209, preserved at Site 1274 because of the lower extent of hydrothermal alteration there.

It is unclear how much of the clinopyroxene observed in Hole 1274A harzburgites is residual or igneous. In most samples, clinopyroxene is spatially associated with orthopyroxene and, in particular, clinopyroxene is interstitial to broken and partly recrystallized orthopyroxene (Fig. F44). In this association, we believe that some of the clinopyroxene could have been exsolved from orthopyroxene during cooling and recrystallization. However, other clinopyroxene is interstitial to olivine, far from any orthopyroxene, and is probably a residual or igneous phase. We infer that the clinopyroxene is not residual. In view of the highly depleted Al, Sc, and V contents of the peridotites, Site 1274 harzburgites probably represent residuum of partial melting that extended beyond the exhaustion of clinopyroxene as a residual phase (>20%–25% melting and melt extraction). If this inference is correct, the observed interstitial clinopyroxene (and, perhaps, some of the clinopyroxene that is spatially associated with orthopyroxene) is igneous. It probably crystallized from cooling melt migrating along grain boundaries after the peridotites had been incorporated into the thermal boundary layer beneath the Mid-Atlantic Ridge. Trace element analyses of whole rocks and clinopyroxene grains during postcruise research will help to evaluate this hypothesis.

Finally, we caution readers that the relatively high CaO in Site 1274 harzburgites may not be entirely due to the presence of clinopyroxene in the rocks. Site 1274 harzburgites also contain more carbonate alteration than most peridotites from previous sites (see "**Hydrothermal Alteration, Metamorphism, and Metasomatism,**" below).

Petrogenesis of Plutonic Rocks

Deformed oxide gabbronorites intrude the peridotite in Hole 1274A. These gabbronorites, while altered and recrystallized, are texturally and mineralogically similar to gabbronorites sampled elsewhere during Leg 209, particularly in Holes 1270B, 1275B, and 1275D.

Hydrothermal Alteration, Metamorphism, and Metasomatism

Metasomatic Changes in Peridotite

Peridotites from Site 1274 include the freshest mantle samples recovered during Leg 209, with up to 35% of the original mantle minerals preserved. However, the peridotites may have been affected by appreciable major element metasomatism during hydrothermal alteration. Figure F45 shows that Hole 1274A peridotites may have been affected by SiO_2 gain or MgO + FeO loss. Dunites have ~5–13 wt% normative orthopyroxene, and five of the six harzburgites have ~26–29 wt% normative orthopyroxene. These proportions of orthopyroxene could be primary [**N9**]. However, these orthopyroxene proportions seem high given the very low Al, Sc, and V contents of the rocks, which reflect high degrees of partial melting.

In addition to possible metasomatic shifts in SiO_2/(MgO+FeO) and despite their apparently high degrees of melt depletion, Site 1274 peridotites generally contain higher proportions of components other than MgO, FeO, and SiO_2, compared to peridotites from previous sites sampled during Leg 209. This may be due to several factors. First, Site 1274 harzburgites contain appreciable clinopyroxene and thus have more CaO than harzburgites from other sites. However, it is not clear that this fully explains the relatively high CaO in Site 1274 peridotites. Site 1274 dunites have less CaO than harzburgites, as expected from their primary mineralogy. However, within the group of harzburgites, CaO is poorly correlated with Al_2O_3 and other indices of pyroxene content and degree of melt depletion.

In addition to CaO in clinopyroxene, peridotites from Site 1274 may have undergone metasomatic enrichment in CaO as a result of carbonate metasomatism. They contain an average of 0.35 wt% CO_2 (1 σ = ±0.03), significantly higher than in peridotites from Site 1268 (CO_2 = 0.07 wt%), Site 1270 (CO_2 = 0.13 wt%, excepting an outlier with 2.2 wt%), Site 1271 (CO_2 = 0.23 wt%, excepting an outlier with 1.5 wt%), and Site 1272 (CO_2 = 0.24 wt%, excepting outliers with 7.3 and 9.3 wt%). Figure F46 summarizes our data on CaO and CO_2 contents of peridotites from Leg 209. In the data set as a whole, carbonate addition clearly accounts for most of the variation in CaO contents of these rocks. As discussed in this and previous site summaries, the poor correlation of CaO with CO_2 in samples with low concentrations may reflect analytical uncertainty, CaO in primary mantle pyroxenes, and CaO in impregnations of igneous pyroxene and plagioclase. However, we emphasize that almost all peridotite samples from Leg 209 contain measurable quantities of CO_2, mostly in aragonite and calcite. This also appears to be true of peridotite samples from Site 920, drilled along the Mid-Atlantic Ridge at 23°20′N during Leg 153 (Cannat, Karson, Miller, et al., 1995; Casey, 1997), though some may contain magnesite. Thus, some of the CaO in all these metaperidotites is probably in carbonate minerals.

It is well established that metaperidotites sometimes lose CaO during serpentinization, apparently because serpentine (as well as talc and brucite) do not readily accept Ca in their crystal structures and other minerals are not stable in the hydrothermal alteration environment. However, although this is not as commonly considered, it is equally clear from our data that metaperidotites sometimes gain CaO during carbonate metasomatism. This may be true of Site 1274 peridotites, despite their relatively low degree of serpentinization.

Aragonite, calcite, and magnesite may contain substantial quantities of Sr and perhaps other trace elements that can form carbonate minerals (e.g., Pb and Ba). Figure F47 shows that Leg 209 metaperidotites with the highest CO_2 also have the highest Sr contents and among the highest Ba contents [**N10**]. During postcruise research, it will be interesting to determine the trace element contents of metasomatic carbonate minerals in peridotites from Leg 209 and the extent to which these minerals influence the whole-rock trace element budget. Meanwhile, interested readers should note that elements that are highly incompatible during partial melting of mantle peridotite may be added to metaperidotites during carbonate metasomatism. As a consequence, whole-rock trace element analyses of hydrothermally altered peridotites, even where they still contain tens of percent of fresh, primary minerals, should be interpreted with caution.

On a different but related topic, Site 1274 samples include ultramafic mud, forming the matrix of fault gouge in several horizons. These muds have high TiO_2 and Al_2O_3 as well as CaO and CO_2 compared to Site 1274 peridotites. Since the fault gouge includes clasts of gabbroic rock as well as peridotite, we infer that the elevated TiO_2 and Al_2O_3 in the muds is due to mechanical mixing of gabbroic material with peridotite, whereas the high CaO may be a consequence of both this mixing process and addition of metasomatic carbonate.

Downward Increase in Serpentinization

There was a clear increase in the extent of alteration of peridotites with increasing depth in Hole 1274A. In general, olivine shows >80% serpentinization, whereas pyroxenes are only 50%–60% altered in the uppermost 60 m, with a gradual increase to nearly 100% alteration of both olivine and pyroxene near the bottom of the hole at 156 mbsf. This gradient of increasing serpentinization away from the seafloor is probably due to alteration associated with large fault zones, represented in the core by extensive fault gouge zones sampled between ~95 and ~145 mbsf. In fact, the degree of alteration may decrease again beneath 145 mbsf, though it is difficult to be sure given our limited sampling below this depth.

The downhole increase in the extent of serpentinization is accompanied by a sharp increase in the proportion of secondary magnetite, reflected in a correlation between magnetic susceptibility and the intensity of alteration as estimated during visual core description (Fig. F48). Density and seismic *P*-wave velocity decrease downhole and are significantly correlated with the intensity of alteration (Fig. F48). These relationships could provide a useful tool in geophysical studies of near-seafloor, partially serpentinized peridotites.

Metamorphic Parageneses

As at Sites 1271 and 1272, brucite is abundant in core from Hole 1274A. This is in keeping with the relatively low SiO_2/(MgO+FeO) for peridotites from all these sites, which are substantially different from the relatively talc-rich, high-SiO_2/(MgO+FeO) peridotites exemplified by samples from Site 1268, but also observed at Site 1270.

Clinopyroxene is relatively abundant in peridotite from Hole 1274A. Where it has been incipiently altered, it is associated with talc and tremolite. This may be explained by hydrothermal metasomatism,

involving substantial input of Mg (±Fe) and extraction of Ca. However, we have no independent evidence for addition of MgO to Site 1274 peridotites and Ca extraction—if any—was limited. As an alternative, formation of tremolite can be explained as a result of reactions involving primary phases present in the peridotites, such as

$$2(Mg,Fe)CaSi_2O_6 + 3(Mg,Fe)_2Si_2O_6 + 3H_2O = Ca_2(Mg,Fe)_5Si_8O_{22}(OH)_2 + (Mg,Fe)_3Si_2O_5(OH)_4,$$

forming tremolite + serpentine from pyroxene or, at higher temperature,

$$4(Mg,Fe)CaSi_2O_6 + 5(Mg,Fe)_2Si_2O_6 + 3H_2O = 2Ca_2(Mg,Fe)_5Si_8O_{22}(OH)_2 + 2(Mg,Fe)_2SiO_4,$$

forming tremolite + olivine. Similarly, talc formation in metaperidotites is generally ascribed to reactions such as

$$3(Mg,Fe)_2Si_2O_6 + 3H_2O = (Mg,Fe)_3Si_4O_{10}(OH)_2 + (Mg,Fe)_3Si_2O_5(OH)_4,$$

or, at higher temperature,

$$5(Mg,Fe)_2Si_2O_6 + 2H_2O = 2(Mg,Fe)_3Si_4O_{10}(OH)_2 + 2(Mg,Fe)_2SiO_4.$$

All of these reactions require only H_2O addition from hydrothermal fluid, and thus may be preferable in cases where independent evidence for metasomatism is lacking.

Brucite is observed in Site 1274 peridotites that also contain pyroxene and/or talc. This assemblage is almost certainly metastable because under most metamorphic conditions brucite and talc break down to form serpentine [N11] via

$$3(Mg,Fe)(OH)_2 + (Mg,Fe)_3Si_4O_{10}(OH)_2 = 2(Mg,Fe)_3Si_2O_5(OH)_4.$$

Thus, the presence of brucite and talc together in serpentinized peridotites from Site 1274 attests to the presence of local disequilibrium, with fluid composition and/or reaction kinetics varying on the scale of a few millimeters. In turn, this suggests that fluid fluxes and fluid/rock ratios may have been low during alteration. Formation of brucite, serpentine, and magnetite is interpreted to reflect local hydration and oxidation of olivine. If so, brucite may be more abundant in the more altered, deeper parts of Hole 1274A that show high magnetic susceptibility associated with relatively large proportions of magnetite.

Ultramafic fault gouge recovered from Site 1274 includes abundant clay, mainly nontronite ($Na_{0.3}Fe^{3+}{}_2[Si,Al]_4O_{10}[OH_2]\cdot nH_2O$). The presence of ferric iron–rich nontronite, as well as the development of aragonite veins with oxidation halos present to depth of 90 mbsf, suggests that water-rock reactions continued at low temperatures under oxidizing conditions. This is striking because the main fault gouge zones are well below the seafloor at depths of ~95 to ~145 mbsf; indications of oxidizing alteration and weathering have been restricted to shallower depths at all previous sites on Leg 209. In addition, this result is somewhat unexpected since the dark green to black color of the fault gouge muds initially suggested to us that they lack hematite and Fe-oxyhydroxides and, thus, that they formed under reducing conditions. It will be interesting to further investigate the redox conditions during fault gouge formation during postcruise research.

Structural Geology

Two main structural features were observed in Hole 1274A. First, as in the peridotites at Sites 1272, 1271, 1270, and 1268, protogranular textures are abundant and porphyroclastic textures are nearly absent. Second, the hole intersected large fault zones, as represented by fault gouge at depths of ~95, 100, 110, 125–135, 140, and 145 mbsf. We discuss each of these in turn.

In Hole 1274A peridotites, it was difficult to even detect and measure a high-temperature foliation. During Leg 209, we increasingly focused on this apparent lack of deformation. In this, as in previous holes, orthopyroxene in mantle peridotites shows little sign of crystal-plastic deformation. Orthopyroxene is commonly interstitial to olivine, with long, narrow projections along olivine grain boundaries. Orthopyroxene crystals are intimately intergrown with complex skeletal spinels that have no discernible shape fabric in three dimensions. Large skeletal spinels, several millimeters long and just a few hundred micrometers wide, with branches at high angles to each other, are also interstitial to olivine where no orthopyroxene is present. Although these observations are qualitative, it is difficult to believe that these textures can have survived significant shear strains.

In the Oman ophiolite, where residual mantle peridotites have been studied extensively on scales of meters to tens of kilometers, high-temperature protogranular textures are restricted to small zones—often interpreted as "diapirs"—with near-vertical spinel lineation. Outside these zones of vertical spinel lineation, residual mantle peridotites have lower-temperature porphyroclastic textures that record pervasive ductile deformation of the upper mantle at 1000°–1200°C, with foliation and spinel lineation that are subhorizontal, roughly parallel to the plane of the crust/mantle boundary [e.g., Boudier and Coleman, 1981; Ceuleneer, 1991; Ceuleneer and Rabinowicz, 1992; Jousselin et al., 1998; Nicolas and Rabinowicz, 1984; Nicolas and Violette, 1982].

In the region investigated during Leg 209, protogranular textures appear to be pervasive and both porphyroclastic textures and well-developed spinel lineations are rare. This observation needs to be checked and quantified by extensive shore-based research. However, it appears that pervasive Moho-parallel deformation in the upper mantle was rare or absent beneath the Mid-Atlantic Ridge from 14°43′ (Site 1270) to 15°39′N (Site 1274). We believe that this cannot be due to an absence of deformation at the plate scale. Substantial shear stresses must have developed in the uppermost mantle in this region as a result of (1) corner flow associated with plate spreading, (2) possible diapiric upwelling of buoyant mantle, and (3) uplift of mantle peridotite from the base of the thermal boundary layer to the seafloor. However, these stresses must have been accommodated by strain localization along the mylonitic shear zones, may of which developed within and near gabbroic veins in peridotite and within gabbroic rocks, as observed at Sites 1268, 1270, and 1271. If this hypothesis is correct, strain localization must have been initiated at temperatures >1200°C.

Tellingly, a single piece of mylonitic peridotite was recovered from Hole 1274. Although this fragment was in Core 209-1274A-2R, we believe that it represents debris that fell from higher in the hole during core recovery. As at Site 1270, where we spudded into a mylonitic fault surface that had been sampled during the dive survey in 1998, we suspect that there is a mylonitic surface at the top of the seafloor outcrop at Site 1274 that was not sampled in the first core, which recovered only 1.1 m of core in 11.9 m of penetration. In general, we have the impression that several Leg 209 holes penetrated into little deformed blocks overlain by poorly sampled, narrow, high-temperature peridotite and gabbro mylonites that form the outcrop surface.

As at Sites 1268, 1270, 1271, and 1272, Hole 1274A encountered numerous zones of poorly consolidated serpentinite + clay fault gouge (Fig. F49). Recovery of gouge was poor at several sites;

therefore, the width of the associated fault zones is uncertain. However, we recovered several meters of continuous gouge at various depths in Holes 1272A and 1274A. These thick gouge zones must represent major faults. The gouge had an unusual rheology, unfamiliar to us, with a pliable claylike texture when it first came on board. We suspect that this type of material has an extremely low plastic yield strength and—once formed as a result of cataclastic deformation during brittle failure—it could undergo continuous aseismic creep. Faults lined with serpentinite + clay fault gouge probably have very low strength and could remain active even at low dip angles.

Peridotite outcrops along the flanks of the Mid-Atlantic rift valley are commonly interpreted to be footwall exposures that were originally overlain by normal fault surfaces. The ubiquity of subsurface faults lined with gouge, found in all holes in peridotite that penetrated deeper than 35 mbsf, suggests that peridotite outcrops along the flanks of the Mid-Atlantic rift valley are also generally underlain by weak faults. Thus, we have formed a tentative picture in which the rift valley walls are underlain by numerous anastomosing fault zones parallel to the regional slope on the order of 100 m apart, perpendicular to the fault plane. Some of these fault zones, particularly in Hole 1268A, clearly overprint earlier high-temperature mylonitic shear zones. Poor recovery associated with most of the fault zones makes it impossible to determine whether this relationship is common. In any case, each of the fault gouges was formed during brittle failure and each represents a weak plane of potential future deformation, whether by normal sense displacement during tectonic extension or as the sole of a landslide.

Paleomagnetic Data and Tectonics

Paleomagnetic data were collected on half cores and individual discrete samples. Using these data, we rotated the measured orientations of foliations, faults, veins, and dikes in individual core pieces around a vertical axis, thereby restoring core pieces to an orientation with a common azimuth for the remanent magnetization vector.

Half-core measurements and discrete peridotite samples all have positive inclinations that are presumable of normal polarity, although the mean inclination (13°) is significantly shallower than the expected dipole inclination at the site (28°), indicating that the rocks are normally polarized. It was difficult to discern high-temperature foliations in peridotite from Hole 1274A, as discussed above. Those that could be identified could only be measured in the cut face of the core, yielding apparent dips in this plane. Since the cut face was generally oriented perpendicular to the serpentine foliation, rotation of the apparent dips of high-temperature foliation into a common remanent magnetization azimuth must yield a cluster of poles with east-northeast strikes. However, in addition to the predictable clustering, the apparent dip data seem to form a girdle on a stereographic projection consistent with folding of the high-temperature foliations striking parallel to the serpentine foliation.

This result is intriguing but remains uncertain. In addition to the difficulties outlined in the previous paragraph, microscopic examination of core yielded foliation directions, based on the presence of elongate orthopyroxene grains and faint spinel trains, that were nearly perpendicular to the serpentine foliation and to the macroscopic fabric marked by alternating light and dark patches visible in core from afar. Our preferred interpretation is that the macroscopic foliation simply represents less serpentinized lenses within the serpentine foliation and is not really a high-temperature feature, in keeping with similar observations and interpretations at ODP Site 920 (Ceuleneer and Cannat, 1997), but uncertainty about this persists. It will be very helpful to measure olivine lattice fabrics in these rocks during postcruise research.

The average remanent inclination for 17 discrete samples of harzburgite is 13.4° (95% CI = +7.4°/–8.1°), and the mean inclination for archive half cores is 18° (95% CI = +2°/–3°). These values are significantly lower than the expected inclination of 28°. These data suggest that block rotation has affected the section sampled at Site 1274, as was also found for Sites 1268, 1270, and 1272, where remanent magnetic inclinations require substantial rotation of the section. For Sites 1268 and 1270, we inferred that rotation axes were probably near horizontal and parallel to the normal faults that form steep slopes along the rift valley. At Site 1272, near the eastern inside corner formed by the Mid-Atlantic Ridge and the 15°20′ Fracture Zone, the choice of a tectonically reasonable rotation axis is less clear. Near Site 1274, there are many south-facing slopes, quite distinct from the east-facing slopes that make up most of the western flank of the rift valley in this region. Thus, the choice of an axis for the rotation of the Site 1274 section is not well constrained. Decreasing the inclination from 28° to ~15° requires a minimum of 13° of clockwise rotation around a horizontal rotation axis with an azimuth of 270° or larger rotations around axes parallel to the trend of the Fracture Zone (~290°) or the rift valley (~020°).

Site 1275

Site 1275 is located along the track of *Shinkai* 6500 Dive 422 on the summit of a topographic dome, known informally as Mt. Mike, ~10 mi west of the Mid-Atlantic rift valley at ~15°44′N. This dome has been interpreted on the basis of bathymetric data as an oceanic core complex, or "megamullion" (Escartin and Cannat, 1999; Escartin et al., in press; Fujiwara et al., 2003; MacLeod et al., 2002). Dive 422 recovered seven samples of gabbro from ~2290 to ~1750 mbsl, mostly from steep blocky outcrops along the southern flank of the dome, and then two samples of peridotite and one sample of gabbro from nearly flat, striated outcrops and overlying talus across the summit of the dome at ~1650–1540 mbsl. In 2001, the *James Clark Ross* made a survey of this dome using the BRIDGE portable wireline rock drill and dredging to sample (Escartin et al., in press; MacLeod et al., 2002). In addition to gabbro and peridotite, short (~1 m) drill cores from the summit of the dome recovered abundant diabase.

Holes 1275A and 1275B were located in an area with horizontal, striated outcrop surfaces extending for ~100 m², ~300 m north of the top of the dome and 90 m north of the northernmost *Shinkai* 6500 sample, 422-R010 (described as highly altered plagioclase-bearing dunite and peridotite, recovered from talus resting on a flat outcrop surface). In an attempt to recover as much material as possible from the upper 5 m of the outcrop, we retrieved the core barrel after 5 m of drilling. Core 209-1275A-1R was composed of a small amount of diabase and carbonate-cemented diabase breccia. Recovering this core involved lifting the drill bit above seafloor, so we immediately spudded Hole 1275B a few meters away. Diabase composed 100% of the rocks from Cores 209-1275B-1R and 2R and >50% of Core 3R, extending to 18 mbsf. Below this depth, core was dominated by gabbroic rocks intruded by a few diabase sills or dikes, except within an interval of troctolite or impregnated dunite from ~30 to ~30–35 mbsf. Given the ultramafic lithology in *Shinkai* 6500 sample 422-R010, we were surprised that the first ultramafic rocks in Hole 1275B were not recovered until the hole reached a depth of 30 mbsf.

After 109 m of drilling in Hole 1275B, it was necessary to change the bit. We marked Hole 1275B for possible reentry but also used the opportunity to move to a position directly above sample 423-R010 to test the resistivity-at-the-bit with coring (RAB-C) coring equipment. The RAB-C test in Hole 1275C recovered very little core, but this included two small pieces of troctolite. Thus, we elected to spud Hole 1275D just a few meters away from Hole 1275C to determine the extent of lateral variability of the lithologies at this site and to provide a complementary rotary core barrel (RCB) hole to fully evaluate the coring potential of the RAB-C equipment. The first three cores in Hole 1275D recovered almost 8 m of

core over ~17.6 m of penetration, the best recovery for the first three cores in any hole drilled during Leg 209. By comparison, Hole 1270C, drilled just a few meters away with the RAB-C bit, recovered just a few tens of centimeters of core over ~21 m of penetration, which was the worst recovery for the first three cores in any hole during Leg 209.

In striking contrast to Hole 1275B, troctolite, or impregnated dunite, was recovered in the first 11 cores of Hole 1275D, extending to ~56 mbsf, though diabase was also present in the first core. Below 56 mbsf, the hole passed into gabbroic rocks intruded by diabase sills or dikes, with a second interval of troctolite between ~80 and 95 mbsf. Thus, although Hole 1275D was only ~90 m south of Hole 1275B, the lithostratigraphy is quite different in the two holes. Correlation of rock units from the two holes is still in an initial stage. However, the simplest interpretation seems to be that the lower troctolite in Hole 1275D, flanked by gabbroic rocks, is correlative to the first (and only) troctolite in Hole 1275B, which is also surrounded by gabbroic rocks. If so and assuming a roughly planar upper contact between troctolite and overlying gabbro, the apparent dip of this contact is ~30° to the south in the plane formed by the two drill holes (Fig. F50). Intriguingly, this dip is parallel to the south slope of the dome along the track of the *Shinkai* 6500 Dive 422 from sample 422-R003 to 422-R008.

Proportions of Igneous Rocks

The igneous and (possibly) residual mantle protoliths of recovered core at Site 1275, weighting the proportions of recovered lithologies by the depths of each hole, were 14% troctolite or impregnated dunite, 74% gabbroic rocks (gabbro, gabbronorite, oxide gabbro, oxide gabbronorite, and olivine gabbro), 10% diabase, and 2% granophyre (Fig. F50). The large proportion of gabbroic rocks and the presence of diabase were no surprise, given past submersible sampling and more recent dredge and BRIDGE drilling results from Mt. Mike. Obviously, Site 1275 is very different from all previous sites drilled during this leg. Drilling at Sites 1274 and the lower portion of Site 1272 recovered just a few percent gabbroic rocks, and at Sites 1268, 1270, and 1271 we recovered ~75% peridotite and ~25% gabbro. Considering all these sites together, without weighting for the different depths of drilling, we can tentatively infer that the crust from 14°39′ to 15°44′ is composed of 20%–40% variably altered gabbroic rocks and 80%–60% partially serpentinized peridotite. As discussed in **"Site 1268,"** it is possible that these proportions of gabbro to peridotite extend to depths below the Moho.

Petrogenesis of Troctolites or Impregnated Dunites

As mentioned above, a lithology termed "troctolite" in lithologic logs and site chapters was recovered in Holes 1275B, 1275C, and 1275D. Several meters of troctolite were recovered from between ~30 and 35 mbsf in Hole 1275B, and tens of meters of troctolite were recovered from the upper 95 m of Hole 127D (Fig. F51). The rocks are highly altered, but relict primary phases remain and the alteration was static so that pseudomorphic assemblages allow unambiguous determination of the primary mineralogy. The protolith of this rock type was composed of 50% to almost 100% olivine with 1%–3% chromian spinel surrounded by poikilitic orthopyroxene and clinopyroxene, and by interstitial plagioclase. Minor brown hornblende in these rocks could be igneous but is probably of metamorphic origin. Olivine crystals are generally rounded and locally embayed, but no reaction rims are present between any of the primary phases.

Because the rock is coarse grained and the proportions of the minerals vary on a centimeter scale, different parts of the troctolite could be classified as dunite, harzburgite, wehrlite, troctolite, or lherzolite. Nonetheless, the different rock types grade into one another and are spatially continuous. Also, chemical

analyses reveal that they are relatively homogeneous from one part of the core to another when sample sizes are a few cubic centimeters. For simplicity, throughout this report we refer to all these rocks as troctolites.

The troctolite is cut by numerous centimeter-scale dikes and veins of gabbroic to felsic material. These are almost all 100% altered to talc + amphibole assemblages. However, the presence of pyroxene oikocrysts that cross contacts between troctolite and intruding gabbroic rock suggests that the two rock types are genetically related. Although the gabbroic dikes and veins that cut the troctolite may be coarser than most gabbroic rocks elsewhere in Holes 1275B and 1275D, the two are probably related. Abundant magnetite is observed in most gabbroic rocks from Site 1275, including the dikes and veins cutting troctolite. We have observed qualitatively in ophiolites that grain size in gabbro increases near intrusive contacts with peridotite (P.B. Kelemen, H.J.B. Dick, and J.F. Casey, pers. comm., 2003). Thus, we interpret the troctolite lenses at 30–35 mbsf in Hole 1275B and 80–95 mbsf in Hole 1275D as rafts of older rock included within a gabbroic pluton and the thick troctolite unit that forms the upper 56 m of Hole 1275D as another raft, cut by the fault that forms the top of the dome, or as a part of the roof of the pluton.

The troctolite is of great interest for two main reasons. First, the apparent equilibrium between igneous olivine, pyroxenes, plagioclase, and spinel places important constraints on the pressure at which this assemblage crystallized. Second, some of the olivine in the troctolite may be relict, residual mantle olivine and thus the presence of the troctolite may indicate that the gabbroic rocks from Site 1275 were intruded into mantle peridotite. We discuss each of these topics in turn in the following paragraphs.

First, we discuss constraints on equilibrium between basaltic liquid, olivine, orthopyroxene, clinopyroxene, spinel, and plagioclase. As is well known to igneous petrologists, the five solid phases in this assemblage are related by reactions such as

$$2(Mg,Fe)_2SiO_4 + CaAl_2Si_2O_8 = (Mg,Fe)_2Si_2O_6 + (Mg,Fe)CaSi_2O_6 + (Mg,Fe)Al_2O_4,$$

which consumes olivine plus the anorthite component in plagioclase, stable at relatively low pressure, to produce orthopyroxene, clinopyroxene, and spinel at higher pressures. Because of constrained Fe/Mg exchange between all these phases, this assemblages is nearly univariant in Ca-Mg-Al-Si-Fe. However, because albite ($NaAlSi_3O_8$) is an important component in plagioclase and Cr spinel (e.g., $MgCr_2O_4$) is an important part of spinel solid solutions in these rocks, there is actually a broad range of pressure and temperature conditions over which this assemblage can be stable. Because this assemblage also contains several geothermometers (e.g., pyroxene solvus and Cr/Al exchange between orthopyroxene and spinel) and because of recent improvements in understanding of spinel solid solutions, during postcruise research it will be possible to constrain the pressure and temperature at which all these solid phases last equilibrated.

Meanwhile, we can infer likely pressures at which basaltic liquid could have been in equilibrium with olivine, orthopyroxene, clinopyroxene, spinel, and plagioclase [**N12**]. The troctolites have whole-rock Mg#s of 86%–89%, similar to and slightly lower than typical values for oceanic residual mantle peridotites. This is fortunate, because an extensive body of experimental work has been devoted to determining the relationships between liquid compositions, pressures, and temperatures for equilibrium between melts and the mineral assemblages in mantle peridotites. The presence of plagioclase in this assemblage indicates that the pressure was less than ~1.2 GPa (e.g., Green and Hibberson, 1970). Conversely, it is well known that the minimum pressure for orthopyroxene saturation in primitive melts is a function of silica content in the melt (e.g., Elthon and Scarfe, 1984; O'Hara, 1965; Stolper, 1980). Thus, primitive tholeiitic basalts with ~49 wt% SiO_2 are last saturated in orthopyroxene at a pressure of ~1 GPa (e.g., Baker and Stolper, 1994), whereas primitive andesites with ~54 wt% SiO_2 can be saturated in

orthopyroxene at ~ 0.5 GPa (e.g., Jaques and Green, 1980) and boninitic melts with ~58 wt% SiO_2 can crystallize orthopyroxene at 0.1 MPa (e.g., Crawford, 1989). In this context, the relatively SiO_2-rich nature of mid-ocean-ridge basalts from the 14° to 16°N region along the Mid-Atlantic Ridge, first noted in "**Site 1268,**" is significant.

Kinzler and Grove (1992, 1993) developed a relatively simple algorithm that relates the composition of melts saturated in olivine, orthopyroxene, clinopyroxene, and plagioclase (± spinel) to pressure and temperature. Although their main goal was to calculate melt compositions given a source peridotite composition, pressure, and temperature, their method can be inverted to estimate pressure and temperature from a melt composition. Figure F52 shows predicted pressures vs. experimental pressures for the suite of olivine + orthopyroxene + clinopyroxene + plagioclase saturated liquid compositions that was used to calibrate the Kinzler and Grove expressions. The agreement between predicted and experimental values is good, with an uncertainty of approximately ±0.2 GPa, similar to the uncertainty in pressure calibrations for the piston cylinder apparatus used in the experiments.

Accordingly, we have taken all published compositions of basaltic glasses from 14° to 16°N along the Mid-Atlantic Ridge and calculated the pressures and temperatures at which each could be saturated in olivine, orthopyroxene, clinopyroxene, and plagioclase. The results are illustrated in Figure F53. Estimates for primitive glass compositions (molar Mg# = 60%–73%) form a tight cluster, averaging 0.54 GPa (2 σ = ±0.14 GPa) and 1220°C (2 σ = ±16°C), though a few glasses yield higher temperature and pressure values. Because the data are tightly clustered, the standard errors of the mean for the average pressure and temperature are very small (~1 MPa and 0.1°C). It should be noted that these calculations are based on the assumption that the MORB glasses could be saturated in olivine, orthopyroxene, clinopyroxene, and plagioclase at some pressure and temperature and does not prove that they were in equilibrium with all these phases at any time. Nevertheless, the more primitive basalt glass compositions are close to Fe/Mg exchange equilibrium with the minerals in the troctolite, whose composition can be inferred from the whole-rock Mg#. Because some of the glasses are very primitive, we conclude that they probably were close to saturation in a mantle phase assemblage.

Thus, we believe that the data in Figure F53 indicate that the Site 1275 troctolites probably formed in equilibrium with a melt at 0.40–0.68 GPa. Because the orthopyroxene, clinopyroxene, and plagioclase in these rocks clearly crystallized from a melt, it follows that conductive cooling and crystallization of rising magma began at a depth of 12–20 km beneath the Mid-Atlantic Ridge, at least in this region. This result is consistent with thermal models for slow-spreading ridges, which predict that the thermal boundary layer extends to depths of ~20 km beneath the Mid-Atlantic Ridge (Braun et al., 2000; Reid and Jackson, 1981; Sleep, 1975). This result is also consistent with fractional crystallization models, which require pressures of 0.4–0.6 GPa to account for observed variation in the composition of genetically related basalts from the Mid-Atlantic Ridge in general (Grove et al., 1992; Meurer et al., 2001; Michael and Chase, 1987) and from the 14° to 16°N region in particular (C. Xia et al., unpubl. data). Finally, in keeping with the observation that residual mantle peridotites are extensively exposed in outcrop in the 14° to 16°N region, this result reminds us that rocks that were incorporated into the plate at great depth have been tectonically uplifted and unroofed on the seafloor. And finally, since the troctolites lack evidence for viscous deformation, we can infer that at depths <12–20 km the tectonic exhumation process involves localized deformation at a temperature less than ~1220°C.

More evolved glass compositions (molar Mg# = 50%–60%) from basalts sampled between 14° and 16°N yield estimated pressures ranging from ~0.6 to ~0.3 GPa and temperatures ranging from 1220° to 1175°C. As can be seen in Figure F53, the pressure-temperature estimates for the evolved glasses form a tight cluster at significantly lower pressures and temperatures compared to the cluster for pressure-temperature

estimates for more primitive glasses. Although further analysis is necessary, this suggests that crystallization of melt in the thermal boundary layer beneath the Mid-Atlantic Ridge is a polybaric process in which increasingly evolved melts crystallize at increasingly shallow depths.

We turn now to the question of whether the olivine in the troctolites is igneous or is relict, residual olivine from mantle peridotite. If the olivine is igneous, the troctolites would be the most primitive igneous cumulates yet recovered from a mid-ocean ridge. If the olivine is derived from mantle peridotite, then the troctolites should be viewed as impregnated dunites, similar to those sampled at Site 1271 and to impregnated peridotites dredged from the mid-ocean ridges and common in some ophiolites. In thin section, some spatially isolated olivine crystals appear to be optically continuous with other nearby olivine grains, though they are now separated by intervening pyroxene and plagioclase. Thus, some rocks may preserve an olivine lattice-preferred orientation, despite the undeformed nature of the pyroxene, plagioclase, and alteration assemblages. If so, this would be consistent with a polygenetic origin for the rocks, composed of older, previously deformed olivine grains that have been partially disaggregated and incorporated in a matrix of younger igneous minerals.

In "**Site 1271**" we argued that covariation of olivine Mg# and Ni contents can be used to distinguish some impregnated dunites from cumulate igneous dunites. Whereas olivine Mg#s are similar to typical values for mantle peridotites, olivine cumulates cannot be distinguished from mantle dunites. However, where the Mg#s are lower, in the range of 88%–85%, then high Ni contents in olivine at a given Mg# are indicative of an origin via melt/rock reaction and impregnation (e.g., Godard et al., 2000; Kelemen, 1986, 1990), whereas lower Ni contents at the same Mg# are consistent with an origin via fractional crystallization (e.g., Hart and Davis, 1978). Because the Site 1275 troctolites are highly altered (some contain up to 9 wt% CO_2), it is difficult to be sure about the composition of the remaining olivine. However, we have inferred the olivine compositions, based on the bulk compositions of samples with 0.2–3 wt% CO_2. To do this, we calculated CIPW norms for the anhydrous bulk composition. These yielded normative proportions ranging from 57 to 78 wt% olivine (with four of six compositions between 70 and 72 wt%), 11 to 30 wt% pyroxene (four of six between 11 and 15 wt%), and 4 to 12 wt% plagioclase (four of six from 9 to 12 wt%). We then estimated the original Ni concentration in olivine, assuming Ni partitioning between olivine and pyroxenes was governed by partitioning at 1250°C, using relationships derived by Kelemen et al. (1998a), and that there is no Ni in plagioclase (or any other phase, including sulfide). The calculated Ni concentrations in olivine are plotted in Figure F54, together with similar estimates for Ni in olivine from mantle harzburgites and dunites recovered at other sites during Leg 209 and with published olivine compositions from dunites, impregnated dunites, and wehrlites in the mantle transition zone of the Oman ophiolite.

It is apparent that the estimated Ni contents of olivine in the Site 1275 troctolites are higher than those predicted for crystal fractionation of olivine. This is consistent with the hypothesis that the troctolites are the products of melt-rock reaction, in which Fe/Mg exchange with migrating melt lowered olivine Mg#s but the original high Ni concentrations were retained in the olivine. Therefore, we tentatively infer that the Site 1275 troctolites are impregnated dunites, containing relict, residual olivine derived from mantle peridotites plus pyroxenes and plagioclase that crystallized from a cooling melt migrating along olivine grain boundaries.

Petrogenesis of Gabbroic Rocks and Diabase

Gabbroic rocks, including gabbro, gabbronorite, oxide gabbro, oxide gabbronorite, and olivine gabbro, compose ~74% of the core from Site 1275. Diabase composes an additional 10% of the core, particularly

in a thick interval at the top of Hole 1275B. The gabbroic rocks are characterized by large variations in mineral proportions and textures on short length scales (Fig. F55), such that the longest interval with homogeneous grain size and mineral proportions is only a few meters. Contacts between contrasting lithologies are generally sharp and planar, though "crenelated" contacts are also observed in dozens of intervals (Fig. F56). Diabase contacts with gabbroic rocks are very sharp. However, there is a gradation in grain size between coarse-grained diabase and fine-grained gabbroic rocks. Thus, the range of grain sizes appears to represent a continuum and we tentatively infer that the gabbroic sections were constructed by multiple intrusions that continued over a range of temperatures and cooling rates. Although steep contacts are locally observed, the great majority of contacts between contrasting gabbro and diabase units have dips <30°, so that—unless the section has undergone tectonic rotations of >30°—it is probable that most of the intrusions were subhorizontal sills.

Diabase and fine-grained gabbros have compositions that resemble basaltic liquid compositions. If they are liquid compositions, the melt was relatively primitive, with Mg# = ~60%. This is striking, because the coarser gabbroic rocks from Site 1275 are probably cumulates formed by crystallization of substantially more evolved melts. We interpret these rocks as cumulates because they have low incompatible element abundances (e.g., low Zr) compared to evolved MORB at the same, or even higher, Mg#. However, there is little sign of the complementary evolved melts that formed these cumulates, either in core from Site 1275 or among erupted lavas from the 14°–16°N region.

Granophric dikes and veins are a minor but ubiquitous part of the gabbroic core. These might conceivably represent melts in equilibrium with the evolved cumulate gabbros, but if so there must be a much larger volume of lava or intrusive rocks with the same composition somewhere else. The granophyres have sharp to completely gradational contacts with host gabbros and probably represent small amounts of highly evolved melt that were extracted from the gabbros in their last stages of crystallization and then ascended to intrude other gabbros higher in the section.

Granophyres locally show complex mingling relationships with host gabbros, and even host diabase. Similarly, some contacts between contrasting gabbroic units also show complex mingling and some fine-grained gabbroic units contain coarse pyroxene crystals that are tentatively interpreted as xenocrysts derived locally from coarser gabbroic host rocks. Thus, the multiple intrusions that constructed the Site 1275 gabbro section occurred while earlier crystallized gabbroic rocks were still partially molten. This process of repeated intrusion led to mingling and, probably, to magma mixing.

Olivine gabbros were only observed in lower portions of Hole 1275D. Unfortunately, these samples were recovered after the shipboard geochemistry laboratory closed for transit to Bermuda. Thus, it is not certain whether these rocks are primitive cumulates, liquidlike compositions, or simply evolved gabbros including olivine.

Aside from the olivine gabbros, the diabases, and one or two fine-grained gabbros with high Mg#s, the gabbroic rocks from Site 1275 that we analyzed have evolved compositions with low Mg# and high incompatible element concentrations. Such evolved compositions appear to be typical of gabbroic intrusions into peridotite that have previously been sampled by dredging and submersibles along the mid-ocean ridges (e.g., Cannat, 1993; Cannat et al., 1992). The common observation of evolved gabbroic intrusions into mantle peridotite poses an interesting conundrum. Evolved lavas with compositions that could crystallize such iron- and titanium-rich gabbroic cumulates have not been sampled in the 14° to 16°N area. By the same token, basalt compositions from the Mid-Atlantic Ridge in this area record fractional crystallization of a relatively primitive cumulate assemblage.

In fact, this problem is more general. As shown in Figures F57 and F58, truly primitive cumulates are rare among oceanic samples, even in the thick gabbroic sequences at ODP Sites 735, 921, and 923 that

have been interpreted as parts of a lower crustal gabbro section beneath sheeted dikes in "typical" layered oceanic crust (e.g., Cannat et al., 1995; Dick et al., 2002; Natland and Dick, 2002). Because average mid-ocean-ridge basalts have about twice as much zirconium and other incompatible elements as primitive mid-ocean-ridge basalts, the average lavas record fractional crystallization of ~50% mafic cumulates, of which at least one-half must have Mg#s > 70%. In contrast, the average Mg# of rocks recovered from Sites 735, 921, and 923 is 67%–71%. It is clear that a substantial proportion of more primitive cumulates has formed beneath the mid-ocean ridges. However, these primitive cumulates have rarely been sampled.

During Leg 209, only the gabbronorites from Site 1268 have the high Mg# and low incompatible element concentrations required for the primitive cumulates complementary to fractionation of typical mid-ocean-ridge basalts. This is intriguing because, as for the troctolites at Site 1275, the Site 1268 gabbronorites include igneous orthopyroxene. Mid-ocean-ridge basalts are saturated in orthopyroxene only at subcrustal pressures (see discussion of troctolite genesis, above). As we outlined in "**Site 1268**," if the Site 1268 gabbronorites formed from primitive basalts, they must have crystallized at relatively high pressure (perhaps ~0.3–0.4 GPa) within an upper mantle thermal boundary layer beneath the Moho. However, we caution readers that the Site 1268 gabbronorites are highly altered, and alteration may have modified the bulk rock Mg#, so that full evaluation of this hypothesis awaits shore-based analysis of relict clinopyroxene crystals.

The depth of crystallization of the relatively evolved gabbroic rocks at Site 1275 is not well constrained. If the earliest formed gabbroic rocks are temporally related to the melts that crystallized impregnations of plagioclase and pyroxene in the troctolites, then they must have crystallized at depths of 12–20 km, driven by slow conductive cooling near the base of the thermal boundary layer, with initial magmatic temperatures of ~1200°C. The aphanitic texture of the diabase intrusions, on the other hand, suggests that they cooled relatively quickly. Since some diabases show mingling with hornblende-bearing granophyre, these diabases must have intruded while the host rocks were still above the fluid-saturated granite/trondjhemite solidus at ~700°C. Other massive diabases, particularly those at the top of Hole 1275B, may have intruded even colder wallrocks, perhaps at shallow depths. Again, we infer that the igneous construction of the gabbroic section took place via multiple intrusions, with wallrock temperatures varying over time from ~1200°C to <700°C. Probably, this process also took place over a range of depths, beginning at 12–20 km and ending near the seafloor. Alternatively, if the crystallization of the gabbroic rocks at Site 1275 was not temporally related to the impregnation of the troctolites, then crystallization of the gabbroic section could have taken place over a more restricted range of temperature and pressure. We hope that oxide-silicate thermobarometry on oxide gabbro and gabbronorite samples from Site 1275 will help to distinguish between these different possibilities.

Hydrothermal Alteration, Metamorphism, and Metasomatism

Metasomatic Changes in Troctolite

As for carbonate-altered peridotites from previous sites on this leg, some troctolites from Site 1275 include abundant carbonate veins. CO_2 contents in these rocks range up to 9 wt% and are correlated with CaO contents. As was proposed in "**Site 1274**" in the discussion of metasomatism of altered peridotites, it could be that the troctolites have been modified by metasomatic addition of Ca as well as CO_2. However, this is unlikely. The troctolites contain substantial Al_2O_3, abundant plagioclase and plagioclase pseudomorphs and only minor amounts of spinel. Thus, most of the Al_2O_3 in these rocks must have originally been in plagioclase. If so, CaO is required to form the anorthite component in the plagioclase. CIPW norms for the anhydrous, CO_2-free compositions of the troctolites include very little

clinopyroxene, and some have trace amounts of normative corundum. Thus, most or all of the calcium currently present in the troctolites is required to balance the Al_2O_3 in plagioclase. As a result, we tentatively conclude that CO_2 was added to the troctolites during hydrothermal metasomatism but that calcium was relatively immobile during this process.

Mainly Static Alteration

Alteration intensity in Holes 1275B and 1275D decreases with increasing depth. Cataclastically deformed gabbroic rocks and diabase and a talc amphibole schist with an ultramafic protolith are abundant in the first five cores of Hole 1275D, and these show 50%–100% amphibolite to greenschist facies alteration. The cataclastic deformation is probably related to the fault(s) that formed the top of the bathymetric dome at Site 1275. However, below this fault-related cataclastic deformation, hydrothermal alteration of the troctolites and gabbroic rocks at Site 1275 took place almost entirely under static conditions along microcracks that lack a systematic preferred orientation and possibly formed during cooling. This static alteration is very different from what has been observed in the thick gabbroic sections at ODP Sites 735, 921, and 923, where alteration intensity is highest in zones of penetrative crystal-plastic deformation that occur throughout the section.

Structural Geology

Crystal-plastic deformation is rare in samples from Site 1275. Only a few gabbros show evidence for dynamic recrystallization of plagioclase. Evidence of minor strain, in the form of bent plagioclase with undulatory extinction and deformation twinning, is present throughout Holes 1275B and 1275D, but this reflects minor high-temperature deformation of the type that may be common during igneous compaction of gabbroic intrusions.

Brittle deformation, in the form of cataclastic breccias and semibrittle schists, is common in the upper 15 m of Hole 1275B and the upper 50 m of Hole 1275D. The difference in depth of cataclastic deformation in the two holes may be related to the greater thickness of relatively weak, altered troctolite in Hole 1275D compared to Hole 1275B. Cataclastic breccias are commonly (always?) developed from gabbroic protoliths, whereas semibrittle schists have mainly ultramafic protoliths. The intensity of brittle deformation decreases markedly downhole in Holes 1275B and 1275D. This is consistent with the hypothesis that the brittle deformation is mainly related to the fault zone that likely forms the top of the topographic dome at Mt. Mike.

Two fascinating observations are that there are fine-grained diabase clasts—and perhaps even chilled diabase material within the matrix—in some cataclastic breccias and that diabase intrusions form deformed lenses, possibly preserving chilled margins, within semibrittle schists. These observations—whose interpretations are still uncertain—may be consistent with the presence of a thick and largely undeformed diabase intrusion in the top 18 m of Hole 1275B. We suggest that diabase sills intruded along the fault zone at the top of Mt. Mike, penecontemporaneously with continued slip on the fault.

Metamorphic veins in core from Site 1275 do not show any preferred orientation and thus may have followed cracks that formed as a consequence of nearly hydrostatic stresses during cooling of the igneous rocks.

Magmatic banding or layering in gabbroic rocks is defined by sharp contacts between lithologies with different proportions of minerals and/or different grain sizes and by plagioclase shape fabrics. This magmatic banding is subhorizontal. Contacts between granophyres and gabbroic host rocks are irregular, but a significant subset have steep dips, >70°. Since the statistical probability of sampling steeply dipping

features in a vertical drill hole is very small compared with the probability of intersecting equally abundant horizontal features (i.e., features with the same width and density), we can infer that near-vertical granophyre veins are much more abundant within the Site 1275 gabbroic rocks than subhorizontal granophyre veins. Because the evolved melt that formed the granophyre was much less dense than the host gabbros, one possible interpretation is that the steeply dipping granophyres crosscut the gabbros as near-vertical dikes and veins (as, for example, in the "transgressive granophyres" of the Skaergaard intrusion [Wager and Brown, 1997, figs. 101 and 105 and accompanying text; Hirschmann et al., 1992]) and thus that the section has not undergone large rotations around near-horizontal axes since the formation of the granophyres. If so, this places an important constraint on the direction and magnitude of possible tectonic rotations of the gabbroic section at Site 1275. Alternatively, the majority of the tranophyres with steep dips could have formed as subhorizontal "segregation sheets" (e.g., review in Boudreau and Philpotts, 2002). In this case, one would infer that the section could have undergone almost 90° of rotation around a nearly horizontal axis.

Five of six diabase/gabbro contacts are subhorizontal. If the gabbroic rocks have not undergone substantial tectonic rotations around a horizontal axis, this indicates that the diabases were intruded as sills emplaced in gabbro. In this case, many of the other subhorizontal magmatic layers could also be sills, intruded into preexisting gabbroic rocks while the growing plutonic complex was at relatively high temperatures. These observations and inferences are consistent with the idea that gabbroic sections beneath some mid-ocean ridges, and perhaps some layered intrusions, form via multiple injection of "sheeted sills" (Bédard et al., 1988; Bernstein et al., 1992, 1996; Browning, 1984; Browning et al., 1989; Kelemen and Aharonov, 1998; Kelemen et al., 1997b; Korenaga and Kelemen, 1997, 1998). Alternatively, if the steeply dipping granophyres at Site 1275 were emplaced as subhorizontal segregation sheets, then most of the contacts between diabase and gabbro and between different gabbro units probably formed with a near-vertical orientation. Whereas dominantly vertical contacts between different gabbroic units are rare in large intrusions, such structures are observed in specific plutons such as the large, shallow-level Lilloise intrusion, intruding Tertiary flood basalts in East Greenland (Chambers and Brown, 1995). And, finally, we emphasize to readers that in presenting two alternative interpretations of these structures, we do not mean to imply that this is an exhaustive list of possibilities. Instead, we simply present two ideas which seem plausible based on our preliminary data.

Paleomagnetic Data and Tectonics

Paleomagnetic data were collected on half cores and individual discrete samples. Using these data, we rotated the measured orientations of foliations, faults, veins, and dikes in individual core pieces around a vertical axis, thereby restoring core pieces to an orientation with a common azimuth for the remanent magnetization vector.

In Hole 1275B, half-core measurements and discrete samples all have negative stable inclinations, suggesting that the rocks are reversely polarized. Rotation of structural features around a vertical axis into a common remanent magnetization direction yields two important results. First, magmatic layering in the gabbroic rocks forms a relatively tight cluster on a lower hemisphere stereo plot, with an average dip of ~20°. Second, although many granophyre/gabbro contacts also have shallow dips, there is a distinct population with near-vertical dips. These are roughly perpendicular to the average attitude of layering in the gabbros. As explained in the previous section of this summary, these observations could be consistent with two different end-member scenarios. In the first scenario, we interpret the steeply dipping granophyre/gabbro contacts as defining the paleovertical direction during granophyre intrusion. In this

view, the nearly horizontal present-day attitude of the gabbro layering probably indicates that these formed as subhorizontal layers. Alternatively, the steeply dipping granophyres could have formed as subhorizontal sheets, in which case the section has undergone large tectonic rotations.

The average remanent inclination for 26 discrete samples of gabbro and diabase from Hole 1275B is –9.5° (95% CI = +3.9°/–3.7°), which agrees well with data on inclination for archive half cores. The average remanent inclination for 34 discrete samples from Hole 1275D is –3.5° (95% CI = +7.0°/–6.7°), also in reasonable agreement with data on inclination for archive half cores. The values for gabbroic rocks are not statistically different.

Discrete sample data for Hole 1275B were all quite similar, but in Hole 1275D there were several samples (particularly troctolites and diabases in the upper 50 m of the hole) that have scattered but positive inclinations. One sample of troctolite contains two nearly antipodal magnetization components. These data suggest that both normal and reversed polarity magnetizations are recorded in Hole 1275D samples. Acquisition of an early reversed polarity magnetization probably occurred via cooling of igneous magnetite through 500°–600°C. Acquisition of a later normal polarity magnetization could have occurred during crystallization of secondary finer-grained metamorphic magnetite associated with serpentinization of olivine in the troctolites and/or during local reheating of fine-grained magnetite in the rocks associated with late intrusion of some of the diabase sills and dikes. Removal of troctolite and diabase samples with positive inclinations from the data set for Hole 1275D yields an average inclination of approximately –12° for the remaining samples, which is even more consistent with the data from Hole 1275B than the average for the entire Hole 1275D data set.

The average inclination of approximately –10° to 12° in gabbroic rocks from Site 1275 is significantly lower than the expected inclination of –28° for rocks with a reversed polarity magnetization. These data suggest that block rotation has affected the section sampled at Site 1275, as found for Sites 1268, 1270, 1272, 1274, and 1275, where remanent magnetic inclinations also require substantial rotation of the section. For Sites 1268 and 1270, we inferred that rotation axes were probably near horizontal and parallel to the normal faults that form steep slopes along the rift valley. At Sites 1272, 1274, and 1275, the choice of a tectonically reasonable rotation axis is less clear.

Decreasing the inclination from –28° to –11° in the gabbroic rocks from Site 1275 requires a minimum of 17° of counterclockwise rotation around a horizontal rotation axis with an azimuth of 270° or larger rotations around axes parallel to the trend of the rift valley (~020°). One option is that the section has indeed been rotated ~17° around a near-horizontal east-west axis. This is consistent with the first structural interpretation discussed above, in which the steeply dipping granophyres formed as near-vertical intrusions into horizontally layered gabbros. However, we cannot rule out the possibility that the steeply dipping granophyres were originally subhorizontal and the section has undergone large rotations, for example, around a nearly horizontal axis parallel to the rift valley walls, as inferred for Sites 1268 and 1270. And again, we emphasize that in listing two alternatives we do not mean to imply that this list is exhaustive. There may be many other interpretations that are consistent with our data.

We are confident that continuing analysis of the structural and paleomagnetic data will place additional constraints on the tectonic history of Mt. Mike. For example, the Hole 1275 data may offer the opportunity for another refinement. There seems to be a significant difference between the magnetic inclinations in gabbroic rocks from ~50 to 140 mbsf, which averages approximately –6°, and magnetic inclinations of approximately –15° in gabbroic rocks from 150 to 209 mbsf (Fig. F59). This may reflect smaller amounts of tectonic rotation in the bottom of Hole 1275D compared to the middle of Hole 1275D and the entire section sampled in Hole 1275B.

OPERATIONS

Port Call: Rio de Janeiro

Leg 209 began at 0956 hr on 6 May 2003 as the first line ashore at Berth 3, Porto Praca Maua, Rio de Janeiro, Brazil, ended Leg 208. Pacing items for the port call included resupply of fuel and drill mud bulk, loading casing scheduled for deployment during Leg 210, and installation of a remote diagnostic system for the active heave compensator (AHC). A complete overhaul and test of the drawworks transmission was also completed during the port call.

Two power outages traced to a faulty transformer occurred on the *JOIDES Resolution* early on the morning of 10 May. Repairing the transformer ultimately became the primary port call pacing item and resulted in a 1-day delay in our scheduled departure. After rotating the ship 180° to load a new spool of drilling cable on the starboard side, mooring lines were released and the last line was brought aboard at 0912 hr on 12 May. The pilot departed at 0954 hr, and the vessel got under way at full speed for the 2627-nmi transit to our first site.

Transit to Site 1268

Transit speed over our first 4 days at sea averaged 11.3 kt. During the transit an air sampling system for airborne microbial study was modified and mounted at the water table level of the derrick.

At 0925 hr on 15 May, the ship's master was informed that the Overseas Drilling Ltd. Electrical Supervisor required medical evacuation. At 0946 hr we changed course to 328° and steamed toward the port of Aracaju, Brazil, 109 nmi away. At 1654 hr we arrived at our rendezvous location (11°18′S, 36°45′W) and proceeded at reduced speed until arrival of a medivac helicopter. Brazilian police helicopter PT-HVA was on board by 1726 hr and departed at 1731 hr. We immediately resumed full speed, changed course to 055°, and proceeded up the eastern coast of Brazil. Overall impact to the leg for the medivac operation was an additional ~60 nmi steaming, or ~5 hr.

During the next 6 days of our transit we averaged 11.7 kt, until a wind heading change and the Equatorial Counter Current slowed our speed. We arrived at Site 1268 at 0500 hr the morning of 22 May. Our transit totaled 2680 nmi at an average speed of 11.4 kt.

Site 1268

The planned location of Site 1268 was revised during transit from Rio de Janeiro after detailed review of the video tapes from *Shinkai* 6500 Dive 427 in 1998. The site was to be in thin sediments at ~3011 meters below sea level (mbsl), overlying a flat, planar outcrop of serpentinized peridotite (probably a fault surface) visible a few meters downslope. Upon arrival at the planned location, the precision depth recorder (PDR) in the underway geophysics laboratory indicated a depth of ~2896 meters below rig floor (mbrf) (2885 mbsl), quite different from the expected depth. Given that submersible dive navigation can be uncertain, we undertook a PDR survey of the seafloor to the southeast (downslope). While making up the drilling assembly, the first 8-1/4-in drill collar, the rig crew discovered a significant crack in the stress relief groove of the pin thread. This collar was laid aside and we decided to magnaflux inspect the remaining eight drill collars in the bottom-hole assembly (BHA). No other cracks were found during the inspection.

While running the drill pipe, we chose a position ~600 m southeast of the originally planned location, with a PDR depth of ~3040 mbsl, to start a camera survey. However, when the camera depth was at ~3080

m, the sonar on the camera sled still could not detect bottom within 100 m. At this point, the ship began moving slowly northwest toward the originally planned site location. Bottom was first detected at ~3180 mbsl at a position ~500 m southeast of the originally planned location. Bathymetry determined during the camera survey conformed closely to bathymetry based on *Shinkai* 6500 Dive 427 at the same latitude and longitude, so we decided that the PDR depths were probably incorrect. At this point, the drill string and camera sled were raised to a bit depth of ~3008 m and the originally planned location for Site 1268 was slowly approached. Again, bathymetry determined from the camera survey at the originally planned location conformed closely to that observed on *Shinkai* 6500 Dive 427, confirming the theory that dive navigation in this case was accurate and PDR depths were incorrect. The close equivalence between camera survey and dive bathymetry indicated that we were very near the originally planned location. Push tests indicated that sediment thickness was ~4 m, slightly thicker than anticipated but within acceptable limits. The positioning beacon was released from the vibration-isolated television (VIT) frame ~20 m away from the identified spud location prior to recovering the VIT.

Hole 1268A

Before initiating coring we deployed the Water Sampling Temperature Probe (WSTP) to obtain a temperature and a seawater sample for a microbiology contamination baseline analysis. Hole 1268A was spudded at 0620 hr on 23 May (Table T1). After cutting Core 209-1268A-1R the AHC was turned off because of erratic performance. The supporting data were recorded both in the newly installed Maritime Hydraulics (MH) diagnostic computer and the Texas A&M University (TAMU) TruVu rig instrumentation system. TruVu was running in the 1-s capture mode. MH-Norway accessed their diagnostic computer remotely and downloaded the data for analysis. Initial reports indicated a possible problem with the AHC motion reference unit (MRU).

Core 209-1268A-1R advanced to 14.0 meters below seafloor, allowing the bit to stay in the hole during the next connection. A standard rotary core barrel (RCB) core barrel was used without a core liner. All subsequent cores were taken using nonmagnetic chrome-plated inner diameter (ID) core barrels. In order to improve recovery, we opted to retrieve cores nominally every 5 m (half cores).

Sepiolite mud sweeps (10 bbl) were circulated every 10 m, and the hole remained stable through Core 209-1268A-28R at 145.1 mbsf with no fill or overpull during connections. After making a connection prior to cutting Core 209-1268A-29R, the driller noted elevated torque and ~1.0 m of fill in the bottom of the hole. After pumping a pair of 20-bbl sepiolite mud sweeps, all drilling parameters returned to normal. While cutting Core 209-1268A- 29R, drilling parameters indicated the hole had collapsed, stalling the top drive and preventing any further rotation or axial movement of the drill string. After an unsuccessful attempt to free the pipe, we decided to sever the drill string above the BHA. The mate to the severed joint cleared the rig floor at 1930 hr, ending Hole 1269A and drilling operations at Site 1268. The average rate of penetration (ROP) for the hole was 3.9 m/hr.

Transit to Site 1269

Using the ship's dynamic positioning system, we moved ~5 nmi to Site 1269. During the move a two-stand BHA was built consisting of six 8.25-in drill collars. This was done to minimize the risk of losing additional drill collars and jeopardizing further operations. As at Site 1268, all collars were inspected before inclusion in the drill string.

Site 1269

Hole 1269A

Prior to initiating Hole 1269A, we undertook a 1.25 hr subsea camera survey to verify our location as compared to site survey video tapes. The drilling target for Site 1269 was along the track of *Shinkai* 6500 submersible Dive 423 in 1998, which recovered samples of peridotite and gabbro from a series of steep outcrops separated by flat, sedimented seafloor along the western flank of the Mid-Atlantic Ridge axial valley. Our camera survey for Hole 1269A began at a depth where the site survey dive had recovered dunite (*Shinkai* 6500 Dive 423, sample R007). After moving downslope 60 m to ensure we were above an outcrop and in sediment free of talus, we released a positioning beacon from the camera frame 30 m east of our selected drilling target, retrieved the camera, and spudded Hole 1269A.

Hole 1269A was initiated at 1005 hr on 27 May with a seafloor tag depth of 2800 mbsl. Coring continued to a depth of 15.3 mbsf before high drilling torque, collapsing hole, and low recovery (2.6%) consisting of only fragments of basalt led us to terminate coring. At 1425 hr 27 May the bit cleared the seafloor, ending Hole 1269A.

Hole 1269B

Our second subsea camera survey at Site 1269 began with the drill pipe over the positioning beacon. We surveyed 60 m west, continuing along a flat sedimented seafloor, free of talus shed from uphill. A push-in test indicated the sediment was <5 m thick, so we retrieved the camera and spudded Hole 1269B.

At 1950 hr on 27 May, Hole 1269B was initiated with a seafloor tag depth of 2799 mbsl. The first core was recovered after 11.1 m penetration and again contained only a few pieces of basalt. As at Hole 1269A, high torque and recovery of only basalt fragments suggested we would not reach our drilling objectives without first drilling through an unknown thickness of unstable basaltic lava, so we abandoned the hole. The bit cleared the seafloor at 2215 hr on 27 May, ending Hole 1269B. Anticipating a move of ~1 km, we recovered the positioning beacon.

Hole 1269C

With two holes at our most promising target yielding only basalt, we elected to move farther uphill (west) for our next hole at Site 1269. After offsetting the drill ship ~1.1 km west, we conducted our third subsea camera survey at this site. This location was near the top of the western rift valley wall, in a flat, sedimented terrain above a moderate slope from which four samples of gabbro were collected during *Shinkai* 6500 Dive 423. After surveying 275 m upslope, we returned to a position ~65 m west of the start of our camera survey to begin Hole 1269C.

Hole 1269C was initiated at 1118 hr on 28 May. Coring was again hampered by high and erratic torque, and the two core barrels (to a depth of 18.3 mbsf) that were recovered contained only a few fragments of basalt. Recognizing that our favored drilling targets at Site 1269 were all covered with a basaltic carapace beneath a few meters of pelagic sediment, we elected to terminate coring at this site and to move to one of our alternate sites. The drill string and positioning beacon were recovered and we completed operations at Site 1269 at 2000 hr on 28 May.

Transit to Site 1270

Site 1270 is the southernmost of all sites occupied during Leg 209, 16 nmi southeast of Site 1269. Originally planned as an alternate site, this location is on the ridge flank at the eastern limit of the axial valley. The site survey dive tapes reveal an exposed fault surface, and samples of mylonitic peridotite were recovered during the dive. We chose to occupy this site as a result of poor hole conditions and low recovery, including only basalt, at Site 1270.

Site 1270

Hole 1270A

On 28 May, we arrived at the Global Positioning System (GPS) coordinates of a position along the dive track of *Shinkai* 6500 Dive 425 just upslope of where serpentinized peridotite had been sampled from a large outcrop (sample R007). A six-collar BHA (nominally 130 m long) was lowered with the drill string, and the subsea camera was deployed. After a ~3.5-hr survey, where we recognized several intervals of bare rock exposure, we selected a drilling target ~150 m west of our camera survey starting position.

Hole 1270A was initiated with slow rotation and low bit weight at 0500 hr on 29 May. The upper guide horn was removed to allow us to keep the subsea camera near the seafloor as we started the hole, to ensure the bit did not track down slope. After 3 m of penetration, the camera was retrieved and coring continued through Core 209-1270A-4R (0.0–26.9 mbsf). Core 4R contained fault gouge, and our attempt to deepen the hole was hampered by erratic torque on the drill string and wall collapse, filling the borehole. After hole cleaning attempts failed, we pulled clear of the seafloor at 1600 hr on 29 May, ending Hole 1270A.

Hole 1270B

We returned to our original camera survey position, redeployed the subsea camera, and began a survey upslope in search of a new drilling location on a bare rock exposure. We moved 100 m east along an azimuth of ~120° over the path followed by *Shinkai* 6500 Dive 425, then turned south to follow a depth contour where outcrop was evident in the dive video tape. After completing a rectangular box survey pattern, we located an extensive exposure of bare rock ~230 m southeast of Hole 1270A and initiated Hole 1270B.

Coring began at Hole 1270B as at Hole 1270A (at 0200 hr on 30 May) by advancing the bit with slow rotation and low bit weight to 3 mbsf while observing the operation with the subsea camera. After retrieving the camera, we cored to a depth of 45.9 mbsf (Cores 209-1270B-1R to 10M). As we began our third coring interval, the bit would not advance past 13.5 mbsf (1 m deeper than the top of Core 209-1270B-2R). At that depth, coring continued as if we had not already drilled the interval between 13.5 and 17.4 mbsf. Core 209-1270B-3M represents rock recovered in generally same interval as Core 209-1270B-2R (13.5–17.4 mbsf) but contains >1 m of cut core cylinders. When the same blockage was encountered at virtually the same depth on our next coring attempt (13.5 mbsf) we cored beyond the bottom depth of Core 209-1270B-2R and 3M, to 22 mbsf. Since we redrilled the upper part of the interval, the recovered core was curated as Core 209-1270B-4M. Normal coring curation and nomenclature was resumed with Core 209-1270B-5R, when we were sure we were coring a new interval from the beginning of the cored interval. Coring progressed steadily with improving recovery until Core 209-1270B-9R. Hard fill in the bottom of the hole prevented advancement and caused high and erratic torque. Since we were still operating with a reduced-length BHA, we chose not to risk getting the pipe stuck and abandoned the hole at 1205 hr on 31 May.

Hole 1270C

We began our third camera survey at the GPS coordinates of sample R008 from *Shinkai* 6500 Dive 425 where mylonitinized peridotite had been sampled. Unlike outcrops at our two previous holes (bare rock free of talus), the dive video tape revealed this outcrop was littered with what appeared to be slabs of rock, albeit more or less in place. We selected this location upslope from our two previous holes, surmising that if the fault gouge encountered at depth in Hole1270A was a result of incipient landsliding, this older, more weathered outcrop might yield better drilling conditions. After a 2.5-hr survey, we selected a drilling target ~240 m east of Hole 1270B.

Hole 1270C was initiated at 1735 hr on 31 May in a similar manner as for our two previous holes. Coring only progressed to 18.5 mbsf (Cores 209-1270C-1R and 2R) before the hole began to fill, restricting circulation. No advancement was possible on our third coring interval even after 2.5 hr of rotation, so the core barrel was recovered (curated as Core 209-1270C-3M) and the hole was abandoned at 0300 hr on 1 June.

Hole 1270D

The survey for Hole 1270D began over the position of Hole 1270C. We moved only a short distance (~30 m east) and selected a drilling target in bare rock. At 0730 hr on 1 May, Hole 1270D was initiated while we watched the operation with the subsea camera. We cored to 3 mbsf before the camera cable appeared to start wrapping around the drill string. While recovering the camera (without rotating the pipe) the driller became concerned when he was required to advance the pipe to maintain a minimum weight on bit. Upon lowering the camera back to the seafloor, the camera image showed that the bit had slid off the outcrop and embedded in sediment. A second hole initiation (at 0934 on 1 June) was successful to 3 mbsf, so the camera was retrieved and coring continued to 57.3 mbsf. After recovering Core 209-1270D-11R, hole conditions deteriorated to the point that no further advance was possible. The bit was pulled clear of the seafloor, ending operations at Site 1270 at 1445 hr on 2 June. ROP at Site 1270 varied from 3 to 7 m/hr.

Transit to Site 1271

Site 1271 is on the southern end of the inside corner high south of the 15°20′N Fracture Zone, ~19 nmi northwest of Site 1270. We again chose to use a six-collar BHA in order to ensure the preservation of sufficient BHA components for future drilling during this leg.

Site 1271

Hole 1271A

Our camera survey for Hole 1271A began at GPS coordinates between samples of gabbro and peridotite collected during *Faranaut* Dive 7. Our target was a smooth, sedimented slope above an outcrop of gabbro. After a 1.75-hr survey, we confirmed our location was on a shallow, eastward-dipping slope of smooth sediment, and our depth (estimated from drill string length) was consistent with our desired drilling location.

Hole 1271A was initiated at 0545 hr on 3 June through 2.5 m of sediment above a peridotite outcrop. The first core required 4.75 hr to advance to 12.9 mbsf. Cores 209-1271A-2R and 3R, however, cored in at total of 50 min. After recovering Core 209-1271A-5R, hole conditions began to deteriorate and the driller

noted the hole had begun to fill between connections. After only advancing 2.0 m on Core 209-1271A-6R, we decided to abandon any further attempt to core deeper. The bit was pulled clear of the seafloor at 0244 hr, ending Hole 1271A. The average ROP for the hole was 4.5 m/hr.

Hole 1271B

Since the shallow sedimented slope where we located Hole 1271A seemed to be our most promising drilling target (based on *Faranaut* Dive 7 video tapes), we decided to move southwest along the same depth contour to position Hole 1271B. Hole 1271B was spudded ~90 m from Hole 1271A.

At 0730 hr on 4 June we began coring Hole 1271B. Cores 209-1271B-1R to 3R were cored without incident, but while drilling Core 4R the driller suspected that a piece of rock had lodged in the bit throat or the bottom of the core barrel. High circulating pressure eventually cleared the obstruction. After cutting Core 209-1271B-4R, the driller had difficulty getting the pipe back to the bottom of the hole through several meters of hard fill.

Coring continued through Core 209-1271B-20R (103.8 mbsf) with low recovery but little or no indication of poor hole conditions. Having achieved a depth >100 mbsf, we chose to curtail coring operations in order to collect wireline logging data. Coring was completed by 1345 hr on 6 June, and the bit was released in the bottom of Hole 1271B. As the driller attempted to pull the bottom of the pipe to logging depth (nominally 30 mbsf), the hole appeared to collapse around the pipe, shutting off circulation. With some difficulty, the pipe was freed and circulation regained.

After securing the pipe at 30 mbsf, the first logging tool was set up and run into the hole. However, the logging tool would not advance more than 6 m past the end of the pipe, indicating catastrophic hole collapse. Our logging attempt was regretfully abandoned. After the pipe was raised to 2300 mbsl, we recovered the positioning beacons and began the short transit (~3.7 nmi) to our next site. Operations at Site 1271 ended at 0745 hr on 7 June. The average ROP for the hole was 4.0 m/hr.

Transit to Site 1272

Site 1272 is the northernmost of our drilling locations on the transect of sites south of the 15°20′N Fracture Zone, on the northwestern flank of the inside corner high. The site was targeted based on reviews of video tapes from *Faranaut* Dives 5 and 2, near the top of the ridge where most of the dive samples were serpentinized peridotite. Site 1272 is ~3.7 nmi north of Site 1271.

Site 1272

Hole 1272A

Having protected our supply of drill collars during earlier operations, we elected to increase the length of our BHA at this site in order to achieve deeper penetration without placing the top of the BHA below the seafloor. A total of 14 8.25-in drill collars (nominally 131 m long) were lowered at the end of the drill string while we positioned the vessel over the GPS coordinates of our camera survey starting position. We surveyed along a shallow-dipping, sediment-covered slope and selected a drilling target located in flat terrain between the depths of *Faranaut* Dive 2 samples FR02-11 and FR-02-12 (both serpentinized peridotite). A push-in test with the drill string indicated the sediment cover was only ~1 m thick.

Hole 1272A was spudded at 2045 hr on 7 June. Core 209-1272A-1R advanced to 12.9 mbsf. Coring continued through Core 209-1272A-27R to a depth of 131.0 mbsf with no difficulty but slow penetration (average ROP = 2.2 m/hr). Because the core we were recovering was clay rich and we encountered several

intervals of drilling-induced disturbance, we elected to use core liners inside the core barrels to see if recovery might improve. Core liners were used on Cores 209-1272A-21R and 23R through 27R, and recovery improved to values as high as 79% (averaging = ~55% as compared to ~30% recovery in similar lithology cored without liners).

The Drill String Accelerometer (DSA) tool was deployed with Cores 209-1272A-12R and 14R. After coring to 131 mbsf with little change in the character of the recovered core or in drilling conditions, we decided to terminate coring and begin wireline logging.

Two logging tool strings were deployed in the hole. Both the triple combination (triple combo) and Formation MicroScanner (FMS)-sonic tool strings reached within 6–7 m of the bottom of the hole. With logging completed, the pipe was pulled clear of the seafloor at 0245 hr on 12 May. By 0730 hr the ship was secured for transit, ending operations at Site 1272.

Transit to Site 1273

Site 1273 is the southernmost drilling target on our transect of sites north of the 15°20′N Fracture Zone. This site was selected based on review of video tapes from *Faranaut* Dive 16, which recovered samples of peridotite and gabbro.

Site 1273

Hole 1273A

At 1716 hr on 12 June we arrived at the coordinates for the Site 1273 camera survey. While we deployed a BHA including 17 8.25-in drill collars (nominally 159 m long) at the end of the drill string, the subsea camera was lowered along with a positioning beacon. Our camera survey track was from west to east starting on a flat, sedimented terrace, moving downslope until we arrived at the edge of a precipitous cliff. During *Faranaut* Dive 16, the submarine traversed upslope >100 m in <5 min until the seafloor slope sharply decreased at the same water depth as our camera survey. Outcrop was exposed along all of this part of the dive track, and a sample of serpentinized peridotite was collected. Inferring that we were near the same outcrop recorded on the dive survey video tapes, we moved 50 m back up the shallow slope to deploy the beacon, and at 0515 hr on 13 June we initiated Hole 1273A ~30 m west of the cliff edge.

Only one core was recovered from Hole 1273A before we were forced to abandon coring because of borehole wall collapse. Hole 1273A ended at 0920 hr on 13 June as the bit was pulled free of the seafloor.

Hole 1273B

Hole 1273B was spudded at 1050 hr on 13 June, after offsetting the ship ~15 m east (closer to the cliff edge). Cores 209-1273B-2R to 3R penetrated quickly (11.6–26.2 mbsf in <2 hr), and, as at Hole 1273A, the driller could not keep the hole cleared of debris. Hole 1273B was completed by 1900 hr on June 13 as the bit was pulled free of the seafloor.

Hole 1273C

Because our site survey bathymetry data indicated the flat terrace where we drilled Holes 1273A and 1273B continued south for at least 500 m, we began a second subsea camera survey tracking south along the top of the cliff. After moving ~100 m while crossing back and forth across the cliff edge, we located a massive outcrop that we considered an ideal target for coring. At 0100 hr on 14 June we spudded Hole

1273C a few meters west of the cliff in sediment <2 m thick. Core 209-1273C-1R was advanced to 18 mbsf because material collapsing into the hole prevented us from setting the pipe to extract the core barrel. Cores 209-1273C-2R and 3R were difficult to core, as material seemed to be falling into the hole as soon as we stopped coring to make a pipe connection. After recovering Core 209-1273C-3R, the drill pipe would not pass 20 mbsf, indicating 8 m of material had fallen into the bottom of the hole. Given that recovery in all three holes was limited to small fragments of basalt with only two small pieces of peridotite, we chose to end coring attempts at Site 1273.

Transit to Site 1274

After a transit from Site 1273 in dynamic positioning mode with the drill string suspended below the ship, we arrived on the GPS position coordinates for the start of the Hole 1274A subsea camera survey at 0030 hr on 15 June.

Site 1274

Our survey began over a sedimented bottom and tracked ~200 m west, up the side of the western wall of the axial valley of the Mid-Atlantic Ridge, following the path of *Shinkai* 6500 Dive 416. During this dive all recovered samples were serpentinized peridotite. After passing an outcrop at the depth of the final sample of peridotite collected during the dive, we selected a drilling target with a thin sediment cover (<2 m) to initiate Hole 1274A.

Hole 1274A

Before beginning our coring operation, we deployed the WSTP to collect a bottom water sample in support of our microbiology program. Coring continued through 155.8 mbsf (Cores 209-1274A-1R to 28R) with little difficulty. The only problems of note were an easily cleared bit blockage experienced after recovering Core 209-1274A-11R and minor amounts of fill collapsing into the hole between pipe connections. Cores 209-1274A-15R, 20R, and 21R were cut as full ~9.6-m intervals (as opposed to the nominal half cores that we recovered throughout the rest of the hole) because of rapid penetration through those depths (74.0–83.7 and 102.9–122.1mbsf, respectively). After we recovered Core 209-1274A-28R, the hole collapsed and cut off circulation through the drill string. Pipe was pulled from the hole while attempting to restore circulation, without success, so we released the bit and abandoned Hole 1274A. The average ROP for Hole 1274A was 4.9 m/hr.

Transit to Site 1275

After a brief ~10-nmi transit west from Site 1274, we arrived at Site 1275.

Site 1275

At 0445 hr on 19 June, we began a camera survey on the top of a large dome, surveyed by the 1998 *Shinkai* 6500 Dive 422. During that dive, gabbro and peridotite were recovered from the southern flank of the dome. Our first drilling target was smooth, slabby outcrops on the north end of the dome summit.

Hole 1275A

Our camera survey for Hole 1275A required <2 hr, and we selected a target on a bare rock outcrop. We initiated coring at 0815 hr at a water depth of 1563 mbsf. In an attempt to recover the uppermost surface of the outcrop, we elected to recover the core barrel after only 5 m of penetration. Because we had to lift the pipe above seafloor in order to have the proper pipe spacing at the rig floor to extract the core barrel, Core 209-1275A-1R was the only core recovered from this hole.

Hole 1275B

In an attempt to remain on or at least very near the outcrop where we cored Hole 1275A, we moved 4 m south in dynamic positioning mode to begin Hole 1275B. Core 209-1275B-1R was cored to a depth of 11.0 mbsf and required >10 hr to drill. Coring continued through Core 209-1275B-22R (108.7 mbsf). Because our rate of penetration early in the hole was so low and the bit had been used for nearly 80 hr of coring, we chose to terminate coring to attempt logging while coring (LWC) at a nearby location. We did not release the bit in the bottom of the hole, so we would have the option to attempt a bare hole reentry, then deepen and log Hole 1275B if time allowed. The location of Hole 1275B was marked with a glass float deployed from the subsea camera frame prior to abandonment. The average ROP for the hole was only 1.4 m/hr.

Hole 1275C

Our target for the LWC operation was, in our estimation, the most optimum location for high recovery occupied during Leg 209. We selected a drilling location at the site of an outcrop where the precruise dive survey had collected serpentinized plagioclase-bearing peridotite. This site was ~90 m south of Holes 1275A and 1275B. Relatively high recovery in hard rock from nearby Hole 1275B (>43%), combined with shallow water and calm seas, should have made for ideal deployment conditions. We deployed a standard eight-collar BHA, as memory on the LWC tool (resistivity at the bit with coring [RAB-C]) is only 70 rotating hr in its current configuration, and we did not expect to penetrate more than ~70 mbsf in that time.

After conducting a brief (1 hr) subsea camera survey, we located an outcrop near the coordinates where peridotite was sampled during the *Shinkai* 6500 dive. Hole 1275C was initiated at 0445 hr on 24 June, with the same slow penetration rate we experienced in Hole 1275B. However, after three cores and nearly 20 hr of operations we had reached only 20.8 mbsf and the three core barrels we recovered were either empty (Core 209-1275C-1R) or contained only one or two small rounded cobbles of rock. Compared to recovery on initial cores from all our previous drilling locations, recovery with the RAB-C was significantly poorer than with our convention rotary system (see Fig. 60). Based on poor recovery, we abandoned Hole 1270C.

Hole 1275D

In an attempt to ensure the deepest penetration possible in the time we had left, we deployed a 22-collar BHA in preparation for coring Hole 1275D. We offset 4 m west from Hole 1275C and began coring Hole 1275D at 1025 hr on 25 June. Coring in the same interval at the RAB-C (Cores 209-1275D-1R to 3R; 0–17.6 mbsf) yielded 32% recovery. This was the highest rate of recovery from the first three cores from any hole drilled during Leg 209. Coring continued through Core 209-1275D-43R (209 mbsf), averaging >50% recovery. We terminated coring at 0915 hr on 30 June in order to leave time for wireline logging.

The average ROP for Hole 1275D was 2.4 m/hr. Wireline logging failed to pass an obstruction at ~103 mbsf, but two tool strings (triple combo and FMS-sonic) were deployed over the interval 103–20 mbsf. The pipe was pulled clear of the seafloor at 0515 hr on July 1, ending operations for Leg 209, and after recovering the pipe, we began our transit to Bermuda.

Transit to Bermuda

The highlight of the transit was a sampling party for shipboard scientists' postcruise research Nearly 400 sections of core (the complete volume of >350 m of core recovered during Leg 209) were arranged throughout the upper two floors of the lab stack.

The 1410-nmi transit was completed at an average speed of 11.6 kt. Leg 209 ended with the first line ashore at Market Wharf, St. George, Bermuda, at 1715 hr on 6 July 2003.

REFERENCES

Agar, S.M., and Lloyd, G.E., 1997. Deformation of Fe-Ti oxides in gabbroic shear zones from the MARK area. *In* Karson, J.A., Cannat, M., Miller, D.J., and Elthon, D. (Eds.), *Proc. ODP, Sci. Results,* 153: College Station, TX (Ocean Drilling Program), 123–141.

Aharonov, E., Whitehead, J.A., Kelemen, P.B., and Spiegelman, M., 1995. Channeling instability of upwelling melt in the mantle. *J. Geophys. Res.*, 100:20433–20450.

Amri, I., Benoit, M., and Ceuleneer, G., 1996. Tectonic setting for the genesis of oceanic plagiogranites: evidence from a paleo-spreading structure in the Oman ophiolite. *Earth Planet. Sci. Lett.,* 139:177–194.

Arai, S., and Matsukage, J.H., 1996. Petrology of gabbro-troctolite-peridotite complex from Hess Deep, equatorial Pacific: implications for mantle–melt interaction within the oceanic lithosphere. *In* Mével, C., Gillis, K.M., Allan, J.F., and Meyer, P.S. (Eds.), *Proc. ODP, Sci. Results,* 147: College Station, TX (Ocean Drilling Program), 135–155.

Axen, G.J., and Bartley, J.M., 1997. Field tests of rolling hinges; existence, mechanical types, and implications for extensional tectonics. *J. Geophys. Res.,* 102:20515–20537.

Baker, M.B., and Stolper, E.M., 1994. Determining the composition of high-pressure mantle melts using diamond aggregates. *Geochim. Cosmochim. Acta,* 58:2811–2827.

Barclay, A.H., Toomey, D.R., and Solomon, S.C., 1998. Seismic structure and crustal magmatism at the Mid-Atlantic Ridge, 35°N. *J. Geophys. Res.*, 103:17827–17844.

Barnouin-Jha, K., Parmentier, E.M., and Sparks, D.W., 1997. Buoyant mantle upwelling and crustal production at oceanic spreading centers: on-axis segmentation and off-axis melting. *J. Geophys. Res.*, 102:11979–11989.

Barth, G.A., and Mutter, J.C., 1996. Variability in oceanic crustal thickness and structure: multichannel seismic reflection results from the northern East Pacific Rise. *J. Geophys. Res.,* 101:17951–17975.

Bédard, J., Sparks, R.S.J., Renner, R., Cheadle, M.J., and Hallworth, M.A., 1988. Peridotite sills and metasomatic gabbros in the Eastern Layered Series of the Rhum complex. *J. Geol. Soc.,* 145:207–224.

Bee, M., and Bibee, L.D., 1989. A seismic refraction study of Cretaceous oceanic lithosphere in the northwest Pacific Basin. *Mar. Geophys. Res.,* 11:239–261.

Behn, M.D., and Kelemen, P.B., in press. Relationship between seismic *P*-wave velocity and the composition of anhydrous igneous and meta-igneous rocks. *Geochem. Geophys. Geosyst.*

Benoit, M., Polve, M., and Ceuleneer, G., 1996. Trace element and isotopic characterization of mafic cumulates in a fossil mantle diapir (Oman ophiolite). *Chem. Geol.,* 134:199–214.

Bernstein, S., Kelemen, P.B., and Brooks, C.K., 1996. Evolution of the Kap Edvard Holm complex: a mafic intrusion at a rifted continental margin. *J. Petrol.,* 37:497–519.

Bernstein, S., Rosing, M.T., Brooks, C.K., and Bird, D.K., 1992. An ocean-ridge type magma chamber at a passive volcanic, continental margin: the Kap Edvard Holm layered gabbro complex, East Greenland. *Geol. Mag.,* 129:437–456.

Bonatti, E., Peyve, A., Kepezhinskas, P., Kurentsova, N., Seyler, M., Skolotnev, S., and Udintsev, G., 1992. Upper mantle heterogeneity below the Mid-Atlantic Ridge, 0°–15°N. *J. Geophys. Res.,* 97:4461–4476.

Boudier, F., and Coleman, R.G., 1981. Cross section through the peridotite in the Samail ophiolite, southeastern Oman Mountains. *J. Geophys. Res.,* 86:2573–2592.

Boudier, F., Godard, M., and Armbruster, C., 2000. Significance of gabbronorite occurrence in the crustal section of the Semail ophiolite. *Mar. Geophys. Res.,* 21:307–326.

Boudier, F., MacLeod, C.J., and Bolou, L., 1996. Structures in peridotites from Site 895, Hess Deep: implications for the geometry of mantle flow beneath the East Pacific Rise. *In* Mével, C., Gillis, K.M., Allan, J.F., and Meyer, P.S. (Eds.), *Proc. ODP, Sci. Results,* 147: College Station, TX (Ocean Drilling Program), 347–356.

Boudier, F., and Nicolas, A., 1995. Nature of the Moho transition zone in the Oman ophiolite. *J. Petrol.,* 36:777–796.

Boudier, F., Nicolas, A., and Ildefonse, B., 1996. Magma chambers in the Oman ophiolite: fed from the top and the bottom. *Earth Planet. Sci. Lett.,* 144:239–250.

Boudreau, A.D., and Philpotts, A.R., 2002. Quantitative modeling of compaction in the Holyoke flood basalt flow, Hartford Basin, Connecticut. *Contrib. Mineral. Petrol.,* 144:176–184.

Bougault, H., Appriou, P., Bienvenu, P., Cambon, P., Charlou, J.L., Collette, B., Donval, J.P., Dosso, L., Floch, G., Fouquet, Y., Morvan, M., Pelle, H., Poncin, J., Thieblemont, D., Vangriesheim, A., and Needham, H.D., 1990. Campagne RIDELENTE: structure de la dorsale Atlantique heterogeniete du manteau et hydrothermalisme. *Spec. Publ.—Oceanol. Acta,* 10:366–381.

Bougault, H., Charlou, J.L., Fouquet, Y., Needham, H.D., Vaslet, N., Appriou, P., Baptiste, P.J., Rona, P.A., Dmitriev, L., and Silantiev, S., 1993. Fast and slow spreading ridges: structure and hydrothermal activity, ultramafic topographic highs, and CH_4 output. *J. Geophys. Res.,* 98:9643–9651.

Bougault, H., Dmitriev, L., Schilling, J.G., Sobolev, A., Joron, J.L., and Needham, H.D., 1988. Mantle heterogeneity from trace elements: MAR triple junction near 14°N. *Earth Planet. Sci. Lett.,* 88:27–36.

Bratt, S.R., and Purdy, G.M., 1984. Structure and variability of oceanic crust on the flanks of the East Pacific Rise between 11° and 13°N. *J. Geophys. Res.,* 89:6111–6125.

Bratt, S.R., and Solomon, S.C., 1984. Compressional and shear wave structure of the East Pacific Rise at 11°20′N: constraints from three-component ocean bottom seismeter data. *J. Geophys. Res.,* 89:6095–6110.

Braun, M.G., Hirth, G., and Parmentier, E.M., 2000. The effects of deep damp melting on mantle flow and melt generation beneath mid-ocean ridges. *Earth Planet. Sci. Lett.,* 176:339–356.

Braun, M.G., and Kelemen, P.B., 2002. Dunite distribution in the Oman ophiolite: implications for melt flux through porous dunite conduits. *Geochem. Geophys. Geosyst.,* 3:10.1029/2001GC000289.

Browning, P., 1984. Cryptic variation within the cumulate sequence of the Oman ophiolite: magma chamber depth and petrological implications. *In* Gass, I.G., Lippard, S.J., and Shelton, A.W. (Eds.), *Ophiolites and Oceanic Lithosphere*. Spec. Publ.—Geol. Soc. London, 13:71–82.

Browning, P., Roberts, S., and Alabaster, T., 1989. Fine-scale modal layering and cyclic units in ultramafic cumumlates from the CY-4 borehole, Troodos ophiolite: evidence for an open system magma chamber, in drillhole CY-4, the Troodos ophiolite, Cyprus. *In* Gibson, I.L., Malpas, J., Robinson, P.T., and Xenophontos, C. (Eds.), *Cyprus Crustal Study Project: Initial Report, Hole CY-4*. Pap.—Geol. Surv. Can., 193–220.

Buck, W.R., and Su, W., 1989. Focused mantle upwelling below mid-ocean ridges due to feedback between viscosity and melting. *Geophys. Res. Lett.,* 16:641–644.

Burnard, P., Graham, D., and Turner, G., 1997. Vesicle-specific noble gas analyses of "popping rock": implications for primordial noble gases in Earth. *Science,* 276:568–571.

Canales, P.J., Detrick, R.S., Bazin, S., Harding, A.J., and Orcutt, J.A., 1998. Off-axis crustal thickness across and along the East Pacific Rise within the MELT area. *Science,* 280:1218–1221.

Canales, P.J., Detrick, R.S., Lin, J., and Collins, J., 2000. Crustal and upper mantle seismic structure beneath the rift mountains and across a nontransform offset at the Mid-Atlantic Ridge (35°N). *J. Geophys. Res.,* 105:2699–2719.

Canales, P.J., Detrick, R.S., Toomey, D.R., and Wilcock, W.S.D., 2003. Segment-scale variations in the crustal structure of 150–300 kyr old fast spreading oceanic crust (East Pacific Rise, 8°15′N–10°5′N) from wide-angle seismic refraction profiles. *Geophys. J. Int.,* 152:766–794.

Cannat, M., 1993. Emplacement of mantle rocks in the seafloor at mid-ocean ridges. *J. Geophys. Res.,* 98:4163–4172.

————, 1996. How thick is the magmatic crust at slow-spreading oceanic ridges? *J. Geophys. Res.,* 101:2847–2857.

Cannat, M., Bideau, D., and Bougault, H., 1992. Serpentinized peridotites and gabbros in the Mid-Atlantic Ridge axial valley at 15°37′N and 16°52′N. *Earth Planet. Sci. Lett.,* 109:87–106.

Cannat, M., and Casey, J.F., 1995. An ultramafic lift at the Mid-Atlantic Ridge: successive stages of magmatism in serpentinized peridotites from the 15°N region. *In* Vissers, R.L.M., and Nicolas, A. (Eds.), *Mantle and Lower Crust Exposed in Oceanic Ridges and Ophiolites:* Dordrecht (Kluwer), 5–34.

Cannat, M., Chatin, F., Whitechurch, H., and Ceuleneer, G., 1997a. Gabbroic rocks trapped in the upper mantle at the Mid-Atlantic Ridge. *In* Karson, J.A., Cannat, M., Miller, D.J., and Elthon, D. (Eds.), *Proc. ODP, Sci. Results,* 153: College Station, TX (Ocean Drilling Program), 243–264.

Cannat, M., Karson, J.A., Miller, D.J., et al., 1995. *Proc. ODP, Init. Repts.,* 153: College Station, TX (Ocean Drilling Program).

Cannat, M., Lagabrielle, Y., Bougault, H., Casey, J., de Coutures, N., Dmitriev, L., and Fouquet, Y., 1997b. Ultramafic and gabbroic exposures at the Mid-Atlantic Ridge: geological mapping in the 15°N region. *Tectonophysics,* 279:193–213.

Cannat, M., Mével, C., Maia, M., Deplus, C., Durand, C., Gente, P., Agrinier, P., Belarouchi, A., Dubuisson, G., et al., 1995. Thin crust, ultramafic exposures, and rugged faulting patterns at the Mid-Atlantic Ridge (22°–24°N). *Geology,* 23:49–52.

Cary, P.W., and Chapman, C.H., 1988. Automatic 1-D waveform inversion of marine seismic refraction data. *Geophys. J. R. Astron. Soc.,* 93:527–546.

Casey, J.F., 1997. Comparison of major- and trace-element geochemistry of abyssal peridotites and mafic plutonic rocks with basalts from the MARK region of the Mid-Atlantic Ridge. *In* Karson, J.A., Cannat, M., Miller, D.J., and Elthon, D. (Eds.), *Proc. ODP, Sci. Results,* 153: College Station, TX (Ocean Drilling Program), 181–241.

Casey, J.F., Braun, M., Kelemen, P.B., Fujiwara, T., Matsumoto, T., and Shipboard Scientific Party, 1998. Megamullions along the Mid-Atlantic Ridge between 14° and 16°N: results of Leg 1, JAMSTEC/WHOI MODE 98 Survey. *Eos, Trans. Am. Geophys. Union,* 79:F920.

Casey, J.F., Bryan, W.F., and Silantyev, S., 1994. Comparison of the geochemistry of basaltic, plutonic and residual mantle rocks from the Mid-Atlantic Ridge: evidence of near fractional melting and mixing. *Eos, Trans. Am. Geophys. Union,* 75:657.

Casey, J.F., Bryan, W.B., Xia, C., Smith, S., Dmitriev, L., Silantiev, S., and Melson, W.G., 1992. Basalt compositional trends, 12° to 38°N along the Mid-Atlantic Ridge: local paradigms. *Eos, Trans. Am. Geophys. Union,* 73:584.

Casey, J.F., Smith, S.E., Bryan, W.B., and Silantyev, S., 1995. Major and trace element geochemistry of basalts, gabbros, and peridotites from the northern MAR: an assessment of the range of subaxial parental and evolved melt compositions. *Eos, Trans. Am. Geophys. Union,* 76:694.

Ceuleneer, G., 1991. Evidences for a paleo-spreading center in the Oman ophiolite: mantle structures in the Maqsad area. *In* Peters, T., Nicolas, A., and Coleman, R.G. (Eds.), *Ophiolite Genesis and Evolution of Oceanic Lithosphere:* Dordrecht (Kluwer), 147–173.

Ceuleneer, G., and Cannat, M., 1997. High-temperature ductile deformation of Site 920 peridotites. *In* Karson, J.A., Cannat, M., Miller, D.J., and Elthon, D. (Eds.), *Proc. ODP, Sci. Results,* 153: College Station, TX (Ocean Drilling Program), 23–34.

Ceuleneer, G., Nicolas, A., and Boudier, F., 1988. Mantle flow patterns at an oceanic spreading centre: the Oman peridotite record. *Tectonophysics,* 151:1–26.

Ceuleneer, G., and Rabinowicz, M., 1992. Mantle flow and melt migration beneath ocean ridges: models derived from observations in ophiolites. *In* Phipps Morgan, J.B., Blackman, D.K., and Sinton, J.M. (Eds.), *Mantle Flow and Melt Generation at Mid-Ocean Ridges.* Geophys. Monogr., Am. Geophys. Union, 71:123–154.

Chambers, A.D., and Brown, P.E., 1995. The Lilloise intrusion, East Greenland: fractionation of a hydrous alkali picritic magma. *J. Petrol.,* 36:933–963.

Chidester, A.H., 1962. Petrology and geochemistry of selected talc-bearing ultramafic rocks and adjacent country rocks in north-central Vermont. *U.S. Geol. Surv. Prof. Pap.*

Christensen, N.I., and Mooney, W.D., 1995. Seismic velocity structure and composition of the continental crust: a global view. *J. Geophys. Res.,* 100:9761–9788.

Christensen, N.I., and Salisbury, M.H., 1975. Structure and constitution of the lower oceanic crust. *Rev. Geophys. Space Phys.,* 13:57–86.

Collins, J.A., Detrick, R.S., Stephen, R.A., Kent, G.M., and Swift, S.A., 1995. Hole 504B seismic experiment: new constraints on the depth of the seismic Layer2/Layer3 boundary. *Eos, Trans. Am. Geophys. Union,* 76:F616.

Collins, J.A., Purdy, M.G., and Brocher, T.M., 1989. Seismic velocity structure at Deep Sea Drilling Project Site 504B, Panama Basin: evidence for thin oceanic crust. *J. Geophys. Res.,* 94:9283–9302.

Collins, M.D., and Brown, J.M., 1998. Elasticity of an upper mantle pyroxene. *Phys. Chem. Miner.,* 26:7–13.

Crane, K., 1985. The spacing of rift axis highs: dependence upon diapiric processes in the underlying asthenosphere. *Earth Planet. Sci. Lett.,* 72:405–414.

Crawford, A.J. (Ed.), 1989. *Boninites and Related Rocks:* London (Unwin Hyman).

Daines, M.J., and Kohlstedt, D.L., 1997. Influence of deformation on melt topology in peridotites. *J. Geophys. Res*., 102:10257–10271.

DePaolo, D.J., 1981. Trace element and isotopic effects of combined wallrock assimilation and fractional crystallization. *Earth Planet. Sci. Lett.,* 53:189–202.

Detrick, R.S., Collins, J.A., Stephen, R.A., and Swift, S.A., 1994. In situ evidence for the nature of the seismic Layer 2/3 boundary in oceanic crust. *Nature,* 370:288–290.

Detrick, R.S., and Purdy, G.M., 1980. The crustal structure of the Kane Fracture Zone from seismic refraction studies. *J. Geophys. Res.,* 85:3759–3777.

Detrick, R.S., Toomey, D.R., and Collins, J.A., 1998. Three-dimensional upper crustal heterogeneity and anisotropy around Hole 504B from seismic topography. *J. Geophy. Res.,* 103:30485–30504.

Detrick, R.S., White, R.S., and Purdy, G.M., 1993. Crustal structure of North Atlantic fracture zones. *Rev. Geophys.,* 31:439–458.

Dick, H.J.B., 1989. Abyssal peridotites, very slow spreading ridges and ocean ridge magmatism. *In* Saunders, A.D., and Norry, M.J. (Eds.), *Magmatism in the Ocean Basins*. Spec. Publ.—Geol. Soc. London, 42:71–105.

Dick, H.J.B., and Bullen, T., 1984. Chromian spinel as a petrogenetic indicator in abyssal and alpine-type peridotites and spatially associated lavas. *Contrib. Mineral. Petrol.,* 86:54–76.

Dick, H.J.B., Fisher, R.L., and Bryan, W.B., 1984. Mineralogic variability of the uppermost mantle along mid-ocean ridges. *Earth Planet. Sci. Lett.,* 69:88–106.

Dick, H.J.B., and Kelemen, P.B., 1992. Light rare earth element enriched clinopyroxene in harzburgites from 15°05′N on the Mid-Atlantic Ridge. *Eos, Trans. Am. Geophys. Union,* 73:584.

Dick, H.J.B., Meyer, P.S., Bloomer, S., Kirby, S., Stakes, D., and Mawer, C., 1991. Lithostratigraphic evolution of an in-situ section of oceanic Layer 3. *In* Von Herzen, R.P., Robinson, P.T., et al., *Proc. ODP, Sci. Results,* 118: College Station, TX (Ocean Drilling Program), 439–538.

Dick, H.J.B., Natland, J.H., Alt, J.C., Bach, W., Bideau, D., Gee, J.S., Haggas, S., Hertogen, J.G.H., Hirth, G., Holm, P.M., Ildefonse, B., Iturrino, G.J., John, B.E., Kelley, D.S., Kikawa, E., Kingdon, A., LeRoux, P.J., Maeda, J., Meyer, P.S., Miller, D.J., Naslund, H.R., Niu, Y., Robinson, P.T., Snow, J., Stephen, R.A., Trimby, P.W., Worm, H.-U., and Yoshinobu, A., 2000. A long in situ section of the lower ocean crust: results of ODP Leg 176 drilling at the Southwest Indian Ridge. *Earth Planet. Sci. Lett.,* 179:31–51.

Dick, H.J.B., Ozawa, K., Meyer, P.S., Niu, Y., Robinson, P.T., Constantin, M., Hebert, R., Natland, J.H., Hirth, G., and Mackie, S.M., 2002. Primary silicate mineral chemistry of a 1.5-km section of very slow spreading lower ocean crust: ODP Hole 735B, Southwest Indian Ridge. *In* Natland, J.H., Dick, H.J.B, Miller, D.J., and Von Herzen, R.P. (Eds.), *Proc. ODP, Sci. Results,* 176, 1–60 [CD-ROM]. Available from: Ocean Drilling Program, Texas A&M University, College Station TX 77845-9547, USA.

Dosso, L., Bougault, H., and Joron, J.L., 1993. Geochemical morphology of the North Atlantic Ridge, 10°–24°N: trace element-isotope complementarity. *Earth Planet. Sci. Lett.,* 120:443–462.

Dosso, L., Hanan, B.B., Bougault, H., Schilling, J.G., and Joron, J.L., 1991. Sr-Nd-Pb geochemical morphology between 10°N and 17°N on the Mid-Atlantic Ridge—a new MORB isotope signature. *Earth Planet. Sci. Lett.,* 106:29–43.

Duennebier, F.K., Lienert, B., Cessaro, R., Anderson, P., and Mallick, S., 1987. Controlled-source seismic experiment at Hole 581C. *In* Duennebier, F.K., Stephen, R., et al., *Init. Repts. DSDP,* 88: Washington (U.S. Govt. Printing Office), 105–125.

Dunn, R.A., and Toomey, D.R., 1997. Seismological evidence for three-dimensional melt migration beneath the East Pacific Rise. *Nature*, 388:259–262.

Elthon, D., and Scarfe, C.M., 1984. High-pressure phase equilibria of a high-magnesia basalt and the genesis of primary oceanic basalts. *Am. Mineral.,* 69:1–15.

Elthon, D., Stewart, M., and Ross, D.K., 1992. Compositional trends of minerals in oceanic cumulates. *J. Geophys. Res.*, 97:15189–15199.

Escartin, J., and Cannat, M., 1999. Ultramafic exposures and the gravity signature of the lithosphere near the Fifteen-Twenty Fracture Zone (Mid-Atlantic Ridge, 14°–16.5°N). *Earth Planet. Sci. Lett.,* 171:411–424.

Escartin, J., Mével, C., MacLeod, C.J., and McCraig, A., in press. Constraints on deformation conditions and the origin of oceanic detachments, the Mid-Atlantic Ridge core complex at 15°45′N. *Geochem. Geophys. Geosyst.*

Forsyth, D.W., Webb, S.C., Dorman, L.M., and Shen, Y., 1998. Phase velocities of Rayleigh waves in the MELT experiment from the East Pacific Rise. *Science*, 280:1235–1237.

Fowler, C.M.R., 1976. Crustal structure of the Mid-Atlantic Ridge crest at 37°N. *Geophys. J. R. Astron. Soc.,* 47:459–491.

————, 1978. The Mid-Atlantic Ridge, structure at 45°N. *Geophys. J. R. Astron. Soc.,* 54:167–183.

Fowler, C.M.R., and Keen, C.E., 1979. Oceanic crustal structure–Mid-Atlantic Ridge at 45°N. *Geophys. J. R. Astron. Soc.,* 56:219–226.

Fujiwara, T., Lin, J., Matsumoto, T., Kelemen, P.B., Tucholke, B.E., and Casey, J., 2003. Crustal evolution of the Mid-Atlantic Ridge near the Fifteen-Twenty Fracture Zone in the last 5 Ma. *Geochem. Geophys. Geosyst.,* 4:10.1029/2002GC000364.

Gaetani, G.A., DeLong, S.E., and Wark, D.A., 1995. Petrogenesis of basalts from the Blanco Trough, northeast Pacific: inferences for off-axis melt generation. *J. Geophys. Res.,* 100:4197–4214.

Ghose, I., Cannat, M., and Seyler, M., 1996. Transform fault effect on mantle melting in the MARK area (Mid-Atlantic Ridge south of the Kane transform). *Geology,* 24:1139–1142.

Gibson, I.L., Beslier, M.-O., Cornen, G., Milliken, K.L., and Seifert, K.E., 1996. Major- and trace-element seawater alteration profiles in serpentinite formed during the development of the Iberia Margin, Site 897. *In* Whitmarsh, R.B., Sawyer, D.S., Klaus, A., and Masson, D.G. (Eds.), *Proc. ODP, Sci. Results,* 149: College Station, TX (Ocean Drilling Program), 519–527.

Ginzburg, A., Whitmarsh, R.B., Roberts, D.G., Montadert, L., Camus, A., and Avedik, F., 1985. The deep seismic structure of the northern continental margin of the Bay of Biscay. *Ann. Geophys.,* 3:499–427.

Godard, M., Jousselin, D., and Bodinier, J.-L., 2000. Relationships between geochemistry and structure beneath a paleo-spreading centre: a study of the mantle section in the Oman ophiolite. *Earth Planet. Sci. Lett.,* 180:133–148.

Green, D.H., and Hibberson, W., 1970. The instability of plagioclase in peridotite at high pressure. *Lithos,* 3:209–221.

Grove, T.L., Kinzler, R.J., and Bryan, W.B., 1992. Fractionation of mid-ocean ridge basalt (MORB). *In* Morgan, J.P., Blackman, D.K., and Sinton, J.M. (Eds.), *Mantle Flow and Melt Generation at Mid-Ocean Ridges*. Geophys. Monogr., Am. Geophys. Union, 71:281–310.

Hacker, B.R., Abers, G.A., and Peacock, S.M., 2003. Subduction factory 1. Theoretical mineralogy, densities, seismic wave speeds, and H_2O contents. *J. Geophys. Res.,* 108:10.1029/2001JB001127.

Hanford, R.F., 1982. Growth of ultramafic reaction zones in greenschist to amphibolite facies metamorphism. *Am. J. Sci.,* 282:543–616.

Hart, S.R., and Davis, K.E., 1978. Nickel partitioning between olivine and silicate melt. *Earth Planet. Sci. Lett.,* 40:203–219.

Hart, S.R., Schilling, J.-G., and Powell, J.L., 1973. Basalts from Iceland and along the Reykjanes Ridge: Sr isotope geochemistry. *Nature,* 246:104–107.

Heling, D., and Schwarz, A., 1992. Iowaite in serpentinite muds at Sites 778, 779, 780, and 784: a possible cause for the low chlorinity of pore waters. *In* Fryer, P., Pearce, J.A., Stokking, L.B., et al., *Proc. ODP, Sci. Results,* 125: College Station, TX (Ocean Drilling Program), 313–323.

Hirschmann, M., 1992. Origin of the transgressive granophyres from the layered series of the Skaergaard intrusion, East Greenland. *J. Volc. Geotherm. Res.,* 52:185–207.

Hofmann, A.W., 1988. Chemical differentiation of the Earth: the relationship between mantle, continental crust and oceanic crust. *Earth Planet. Sci. Lett.,* 90:297–314.

Hooft, E.E.E., Detrick, R.S., Toomey, D.R., Collins, J.A., and Lin, J., 2000. Crustal and upper mantle structure along three contrasting spreading segments of the Mid-Atlantic Ridge (33.5°–35° N). *J. Geophys. Res.,* 105:8205–8226.

Hurst, S.D., Gee, J.S., and Lawrence, R.M., 1997. *Data report:* Reorientation of structural features at Sites 920 to 924 using remanent magnetization and magnetic characteristics. *In* Karson, J.A., Cannat, M., Miller, D.J., and Elthon, D. (Eds.), *Proc. ODP, Sci. Results,* 153: College Station, TX (Ocean Drilling Program), 547–559.

Ishizuka, H., Fujimoto, H., Bryan, W., Fujiwara, T., Furuta, T., Kelemen, P., Kinoshita, H., Kobayashi, K., Matsumoto, T., Takeuchi, A., and Tivey, M., 1995. Oceanic lower crust and upper mantle materials in transform fault zone of WMARK. *JAMSTEC J., Deep-Sea Res*., 11:37–52. (Japanese with English abstr.)

Jacques, A.L., and Green, D.H., 1980. Anhydrous melting of peridotite at 0–15 kb pressure and the genesis of tholeiitic basalts. *Contrib. Mineral. Petrol.,* 73:287–310.

Javoy, M., and Pineau, F., 1991. The volatiles record of a "popping" rock from the Mid-Atlantic Ridge at 14°N: chemical and isotopic composition of gas trapped in the vesicles. *Earth Planet. Sci. Lett.,* 107:598–611.

Jha, K., Parmentier, E.M., and Phipps Morgan, J., 1994. The role of mantle-depletion and melt-retention buoyancy in spreading-center segmentation. *Earth Planet. Sci. Lett.*, 125:221–234.

John, B.E., 1987. Geometry and evolution of a mid-crustal extensional fault system; Chemehuevi Mountains, southeastern California. *In* Coward, M.P., Dewey, J.F., and Hancock, P.L. (Eds.), *Continental Extensional Tectonics,* Spec. Publ.—Geol. Soc. Am., 28:313–335.

John, B.E., and Foster, D.A., 1993. Structural and thermal constraints on the initiation angle of detachment faulting in the Southern Basin and Range, the Chemehuevi Mountains case study. *Bull. Geol. Soc. Am.,* 105:1091–1108.

Jousselin, D., Nicolas, A., and Boudier, F., 1998. Detailed mapping of a mantle diapir below a paleo-spreading center in the Oman ophiolite. *J. Geophys. Res*., 103:18153–18170.

Kelemen, P.B., 1986. Assimilation of ultramafic rocks in subduction-related magmatic arcs. *J. Geol.,* 94:829–843.

————, 1990. Reaction between ultramafic rock and fractionating basaltic magma, I. Phase relations, the origin of calc-alkaline magma series, and the formation of discordant dunite. *J. Petrol.,* 31:51–98.

Kelemen, P.B., and Aharonov, E., 1998. Periodic formation of magma fractures and generation of layered gabbros in the lower crust beneath oceanic spreading centers. *In* Buck, R., Delaney, P.T., Karson, J.A., and Lagabrielle, Y. (Eds.), *Faulting and Magmatism at Mid-Ocean Ridges*. Geophys. Monogr., 106:267–289.

Kelemen, P.B., Braun, M.G., and Hirth, G., 2000. Spatial distribution of melt conduits in the mantle beneath oceanic spreading ridges: observations from the Ingalls and Oman ophiolites. *Geochem., Geophys., Geosyst.,* 1:1029/1999GC000012.

Kelemen, P.B., Hart, S.R., and Bernstein, S., 1998a. Silica enrichment in the continental upper mantle via melt/rock reaction. *Earth Planet. Sci. Lett.,* 164:387–406.

Kelemen, P.B., Hirth, G., Shimizu, N., Spiegelman, M., and Dick, H.J.B., 1997a. A review of melt migration processes in the asthenospheric mantle beneath oceanic spreading centers. *Philos. Trans. R. Soc. London, Ser. A,* 355:283–318.

Kelemen, P.B., Koga, K., and Shimizu, N., 1997b. Geochemistry of gabbro sills in the crust–mantle transition zone of the Oman ophiolite: implications for the origin of the oceanic lower crust. *Earth Planet Sci. Lett.,* 146:475–488.

Kelemen, P.B., Matsumoto, T., and Shipboard Scientific Party, 1998b. Geological results of MODE 98, Leg 1: JAMSTEC/WHOI *Shinkai* 6500 cruise to 15°N, Mid-Atlantic Ridge. *Eos, Trans. Am., Geophys. Union,* 79:F45.

Kelemen, P.B., Shimizu, N., and Salters, V.J.M., 1995a. Extraction of mid-ocean-ridge basalt from the upwelling mantle by focused flow of melt in dunite channels. *Nature,* 375:747–753.

Kelemen, P.B., Whitehead, J.A., Aharonov, E., and Jordahl, K.A., 1995b. Experiments on flow focusing in soluble porous media, with applications to melt extraction from the mantle. *J. Geophys. Res.,* 100:475–496.

Kelso, P.R., Richter, C., and Pariso, J.E., 1996. Rock magnetic properties, magnetic mineralogy, and paleomagnetism of peridotites from Site 895, Hess Deep. *In* Mével, C., Gillis, K.M., Allan, J.F., and Meyer, P.S. (Eds.), *Proc. ODP, Sci. Results,* 147: College Station, TX (Ocean Drilling Program), 405–413.

Kikawa, E., Kelso, P.R., Pariso, J.E., and Richter, C., 1996. Paleomagnetism of gabbroic rocks and peridotites from Sites 894 and 895, Leg 147, Hess Deep: results of half-core and whole-core measurements. *In* Mével, C., Gillis, K.M., Allan, J.F., and Meyer, P.S. (Eds.), *Proc. ODP, Sci. Results,* 147: College Station, TX (Ocean Drilling Program), 383–391.

Kinzler, R.J., and Grove, T.L., 1992. Primary magmas of mid-ocean ridge basalts, 2. Applications. *J. Geophys. Res.,* 97:6907–6926.

————, 1993. Corrections and further discussion of the primary magmas of mid-ocean ridge basalts, 1 and 2. *J. Geophys. Res.,* 98:22339–22347.

Koga, K.T., Kelemen, P.B., and Shimizu, N., 2001. Petrogenesis of the crust-mantle transition zone and the origin of lower crustal wehrlite in the Oman ophiolite. *Geochem. Geophys. Geosyst.,* 2:10.1029/2000GC000132.

Kohlstedt, D.L., and Zimmerman, M.E., 1996. Rheology of partially molten mantle rocks. *Annu. Rev. Earth Planet. Sci.,* 24:41–62.

Korenaga, J., Holbrook, W.S., Kent, G.M., Kelemen, P.B., Detrick, R.S., Larsen, H.-C., Hopper, J.R., and Dahl-Jensen, T., 2000. Crustal structure of the Southeast Greenland margin from joint refraction and reflection seismic tomography. *J. Geophys. Res., [Solid Earth Planets],* 105:21259–21614.

Korenaga, J., and Kelemen, P.B., 1997. Origin of gabbros sills in the Moho transition zone of the Oman ophiolite: implications for magma transport in the oceanic lower crust. *J. Geophys. Res.,* 102:27.

————, 1998. Melt migration through the oceanic lower crust: a constraint from melt percolation modeling with finite solid diffusion. *Earth Planet. Sci. Lett.,* 156:1–11.

Korenaga, J., Kelemen, P.B., and Holbrook, W.S., 2002. Methods for resolving the origin of large igneous provinces from crustal seismology. *J. Geophys. Res., [Solid Earth Planets],* 107:27.

Kuo, B.-Y., and Forsyth, D.W., 1988. Gravity anomalies of the ridge-transform system in the South Atlantic between 31° and 34.5°S: upwelling centers and variations in crustal thickness. *Mar. Geophys. Res.,* 10:205–232.

Langmuir, C.H., and Bender, J.F., 1984. The geochemistry of oceanic basalts in the vicinity of transform faults: observations and implications. *Earth Planet. Sci. Lett.,* 69:107–127.

Lawrence, R.M., Gee, J.S., and Hurst, S.D., 1997. Magnetic anisotropy in serpentinized peridotites from Site 920: its origin and relationship to deformation fabrics. *In* Karson, J.A., Cannat, M., Miller, D.J., and Elthon, D. (Eds.), *Proc. ODP, Sci. Results,* 153: College Station, TX (Ocean Drilling Program), 419–427.

Lewis, B.T.R., and Garmany, J.D., 1982. Constraints on the structure of the East Pacific Rise from seismic refraction data. *J. Geophys. Res.,* 87:8417–8425.

Lewis, B.T.R., and Snydsman, W.E., 1979. Fine structure of the oceanic crust on the Cocos plate. *Tectonophysics,* 55:87–105.

Lin, J., and Phipps Morgan, J., 1992. The spreading rate dependence of three-dimensional midocean ridge gravity structure. *Geophys. Res. Lett.,* 19:13–16.

Lin, J., Purdy, G.M., Schouten, H., Sempéré, J.-C., and Zervas, C., 1990. Evidence from gravity data for focused magmatic accretion along the Mid-Atlantic Ridge. *Nature,* 344:627–632.

MacLeod, C.J., Escartin, J., Banerji, D., Banks, G.J., Gleeson, M., Irving, D.H.B., Lilly, R.B., McCraig, A., Niu, Y., Allerton, S., and Smith, D.K., 2002. Direct geological evidence for oceanic detachment faulting. *Geology,* 30:879–882.

Magde, L.S., Dick, H.J.B., and Hart, S.R., 1995. Tectonics, alteration and the fractal distribution of hydrothermal veins in the lower ocean crust. *Earth Planet. Sci. Lett.,* 129:103–119.

Magde, L.S., Sparks, D.W., and Detrick, R.S., 1997. The relationship between buoyant mantle flow, melt migration, and gravity bull's eyes at the Mid-Atlantic Ridge between 33°N and 35°N. *Earth Planet. Sci. Lett.,* 148:59–67.

Matsumoto, T., Kelemen, P.B., and Party, O.S., 1998. Preliminary results of the precise geological and geophysical mapping of the Mid-Atlantic Ridge 14–16°N—tectonic extension along the magma-poor ridge axis. *Eos, Trans. Am. Geophys. Union,* 79:F46.

Matveev, S., and Ballhaus, C., 2002. Role of water in the origin of podiform chromitite deposits. *Earth Planet. Sci. Lett.,* 203:235–243.

McClain, J.S., and Atallah, C.A., 1986. Thickening of the oceanic crust with age. *Geology,* 14:574–576.

Melson, W.G., Byerly, G.R., Nelen, J.A., O'Hearn, T., Wright, T.L., and Vallier, T., 1977. A catalog of the major element chemistry of abyssal volcanic glasses. *Smithsonian Contrib. Earth Sci.,* 19:31–60.

MELT Team, T.M.S., 1998. Imaging the deep seismic structure beneath a mid-ocean ridge: the MELT experiment. *Science,* 280:1215–1218.

Meurer, W.P., Sturm, M.A., Klein, E.M., and Karson, J.A., 2001. Basalt compositions from the Mid-Atlantic Ridge at the SMARK area (22°30′N to 22°50′N): implications for parental liquid variability at isotopically homogeneous spreading centers. *Earth Planet. Sci. Lett.,* 186:451-469.

Michael, P.J., and Chase, R.L., 1987. The influence of primary magma composition, H_2O and pressure on mid-ocean ridge basalt differentiation. *Contrib. Mineral. Petrol.,* 96:245–263.

Miller, D.J., and Christensen, N.I., 1997. Seismic velocities of lower crustal and upper mantle rocks from the slow-spreading Mid-Atlantic Ridge, south of the Kane Transform Zone (MARK). *In* Karson, J.A., Cannat, M., Miller, D.J., and Elthon, D. (Eds.), *Proc. ODP, Sci. Results,* 153: College Station, TX (Ocean Drilling Program), 437–454.

Minshull, T.A., White, R.S., Mutter, J.C., Buhl, P., Detrick, R.S., Williams, C.A., and Morris, E., 1991. Crustal structure at the Blake Spur Fracture Zone from expanding spread profiles. *J. Geophys. Res.,* 96:9955–9984.

Mithal, R., and Mutter, J.C., 1989. A low-velocity zone within the Layer 3 region of 118 Myr old oceanic crust in the western Atlantic. *Geophys. J. R. Astron. Soc.,* 97:275–294.

Moore, J.G., Batchelder, J.N.N., and Cunningham, C.G., 1977. CO_2 filled vesicles in mid-ocean ridge basalts. *J. Volcanol. Geotherm. Res.,* 2:309–374.

Moreira, M., Kunz, J., and Allègre, C., 1998. Rare gas systematics in popping rock: isotopic and elemental compositions in the upper mantle. *Science*, 279:1178–1181.

Morris, E., Detrick, R.S., Minshull, T.A., Mutter, J.C., White, R.S., Su, W., and Buhl, P., 1993. Seismic structure of oceanic crust in the western North Atlantic. *J. Geophys. Res.,* 98:13879–13903.

Natland, J.H., and Dick, H.J.B., 1996. Melt migration through high-level gabbroic cumulates of the East Pacific Rise at Hess Deep: the origin of magma lenses and the deep crustal structure of fast-spreading ridges. *In* Mével, C., Gillis, K.M., Allan, J.F., and Meyer, P.S. (Eds.), *Proc. ODP, Sci. Results,* 147: College Station, TX (Ocean Drilling Program), 21–58.

————, 2002. Stratigraphy and composition of gabbros drilled at Ocean Drilling Program Hole 735B, Southwest Indian Ridge: a synthesis of geochemical data. *In* Natland, J.H., Dick, H.J.B., Miller, D.J., and Von Herzen, R.P. (Eds.), *Proc. ODP, Sci. Results,* 176, 1–69 [CD-ROM]. Available from: Ocean Drilling Program, Texas A&M University, College Station TX 77845-9547, USA.

Natland, J.H., Meyer, P.S., Dick, H.J.B., and Bloomer, S.H., 1991. Magmatic oxides and sulfides in gabbroic rocks from Hole 735B and the later development of the liquid line of descent. *In* Von Herzen, R.P., Robinson, P.T., et al., *Proc. ODP, Sci. Results,* 118: College Station, TX (Ocean Drilling Program), 75–111.

Navon, O., and Stolper, E., 1987. Geochemical consequences of melt percolation: the upper mantle as a chromatographic column. *J. Geol.,* 95:285–307.

Nicolas, A., 1986. A melt extraction model based on structural studies in mantle peridotites *J. Petrol.,* 27:999–1022.

————, 1990. Melt extraction from mantle peridotites: hydrofracturing and porous flow, with consequences for oceanic ridge activity. *In* Ryan, M.P. (Ed.), *Magma Transport and Storage:* Chichester (Wiley), 159–173.

Nicolas, A., and Boudier, F., 1995. Mapping oceanic ridge segments in Oman ophiolites. *J. Geophys. Res.,* 100:6179–6197.

Nicolas, A., Boudier, F., and Ildefonse, B., 1996. Variable crustal thickness in the Oman ophiolite: implication for oceanic crust. *J. Geophys. Res.,* 101:17941–17950.

Nicolas, A., and Rabinowicz, M., 1984. Mantle flow pattern at oceanic spreading centres: relation with ophiolitic and oceanic structures. *In* Gass, I.G., Lippard, S.J., and Shelton, A.W. (Eds.), *Ophiolites and Oceanic Lithosphere.* Spec. Publ.—Geol. Soc. London, 13:147–151.

Nicolas, A., and Violette, J.F., 1982. Mantle flow at oceanic spreading centers: models derived from ophiolites. *Tectonophysics,* 81:319–339.

Niu, Y., Gilmore, T., Mackie, S., Greig, A., and Bach, W., 2002. Mineral chemistry, whole-rock compositions, and petrogenesis of Leg 176 gabbros: data and discussion. *In* Natland, J.H., Dick, H.J.B., Miller, D.J., and Von Herzen, R.P. (Eds.), *Proc. ODP, Sci. Results,* 176, 1–60 [CD-ROM]. Available from: Ocean Drilling Program, Texas A&M University, College Station TX 77845-9547, USA.

O'Hara, M.J., 1965. Primary magmas and the origin of basalts. *Scott. J. Geol.,* 1:19–40.

Orcutt, J.A., Kennett, B., and Dorman, L., 1976. Structure of the East Pacific Rise from an ocean bottom seismometer survey. *Geophys. J. R. Astron. Soc.,* 45:305–320.

Ozawa, K., Meyer, P.S., and Bloomer, S.H., 1991. Mineralogy and textures of iron titanium oxide gabbros and associated olivine gabbros from Hole 735B. *In* Von Herzen, R.P., Robinson, P.T., et al., *Proc. ODP, Sci. Results,* 118: College Station, TX (Ocean Drilling Program), 41–73.

Pallister, J.S., and Hopson, C.A., 1981. Samail ophiolite plutonic suite: field relations, phase variation, cryptic variation and layering, and a model of a spreading ridge magma chamber. *J. Geophys. Res.,* 86:2593–2644.

Parmentier, E.M., and Phipps Morgan, J., 1990. Spreading rate dependence of three-dimensional structure in oceanic spreading centers. *Nature*, 348:325–328.

Pettigrew, T.L., Casey, J.F., Miller, D.J., et al., 1999. *Proc. ODP, Init. Repts.,* 179 [CD-ROM]. Available from: Ocean Drilling Program, Texas A&M University, College Station, TX 77845-9547, U.S.A.

Peyve, A.A., Suchevskaya, N.M., Lyapunov, S.M., and Konokova, N.N., 1988. Peculiarities of tholeiitic magmatism in the area of the Cape Verde Fracture Zone in the Atlantic (13–15°N). *Dokl. Akad. Nauk USSR,* 302:1174–1178. (in Russian)

Phipps, S.P., and Ballotti, D., 1992. Rheology of serpentinite muds in the Mariana–Izu Bonin forearc. *In* Freyer, P., Pearce, J.A., Stokking, L.B., et al., *Proc. ODP, Sci. Results,* 125, College Station, TX (Ocean Drilling Program), 363–372.

Phipps Morgan, J., 1987. Melt migration beneath mid-ocean spreading centers. *Geophys. Res. Lett.*, 14:1238–1241.

Phipps Morgan, J., and Forsyth, D.W., 1988. Three-dimensional flow and temperature perturbations due to a transform offset: effects on oceanic crustal and upper mantle structure. *J. Geophys. Res.,* 93:2955–2966.

Pineau, F., Javoy, M., and Bottinga, Y., 1976. $^{13}C/^{12}C$ ratios of rocks and inclusions in popping rocks of the Mid-Atlantic Ridge. *Earth Planet. Sci. Lett.,* 29:413–421.

Purdy, G.M., 1983. The seismic structure of 140 Myr old crust in the western central Atlantic Ocean. *Geophys. J. R. Astron. Soc.,* 72:115–137.

Purdy, G.M., and Detrick, R.S., 1986. Crustal structure of the Mid-Atlantic Ridge at 23°N from seismic refraction studies. *J. Geophys. Res.,* 91:3739–3762.

Rabinowicz, M., Ceuleneer, M., and Nicolas, A., 1987. Melt segregation and flow in mantle diapirs below spreading centers: evidence from the Oman ophiolites. *J. Geophys. Res.,* 92:3475–3486.

Rabinowicz, M., Nicolas, A., and Vigneresse, J.L., 1984. A rolling mill effect in asthenosphere beneath oceanic spreading centers. *Earth Planet. Sci. Lett.,* 67:97–108.

Reid, I., and Jackson, H.R., 1981. Oceanic spreading rate and crustal thickness. *Mar. Geophys. Res.,* 5:165–172.

Richter, C., Kelso, P.R., and MacLeod, C.J., 1996. Magnetic fabrics and sources of magnetic susceptibility in lower crustal and upper mantle rocks from Hess Deep. *In* Mével, C., Gillis, K.M., Allan, J.F., and Meyer, P.S. (Eds.), *Proc. ODP, Sci. Results,* 147: College Station, TX (Ocean Drilling Program), 393–403.

Roeder, P.L., and Emslie, R.F., 1970. Olivine liquid equilibrium. *Contrib. Mineral. Petrol.,* 29:275–289.

Sarda, P., and Graham, D., 1990. Mid-ocean ridge popping rocks: implications for degassing at ridge crests. *Earth Planet. Sci. Lett.,* 97:268–289.

Schilling, J.-G., 1973. Iceland mantle plume: geochemical study of Reykjanes Ridge. *Nature,* 242:565–571.

Schouten, H., Klitgord, K.D., and Whitehead, J.A., 1985. Segmentation of mid-ocean ridges. *Nature,* 317:225–229.

Seyler, M., and Bonatti, E., 1997. Regional-scale melt-rock interaction in lherzolitic mantle in the Romanche Fracture Zone (Atlantic Ocean). *Earth Planet. Sci. Lett.,* 146:273–287.

Shearer, P., and Orcutt, J.A., 1986. Compressional- and shear-wave anisotropy in the oceanic lithosphere—the Ngendei seismic refraction experiment. *Geophys. J. R. Astron. Soc.,* 87:967–1003.

Shen, Y., and Forsyth, D.W., 1995. Geochemical constraints on initial and final depths of melting beneath mid-ocean ridges. *J. Geophys. Res.,* 100:2211–2237.

Silantyev, S.A., Dmitriev, L.V., Bazylev, B.A., Casey, J.F., Bougault, H., Levsky, L.K., Belyatsky, B.V, and Ovchinikova, G.V., 1996. An examination of genetic conformity between co-existing basalt, gabbro and residual peridotites from 15°20′N fracture zone, central Atlantic: evidence from isotope composition of Sr, Nd, and Pb. *InterRidge Newsl.*, 4:18–21.

Sisson, T.W., and Grove, T.L., 1993a. Experimental investigations of the role of H_2O in calc-alkaline differentiation and subduction zone magmatism. *Contrib. Mineral. Petrol.,* 113:143–166.

————, 1993b. Temperatures and H_2O contents of low MgO high-alumina basalts. *Contrib. Mineral. Petrol.,* 113:167–184.

Sleep, N.H., 1975. Formation of oceanic crust: some thermal constraints. *J. Geophys. Res.,* 80:4037–4042.

Smewing, J.D., 1981. Mixing characteristics and compositional differences in mantle-derived melts beneath spreading axes: evidence from cyclically layered rocks in the ophiolite of North Oman. *J. Geophys. Res.,* 86:2645–2659.

Snow, J.E., and Dick, H.J.B., 1995. Pervasive magnesium loss by marine weathering of perdotite. *Geochim. Cosmochim. Acta,* 59:4219–4235.

Sobolev, A.V., Dmitriev, L.V., Tsamerian, O.P., Simonov, V.A., Skolotnev, S.G., and Basilev, B.A., 1992a. On the structure and origin of geochemical anomaly in basalts from Mid-Atlantic Ridge between 12 and 18°N. *Dok. Akad. Nauk USSR*, 326:541–546. (in Russian)

Sobolev, A.V., Tsamerian, O.P., and Dmitriev, L.V., 1992b. The geochemical anomaly in Mid-Atlantic Ridge basalts between 12°–18°N: geochemical structure and origin. *Proc. 29th Int. Geol. Cong.,* 29:58.

Sobolov, A.V., Tsamerian, G.P., Dmitriev, L.V., and Basilev, B., 1992c. The correlation between the mineralogy of basalt and the associated peridotites: the data from the MAR between 8°–18°N. *Eos, Trans. Am. Geophys. Union,* 73:584.

Sparks, D.W., and Parmentier, E.M., 1991. Melt extraction from the mantle beneath spreading centers. *Earth Planet. Sci. Lett.*, 105:368–377.

————, 1993. The structure of three-dimensional convection beneath oceanic spreading centres. *Geophys. J. Int.*, 112:81–91.

————, 1994. The generation and migration of partial melt beneath oceanic spreading centers. *In* Ryan, M.P. (Ed.), *Magmatic Systems,* San Diego CA (Academic Press, Inc.), 55–76.

Sparks, D.W., Parmentier, E.M., and Phipps Morgan, J., 1993. Three-dimensional mantle convection beneath a segmented spreading center: implications for along-axis variations in crustal thickness and gravity. *J. Geophys. Res.*, 98:21977–21995.

Spiegelman, M., 1993. Physics of melt extraction: theory, implications and applications. *Philos. Trans. R. Soc. London, Ser. A.,* 342:23–41.

Spiegelman, M., and McKenzie, D., 1987. Simple 2-D models for melt extraction at mid-ocean ridges and island arcs. *Earth Planet. Sci. Lett.,* 83:137–152.

Spudich, P., and Orcutt, J., 1980. Petrology and porosity of an oceanic crustal site: results from wave form modeling of seismic refraction data. *J. Geophys. Res.,* 85:1409–1433.

Staudacher, T., Sarda, P., Richardson, S.H., Allegré, C.J., Sagna, I., and Dimitriev, L.V., 1989. Noble gases in basalt glasses from a Mid-Atlantic Ridge topographic high at 14°N: geodynamic consequences. *Earth Planet. Sci. Lett.,* 96:119–133.

Stolper, E., 1980. A phase diagram for mid-ocean ridge basalts: preliminary results and implications for petrogenesis. *Contrib. Mineral. Petrol.,* 78:13–27.

Su, W., and Buck, W.R., 1993. Buoyancy effects on mantle flow under mid-ocean ridges. *J. Geophys. Res.*, 98:12191–12205.

Thompson, J.B., Jr., 1959. Local equilibrium in metasomatic processes. *Res. Geochem.,* 1:427–457.

Tolstoy, M.A., Harding, J.A., and Orcutt, J.A., 1992. Crustal thickness at the Mid-Atlantic Ridge: bull's eye gravity anomalies and focused accretion. *Science,* 262:726–729.

Toomey, D.R., Wilcock, W.S.D., Solomon, S.C., Hammond, W.C., and Orcutt, J.A., 1998. Mantle seismic structure beneath the MELT region of the East Pacific Rise from *P*- and *S*-wave tomography. *Science,* 280:1224–1227.

Tucholke, B.E., Lin, J., Kleinrock, M.C., Tivey, M.A., Reed, T.B., Goff, J., and Jaroslow, G., 1997. Segmentation and crustal structure of the western Mid-Atlantic Ridge flank, 25°25′–27°10′N and 0–29 m.y. *J. Geophys. Res.*, 102:10203–10223.

Turcotte, D.L., and Phipps Morgan, J., 1992. The physics of melt migration and mantle flow beneath a mid-ocean ridge. *In* Phipps Morgan, J., Blackman D., and Sinton, J. (Eds.), *Mantle Flow and Melt Generation at Mid-Ocean Ridges.* Geophys. Monogr., 71:155–182.

Vera, E.E., Mutter, J.C., Buhl, P., Orcutt, J.A., Harding, A.J., Kappus, M.E., Detrick, R.S., and Brocher, T.M., 1990. The structure of 0- to 0.2-m.y.-old oceanic crust at 9°N on the East Pacific Rise from expanded spread profiles. *J. Geophys. Res.,* 95:15529–15556.

Wager, L.R., and Brown, G.M., 1968. *Layered Igneous Rocks:* Edinburgh (Oliver and Boyd).

Waldron, D.A., Clowes, R.M., and White, D.J., 1990. Seismic structure of the subducting oceanic plate off western Canada. *In* Green, A.G. (Ed.), *Studies of Laterally Heterogeneous Structures Using Seismic Refraction and Reflection Data.* Pap.—Geol. Surv. Can., 105–113.

White, R.S., 1979. Oceanic upper crustal structure from variable angle seismic reflection-refraction profiles. *Geophys. J. R. Astron. Soc.,* 57:683–726.

White, R.S., McKenzie, D., and O'Nions, R.K., 1992. Oceanic crustal thickness from seismic measurements and rare earth element inversions. *J. Geophys. Res.,* 97:19683–19715.

Whitehead, J.A., Dick, H.J.B., and Shouten, H., 1984. A mechanism for magmatic accretion under spreading centers. *Nature,* 312:146–148.

Whitmarsh, R.B., and Calvert, A.J., 1986. Crustal structure of Atlantic fracture zones. *Geophys. J. R. Astron. Soc.,* 85:107–138.

Whitmarsh, R.B., Ginzburg, A., and Searle, R.C., 1982. The structure and origin of the Azores-Biscay Rise, northeast Atlantic Ocean. *Geophys. J. R. Astron. Soc.,* 70:79–108.

Whitmarsh, R.B., Miles, P.R., and Mauffret, A., 1990. The ocean-continent boundary off the western continental margin of Iberia, I. Crustal structure at 40°30′N. *Geophys. J. Int.,* 103:509–531.

Xia, C., Casey, J.F., Silantiev, S., and Dmitriev, L., 1991. Geochemical structure of the 14°N mantle source anomaly along the Mid-Atlantic Ridge and geochemical changes across the 15°20′N Fracture Zone. *Eos, Trans. Am. Geophys. Union,* 72:518.

Xia, C., Casey, J.F., Silantiev, S., Dmitriev, L., and Bougault, H., 1992. Geochemical variations between 12 to 16°N, Mid-Atlantic Ridge: a region with high degrees of partial melting yet magma starved? *Eos, Trans. Am. Geophys. Union,* 73:553.

TABLE CAPTION

Table T1. Leg 209 coring summary.

FIGURE CAPTIONS

Figure F1. Preliminary calculation of Mantle Bouger Anomaly (e.g., Lin et al., 1990) from shipboard gravity measurements taken in 1998 (Kelemen et al., 1998a; Matsumoto et al., 1998; Casey et al., 1998). Both figures use the same range of colors, representing slightly different values. **A.** Range is from about –35 (red) to +40 (pink) mGal north of the 15°20′N Fracture Zone. **B.** Range is from about –60 (red) to +45 (pink) Mgal south of the 15°20′N Fracture Zone. These data suggest that the magma-starved region with abundant peridotite outcrops from 14°40′ to 15°40′N lies on the periphery of large magmatic segments centered at ~14° and 16°N, with thick igneous crust in the segment centers.

Figure F2. Bathymetry and geology from 14° to 16°N along the Mid-Atlantic Ridge. Depth range is ~5400 (violet) to 1600 (red) m. Sample lithologies are compiled from all known dredging and submersible results. **A.** North of the 15°20′N Fracture Zone. **B.** South of the 15°20′N Fracture Zone. **C.** View from the north of the "megamullion" dive site, where a large low-angle normal fault is exposed on the seafloor. Open circles = mantle peridotite, solid circles = basalt.

Figure F3. Geochemical data for samples from the Mid-Atlantic Ridge. **A.** Low Na_2O (upper panel = equator–70°N data; lower panel = 10°–20°N data) in basalts. **B.** High Cr/(Cr+Al) in spinel (lower panel) and shallow axial depth (upper panel) can all be taken to indicate high degrees of partial melting. **C.** High La/Sm (upper panel = data from the equator to 70°N; lower panel = data from 10° to 20°N). **D.** High $^{207}Pb/^{204}Pb$ (upper panel) and high $^{87}Sr/^{86}Sr$ (lower panel). C and D are indicative of long-term enrichment of the mantle source in incompatible trace elements. All of these characteristics are observed along the Mid-Atlantic Ridge just south of the 15°20′N Fracture Zone (FZ). Basalt data compiled by Xia et al. (1991, 1992, unpubl. data) and Casey et al. (1992). Spinel data and bathymetry from Bonatti et al. (1992) and Sobolev et al. (1991, 1992a).

Figure F4. **A.** Maps showing locations of conventional seismic refraction profiles (long white lines) and NOBEL experiments (numbered black lines) in 1997. **B–D.** Preliminary interpretation of data from the long refraction profile (R. Detrick and J. Collins, pers. comm., 1998); (B) two-dimensional velocity model with contours labeled in kilometers per second, (C) indication of data coverage, which is sparse in the lower crust but sufficient to define large lateral velocity variations (contours labeled in kilometers per second), and (D) traveltime data (circles) with model calculations (shading) for comparison. **E.** Comparison of two one-dimensional sections through the velocity model with a typical one-dimensional section for oceanic crust at the East Pacific Rise (EPR). MAR = Mid-Atlantic Ridge.

Figure F5. Leg 209 drill site locations.

Figure F6. **A.** Schematic diagram drawn after Barnouin-Jha et al. (1997) showing results for the upper 50 km in a dynamic model of buoyancy-driven three-dimensional (3-D) mantle flow beneath a slow-spreading ridge. Red = flow vectors in the horizontal plane, yellow = flow vectors in the vertical ridge-axis plane, blue = flow vectors in the vertical ridge-normal plane. This illustrates along-axis flow in the shallow mantle from segment centers to segment ends. Note spacing between upwelling centers is ~400 km and the region of melt generation is almost as long as the ridge segments. **B.** From Ceuleneer (1991), illustrating ductile flow

vectors and shear sense inferred from peridotite fabrics in the mantle section of the Maqsad area, Oman ophiolite. Map area is ~17 km long × 14 km wide. Approximate location of inferred paleoridge axis is shown as a red line. **C.** Schematic diagram from Jousselin et al. (1998) showing their vision of mantle flow, loosely based on observations from the Oman ophiolite, with a narrow zone of upwelling and a thin region of corner flow feeding a ridge segment that is three times longer than the diameter of the mantle upwelling zone. This model requires extensive subhorizontal ridge-parallel flow of residual mantle peridotite from the segment center to the segment ends. Although this geometry seems somewhat extreme and has not been produced in any 3-D dynamic model to date, it illustrates the type of highly focused solid upwelling that could produce the observed along-axis variation in crustal thickness on the Mid-Atlantic Ridge via 3-D focusing of mantle flow. Dynamic models such as that illustrated in A do not have sufficiently narrow zones of mantle upwelling and cannot reproduce the lengths of observed magmatic segments (~30–100 km). MOHO = Mohorovicic seismic discontinuity.

Figure F7. Downhole lithologic distributions in Hole 1268A are shown as percentages for each section (left panel) and as volume percent recovery. The lithologies are grouped as dunites (rocks with 90% olivine), harzburgites (includes all ultramafic rocks exclusive of dunites, but the bulk are harzburgites in the strict sense), gabbros (includes gabbronorites, microgabbros, and gabbroic rocks of undeterminable mineralogy), and breccias (mixtures of highly altered, probably originally gabbroic material and ultramafic host). TD = total depth.

Figure F8. **A.** Data on the seismic velocity of the mantle beneath oceanic crust (depths >7 km) from seismic refraction experiments, as a function of oceanic plate age. Data compiled from Beé and Bibee (1989), Bratt and Purdy (1984), Bratt and Solomon (1984), Canales et al. (1998, 2000, 2003), Cary and Chapman (1988a), Collins et al. (1989, 1995), Collins and Brown (1998), Detrick et al. (1993, 1994, 1998), Detrick and Purdy (1980), Duennebier et al. (1987), Fowler (1976, 1978), Fowler and Keen (1979), Ginzburg et al. (1985), Hooft et al. (2000), Lewis and Garmany (1982), Lewis and Snydsman (1979), McClain and Atallah (1986), Minshull et al. (1991), Mithal and Mutter (1989), Morris et al. (1993), Orcutt et al. (1976), Purdy (1983), Purdy and Detrick (1986), Shearer and Orcutt (1986), Spudich and Orcutt (1980), Vera et al. (1990), Waldron et al. (1990), White (1979), White et al. (1992), Whitmarsh and Calvert (1986), Whitmarsh et al. (1982, 1990). **B.** Calculated *P*-wave velocity for polycrystalline dunite and pyroxenite at 25°C as a function of pressure, with 1 σ error estimates, from Christensen and Mooney (1995). Based on these estimates, harzburgite with 20% orthopyroxene at the base of oceanic crust would have a *P*-wave velocity = ~8.2 ± 0.1 km/s at 25°C, or ~ 8.1 km/s at 200°C.

Figure F9. **A.** Close-up photograph of hand specimen of a typical example of completely serpentinized harzburgite (interval 209-1268A-19R-1, 50–62 cm). **B.** X-ray diffraction spectrum of that sample shows that it consists almost entirely of lizardite (chrysotile[?]) and magnetite.

Figure F10. **A.** Close-up photograph of partially talc-altered serpentinite (interval 209-1268A-23R-2, 15–28 cm) with remnants of serpentine pseudomorphs after orthopyroxene. Arrows indicate approximate position of thin section photographs. **B, C.** Photomicrograph showing pervasive talc alteration (Sample 209-1268A-23R-2, 18–21 cm) (cross polarized light: blue filter; field of view - 2.75 mm). (B) Talc alteration has completely overprinted the matrix texture of the serpentinized harzburgite. A bastite pseudomorph after orthopyroxene (left) is being replaced by veinlets of massive talc (image 1268A_040). (C) Talc replacing orthopyroxene (to the left of prominent spinel crystal in center of image) and former serpentine-

chrysotile veins (left). Talc has completely erased the mesh texture of the serpentinized harzburgite (image 1268A_039).

Figure F11. Primitive glasses (Mg# > 60%) from the 14°–16°N region of the Mid-Atlantic Ridge (Melson et al., 1977; C. Xia et al., unpubl. data) extend to >52 wt% SiO_2 and are among the most SiO_2-rich primitive glasses that have been recovered from the mid-ocean ridges. Mid-ocean-ridge glass data, including data from the Melson et al. catalog, were downloaded in April 2003 from PetDB (online at **petdb.ldeo.columbia.edu/petdb/**).

Figure F12. Thin section photomicrograph showing the core of an orthopyroxene crystal pseudomorphed by talc and pyrite. The core is surrounded by a corona of pleochroic serpentine. Pseudomorphic talc and pleochroic serpentine are replaced by late, nonpseudomorphic talc (bottom) (Sample 209-1268A-13R-2, 3–6 cm) (cross polarized light: blue filter; field of view = 2.75 mm; image 1268A_016).

Figure F13. **A.** Anhydrous major element compositions of hydrothermally altered peridotite samples from Site 1268, plotted in terms of mole fraction of SiO_2 vs. mole fraction of MgO + FeO, compared to anhydrous compositions of end-member minerals (speciation is SiO_2, TiO_2, Al_2O_3, Cr_2O_3, FeO, MnO, MgO, CaO, Na_2O, K_2O, P_2O_5, with all Fe as FeO). **B.** Expanded plot of A, with weight percent pyroxene proportions added. Talc-altered peridotites approach the composition of end-member talc. Even serpentinized peridotites have ~25 wt% normative orthopyroxene, indicative of substantial addition of SiO_2 and/or loss of MgO + FeO. Slight divergence of the peridotite compositions from the MgO + FeO to SiO_2 mixing line is due to the minor presence of other oxides, mainly in the form of a few percent Cr-Al spinel in most peridotite samples.

Figure F14. **A–D.** Anhydrous major element compositions of hydrothermally altered gabbronorite samples from Site 1268, plotted in terms of oxide mole fractions (speciation as for Fig. F13). Calcic amphibole end-members are tremolite/actinolite, hornblende, edenite, pargasite, and tschermakite. Chlorite end-member is clinochlore. Bold triangles in panels B, C, and D enclose possible gabbronorite assemblages with calcic plagioclase. Light gray arrows show trend of increasing alteration and metasomatism for Site 1268 gabbronorites. The freshest samples have compositions similar to igneous gabbronorites, whereas the most altered samples approach the composition of talc-chlorite-quartz mixtures, in accord with the observed alteration assemblage. Cpx = clinopyroxene, opx = orthopyroxene, serp = serpentinite.

Figure F15. Close-up photograph of pegmatitic textured gabbro (interval 209-1268A-21R-1, 10–21 cm).

Figure F16. Magnetic inclination as a function of the amount of rotation around a horizontal axis, for rocks that initially are normally magnetized with a magnetic inclination of 28° and a declination of 0°. Inclinations of 15°, the average value in gabbronorite from Hole 1268A, and 36°, the average value in talc-altered peridotite from Hole 1268A, are shown for reference. Small rotations around an east-west axis could produce inclinations different from 28°. However, this would require opposite senses of rotation for the gabbronorites and the peridotites. Geological reasoning suggests that tectonic rotations in this area are likely to be counterclockwise around a ridge-parallel, nearly horizontal axis striking 020°. Large rotations around a horizontal axis striking 020° could produce the observed 15° inclination in gabbronorites, whereas smaller counterclockwise rotations could produce the observed 36° inclination in peridotites. We hypothesize the gabbronorites acquired their remanent magnetization at somewhat higher temperature than the peridotite during slow cooling of the rocks as they were uplifted toward the seafloor. Peridotites acquired their remanent magnetization at a later time, during magnetite growth associated with hydrothermal alteration and serpentinization at ~300°C. Rotation began before serpentinization of the

peridotites, so the peridotites record only part of the tectonic rotation. CW = clockwise, CCW = counterclockwise.

Figure F17. Magnetic inclination as a function of the amount of rotation around an axis with an azimuth of 020° for rocks which initially are normally magnetized with a magnetic inclination of 28° and a declination of 0°, showing the effect of different plunges of the rotation axis.

Figure F18. Spherical projections illustrating the effects of rotation of a remanent magnetic vector initially striking 360° with an inclination of 28° around axes striking 360°–040° and plunging –10° to +10°. The initial position of the vector is indicated with a black cross. The rotation axis is shown as a square. Closed symbols = projection points in the lower hemisphere, open symbols = projection points in the upper hemisphere. Small circles = projection points of the rotating magnetic vector plotted at 20° rotation intervals, large circles = magnetic inclinations of 28° (blue = expected at this latitude), 15° (black = average observed in gabbroic rocks), 28°, and 36° (dashed = average observed in talc-altered peridotites). Effects on the inclination are relatively large and are sufficient to account for the observed inclinations in gabbronorite and peridotite in Hole 1268A. Also, in some cases, the effects on the azimuth of the remanent magnetization vector are large. For example, in the most extreme case illustrated, the azimuth changes by almost 90° of counterclockwise rotation around an axis striking 040° and plunging 10° to the south (lower left). CW = clockwise, CCW = counterclockwise.

Figure F19. Close-up photograph of highly (>15 vol%) vesicular basalt (interval 209-1269B-1R-1, 39.5–47 cm).

Figure F20. Proportions of lithogies recovered from Holes 1270A, 1270B, 1270C, and 1270D. TD = total depth.

Figure F21. Photomicrographs depicting the variations in deformation of the oxide gabbronorites ranging from relatively undeformed to strongly deformed. **A–C.** This oxide gabbronorite has an undeformed igneous texture with lath-shaped euhedral plagioclase, subhedral to euhedral clinopyroxenes, subhedral orthopyroxene, and interstitial oxides (Sample 209-1270B-10M-1, 117–120 cm). (A) The red box indicates the position of the magnified image in B (field of view [FOV] = 11 mm; plane-polarized light: blue + dark gray filters; image 1270B_033). (B) Close up of A showing that although the texture is magmatic the rock has experienced some deformation as indicated by kinked plagioclase and release of strain associated with the polysynthetic twinning (cross polarized light [XPL]: blue + dark gray filters; FOV = 2.75 mm; image 1270B_034). (C) Preservation of an optically zoned core (outlined in red) in a slightly deformed plagioclase (XPL: blue filter; FOV = 1.4 mm; image 1270B_013). **D.** Ribbon-textured plagioclase surrounded by plagioclase neoblasts in a strongly deformed oxide gabbronorite (Sample 209-1270B-1R-1, 90–93 cm) (XPL: blue filter; FOV = 2.75 mm; image 1270B_036). E, F. Wide view and detail of a stretched orthopyroxene grain (Sample 209-1270B-4M-1, 108–111 cm) (XPL: blue filter). (E) The stretched orthopyroxene grain is outlined in red. It sits in a matrix of plagioclase neoblasts and has neoblast of orthopyroxene in the middle of the grain where it has failed. The yellow box shows the location of a detailed view of the central boudinaged part of this grain (FOV = 11 mm; image 1270B_037). (F) Detail of a boudinaged orthopyroxene crystal with neoblasts of orthopyroxene and plagioclase (FOV = 2.75 mm; image 1270B_038).

Figure F22. Anhydrous major element compositions of gabbronorite samples from Hole 1270B, plotted in terms of oxide mole fractions (mole fractions calculated for SiO_2, TiO_2, Al_2O_3, Cr_2O_3, FeO, MnO, MgO, CaO, Na_2O, K_2O, P_2O_5, with all Fe as FeO). Calcic amphibole end-members are tremolite/actinolite, hornblende,

edenite, pargasite, and tschermakite. Chlorite end-member is clinochlore. The bold triangle encloses possible pyroxene gabbro and gabbronorite assemblages with calcic plagioclase. All of the Hole 1270B gabbronorites lie outside this triangle, indicating that they must have contained substantial proportions of igneous olivine (dashed lines) and/or Fe-Ti oxides (thin lines). Olivine could have been consumed by subsolidus or near-solidus oxidation reactions that produced pyroxene + magnetite. However, the high Ti contents of all Hole 1270B gabbronorites require substantial proportions of normative ilmenite and/or magnetite, so it is very likely that these rocks all contain igneous Fe-Ti oxides.

Figure F23. Glasses from the 14° to 16°N region of the Mid-Atlantic Ridge (Melson et al., 1977; C. Xia et al., unpubl. data) have a minimum Mg# = ~50%. Glasses with Mg#s < 50% are rare along the Mid-Atlantic Ridge. Mid-ocean-ridge glass data, including data from the Melson et al., Smithsonian catalog, were downloaded in April 2003 from PetDB (online at **petdb.ldeo.columbia.edu/petdb/**).

Figure F24. Photomicrograph of zircon crystals (Sample 207-1270D-4R-1 [Piece 7, 33–37 cm]) (cross polarized light: blue filter; field of view = 0.7 mm; image 1270D_002).

Figure F25. Anhydrous major element compositions of hydrothermally altered peridotite samples from Sites 1268 and 1270, plotted in terms of mole fraction of SiO_2 vs. mole fraction of MgO + FeO, compared to anhydrous compositions of end-member minerals (speciation as for Fig. F22). Tick marks along the vector connecting olivine and pyroxene are for variations in normative orthopyroxene content in terms of weight percent orthopyroxene/(orthopyroxene+olivine), assuming olivine Mg# = orthopyroxene Mg#. All but two of the serpentinized peridotites from these sites have >30 wt% normative orthopyroxene, indicative of substantial addition of SiO_2 and/or loss of MgO + FeO. Slight divergence of the peridotite compositions from the MgO+FeO to SiO_2 mixing line is due to the minor presence of other oxides, mainly in the form of a few percent Cr-Al spinel in most peridotite samples.

Figure F26. Photograph of *Shinkai* 6500 dive sample 425-R007, a peridotite mylonite ~45 cm long, recovered from a planar, striated outcrop surface dipping ~20° to the west, just a few tens of meters from the site of Hole 1270A. Textures in this sample record localized mylonitic deformation of peridotite at ~600°C, strikingly different from textures in peridotites from Holes 1270A, 1270C, and 1270D, which record protogranular to mildly porphyroclastic deformation at temperatures >1000°C, except within a few millimeters of gabbro-hosted, mylonitic shear zones.

Figure F27. **A, B.** Data from Hole 1270B gabbronorites, comparing the intensity of crystal-plastic deformation (estimated during visual core description, supplemented with thin section observation) to the proportion of magnetite estimated from magnetic susceptibility measurements on large individual core pieces. Deformation intensities vary on a small scale, due to the presence of anastomosing shear zones around less deformed gabbroic rocks, so the deformation intensity data in both A and B are smoothed using a 10-piece running average, weighted by piece length. The estimated proportion of magnetite also shows large variations on short length scales, as can be seen in A. Thus, in B, the magnetite proportions are presented as a 5-point running median. Magnetite proportions have not been estimated for every core piece and the spacing of estimates downhole is not uniform, but the data are so sparse that there is no way to weight the observations by length. For this reason, the comparison illustrated here is only preliminary. However, this provisional comparison supports the hypothesis that deformation intensity and magnetite proportions are correlated within some intervals of the core, as has been proposed for ODP Holes 735B and 1105A (e.g., Dick et al., 1991, 2000, 2002; Natland and Dick, 2002; Natland et al., 1991; Niu et al., 2002; Ozawa et al., 1991; Pettigrew, Casey, Miller, et al., 1999).

Figure F28. Schematic illustration of possible dips of high-temperature crystal-plastic foliations in gabbroic rocks from Hole 1270B, and peridotites from Holes 1270C and 1270D. Gabbroic rocks record dominantly negative magnetic inclinations, suggesting that these rocks may be reversely magnetized, consistent with—but not required by—their position ~13–18 km east of the rift axis. Based on this assumption, rotation of crystal-plastic foliations around a vertical axis to reorient core so that remanent magnetizations have a constant azimuth planes that dipped east at ~45° when the remanent magnetization vector pointed south. **A.** If both gabbroic rocks and peridotites are reversely magnetized, the crystal-plastic foliations in peridotites dipped west at ~45° when the remanent magnetization vector pointed south, at a 90° angle to the fabrics in gabbroic rocks. **B.** If, instead, both gabbroic rocks in Hole 1270B and peridotites in Holes 1270C and 1270D are normally magnetized, high-temperature crystal-plastic foliations in gabbroic rocks from Hole 1270B dipped east at ~45° when the remanent magnetization vector pointed north and mylonite zones in peridotites from Holes 1270C and 1270D dipped west at ~45° when the remanent magnetization vector pointed north. **C.** It is assumed that the peridotites were magnetized later than the gabbroic rocks and record normal polarity. With this assumption, crystal-plastic fabrics in Holes 1270B, 1270C, and 1270D are parallel and dipped ~45° to the east when the remanent magnetization vector in Hole 1270B pointed south and the remanent magnetization vector in Holes 1270C and 1270D pointed north.

Figure F29. Magnetic inclination as a function of the amount of rotation around a horizontal axis for rocks with a magnetic inclination of ±28° and a declination of 0°. Inclinations of –14°, the average value in gabbro and gabbronorite from Hole 1270B, and –3°, the average value in peridotite from Holes 1270C and 1270D, are shown for reference. Relatively small rotations around a horizontal east-west axis could produce the inclinations in the gabbroic rocks and the peridotites. However, this is problematic if gabbroic rocks are reversely magnetized and peridotites are normally magnetized, as in Figure F28C. If all samples are normally magnetized, as in Figure F28B, then clockwise rotations of 42° and 31° around an east-west axis could produce the inclinations in the gabbroic rocks and the peridotites, respectively. However, there is little evidence for east-west—striking, north-dipping faults in bathymetric data from the region around Site 1270 (e.g., Fujiwara et al., 2003). Instead, geological reasoning suggests that tectonic rotations in this area are likely to be clockwise around a ridge-parallel, nearly horizontal axis striking 020°. Large rotations around a horizontal axis striking 020° could produce the observed –14° inclination in gabbroic rocks, whereas somewhat smaller clockwise rotations could produce the observed –3° inclination in peridotites. For the scenario in Figure F28C, in which gabbroic rocks are reversely magnetized (dashed curves) while peridotites are normally magnetized (solid curves), this requires ~45°–50° of clockwise rotation after both rock types acquired their remanent magnetization. For the scenario in Figure F28B, in which both gabbroic rocks and peridotites are normally magnetized (solid curves), we hypothesize the gabbronorites acquired their remanent magnetization at the magnetite blocking temperature (~500°–570°C) during slow cooling of the rocks as they were uplifted toward the seafloor. Peridotites acquired their remanent magnetization at a later time, during magnetite growth associated with hydrothermal alteration and serpentinization at ~300°C. Rotation began before serpentinization of the peridotites, so the peridotites record only part of the tectonic rotation.

Figure F30. Magnetic inclination as a function of the amount of rotation around an axis with an azimuth of 020° for rocks which initially have a magnetic inclination of ±28° and a declination of 0°, showing the effect of different plunges of the rotation axis. Solid curves = normally polarized rocks, dashed curves = reversely polarized rocks.

Figure F31. Lithostratigraphic summary for Holes 1271A and 1271B. TD = total depth.

Figure F32. Close-up photograph of network of gabbro intrusions in dunite (interval 209-1271A-1R-1, [Piece 9, 37–51 cm]). A large crystal of clinopyroxene (now amphibole) is included in the dunite at 46–51 cm.

Figure F33. Anhydrous major element compositions of hydrothermally altered peridotite samples from Sites 1268, 1270, and 1271, plotted in terms of mole fraction of SiO_2 vs. mole fraction of MgO + FeO + CaO, compared to anhydrous compositions of end-member minerals (speciation as for Fig. F22). Tick marks along the vector connecting olivine and pyroxene indicate variations in normative orthopyroxene content, in terms of weight percent orthopyroxene/(orthopyroxene+olivine), assuming olivine Mg# = orthopyroxene Mg#. Most serpentinized dunites and harzburgites from Site 1271 have <30 wt% normative orthopyroxene and so do not require metasomatic increases in Si/(Mg+Fe) during alteration. Substantial divergence of the Site 1271 peridotite compositions from the MgO+FeO to SiO_2 mixing line is due to the presence of interstitial gabbroic material, originally including plagioclase and/or igneous amphibole, especially in the impregnated dunite sample. Site 1270 dunites also include relatively abundant Cr-Al spinel.

Figure F34. Molar Mg# vs. Ni concentration for peridotite samples from Sites 1270 and 1271. Whole-rock Mg#s are assumed to be close to original olivine Mg#s in all samples. The whole-rock Ni content in dunites is a good approximation for the Ni concentration in olivine in these samples. Ni concentrations in olivine in the harzburgites were estimated using an olivine/orthopyroxene Ni distribution coefficient of 4 at ~1250°C (Kelemen et al., 1998a), appropriate for igneous conditions beneath a mid-ocean ridge, and bounds of 10 and 30 wt% on the modal proportion of orthopyroxene. The Ni concentration in olivine in a sample of impregnated dunite was calculated in the same way. The olivine crystallization curve shows the composition of olivine in equilibrium with liquid during fractional crystallization of olivine from primitive mid-ocean-ridge basalt (MORB). The initial liquid composition was an estimated 10% melt of the MORB source, assuming polybaric incremental melting with an average pressure of 1 GPa (Kinzler and Grove, 1992, 1993). We used an olivine/liquid Fe/Mg K_d of 0.3 (Roeder and Emslie, 1970) and the dependence of the olivine/liquid Ni distribution coefficient on MgO content of the liquid determined by Hart and Davis (1978). Light gray symbols in the background are olivine compositions from the crust–mantle transition zone (MTZ) in the Samail and Wadi Tayin massifs of the Oman ophiolite (Godard et al., 2000; Koga et al., 2001). The Site 1271 dunites with the lowest Mg# have olivine Ni concentrations comparable to Ni in olivine in the most depleted residual harzburgites from Sites 1270 and 1271. These data are consistent with formation of the dunites by reaction between relatively low Mg# melt and residual mantle olivine and inconsistent with formation of the dunites as olivine cumulates during fractional crystallization of olivine from primitive MORB. Opx = orthopyroxene, harz = harzburgite.

Figure F35. Close-up photograph of chromitite pod in dunite. The matrix surrounding chromite in the chromitite pod consists of chlorite (possibly replacing plagioclase) and amphibole. The host dunite intruded by the chromitite is also rich in chromian spinel (interval 209-1271B-4R-2 [Piece 2, 38–48 cm]).

Figure F36. Close-up photograph of brown amphibole gabbro (interval 209-1271B-6R-1, 21–27 cm).

Figure F37. Photomicrographs showing that the evolution of brown amphibole gabbro during deformation and metamorphism is complex and involves several stages. **A–C.** Sample 209-1271B-14R-1, 25–29 cm (cross polarized light [XPL]: blue filter). (A) Ductile deformation. Amphibole porphyroclast with wavy extinction (a(p)) represents a microboudin that has been syntectonically recrystallized to fine-grained amphibole neoblasts (a(n)) along its margins (field of view [FOV] = 5.5 mm; image 1271B_058). (B) Amphibole

porphyroclasts (a(p)) have been partially replaced by amphibole neoblasts (a(n)). The amphibole is surrounded by bands of former plagioclase neoblasts that have been statically altered to sericite (sc(n)) (FOV = 5 mm; image 1271B_059). (C) The outline of a "ghost" plagioclase porphyroclast replaced by sericite (sc(p)) can be recognized in this sample. The original polysynthetic twinning of the plagioclase porphyroclasts (white arrows) is pseudomorphed by sericite with different orientations. Former plagioclase neoblasts are pseudomorphically replaced by sericite aggregates (sc(n); red arrows) (FOV = 2.75 mm; image 1271B_060). **D, E.** Sample 209-1271B-11R-1, 44–46 cm (XPL: blue + dark gray filters; FOV = 1.4 mm). (D) Intergrowth of fibrous amphibole (a2) and chlorite after former high-temperature amphibole. Fibrous amphibole and chlorite are stretched and deformed along shear bands (image 1271B_049). (E) Amphibole-chlorite schists after gabbroic protolith. The secondary fibrous amphibole (a2), sericite (sc), and chlorite (ch) are stretched and banded, defining the schistosity (image 1271B_048). **F.** Fold of fibrous amphibole (a2) in a amphibole-chlorite schists after gabbro. Chlorite (ch) crystallized in the pressure shadow of the inner part of the fold. The matrix is composed of fine fibrous aggregates of secondary amphibole (a2) and chlorite (a2) (may by replacing former high-temperature amphibole) alternating with dark bands of sericite and hydrogrossular (sc and hgr) (may by replacing former plagioclase) (Sample 209-1271B-11R-1, 55–57 cm) (plane polarized light: blue + dark gray filters; FOV = 5.5 mm; image 1271B_053).

Figure F38. Stratigraphic distribution of lithologic proportions, lithologic variability, and modal orthopyroxene in peridotites are shown along with the graphical depiction of the recovery for each interval. TD = total depth.

Figure F39. Core photographs of alternating bands of dunite (D) and harzburgite (H). Harzburgite at the bottom is enriched in orthopyroxene (opx) (interval 209-1272A-23R-1 [Pieces 2, 3, 4–77 cm]).

Figure F40. **A.** Comparison of compositions of diabase and miarolitic gabbro from Hole 1272A with compositions of Mid-Atlantic Ridge basalt glasses. The Hole 1272A samples have compositions that lie within the range of observed glass compositions, consistent with the hypothesis that all preserve liquid, rather than cumulate, compositions. **B.** Like glasses from the 14° to 16°N region, the samples from Site 1272 fall at the high end of the range of SiO_2 and Zr concentration in Mid-Atlantic Ridge glasses at a given Mg#. Glass compositions from the 14° to 16°N region of the Mid-Atlantic Ridge are from Melson et al. (1977) and C. Xia et al. (unpubl. data). Mid-ocean-ridge glass data, including data from the Melson et al. catalog, were downloaded in April 2003 from PetDB (online at **petdb.ldeo.columbia.edu/petdb/**).

Figure F41. Anhydrous major element compositions of hydrothermally altered peridotite samples from Sites 1268, 1270, 1271, and 1272, plotted in terms of mole fraction of SiO_2 vs. mole fraction of MgO + FeO, compared to anhydrous compositions of end-member minerals (speciation as for Figure 22). Tick marks along the vector connecting olivine and pyroxene are for variations in normative orthopyroxene content, in terms of weight percent orthopyroxene/(orthopyroxene+olivine), assuming olivine Mg# = orthopyroxene Mg#. Most serpentinized dunites and harzburgites from Site 1272 have <25 wt% normative orthopyroxene and so do not require metasomatic increases in Si/(Mg+Fe) during alteration. Substantial divergence of two Site 1272 peridotite compositions from the MgO + FeO to SiO_2 mixing line is due to the presence of carbonate alteration in veins and perhaps also in the serpentinite matrix.

Figure F42. Close-up photographs of examples of semiplastic fault gouges from Hole 1272A. The fault gouges were semicohesive fault breccias with matrix-supported clasts. **A.** Interval 209-1272A-18R-1, 134–149 cm. **B.** Interval 209-1272A-18R-2, 1–19 cm. **C.** Interval 209-1272A-19R-1, 138–150 cm. **D. E.** Interval 209-1272A-19R-2, 1–18 cm. **F.** Interval 209-1272A-25R-2, 8–26 cm.

Figure F43. Stratigraphic distribution of lithologic proportions and lithologic variability in Hole 1274A with a graphical depiction of the recovery for each interval. TD = total depth.

Figure F44. Photomicrographs of Sample 209-1274A-8R-1, 15–18 cm (cross polarized light). **A.** Clinopyroxene-spinel symplectite at the contact between protogranular orthopyroxene and olivine. The symplectite extends into the olivine (field of view = 2.75 mm; image 1274A_049). **B.** Close up showing that the clinopyroxene is a single crystal with undulatory extinction (field of view = 1.4 mm; image 1274A_050).

Figure F45. Anhydrous major element compositions of hydrothermally altered peridotite samples from Sites 1268, 1270, 1271, 1272, and 1274, plotted in terms of mole fraction of SiO_2 vs. mole fraction of MgO + FeO, compared to anhydrous compositions of end-member minerals (speciation as for Figure F22). Tick marks along the vector connecting olivine and pyroxene are for variations in normative orthopyroxene content, in terms of weight percent pyroxene/(pyroxene+olivine), assuming olivine Mg# = pyroxene Mg#. Partially serpentinized "dunites" from Site 1274 have ~5–13 wt% normative pyroxene. Five of six partially serpentinized harzburgites from Site 1274 have 26–29 wt% normative pyroxene, more than expected for highly depleted residual peridotites, and so may have undergone metasomatic increases in Si/(Mg+Fe) during alteration. Divergence of a Site 1274 fault gouge mud from the MgO + FeO + CaO to SiO_2 mixing line is probably due mechanical mixing of gabbroic and ultramafic material in the fault gouge.

Figure F46. Weight percent CO_2 vs. weight percent CaO in metaperidotite samples from ODP Legs 153 and 209. Leg 153 data from Cannat, Karson, Miller, et al. (1995) and Casey (1997). The upper diagram shows that most samples with high CaO have high CO_2 and lie along a mixing line toward calcite and aragonite $CaCO_2$. A few samples with high CaO and low CO_2 are impregnated peridotites, which include igneous plagioclase and clinopyroxene precipitated from melts migrating along grain boundaries. The lower diagram shows more detail for samples with low CO_2 and CaO contents. Although the data are scattered, much of this may be due to analytical uncertainty. Most metaperidotites from Legs 153 and 209 contain appreciable CO_2, mainly in aragonite and calcite. Thus, carbonate alteration accounts for a significant fraction of the whole-rock CaO budget in these rocks. This suggests, but does not prove, that CaO may have been metasomatically added to these rocks along with CO_2 during hydrothermal alteration.

Figure F47. Sr and Ba concentrations vs. weight percent CO_2 in metaperidotite samples from Leg 209. The samples with the highest Sr contents all include substantial proportions of carbonate; thus, carbonate minerals probably are the primary host for Sr in Leg 209 metaperidotites and much of the Sr may have been introduced during hydrothermal metasomatism. A few samples with high Ba and low CO_2 are impregnated peridotites, which include igneous plagioclase and clinopyroxene precipitated from melts migrating along grain boundaries. However, other samples with high Ba also have high CO_2 contents, consistent with the hypothesis that metasomatically introduced Ba in hydrothermal carbonate provides most of the Ba in the whole-rock budget for many Leg 209 metaperidotites.

Figure F48. Percent of hydrothermal alteration in Sites 1272 and 1274 metaperidotites (estimated during visual core description) vs. density and magnetic susceptibility. Variations in these parameters, as well as data on seismic *P*-wave velocity and porosity, are moderately well correlated.

Figure F49. Close-up photograph of mud interval from the fault gouge zone recovered in Hole 1274A (interval 209-1274A-24R-1, 3–29 cm).

Figure F50. Stratigraphic distribution of lithologic proportions and lithologic variability of Holes 1275B and 1275D plotted at the same vertical scale. Recovery columns are set at 90 m apart on the same scale (which is the approximate distance between holes). Dashed lines connect intervals of troctolite. TD = total depth.

Figure F51. Close-up photograph of troctolite with intergranular gabbroic material cut by altered gabbroic veins (interval 209-1275D-9R-1, 79–109 cm).

Figure F52. Comparison of experimental pressures for melts equilibrated with olivine + orthopyroxene + clinopyroxene + plagioclase ± spinel, with pressures calculated using the method of Kinzler and Grove (1992, 1993). Pressures were calculated for each of four expressions using normative olivine, plagioclase, quartz, and clinopyroxene in the melt compositions. These four pressures were then averaged, as recommended by Kinzlier and Grove. The error bars on the calculated pressures show the range from maximum to minimum pressure calculated from the four expressions. As the figure shows, this method reproduces the experimental data on which it is calibrated with a precision of about ±0.2 GPa.

Figure F53. Estimated conditions for equilibration of MORB glass compositions from 14° to 16°N along the Mid-Atlantic Ridge with olivine + orthopyroxene + clinopyroxene + plagioclase ± spinel. Equilibration pressures were calculated as described in the caption for Figure F52. Equilibration temperatures were calculated using each of the four pressure estimates for each glass composition, and then averaged. For both pressure and temperature (P-T), the error bars for each individual composition show the range from maximum to minimum calculated pressure and temperature. Error bars for the average P-T estimate for primitive glasses, with molar Mg# > 0.6, are for 2 standard deviations from the mean pressure and temperature. The standard error of the mean for the average pressure-temperature estimate for primitive glasses is about 90 times smaller than the standard deviation.

Figure F54. Estimated molar Mg# vs. Ni concentration in olivine in Site 1275 troctolites, compared to similar estimates for peridotite samples from Sites 1270, 1271, 1272, and 1274. Whole-rock Mg#s are assumed to be close to original olivine Mg#s in all samples. We estimated the olivine Ni concentrations in the troctolites based on the bulk compositions of samples with 0.2–3 wt% CO_2. To do this, we calculated CIPW norms for the anhydrous CO_2-free bulk composition. We then estimated the original Ni concentration in olivine, assuming Ni partitioning between olivine and pyroxenes was governed by partitioning at 1250°C, using relationships derived by Kelemen et al. (1998a), and that there is no Ni in plagioclase (or any other phase, including sulfide). The whole-rock Ni content in dunites is a good approximation for the Ni concentration in olivine in these samples. Ni concentrations in olivine in the harzburgites were estimated using an olivine/orthopyroxene Ni distribution from Kelemen et al. (1998a) and bounds of 10 and 30 wt% on the modal proportion of orthopyroxene. The olivine crystallization curve shows the composition of olivine in equilibrium with liquid during fractional crystallization of olivine from primitive mid-ocean-ridge basalt (MORB). The initial liquid composition was an estimated 10% melt of the MORB source, assuming polybaric incremental melting with an average pressure of 1 GPa (Kinzler and Grove, 1992, 1993). We used an olivine/liquid Fe/Mg K_d of 0.3 (Roeder and Emslie, 1970) and the dependence of the olivine/liquid Ni distribution coefficient on MgO content of the liquid determined by Hart and Davis (1978). Light gray symbols in the background are olivine compositions in dunites, impregnated dunites, and wehrlites from the crust–mantle transition zone (MTZ) in the Samail and Wadi Tayin massifs of the Oman ophiolite (Godard et al., 2000; Koga et al., 2001). Like most Site 1271 dunites and some Oman MTZ dunites, the estimated olivine compositions in the Site 1275 troctolites have olivine Ni concentrations comparable to Ni in olivine in the most depleted residual harzburgites from Sites 1270

and 1271. These Mg#s are consistent with formation of the troctolites by reaction between relatively low Mg# melt and residual mantle olivine and inconsistent with formation of the dunites as olivine cumulates during fractional crystallization of olivine from primitive MORB. Readers should keep in mind that the method of estimating olivine composition, using the bulk composition of highly altered troctolites, is uncertain, so this result is preliminary. Opx = orthopyroxene.

Figure F55. Close-up photograph of gabbro with mixed grain sizes showing patches of fine-grained gabbro in a matrix of coarse-grained gabbro (interval 209-1275B-5R-1, 113–120 cm).

Figure F56. Close-up photographs of gabbro with various grain size domains in curviplanar and sharp (crenulate) contacts. **A.** Interval 209-1275B-13R-1, 75–91 cm. **B.** Interval 209-1275D-18R-1, 55–74 cm.

Figure F57. Histograms for molar Mg# in gabbroic rocks from sites drilled during this leg, Site 923 in the Kane Fracture Zone (MARK) area (Agar and Lloyd, 1997), and Site 735B along the Southwest Indian Ridge (Natland and Dick, 2002). Cumulate oxide gabbros and oxide gabbronorites dominate the gabbroic rocks recovered during Leg 209, especially at Sites 1270 and 1275. Diabases and miarolitic gabbros from Sites 1275 and 1272 have higher Mg#s than the oxide gabbros and closely approximate liquid compositions (see the "**Site 1272**" summary and Fig. F58). Site 1275 troctolites are probably hybrid rocks, formed by interaction between migrating melt and residual mantle olivine. Only at Site 1268 were gabbroic rocks with primitive cumulate compositions sampled. These rocks were gabbronorites. However, extensive alteration makes it difficult to be certain that their high Mg# is a primary igneous feature. In general, the Leg 209 gabbro samples, and particularly the gabbroic rocks from Site 1275, are the most evolved suite of plutonic rocks recovered by ODP drilling along a mid-ocean ridge. However, although some primitive gabbroic cumulates were sampled at Sites 921, 923, and 735B, the abundance of evolved gabbros leads to average compositions with intermediate Mg#s at these other sites. Thus, with the possible exception of Site 1268 gabbronorites and of impregnated peridotites from, for example, Sites 1271 and 1275, no plutonic suite recovered by ODP drilling provides an example of the refractory cumulates (80% < Mg# < 90%) required to balance crystal fractionation of MORB.

Figure F58. Plot of molar Mg# vs. ppm Zr in gabbroic rocks recovered during Leg 209. Also shown are the compositional field defined by mid-ocean-ridge basalt (MORB) glasses from the Mid-Atlantic Ridge, the average of Mid-Atlantic Ridge (MAR) MORB glass compositions, the composition of "normal MORB" (N-MORB) (from Hofmann, 1988), and average compositions of gabbros from ODP Sites 735B (Natland and Dick, 2002), and 923 (Agar and Lloyd, 1997). MORB glass data were downloaded in April 2003 from PetDB (online at **petdb.ldeo.columbia.edu/petdb/**). Because (1) Zr is an incompatible element that is almost completely retained in the melt during fractional crystallization of basalt, (2) primitive MORB glasses have ~50 ppm Zr, and (3) average MORB has ~100 ppm Zr, it follows that average MORB probably records ~50% crystal fractionation over the span of liquid Mg#s from ~70% in mantle-derived melts to 60% in average MORB. Gabbroic cumulates in equilibrium with melts in this compositional range should have high Mg#s. For example, using an Fe/Mg clinopyroxene/liquid K_d of 0.23 (e.g., Sisson and Grove, 1993a, 1993b) and assuming that 90% of the iron in melt is ferrous, we estimate that Mid-Atlantic Ridge glasses with Mg#s from 73% to 50% should crystallize clinopyroxene with Mg#s of ~93%–82%. Thus, there must be a mass of primitive gabbroic rocks with Mg#s substantially >70% and low Zr concentrations that is approximately equal to the mass of erupted volcanics and sheeted dikes. However, as also noted in the text and in the caption to Figure F57, very few gabbroic rocks sampled from the mid-ocean ridges to date have these characteristics. For example, the average gabbroic rocks from Sites 735 and 923 do not have appropriate

compositions to be the complementary cumulates required by MORB fractionation. During Leg 209, only the gabbronorites from Site 1268 and perhaps impregnated peridotites from, for example, Sites 1271 and 1275 could represent part of this complementary refractory cumulate reservoir. Diabases and miarolitic gabbros from Sites 1272 and 1275, together with a few fine-grained gabbroic rocks from Site 1275, have compositions very similar to MORB and are probably chilled liquid compositions. Most of the gabbroic rocks from Site 1275, together with more than one-half of those from Hole 1270B, have such low Mg#s that they cannot play a significant role in the main process of MORB crystal fractionation. Instead, they must crystallize from highly evolved, rarely sampled melts.

Figure F59. Histograms of stable remanent inclinations determined for archive-halves from Hole 1275D, illustrating how different depth intervals preserve distinctly different remanence inclinations. The top 50 m of the hole apparently records a mixture of normally and reversely polarized magnetization. The middle of the hole, from 50 to 140 mbsf, preserves a well-defined shallow negative inclination. Below a relatively sharp break at ~140 mbsf, the lower portion of the hole has a significantly higher negative inclination.

Figure F60. Comparison of rotary core barrel (RCB) and resistivity at the bit while coring (RAB-C) in the first three cores for each hole drilled during Leg 209.

NOTES

N1. Some undeformed gabbronorites may post-date the high temperature deformation, or - our preferred hypothesis - localization of the high temperature deformation preserved undeformed, pre-kinematic gabbronorites below the mylonitic shear zones

N2. It might seem simpler to envision 13° of clockwise rotation around a horizontal axis striking 270° to account for the shallow 15° inclination in the gabbros. However, to explain the steep 36° inclination in the peridotites via rotation around the same west-striking axis would require an antithetical, counter-clockwise rotation of 8°. It seems unlikely that rocks from the same hole would have undergone antithetical rotations.

N3. The discussion in the previous paragraphs considers only changes in the magnetic inclination due to rotation. However, tectonic rotations after acquisition of the magnetic remanence will also affect the magnetic declination and, hence, influence the reorientation of structural features. Figure F18 illustrates this effect, which can be as much as 50° for counterclockwise rotation around a horizontal or gently plunging axis striking 020°.

N4. In Figure F27, the approximate proportion of magnetite is quantified using measurements of magmatic susceptibility made on large individual core pieces. However, there are numerous uncertainties associated with this procedure. For example, the proportion of nonmagnetic ilmenite is not quantified, and the presence of Ti as ulvospinel component in the magnetite solid solution reduces its magnetic susceptibility, leading to an underestimate of magnetite proportion. Magnetite content inferred from susceptibility does not correlate well with estimates of oxide proportion in the visual core description, nor with estimates of oxide proportion based on chemical analyses and calculated mineral proportions, nor with estimates of oxide proportion based on thin section observations. However, these other estimates are not available on many samples and may be subject to a "nugget effect," leading to large variations in oxide proportion observed in thin sections on the centimeter scale, and inferred from geochemical analyses of small samples, so we have used the more continuous (and internally consistent?) data set derived from interpretation of magnetic susceptibility.

N5. If the constraint that tectonic rotation axes were parallel to the rift axis is dropped, smaller rotations around a horizontal axis striking 270° can account for the inclinations in the gabbroic rocks and the peridotites. However, this is problematic if Hole 1270B rocks are reversely magnetized, whereas Hole 1270C and 1270D samples are normally magnetized, because it requires opposite senses of rotation for the samples from the different holes. Alternatively, if all are normally magnetized, a minimum of 42° of clockwise rotation can account for the –14° inclination in the gabbroic rocks from Hole 1270B and a minimum rotation of 31° of clockwise rotation can account for the –3° inclination in the peridotites from Holes 1270C and 1270D. Given the scarcity of north- and south-

facing slopes in the rift mountains flanking the Mid-Atlantic Ridge in this area, such large tectonic rotations around east-west axes seem unlikely.

N6. The discussion in the previous paragraphs considers only changes in the magnetic inclination due to rotation. However, tectonic rotations after acquisition of the magnetic remanence will also affect the magnetic declination and, hence, influence the reorientation of structural features. See **"Site 1268"** and Figure F18, and accompanying text for further discussion.

N7. About 7% of the recovered core from Hole 1274A consisted of poorly consolidated mud and matrix supported, cataclastic breccia, interpreted as fault gouge. This material had a dominantly ultramafic protolith, but observation of gabbroic clasts as well as peridotite clasts, and geochemical data indicate that it is a mixture including a substantial proportion of gabbroic material.

N8. Note that at Site 1271, just a few kilometers south of Site 1272, we recovered abundant gabbroic rocks that were clearly intrusive into harzburgite.

N9. If the normative proportions of orthopyroxene are primary, then some harzburgites have been incorrectly classified as orthopyroxene-bearing dunites

N10. Plagioclase contains more Sr and Ba than olivine, pyroxene, and spinel in residual peridotites, so that impregnated peridotites, together with carbonate-rich metaperidotites, have high Sr and Ba compared to other samples.

N11. The fact that H_2O is conserved in this reaction suggests that it may be pressure sensitive, so perhaps there are conditions under which the assemblage brucite + talc is stable; however, this is doubtful for low-pressure hydrothermal alteration.

N12. Note that this analysis assumes that a melt was in equilibrium with olivine but does not assume that the olivine in the troctolites crystallized from that melt. It is not important for this discussion whether the olivine in the troctolites is entirely igneous in origin, or whether some of the olivine is relict, residual olivine from mantle peridotite.

Table T1. Leg 209 coring summary.

Site	Hole	Rotary core barrel (RCB) system				RAB-C System				Site coring totals			
		Cores	Cored (m)	Recovered (m)	Recovery (%)	Cores	Cored (m)	Recovered (m)	Recovery (%)	Cores	Cored (m)	Recovered (m)	Recovery (%)
MAR-4S	1268A	29	147.6	78.69	53.3%	0	0.0	0.00	NA	29	147.6	78.69	53.3%
Site 1268 totals:		29	147.6	78.69	53.3%	0	0.0	0.00	0.0%	29	147.6	78.69	53.3%
MAR-3S	1269A	1	15.3	0.39	2.5%	0	0.0	0.00	NA	1	15.3	0.39	2.5%
	1269B	1	11.1	0.53	4.8%	0	0.0	0.00	NA	1	11.1	0.53	4.8%
	1269C	2	18.3	0.26	1.4%	0	0.0	0.00	NA	2	18.3	0.26	1.4%
Site 1269 totals:		4	44.7	1.18	2.6%	0	0.0	0.00	0.0%	4	44.7	1.18	2.6%
MAR-Alt2S	1270A	4	26.9	3.28	12.2%	0	0.0	0.00	NA	4	26.9	3.28	12.2%
	1270B	10	45.9	17.17	37.4%	0	0.0	0.00	NA	10	45.9	17.17	37.4%
	1270C	3	18.6	1.98	10.6%	0	0.0	0.00	NA	3	18.6	1.98	10.6%
	1270D	11	57.3	7.68	13.4%	0	0.0	0.00	NA	11	57.3	7.68	13.4%
Site 1270 totals:		28	148.7	30.11	20.2%	0	0.0	0.00	0.0%	28	148.7	30.11	20.2%
MAR-2S	1271A	6	44.8	5.76	12.9%	0	0.0	0.00	0.0%	6	44.8	5.76	12.9%
	1271B	20	103.8	15.90	15.3%	0	0.0	0.00	0.0%	20	103.8	15.90	15.3%
	1271C	0	0.0	0.00	0.0%					0	0.0	0.00	
Site 1271 totals:		26	148.6	21.66	14.6%	0	0.0	0.00	0.0%	26	148.6	21.66	14.6%
MAR-1S	1272A	27	131.0	37.50	28.6%	0	0.0	0.00	0.0%	27	131.0	37.50	28.6%
Site 1272 totals:		27	131.0	37.50	28.6%	0	0.0	0.00	0.0%	27	131.0	37.50	28.6%
MAR-3N	1273A	1	13.6	0.39	2.9%	0	0.0	0.00	0.0%	1	13.6	0.39	2.9%
	1273B	3	26.2	0.46	1.8%	0	0.0	0.00	0.0%	3	26.2	0.46	1.8%
	1273C	3	27.7	0.62	2.2%	0	0.0	0.00	NA	3	27.7	0.62	2.2%
Site 1273 totals:		7	67.5	1.47	2.2%	0	0.0	0.00	0.0%	7	67.5	1.47	2.2%
MAR-1N	1274A	28	155.8	34.65	22.2%	0	0.0	0.00	0.0%	28	155.8	34.65	22.2%
Site 1274 totals:		28	155.8	34.65	22.2%	0	0.0	0.00	0.0%	28	155.8	34.65	22.2%
MAR-Alt1N	1275A	1	5.0	0.13	2.6%	0	0.0	0.00	0.0%	1	5.0	0.13	2.6%
	1275B	22	108.7	46.90	43.1%	0	0.0	0.00	0.0%	22	108.7	46.90	43.1%
	1275C	0	0.0	0.00	NA	3	20.8	0.17	0.8%	3	20.8	0.17	0.8%
	1275D	43	209.0	104.63	50.1%	0	0.0	0.00	NA	43	209.0	104.63	50.1%
Site 1275 totals:		66	322.7	151.66	47.0%	3	20.8	0.17	0.8%	69	343.5	151.83	44.2%
Leg 209 totals:		215	1166.6	356.92	30.6%	3	20.8	0.17	0.8%	218	1187.4	357.09	30.1%

Note: RAB-C = resistivity at the bit while coring.

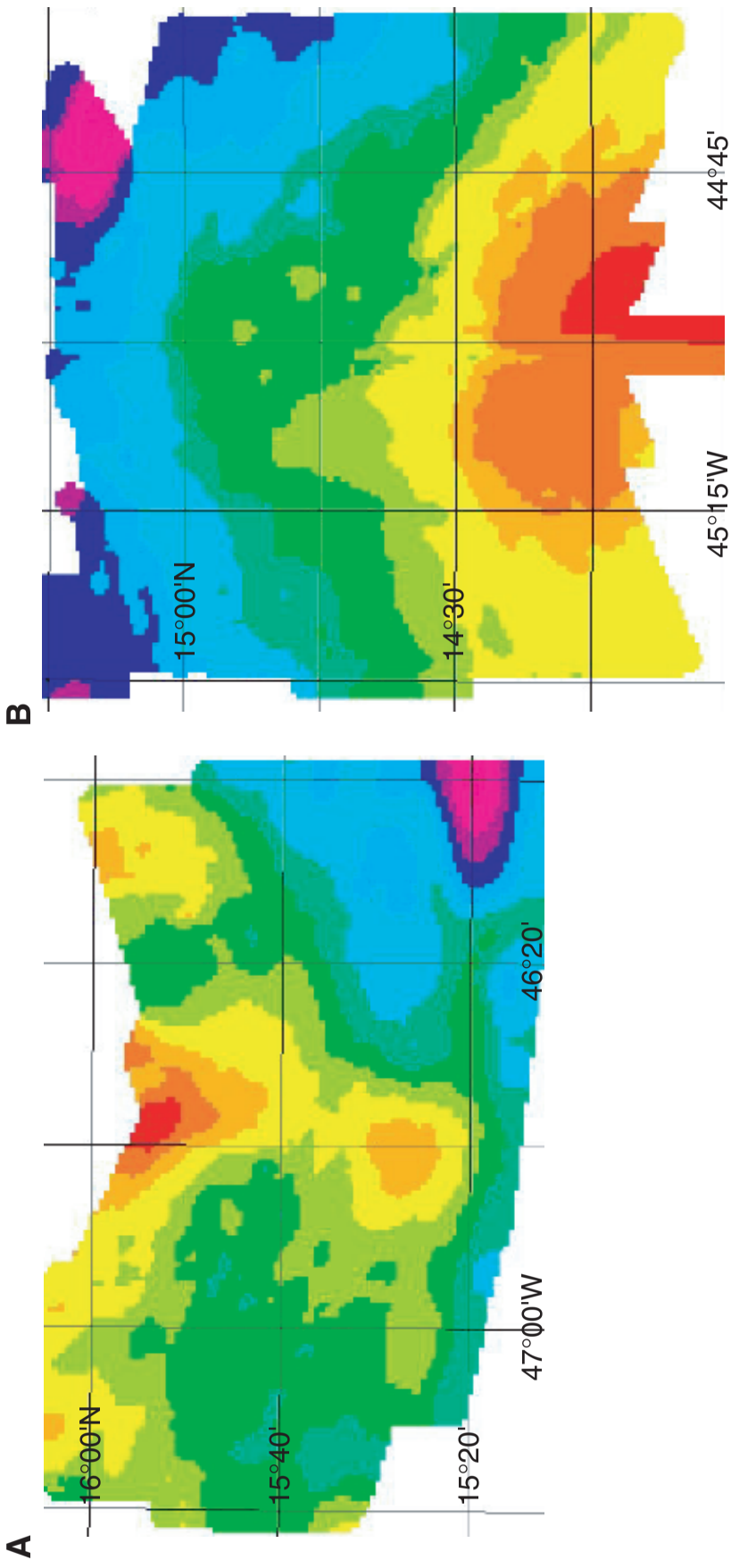

Figure F1

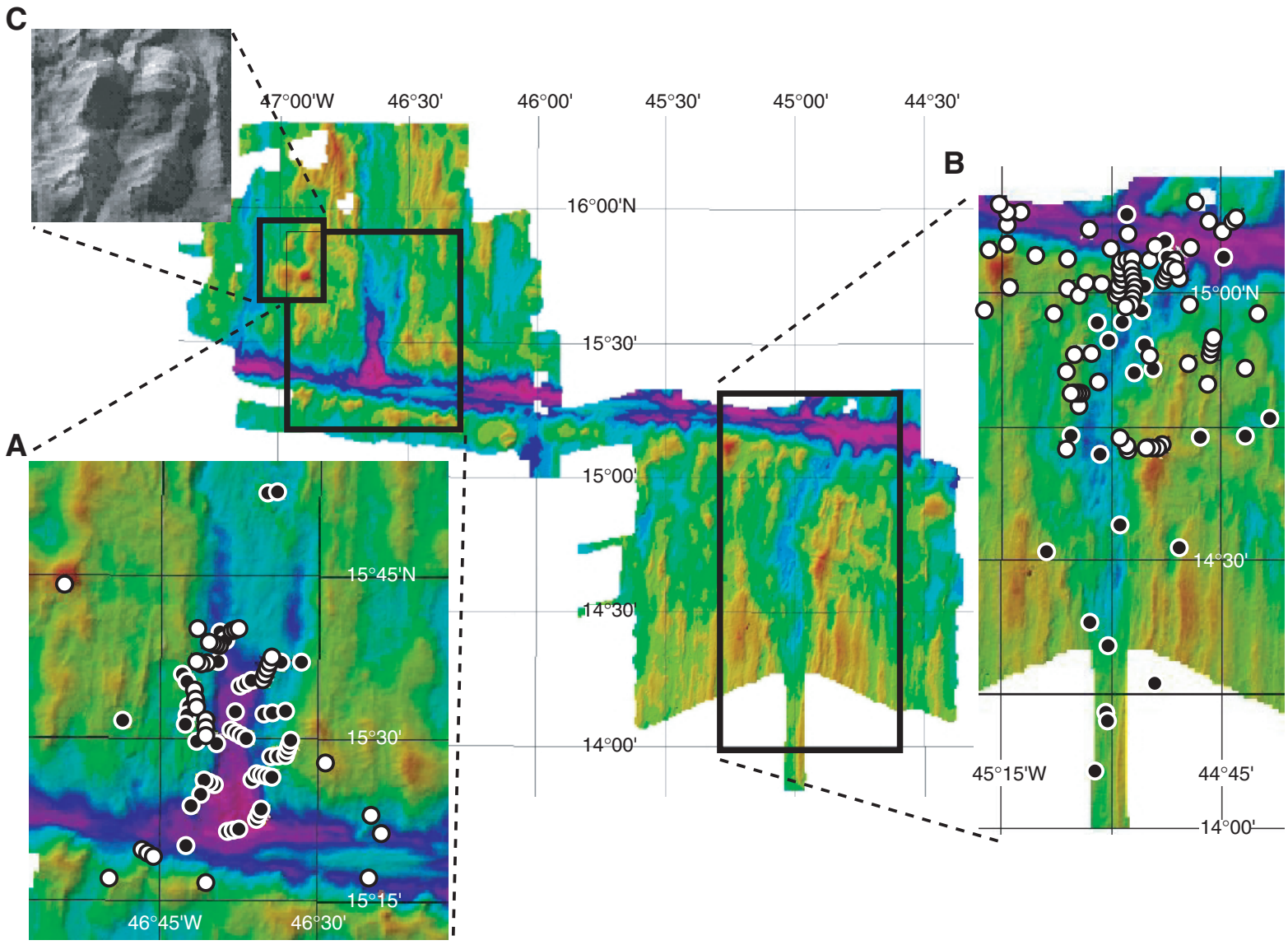
C
47°00'W
46°30'
46°00'
45°30'
45°00'
44°30'
16°00'N
15°30'
15°00'
14°30'
14°00'
B
15°00'N
14°30'
45°15'W
44°45'
14°00'
A
15°45'N
15°30'
15°15'
46°45'W
46°30'

Figure F2

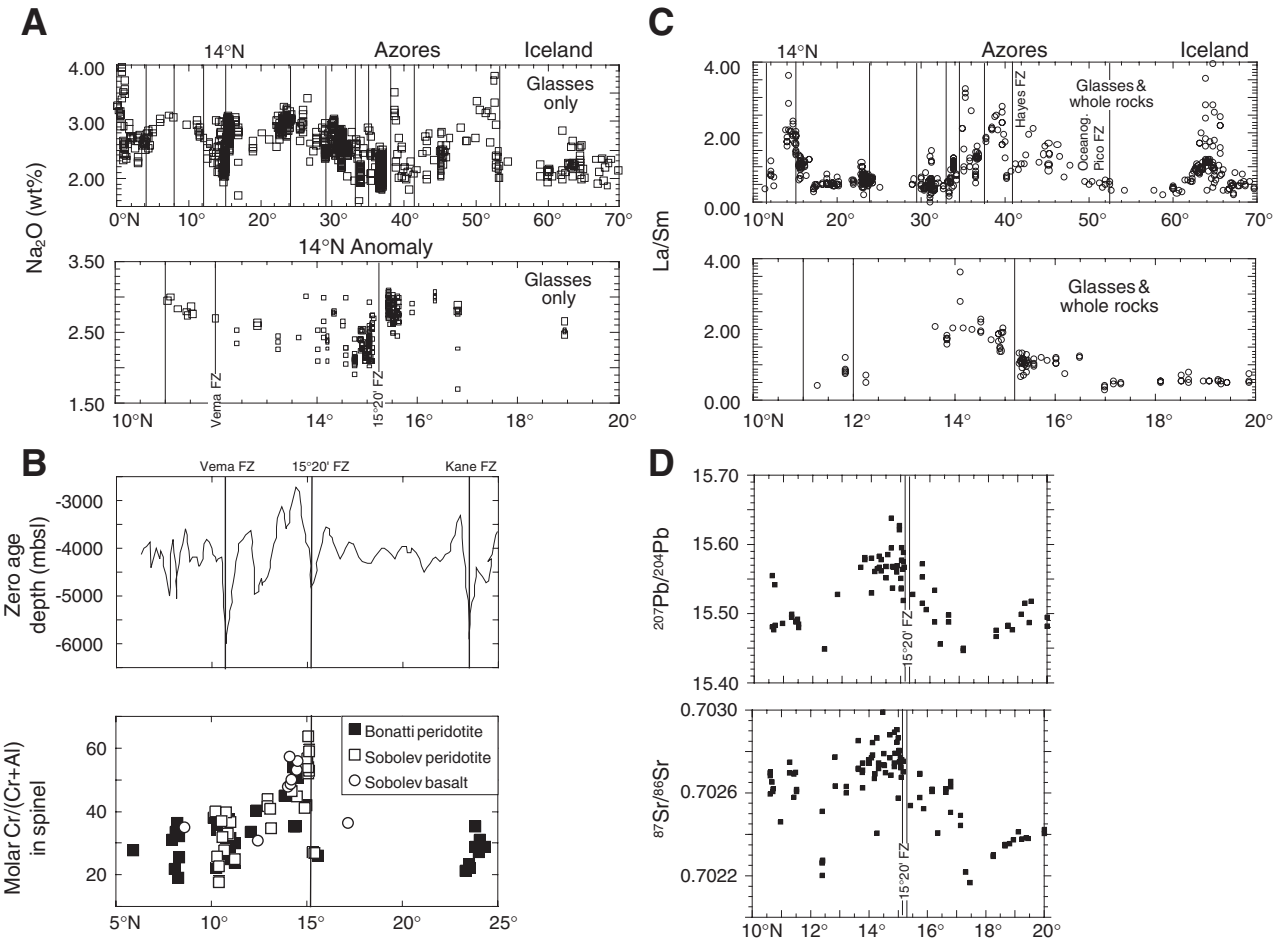
A
14°N
Azores
Iceland
Glasses only
Na2O (wt%)
14°N Anomaly
Vema FZ
15°20' FZ
B
Vema FZ
15°20' FZ
Kane FZ
Zero age depth (mbsl)
Molar Cr/(Cr+Al) in spinel
Bonatti peridotite
Sobolev peridotite
Sobolev basalt
C
Glasses & whole rocks
Hayes FZ
Oceanog.
Pico FZ
La/Sm
D
207Pb/204Pb
87Sr/86Sr

Figure F3

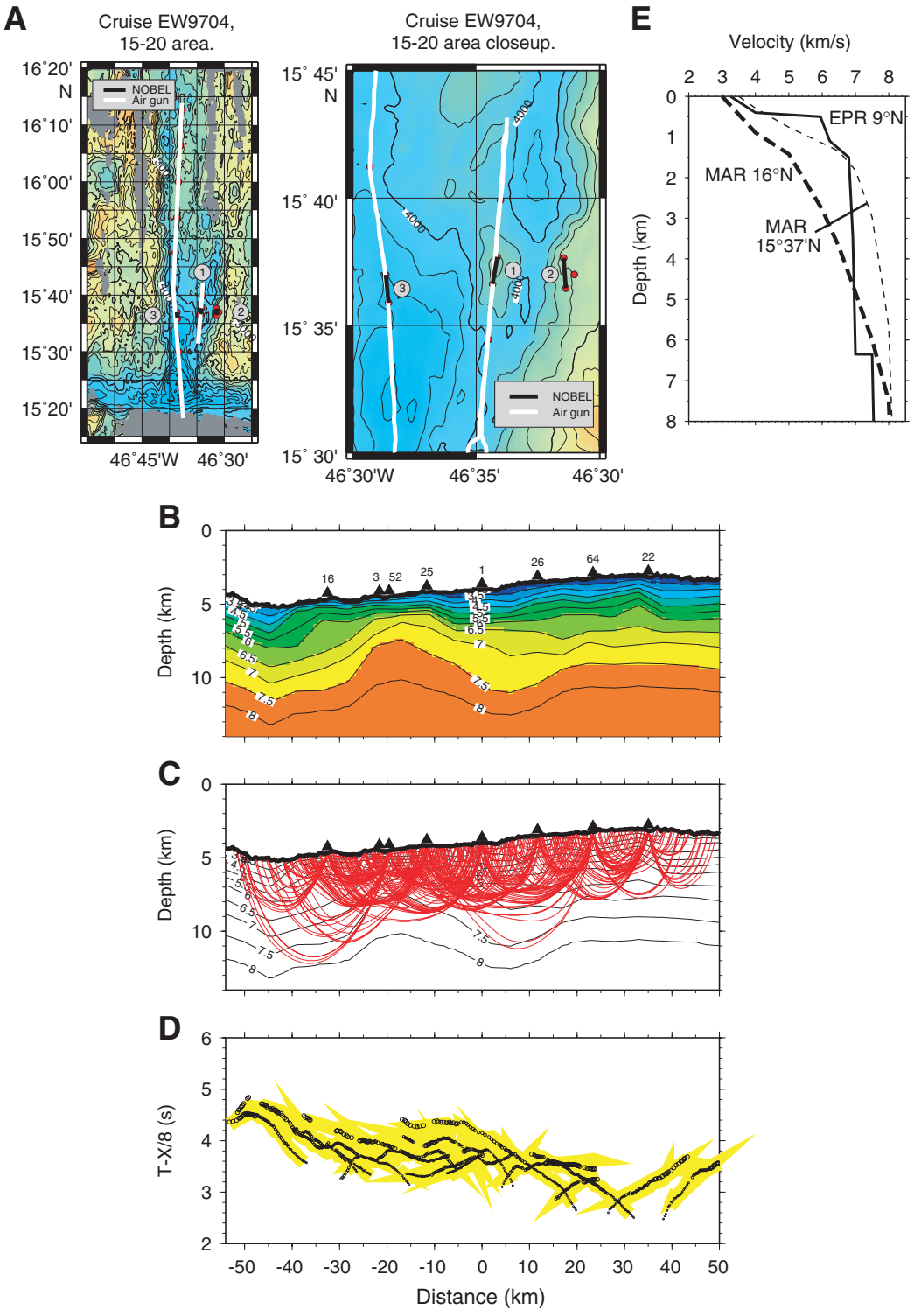
A
Cruise EW9704,
15-20 area.
NOBEL
Air gun
16°20' N
16°10'
16°00'
15°50'
15°40'
15°30'
15°20'
46°45'W
46°30'
Cruise EW9704,
15-20 area closeup.
15° 45' N
15° 40'
15° 35'
15° 30'
46°30'W
46°35'
46°30'
4000
E
Velocity (km/s)
2 3 4 5 6 7 8
EPR 9°N
MAR 16°N
MAR
15°37'N
Depth (km)
B
Depth (km)
16 3 52 25 1 26 64 22
C
Depth (km)
D
T-X/8 (s)
-50 -40 -30 -20 -10 0 10 20 30 40 50
Distance (km)

Figure F4

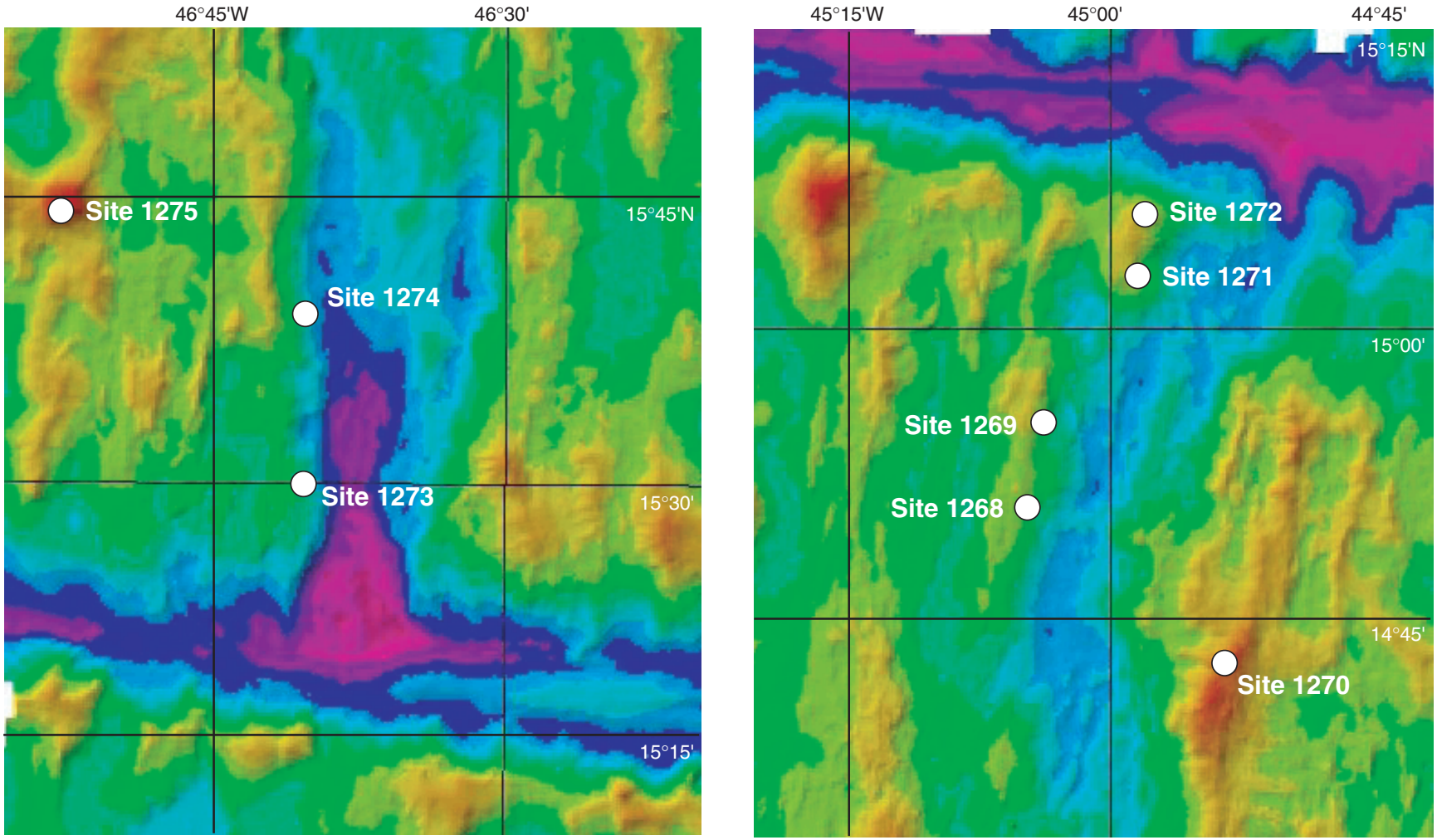
46°45'W
46°30'
15°45'N
15°30'
15°15'
Site 1275
Site 1274
Site 1273
45°15'W
45°00'
44°45'
15°15'N
15°00'
14°45'
Site 1272
Site 1271
Site 1269
Site 1268
Site 1270

Figure F5

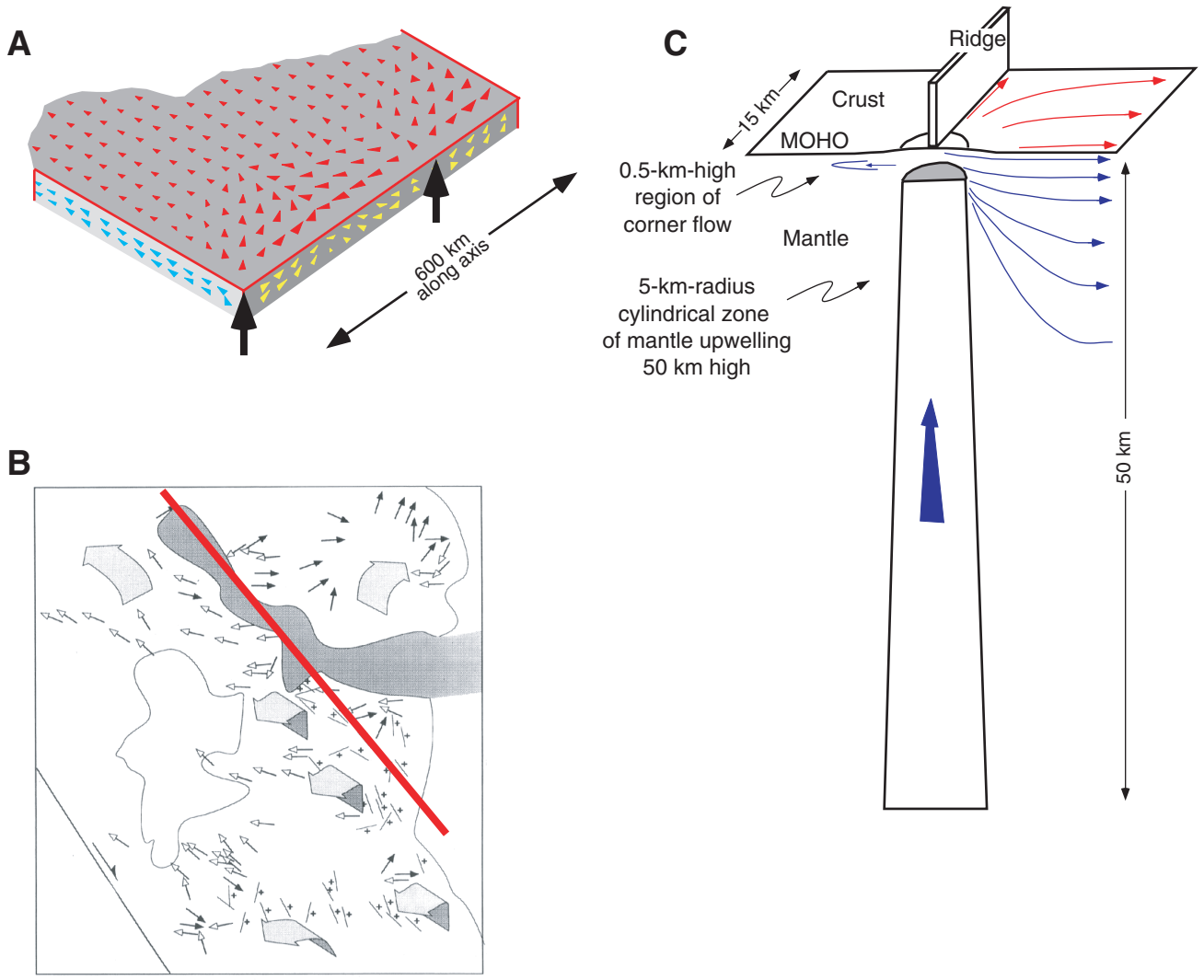
A
600 km
along axis
B
C
Ridge
15 km
Crust
MOHO
0.5-km-high
region of
corner flow
Mantle
5-km-radius
cylindrical zone
of mantle upwelling
50 km high
50 km

Figure F6

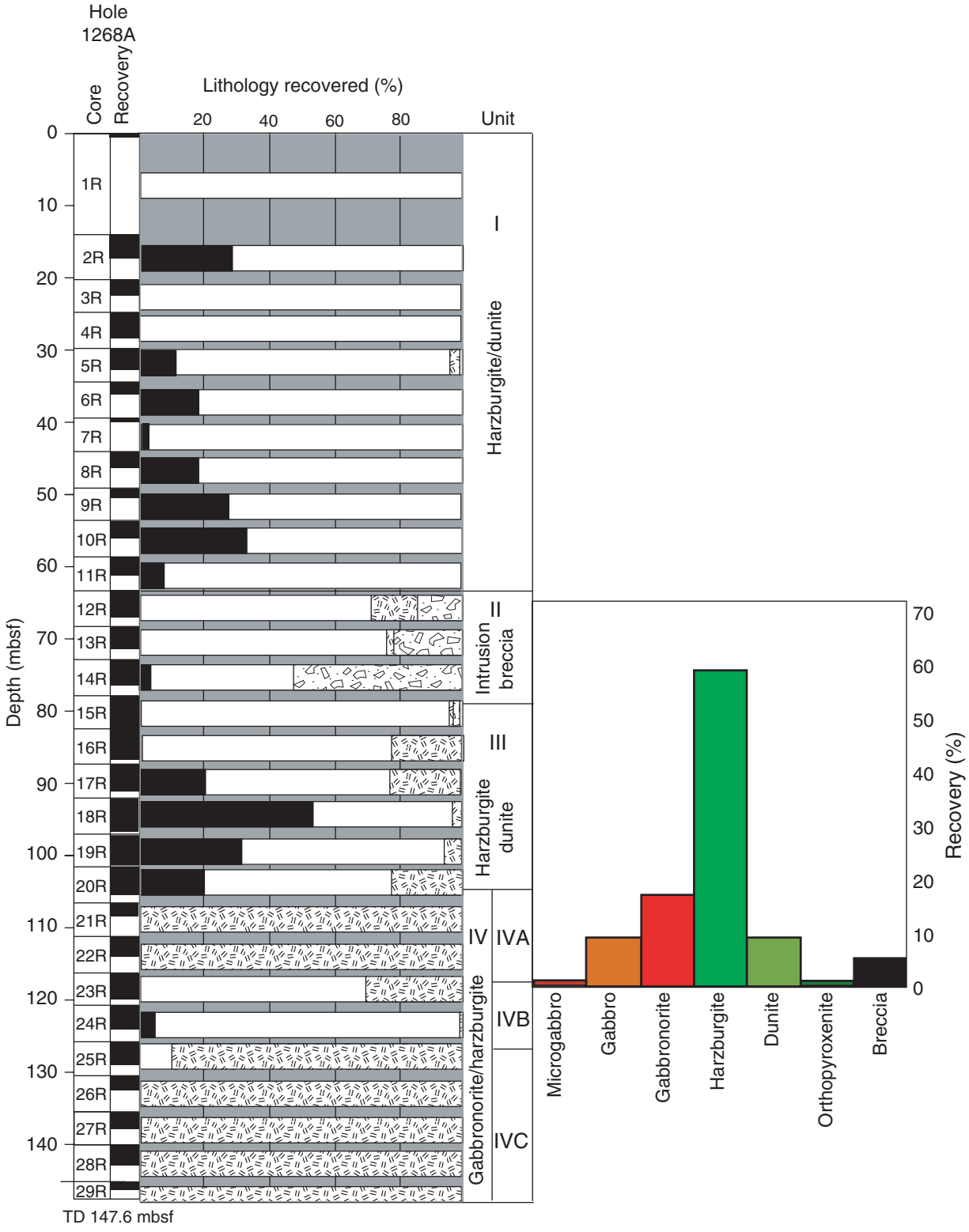
Hole 1268A
Core
Recovery
Lithology recovered (%)
20
40
60
80
Unit
Depth (mbsf)
0
10
20
30
40
50
60
70
80
90
100
110
120
130
140
1R
2R
3R
4R
5R
6R
7R
8R
9R
10R
11R
12R
13R
14R
15R
16R
17R
18R
19R
20R
21R
22R
23R
24R
25R
26R
27R
28R
29R
I
Harzburgite/dunite
II
Intrusion breccia
III
Harzburgite dunite
IV
IVA
IVB
IVC
Gabbronorite/harzburgite
TD 147.6 mbsf
Microgabbro
Gabbro
Gabbronorite
Harzburgite
Dunite
Orthopyroxenite
Breccia
Recovery (%)
0
10
20
30
40
50
60
70

Figure F7

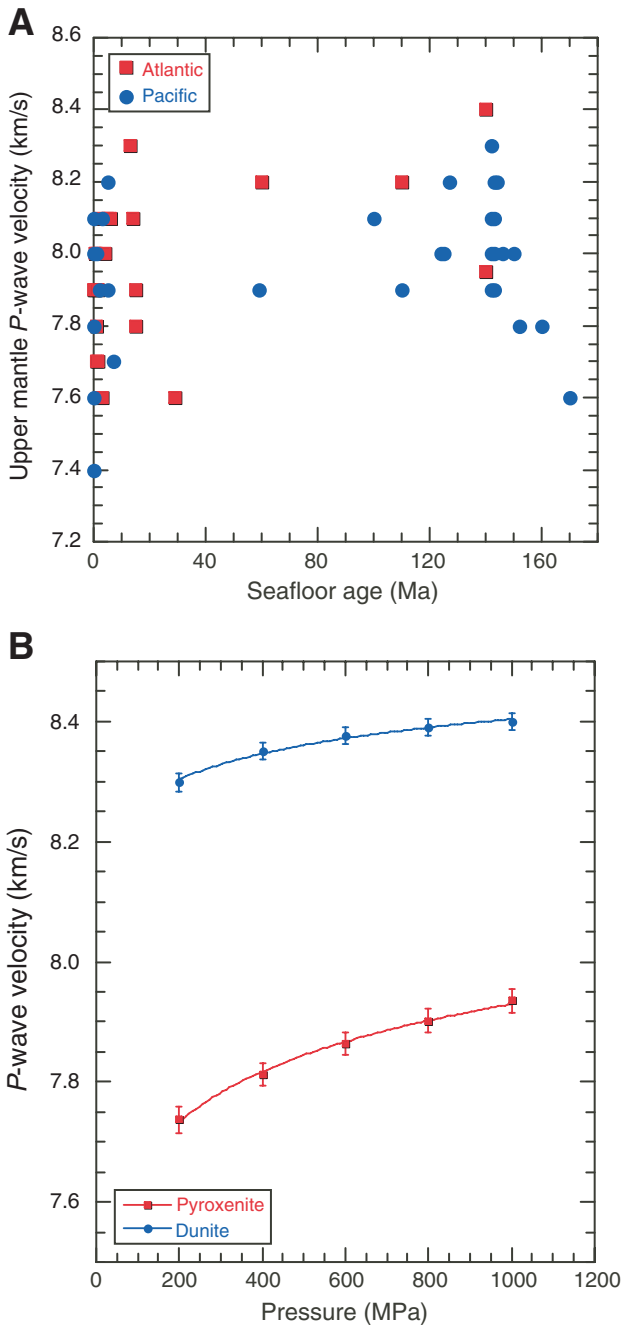
A
Atlantic
Pacific
Upper mantle P-wave velocity (km/s)
8.6
8.4
8.2
8.0
7.8
7.6
7.4
7.2
0
40
80
120
160
Seafloor age (Ma)
B
P-wave velocity (km/s)
8.4
8.2
8.0
7.8
7.6
Pyroxenite
Dunite
0
200
400
600
800
1000
1200
Pressure (MPa)

Figure F8

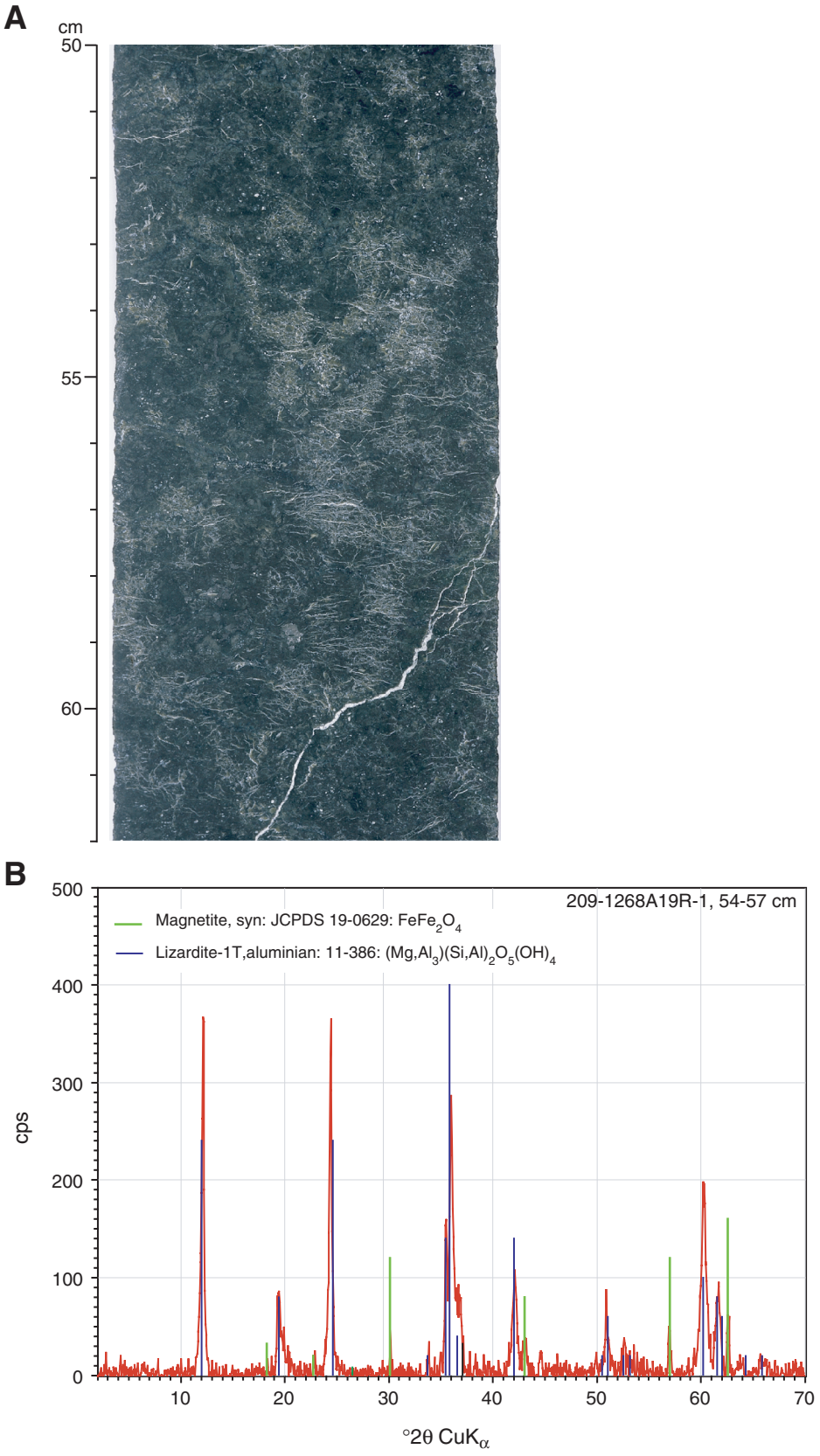
A
cm
50
55
60
B
209-1268A19R-1, 54-57 cm
Magnetite, syn: JCPDS 19-0629: FeFe2O4
Lizardite-1T,aluminian: 11-386: (Mg,Al3)(Si,Al)2O5(OH)4
cps
500
400
300
200
100
0
10
20
30
40
50
60
70
°2θ CuKα

Figure F9

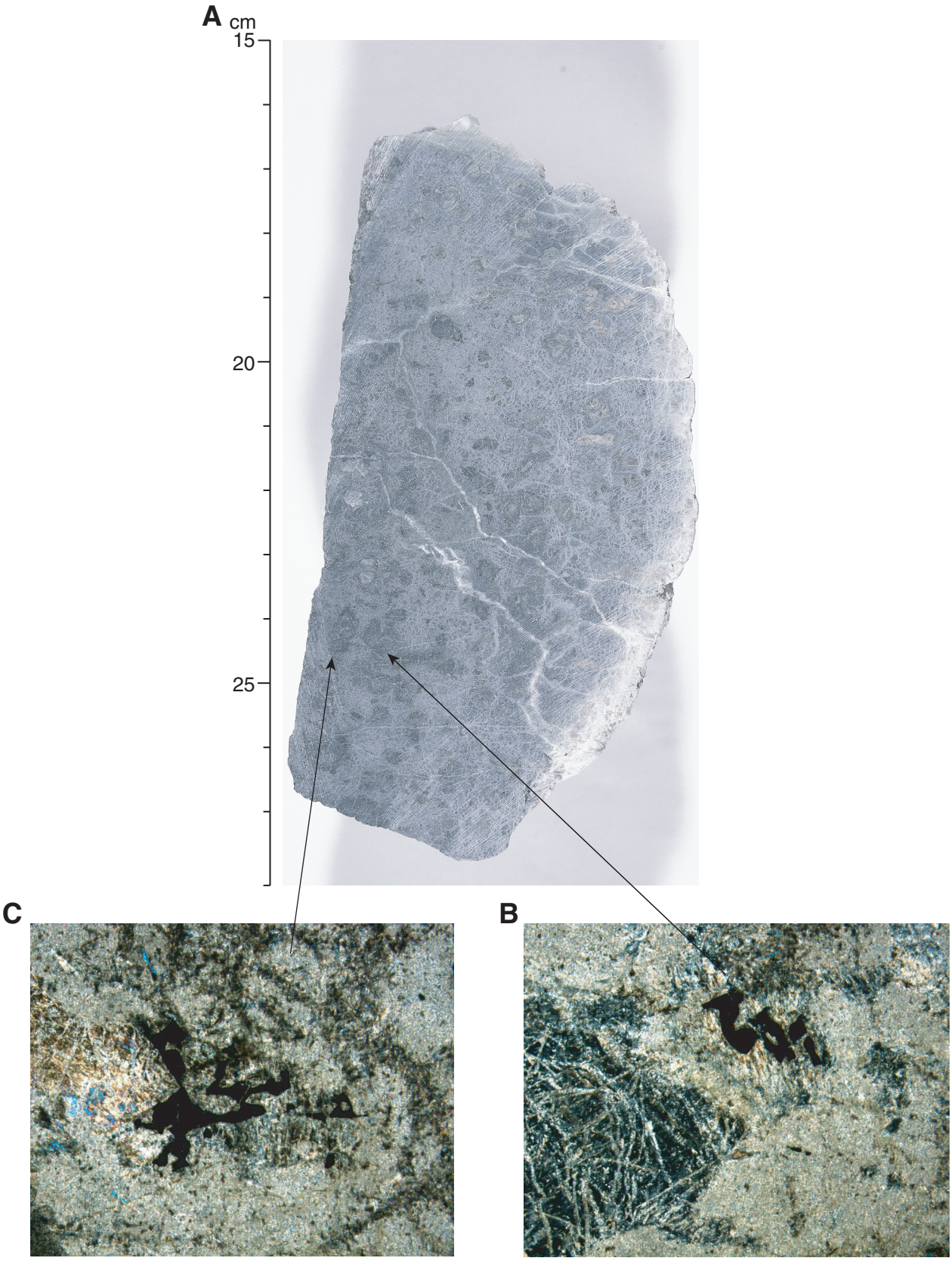

Figure F10

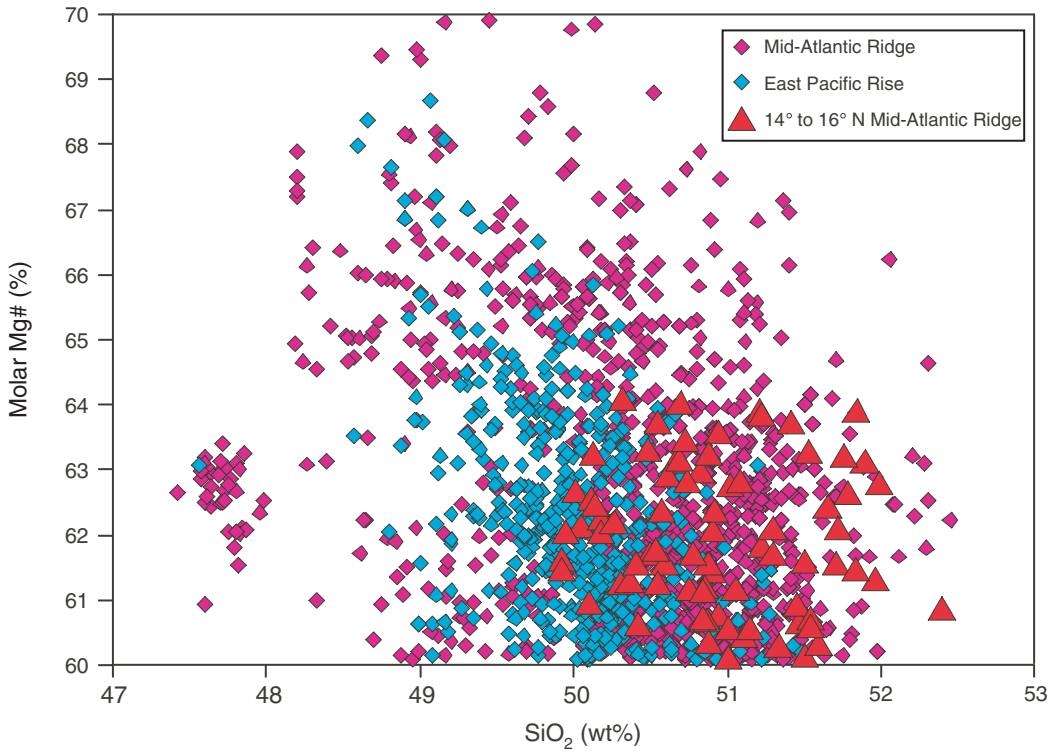
Mid-Atlantic Ridge
East Pacific Rise
14° to 16° N Mid-Atlantic Ridge
Molar Mg# (%)
70
69
68
67
66
65
64
63
62
61
60
47
48
49
50
51
52
53
SiO2 (wt%)

Figure F11

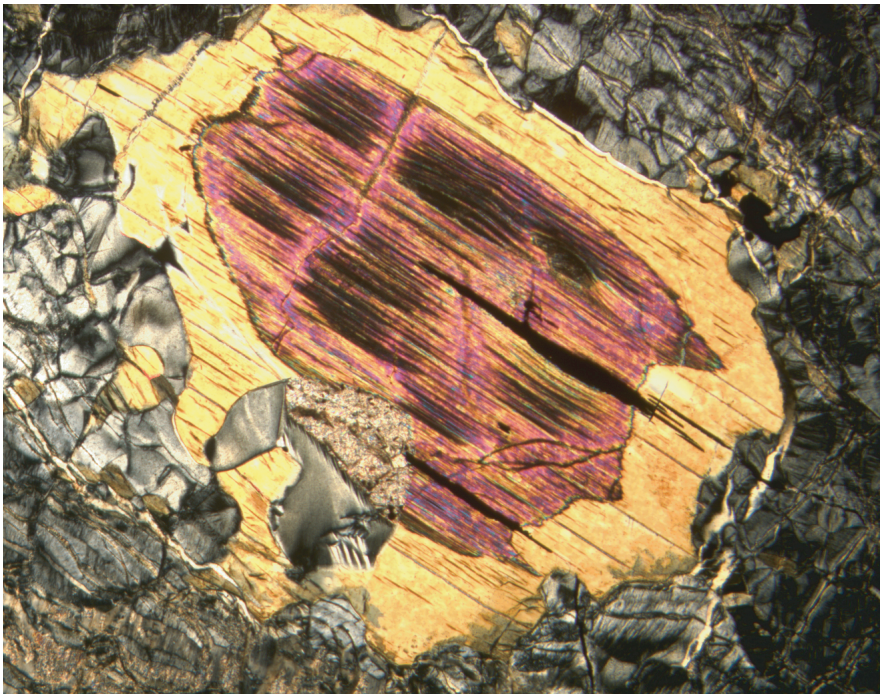

Figure F12

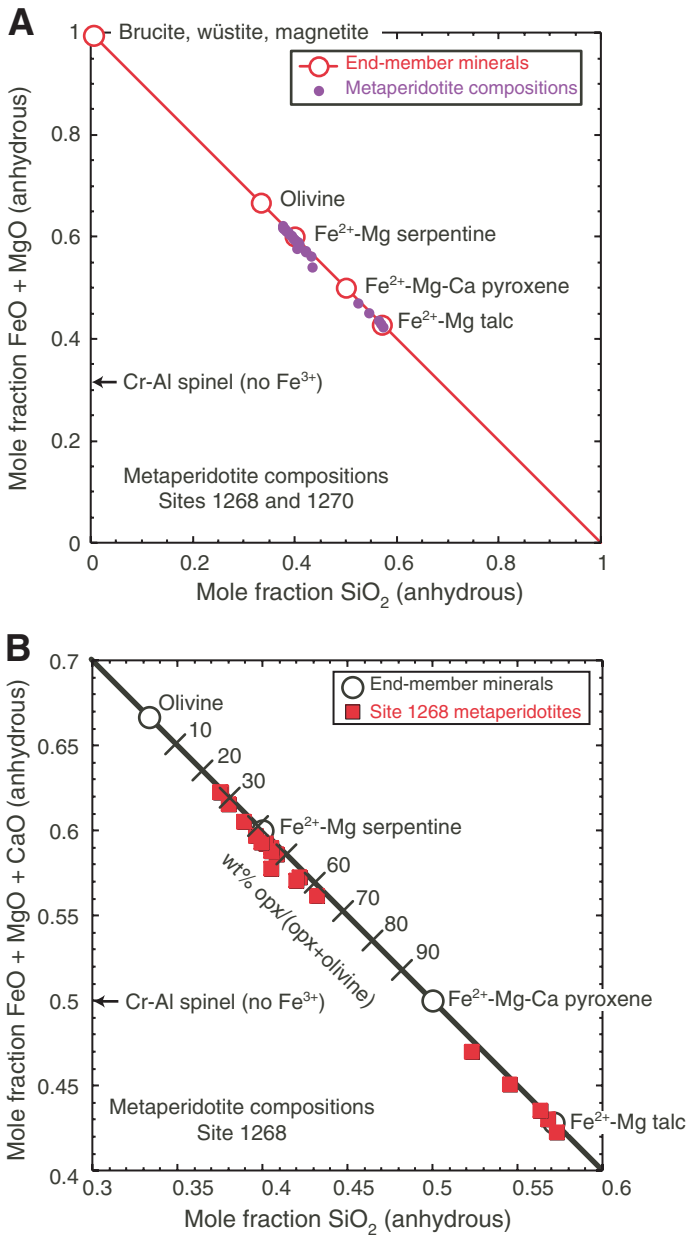
A
Brucite, wüstite, magnetite
End-member minerals
Metaperidotite compositions
Olivine
Fe2+-Mg serpentine
Fe2+-Mg-Ca pyroxene
Fe2+-Mg talc
Cr-Al spinel (no Fe3+)
Metaperidotite compositions
Sites 1268 and 1270
Mole fraction FeO + MgO (anhydrous)
Mole fraction SiO2 (anhydrous)
0
0.2
0.4
0.6
0.8
1
B
End-member minerals
Site 1268 metaperidotites
Olivine
10
20
30
Fe2+-Mg serpentine
60
70
80
90
wt% opx/(opx+olivine)
Cr-Al spinel (no Fe3+)
Fe2+-Mg-Ca pyroxene
Fe2+-Mg talc
Metaperidotite compositions
Site 1268
Mole fraction FeO + MgO + CaO (anhydrous)
Mole fraction SiO2 (anhydrous)
0.3
0.35
0.4
0.45
0.5
0.55
0.6
0.65
0.7

Figure F13

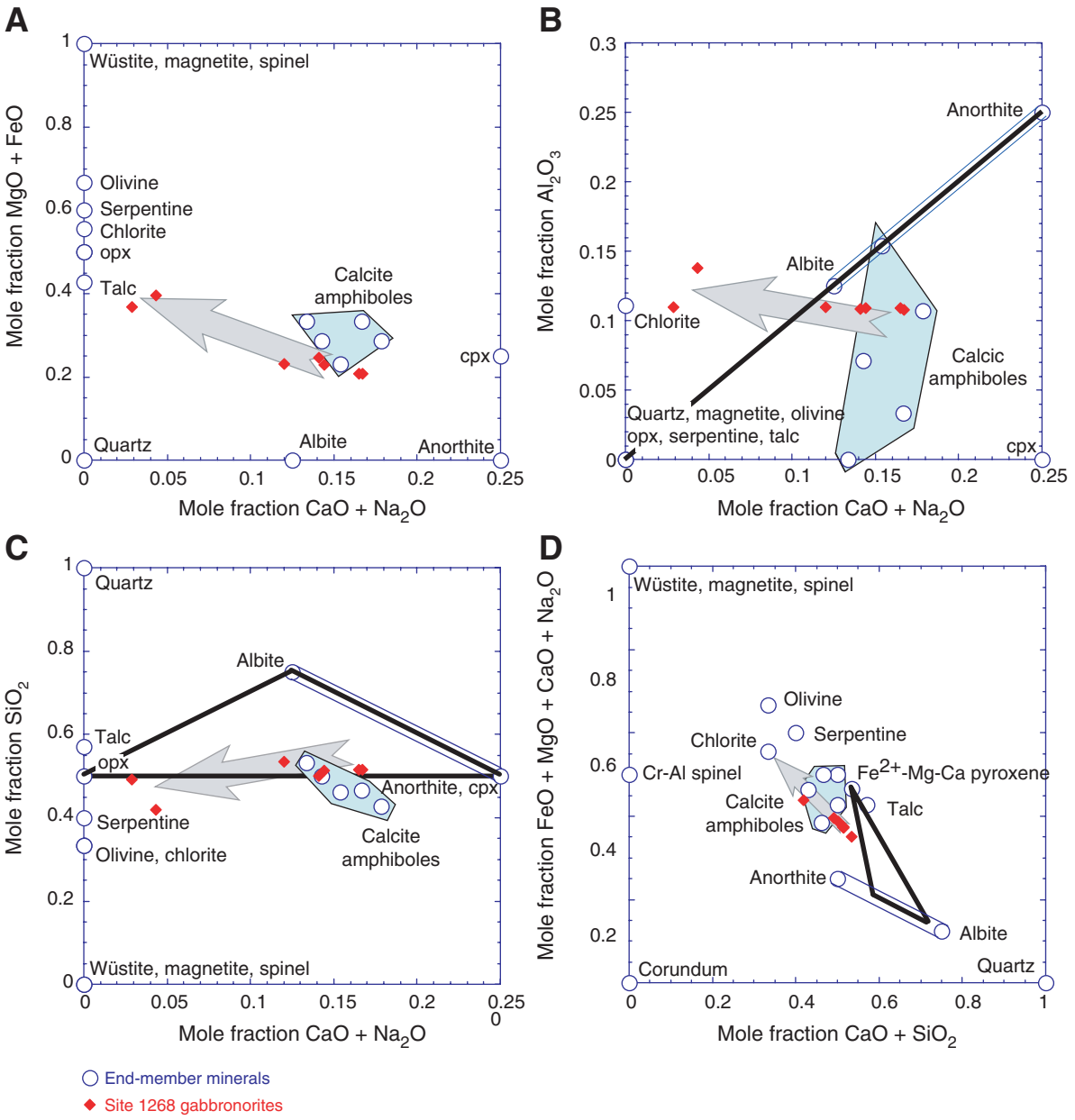
A
Wüstite, magnetite, spinel
Olivine
Serpentine
Chlorite
opx
Talc
Calcite amphiboles
cpx
Quartz
Albite
Anorthite
Mole fraction MgO + FeO
Mole fraction CaO + Na2O
B
Anorthite
Albite
Chlorite
Calcic amphiboles
Quartz, magnetite, olivine opx, serpentine, talc
cpx
Mole fraction Al2O3
Mole fraction CaO + Na2O
C
Quartz
Albite
Talc
opx
Anorthite, cpx
Serpentine
Olivine, chlorite
Calcite amphiboles
Wüstite, magnetite, spinel
Mole fraction SiO2
Mole fraction CaO + Na2O
D
Wüstite, magnetite, spinel
Olivine
Chlorite
Serpentine
Cr-Al spinel
Fe2+-Mg-Ca pyroxene
Calcite amphiboles
Talc
Anorthite
Albite
Corundum
Quartz
Mole fraction FeO + MgO + CaO + Na2O
Mole fraction CaO + SiO2
End-member minerals
Site 1268 gabbronorites

Figure F14

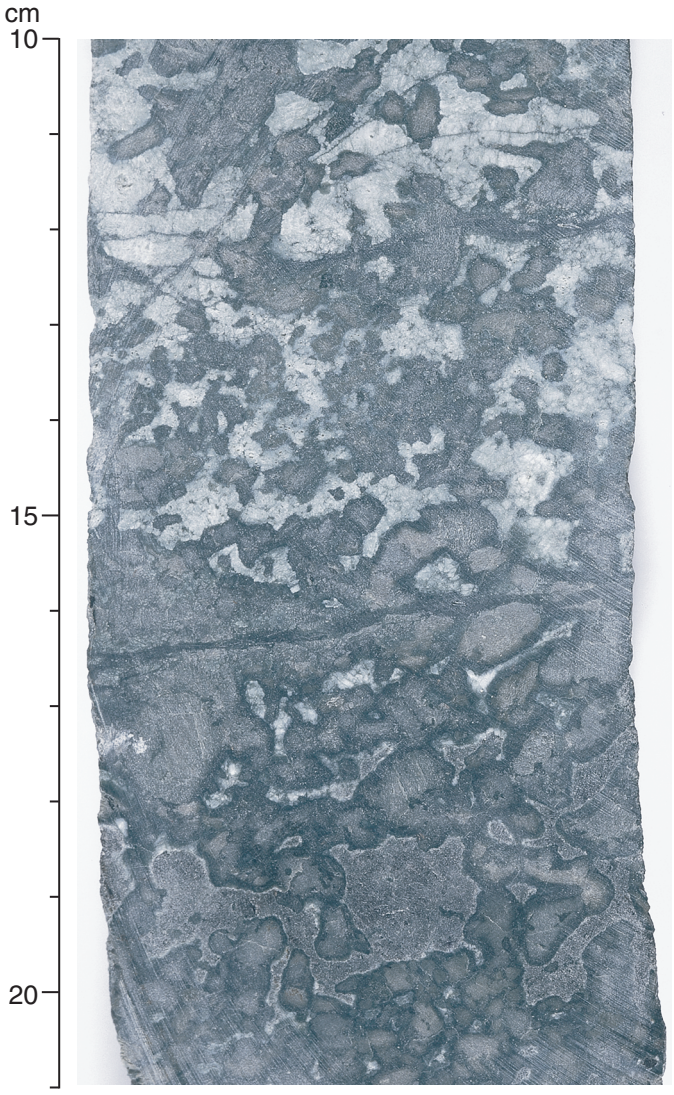

Figure F15

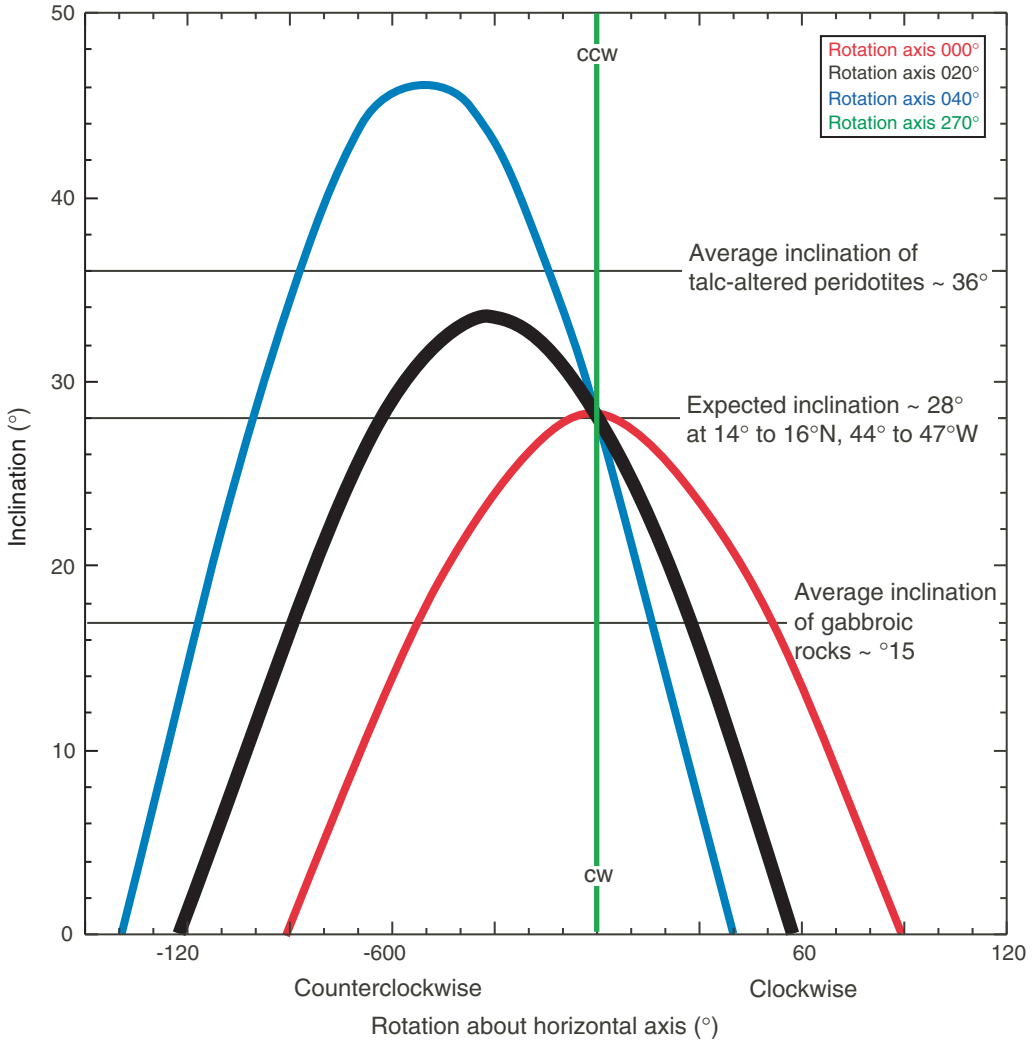
Rotation axis 000°
Rotation axis 020°
Rotation axis 040°
Rotation axis 270°
ccw
cw
Average inclination of
talc-altered peridotites ~ 36°
Expected inclination ~ 28°
at 14° to 16°N, 44° to 47°W
Average inclination
of gabbroic
rocks ~ °15
Inclination (°)
50
40
30
20
10
0
-120
-600
60
120
Counterclockwise
Clockwise
Rotation about horizontal axis (°)

Figure F16

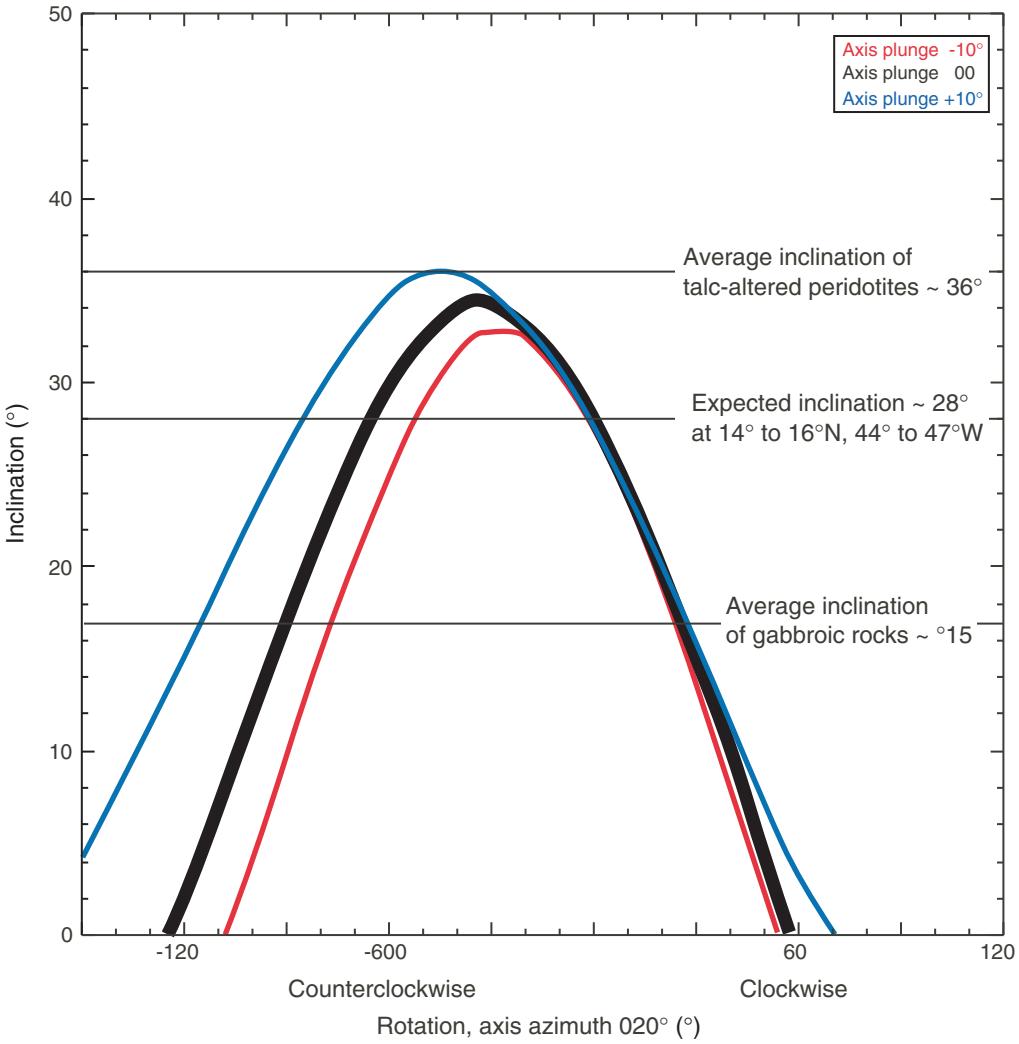
Axis plunge -10°
Axis plunge 00
Axis plunge +10°
Average inclination of
talc-altered peridotites ~ 36°
Expected inclination ~ 28°
at 14° to 16°N, 44° to 47°W
Average inclination
of gabbroic rocks ~ °15
Inclination (°)
50
40
30
20
10
0
-120
-600
60
120
Counterclockwise
Clockwise
Rotation, axis azimuth 020° (°)

Figure F17

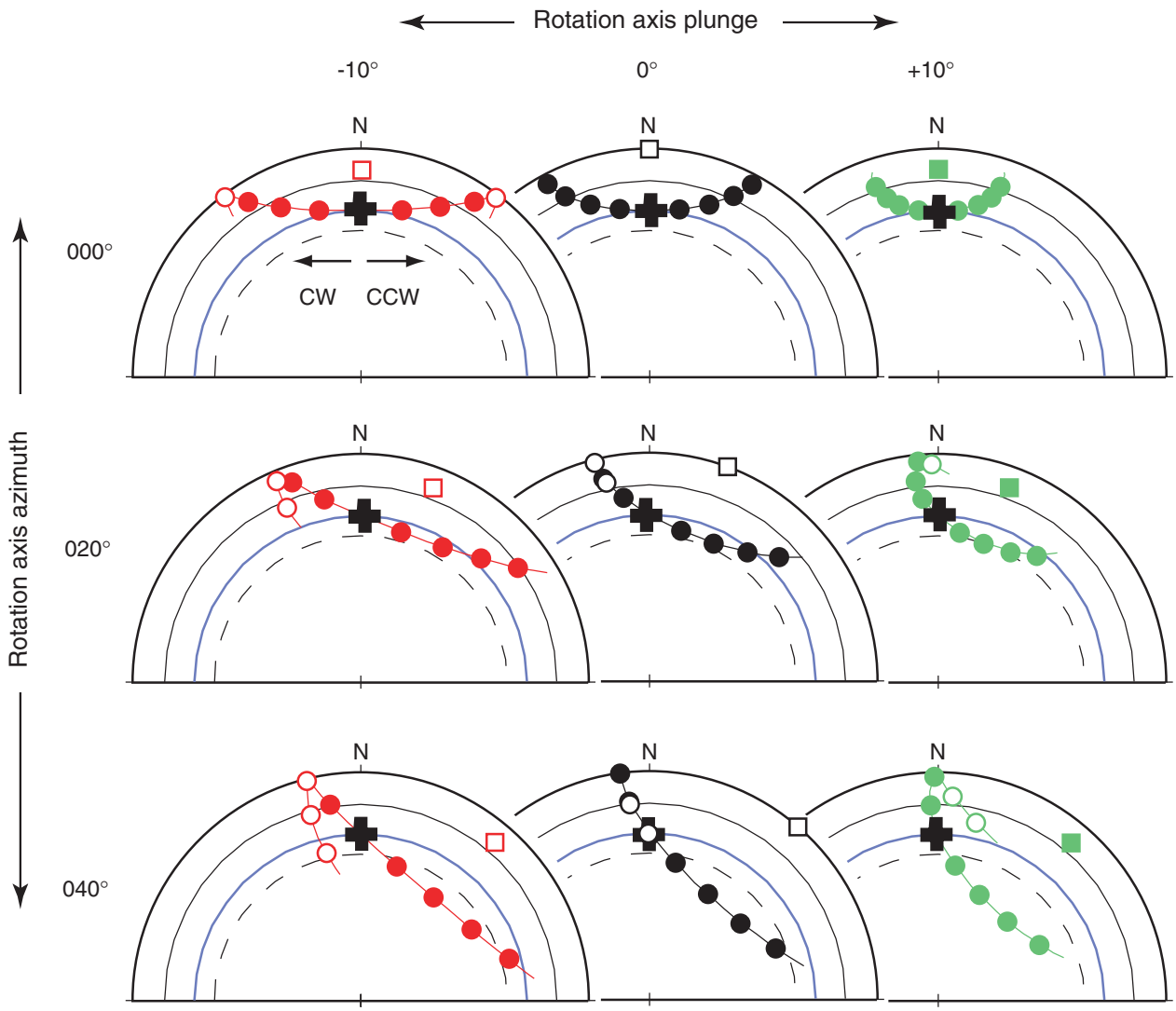
Rotation axis plunge
-10°
0°
+10°
N
000°
CW
CCW
020°
040°
Rotation axis azimuth

Figure F18

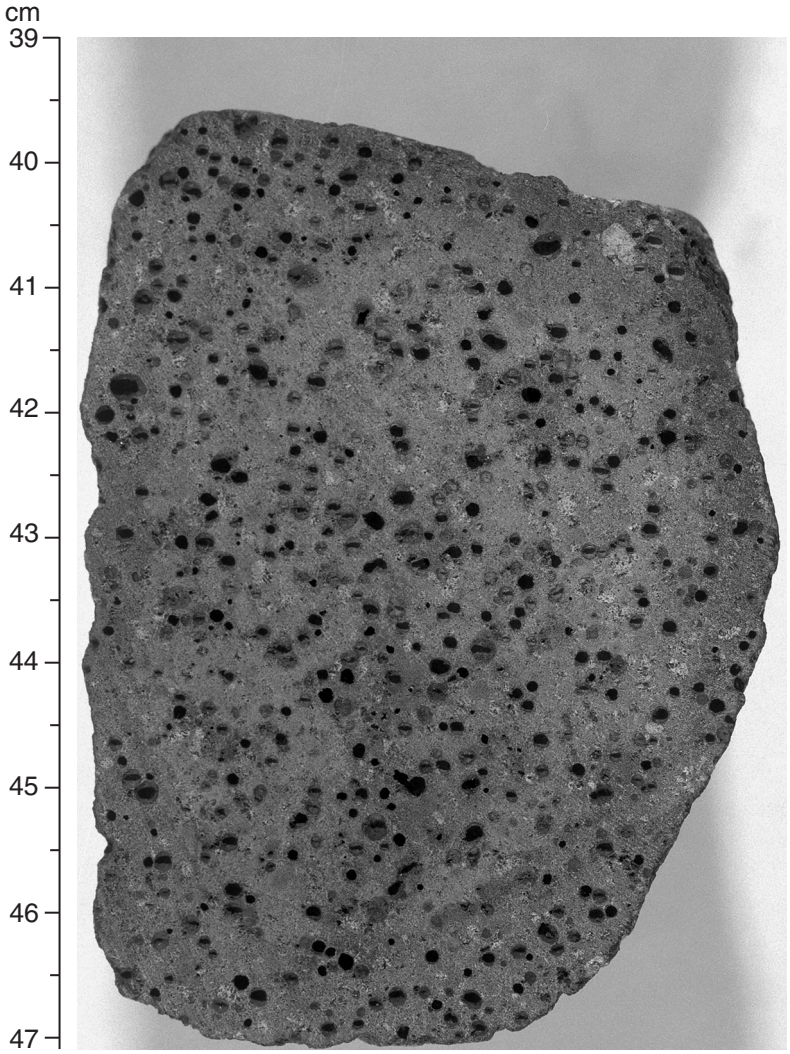

Figure F19

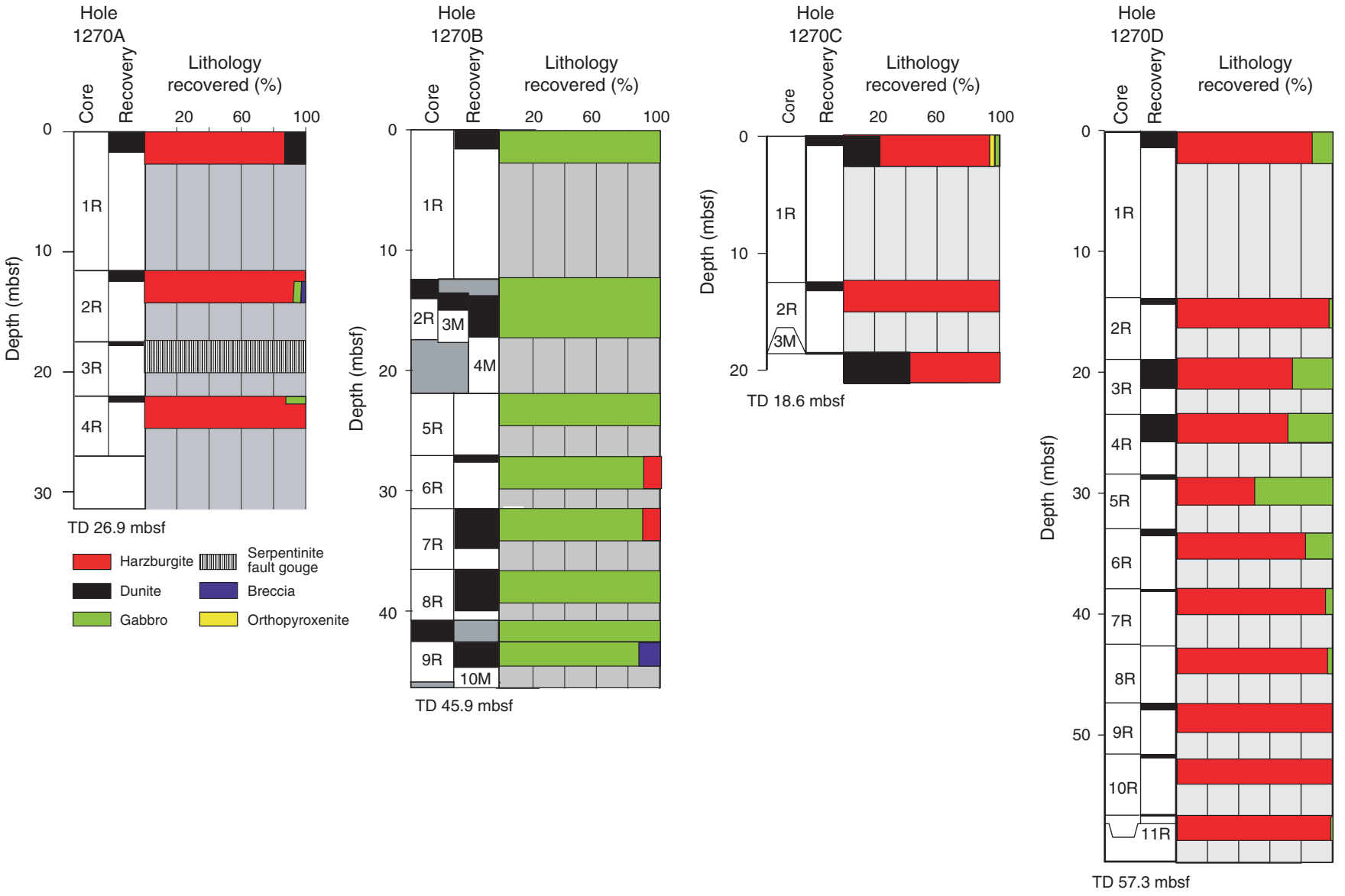
Hole 1270A
Core
Recovery
Lithology recovered (%)
0
20
60
100
Depth (mbsf)
0
10
20
30
1R
2R
3R
4R
TD 26.9 mbsf
Harzburgite
Dunite
Gabbro
Serpentinite fault gouge
Breccia
Orthopyroxenite
Hole 1270B
Core
Recovery
Lithology recovered (%)
Depth (mbsf)
0
10
20
30
40
1R
2R
3M
4M
5R
6R
7R
8R
9R
10M
TD 45.9 mbsf
Hole 1270C
Core
Recovery
Lithology recovered (%)
Depth (mbsf)
0
10
20
1R
2R
3M
TD 18.6 mbsf
Hole 1270D
Core
Recovery
Lithology recovered (%)
Depth (mbsf)
0
10
20
30
40
50
1R
2R
3R
4R
5R
6R
7R
8R
9R
10R
11R
TD 57.3 mbsf

Figure F20

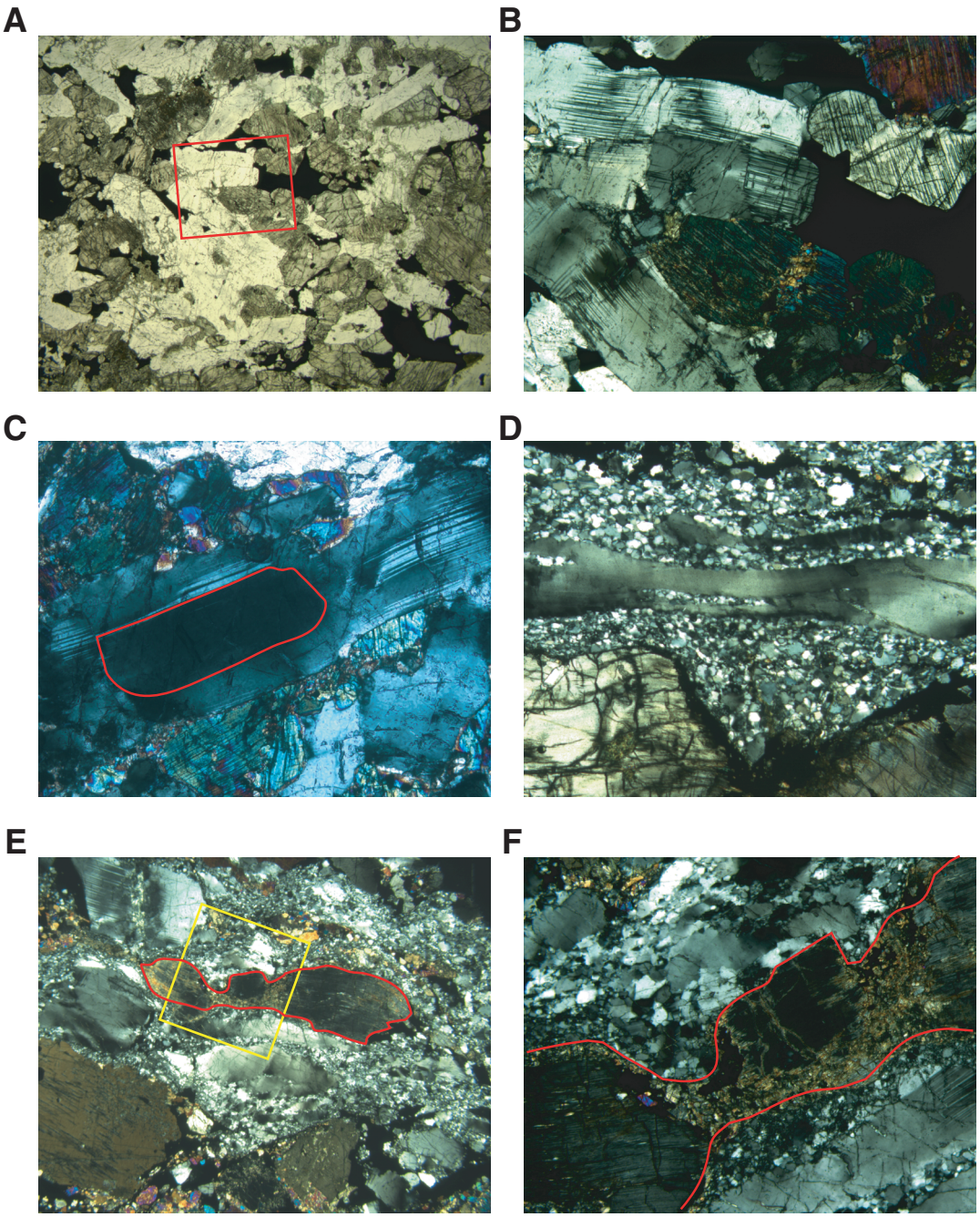

Figure F21

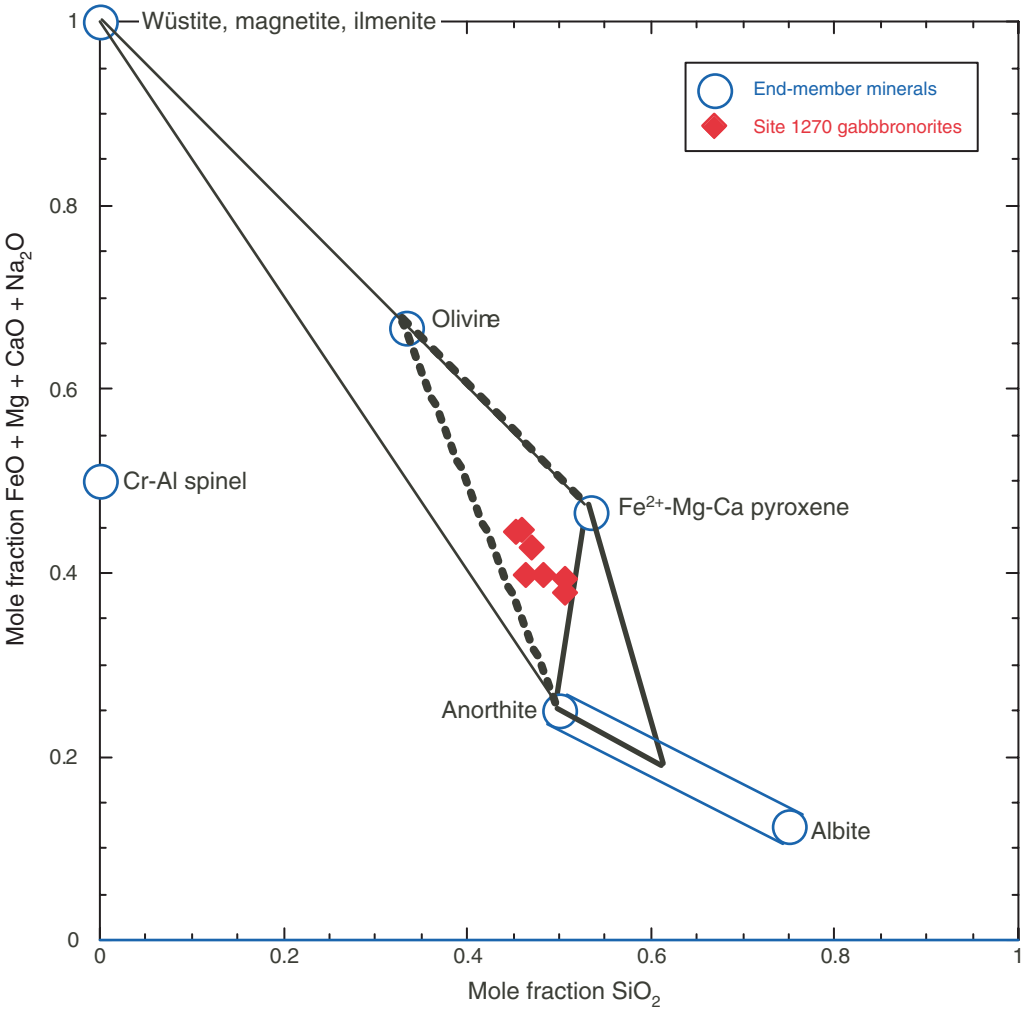
Wüstite, magnetite, ilmenite
End-member minerals
Site 1270 gabbbronorites
Olivine
Cr-Al spinel
Fe2+-Mg-Ca pyroxene
Anorthite
Albite
Mole fraction FeO + Mg + CaO + Na2O
Mole fraction SiO2
0
0.2
0.4
0.6
0.8
1

Figure F22

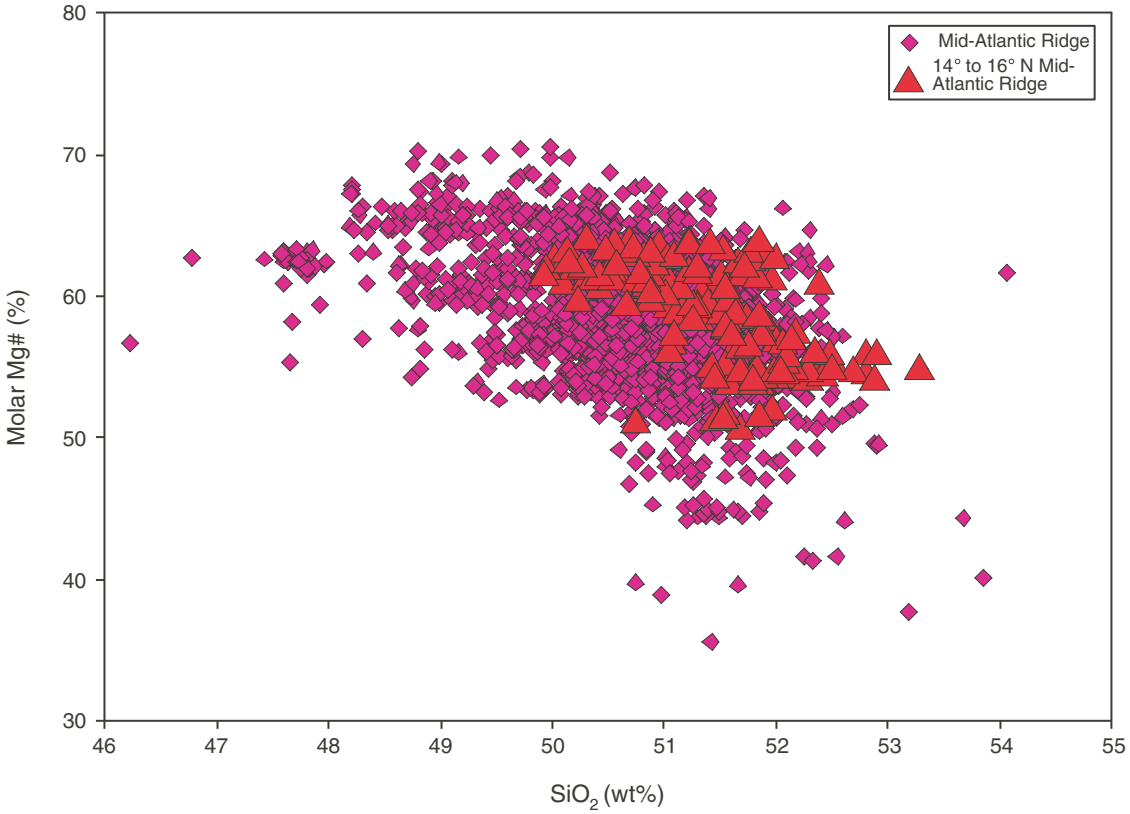
Mid-Atlantic Ridge
14° to 16° N Mid-Atlantic Ridge
Molar Mg# (%)
80
70
60
50
40
30
46
47
48
49
50
51
52
53
54
55
SiO2 (wt%)

Figure F23

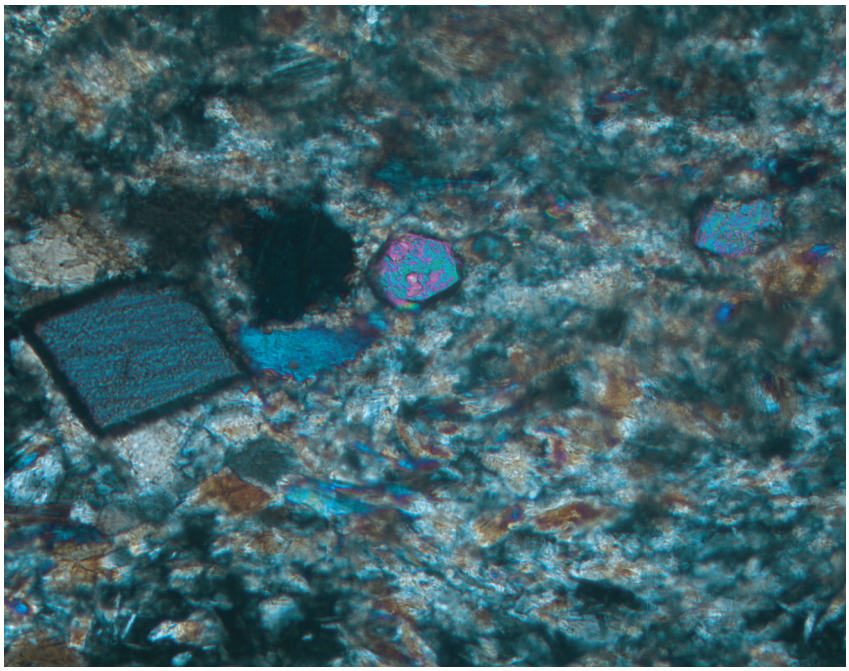

Figure F24

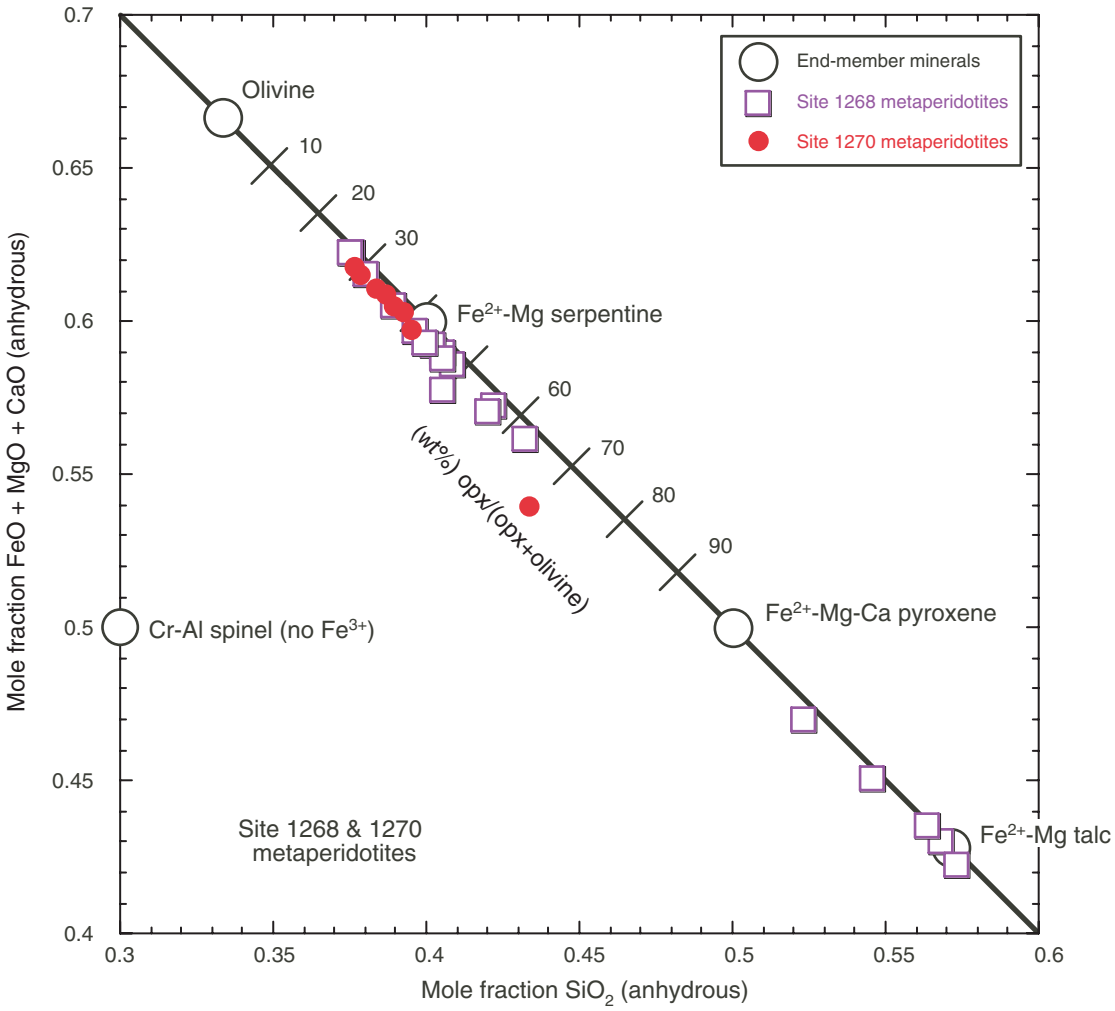
End-member minerals
Site 1268 metaperidotites
Site 1270 metaperidotites
Olivine
10
20
30
Fe2+-Mg serpentine
60
70
80
90
(wt%) opx/(opx+olivine)
Fe2+-Mg-Ca pyroxene
Cr-Al spinel (no Fe3+)
Site 1268 & 1270
metaperidotites
Fe2+-Mg talc
Mole fraction FeO + MgO + CaO (anhydrous)
Mole fraction SiO2 (anhydrous)
0.7
0.65
0.6
0.55
0.5
0.45
0.4
0.3
0.35
0.4
0.45
0.5
0.55
0.6

Figure F25

Figure F26

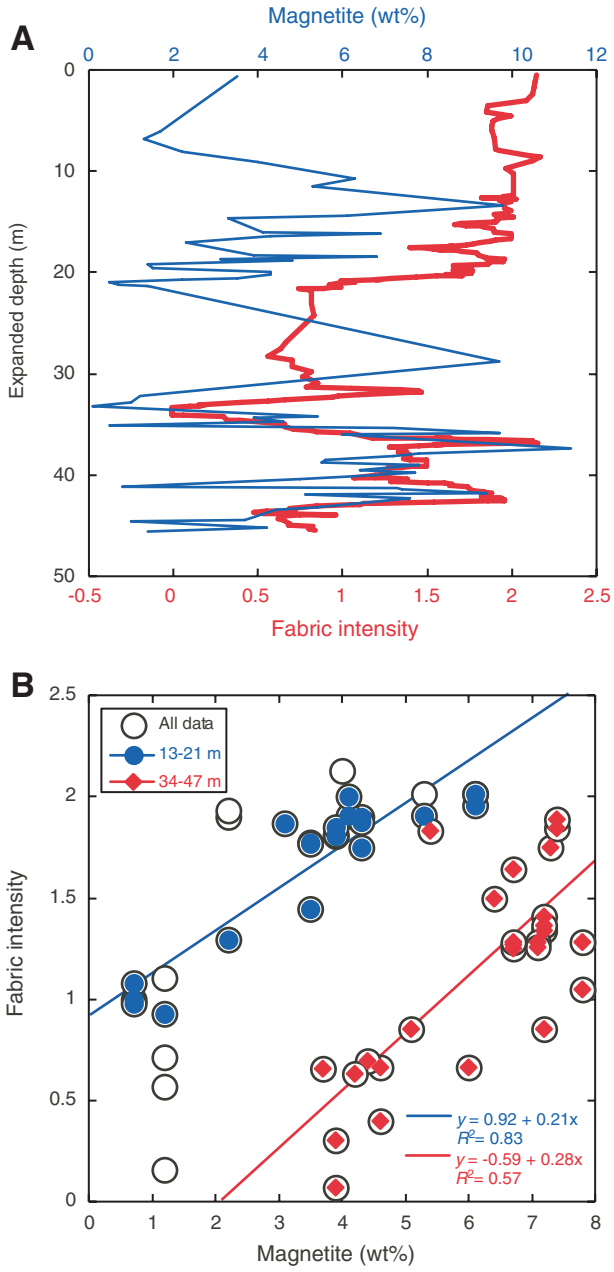
A
Magnetite (wt%)
0
2
4
6
8
10
12
Expanded depth (m)
0
10
20
30
40
50
-0.5
0
0.5
1
1.5
2
2.5
Fabric intensity
B
All data
13-21 m
34-47 m
Fabric intensity
0
0.5
1
1.5
2
2.5
0
1
2
3
4
5
6
7
8
Magnetite (wt%)
y = 0.92 + 0.21x
R2= 0.83
y = -0.59 + 0.28x
R2= 0.57

Figure F27

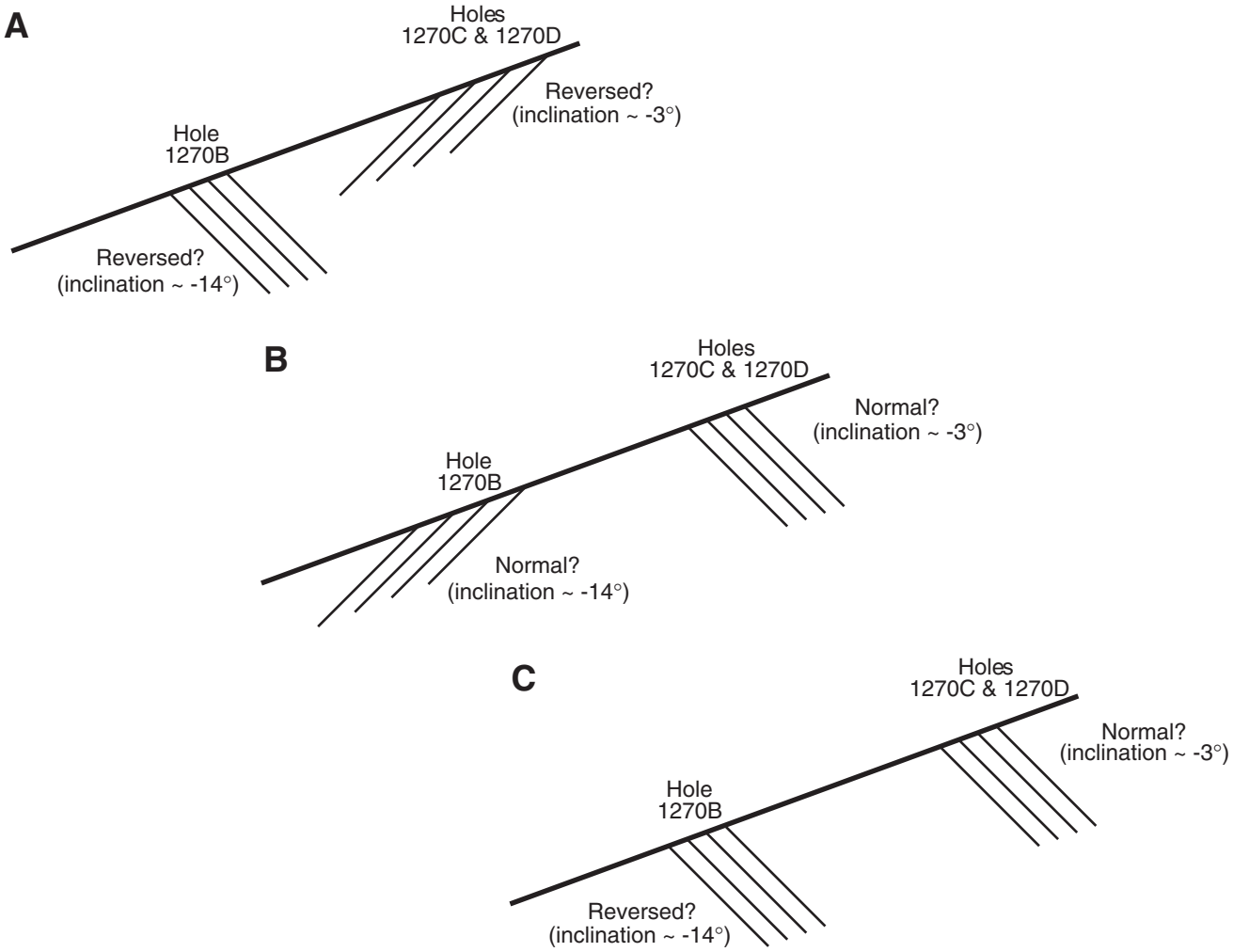
A
Holes
1270C & 1270D
Reversed?
(inclination ~ -3°)
Hole
1270B
Reversed?
(inclination ~ -14°)
B
Holes
1270C & 1270D
Normal?
(inclination ~ -3°)
Hole
1270B
Normal?
(inclination ~ -14°)
C
Holes
1270C & 1270D
Normal?
(inclination ~ -3°)
Hole
1270B
Reversed?
(inclination ~ -14°)

Figure F28

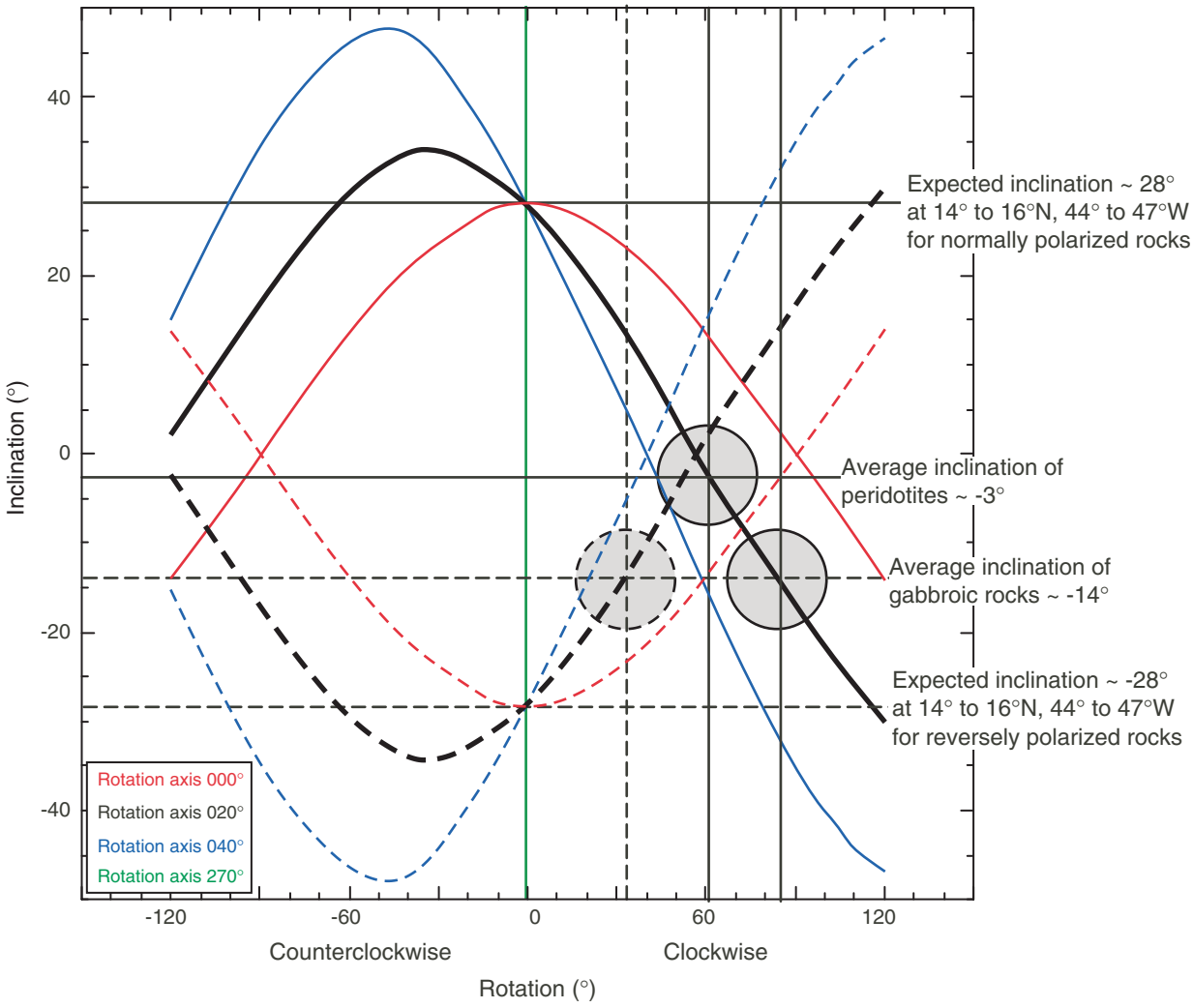
40
20
0
-20
-40
Inclination (°)
-120
-60
0
60
120
Counterclockwise
Clockwise
Rotation (°)
Rotation axis 000°
Rotation axis 020°
Rotation axis 040°
Rotation axis 270°
Expected inclination ~ 28°
at 14° to 16°N, 44° to 47°W
for normally polarized rocks
Average inclination of
peridotites ~ -3°
Average inclination of
gabbroic rocks ~ -14°
Expected inclination ~ -28°
at 14° to 16°N, 44° to 47°W
for reversely polarized rocks

Figure F29

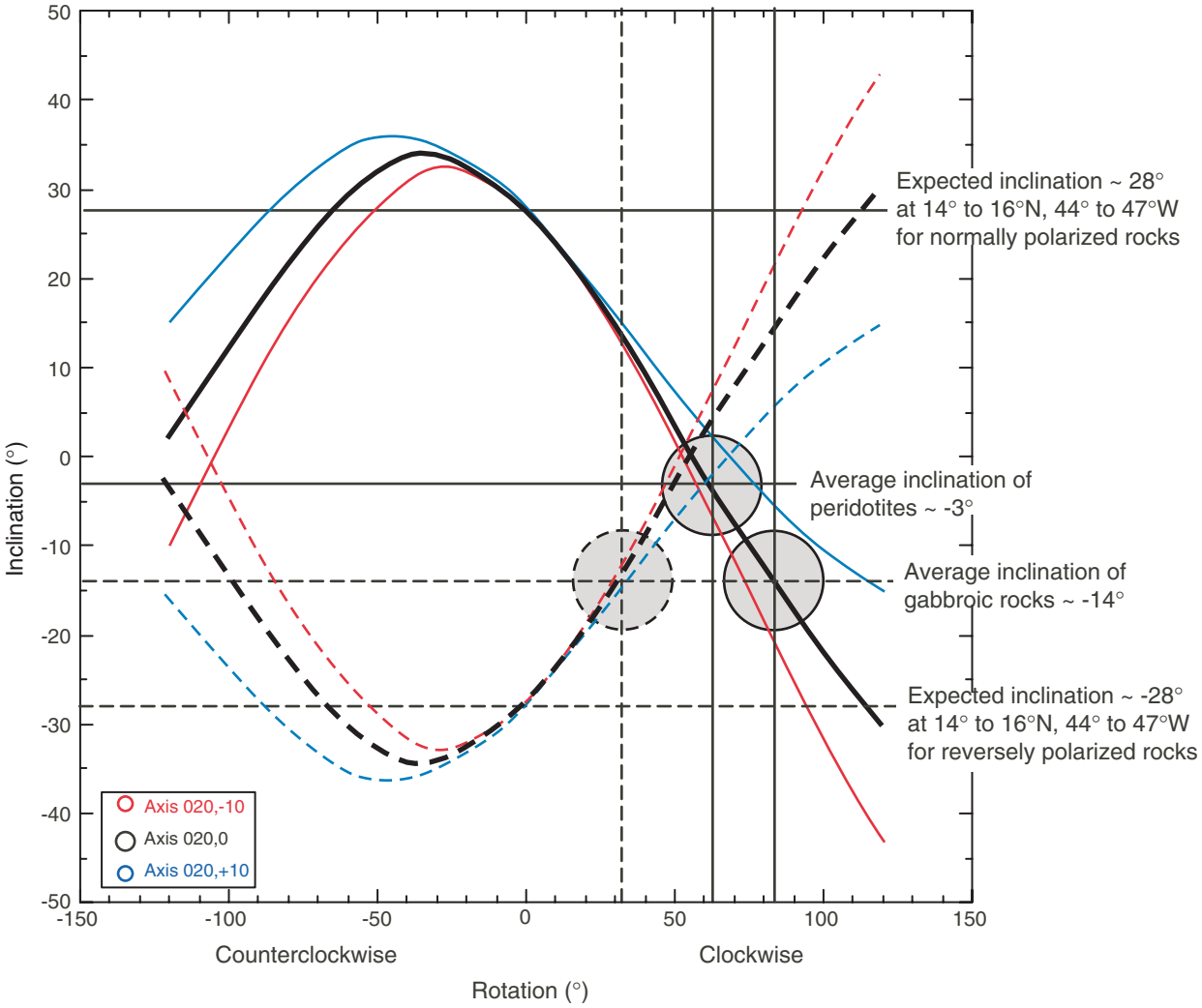
Inclination (°)
Rotation (°)
Counterclockwise
Clockwise
Axis 020,-10
Axis 020,0
Axis 020,+10
Expected inclination ~ 28°
at 14° to 16°N, 44° to 47°W
for normally polarized rocks
Average inclination of
peridotites ~ -3°
Average inclination of
gabbroic rocks ~ -14°
Expected inclination ~ -28°
at 14° to 16°N, 44° to 47°W
for reversely polarized rocks

Figure F30

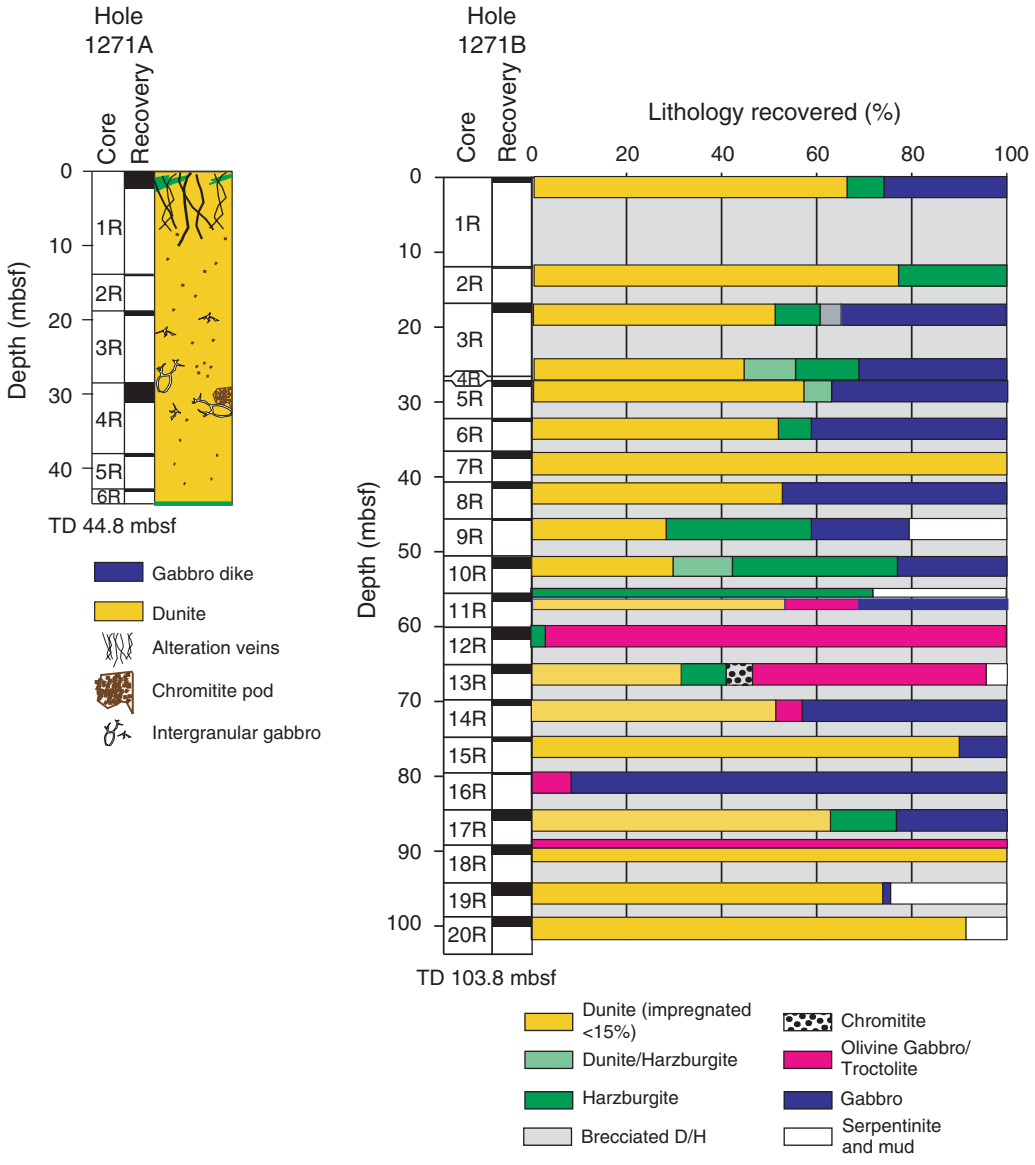
Hole 1271A
Core
Recovery
Depth (mbsf)
0
10
20
30
40
1R
2R
3R
4R
5R
6R
TD 44.8 mbsf
Gabbro dike
Dunite
Alteration veins
Chromitite pod
Intergranular gabbro
Hole 1271B
Core
Recovery
Lithology recovered (%)
0
20
40
60
80
100
Depth (mbsf)
0
10
20
30
40
50
60
70
80
90
100
1R
2R
3R
4R
5R
6R
7R
8R
9R
10R
11R
12R
13R
14R
15R
16R
17R
18R
19R
20R
TD 103.8 mbsf
Dunite (impregnated <15%)
Dunite/Harzburgite
Harzburgite
Brecciated D/H
Chromitite
Olivine Gabbro/ Troctolite
Gabbro
Serpentinite and mud

Figure F31

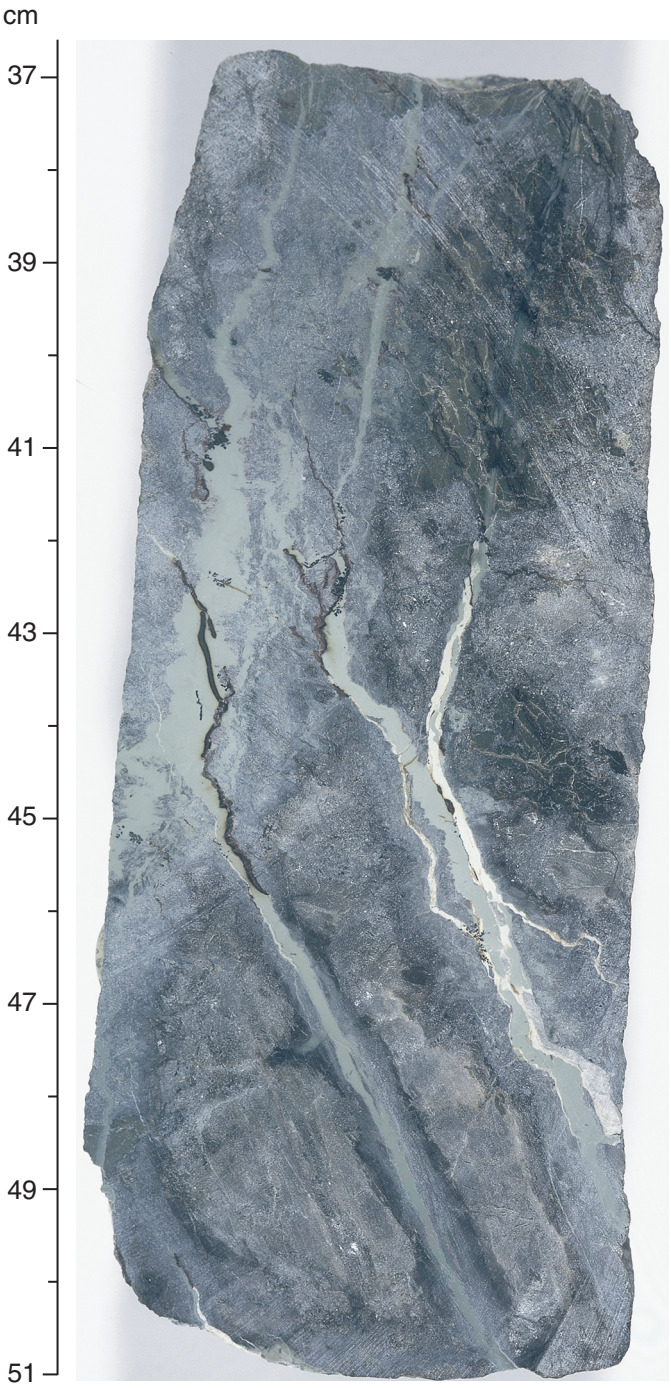

Figure F32

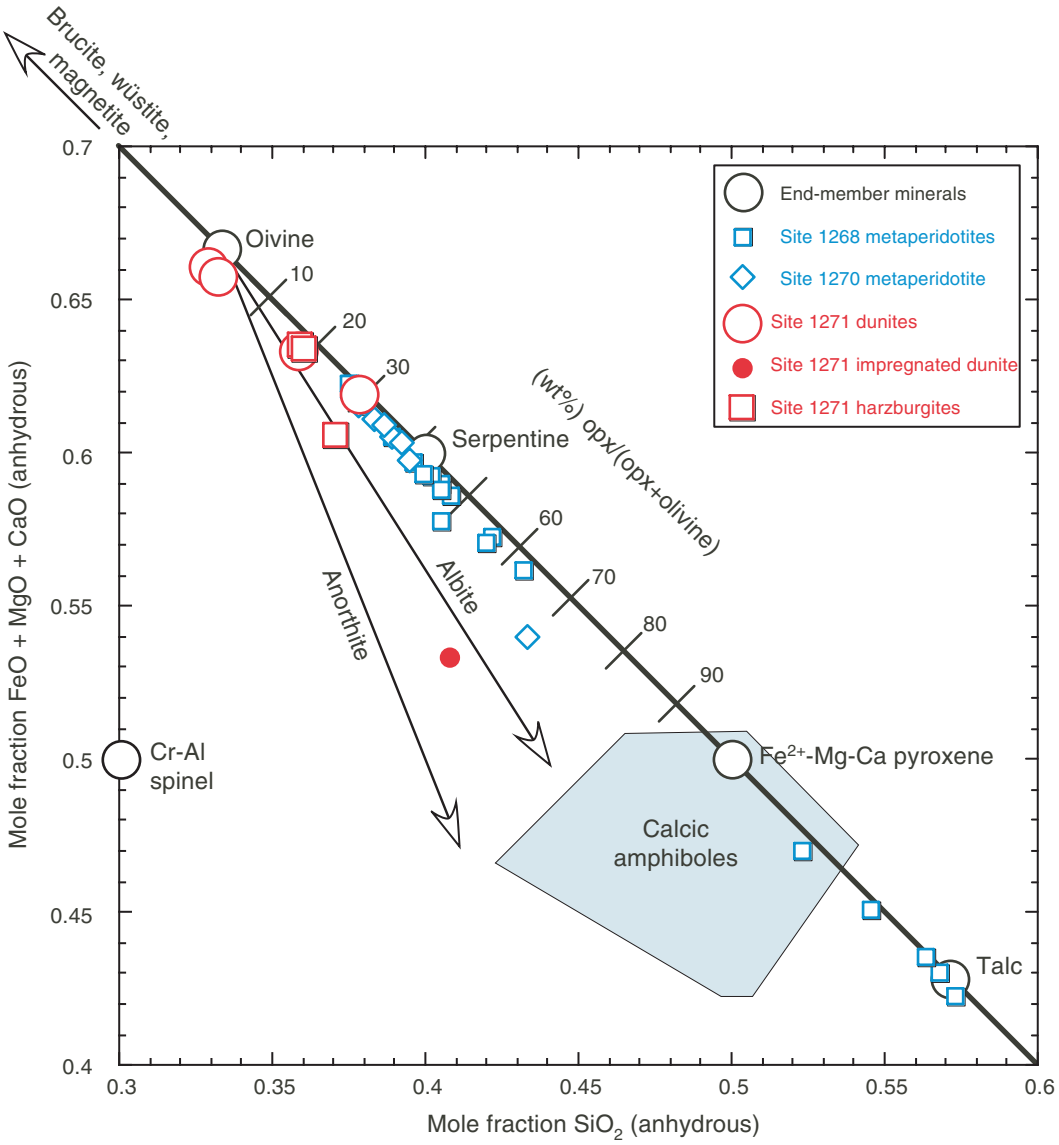
Brucite, wüstite, magnetite
End-member minerals
Site 1268 metaperidotites
Site 1270 metaperidotite
Site 1271 dunites
Site 1271 impregnated dunite
Site 1271 harzburgites
Olivine
Serpentine
Cr-Al spinel
Fe2+-Mg-Ca pyroxene
Talc
Calcic amphiboles
Anorthite
Albite
(wt%) opx/(opx+olivine)
10
20
30
60
70
80
90
Mole fraction FeO + MgO + CaO (anhydrous)
Mole fraction SiO2 (anhydrous)
0.7
0.65
0.6
0.55
0.5
0.45
0.4
0.3
0.35
0.4
0.45
0.5
0.55
0.6

Figure F33

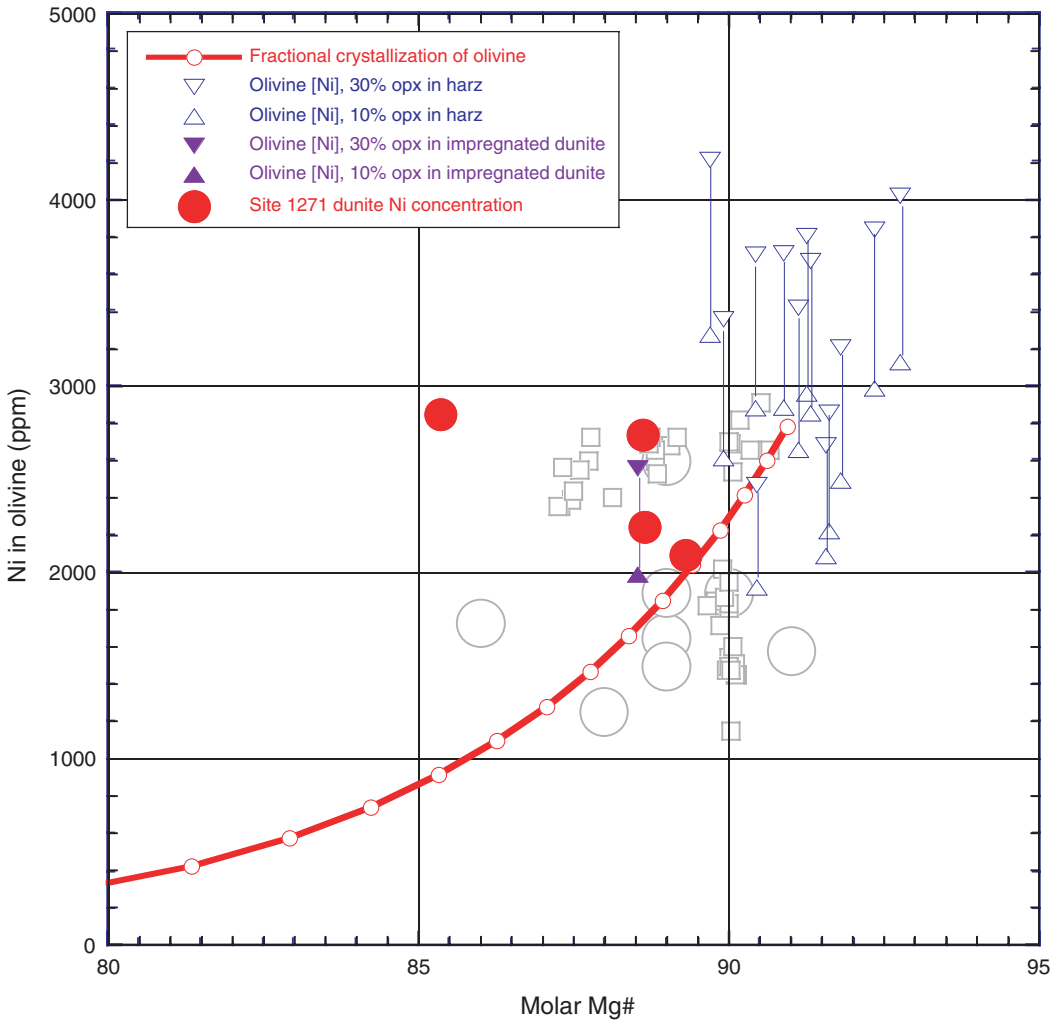
Fractional crystallization of olivine
Olivine [Ni], 30% opx in harz
Olivine [Ni], 10% opx in harz
Olivine [Ni], 30% opx in impregnated dunite
Olivine [Ni], 10% opx in impregnated dunite
Site 1271 dunite Ni concentration
Ni in olivine (ppm)
5000
4000
3000
2000
1000
0
80
85
90
95
Molar Mg#

Figure F34

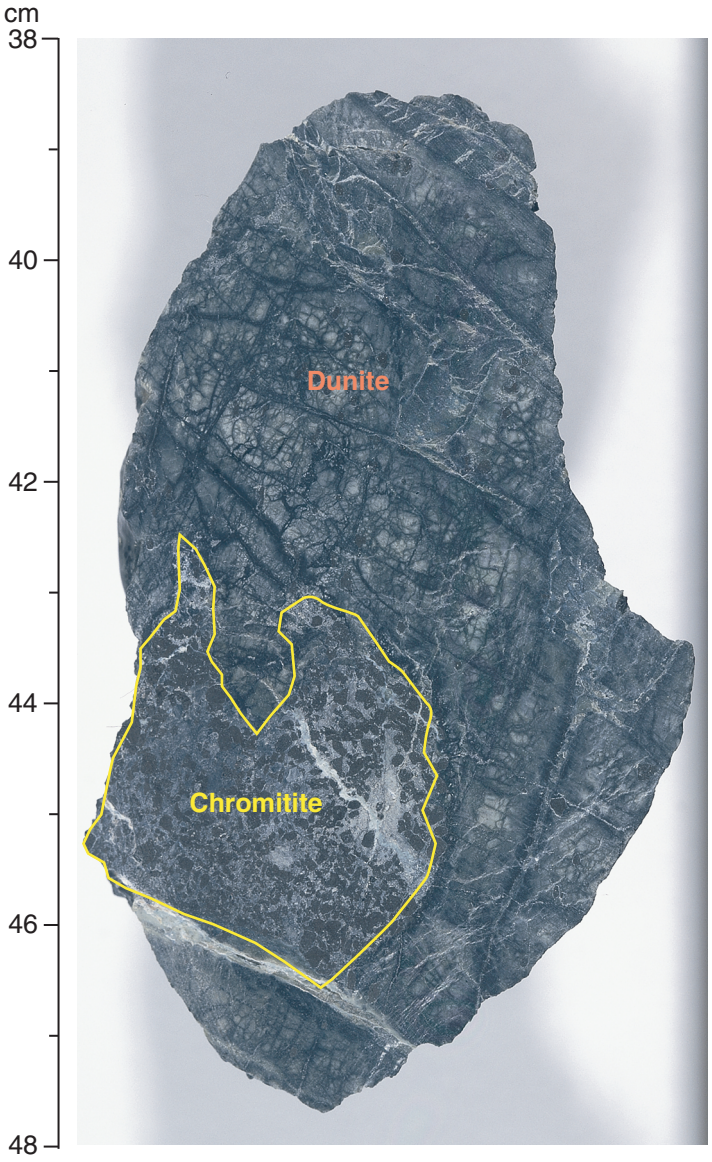

Figure F35

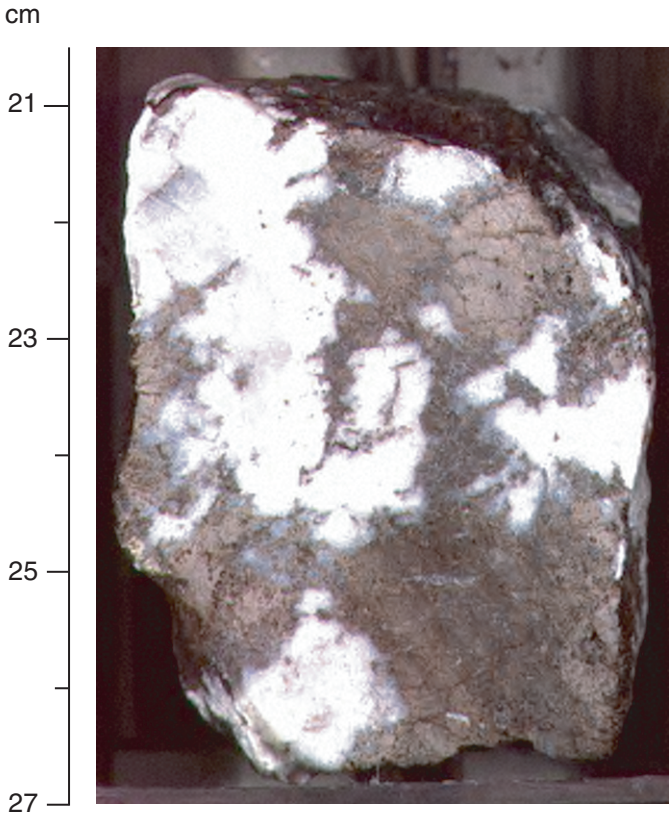

Figure F36

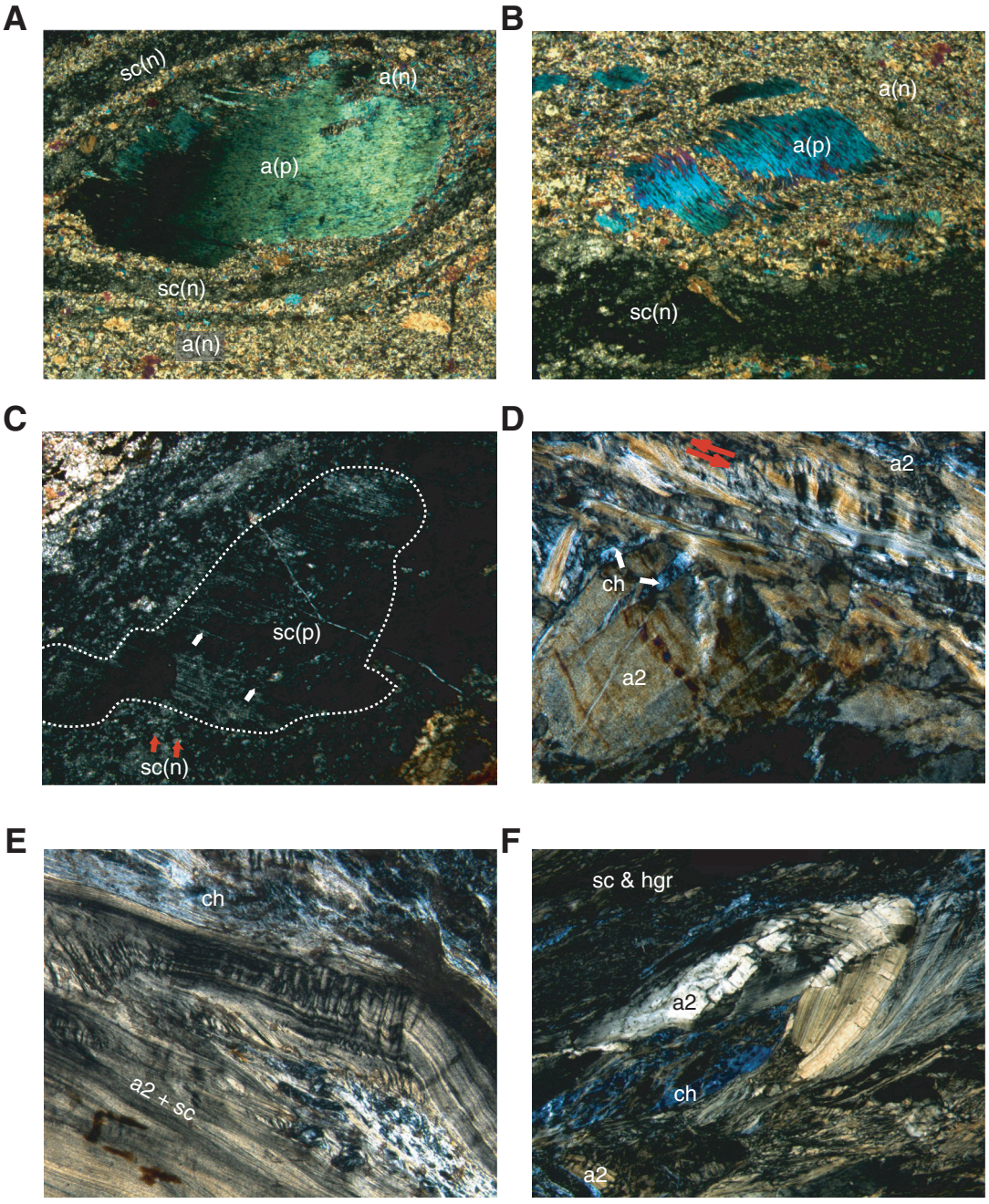
A
sc(n)
a(n)
a(p)
sc(n)
a(n)
B
a(n)
a(p)
sc(n)
C
sc(p)
sc(n)
D
a2
ch
a2
E
ch
a2 + sc
F
sc & hgr
a2
ch
a2

Figure F37

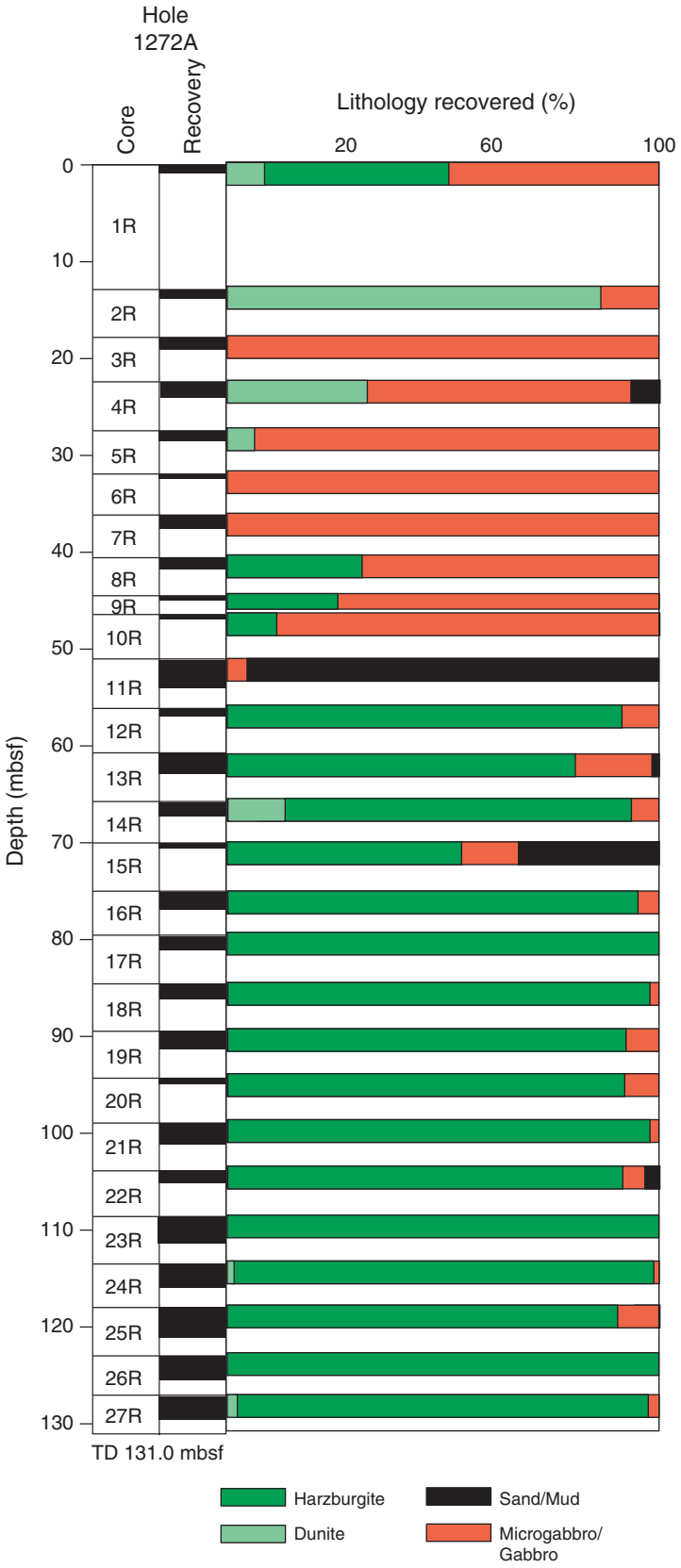
Hole
1272A
Core
Recovery
Lithology recovered (%)
20
60
100
Depth (mbsf)
0
10
20
30
40
50
60
70
80
90
100
110
120
130
1R
2R
3R
4R
5R
6R
7R
8R
9R
10R
11R
12R
13R
14R
15R
16R
17R
18R
19R
20R
21R
22R
23R
24R
25R
26R
27R
TD 131.0 mbsf
Harzburgite
Dunite
Sand/Mud
Microgabbro/
Gabbro

Figure F38

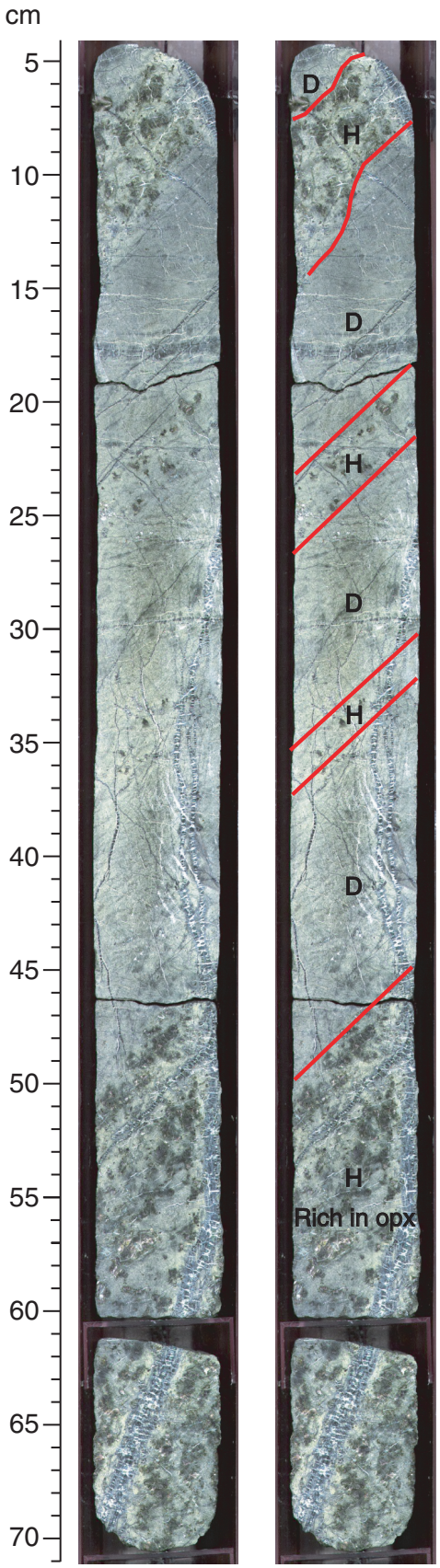

Figure F39

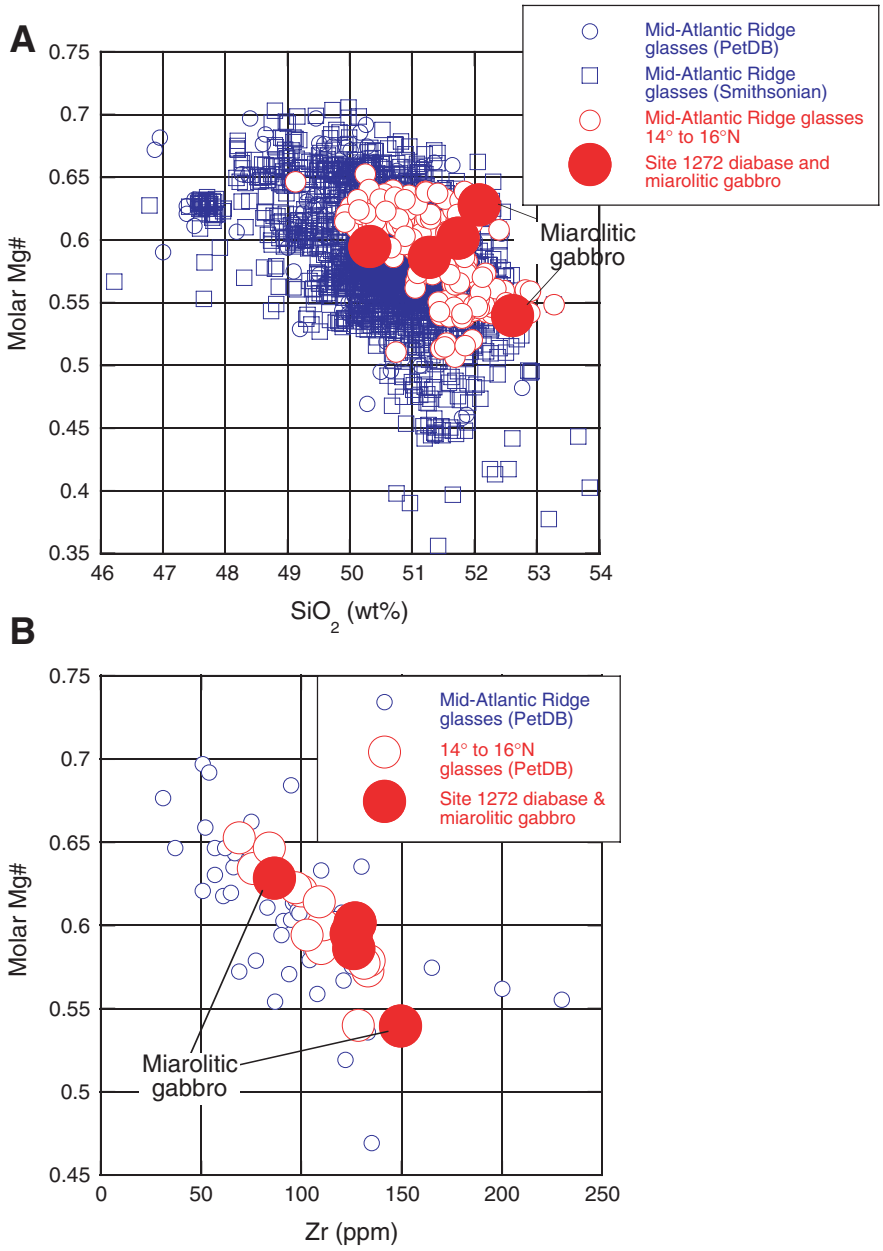
A
Mid-Atlantic Ridge glasses (PetDB)
Mid-Atlantic Ridge glasses (Smithsonian)
Mid-Atlantic Ridge glasses 14° to 16°N
Site 1272 diabase and miarolitic gabbro
Miarolitic gabbro
Molar Mg#
0.75
0.7
0.65
0.6
0.55
0.5
0.45
0.4
0.35
46
47
48
49
50
51
52
53
54
SiO2 (wt%)
B
Mid-Atlantic Ridge glasses (PetDB)
14° to 16°N glasses (PetDB)
Site 1272 diabase & miarolitic gabbro
Miarolitic gabbro
Molar Mg#
0.75
0.7
0.65
0.6
0.55
0.5
0.45
0
50
100
150
200
250
Zr (ppm)

Figure F40

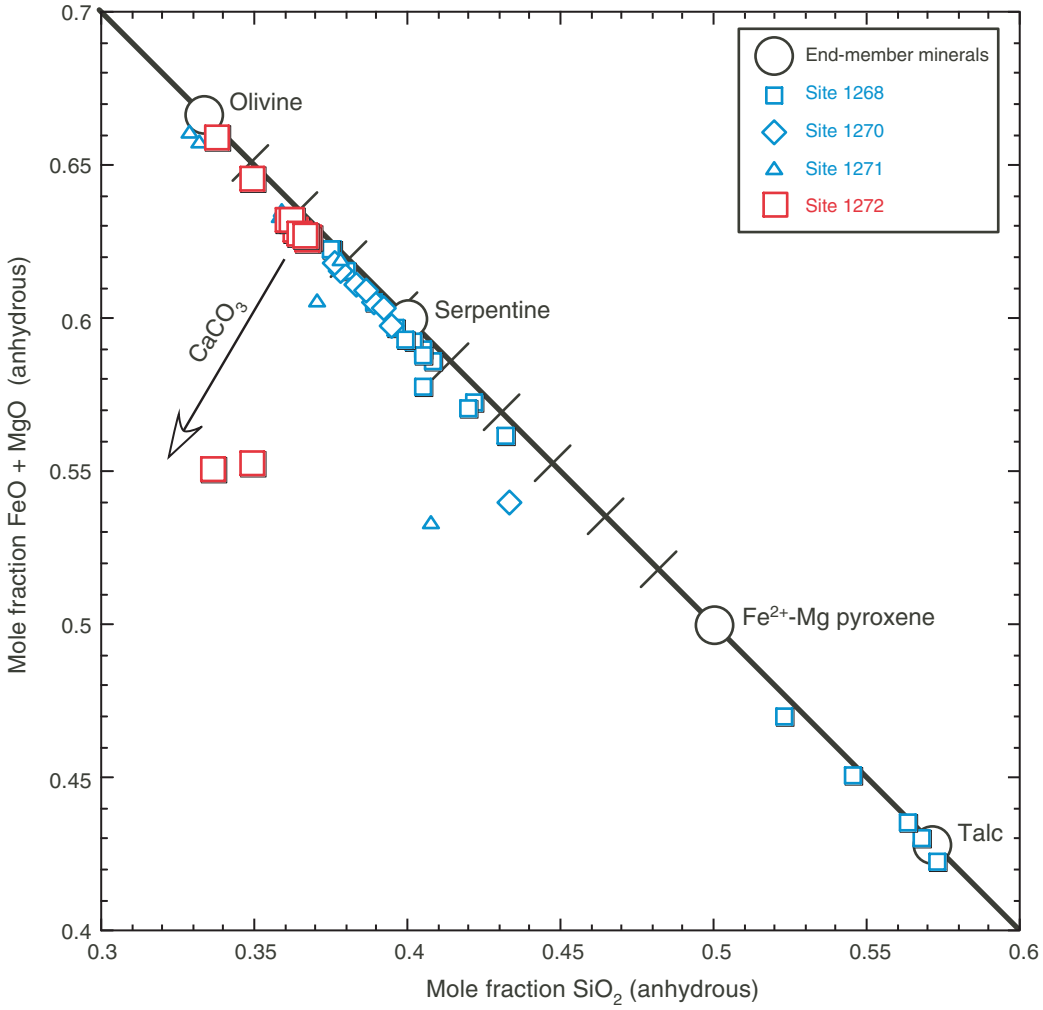
End-member minerals
Site 1268
Site 1270
Site 1271
Site 1272
Olivine
Serpentine
Fe2+-Mg pyroxene
Talc
CaCO3
Mole fraction FeO + MgO (anhydrous)
Mole fraction SiO2 (anhydrous)
0.7
0.65
0.6
0.55
0.5
0.45
0.4
0.3
0.35
0.4
0.45
0.5
0.55
0.6

Figure F41

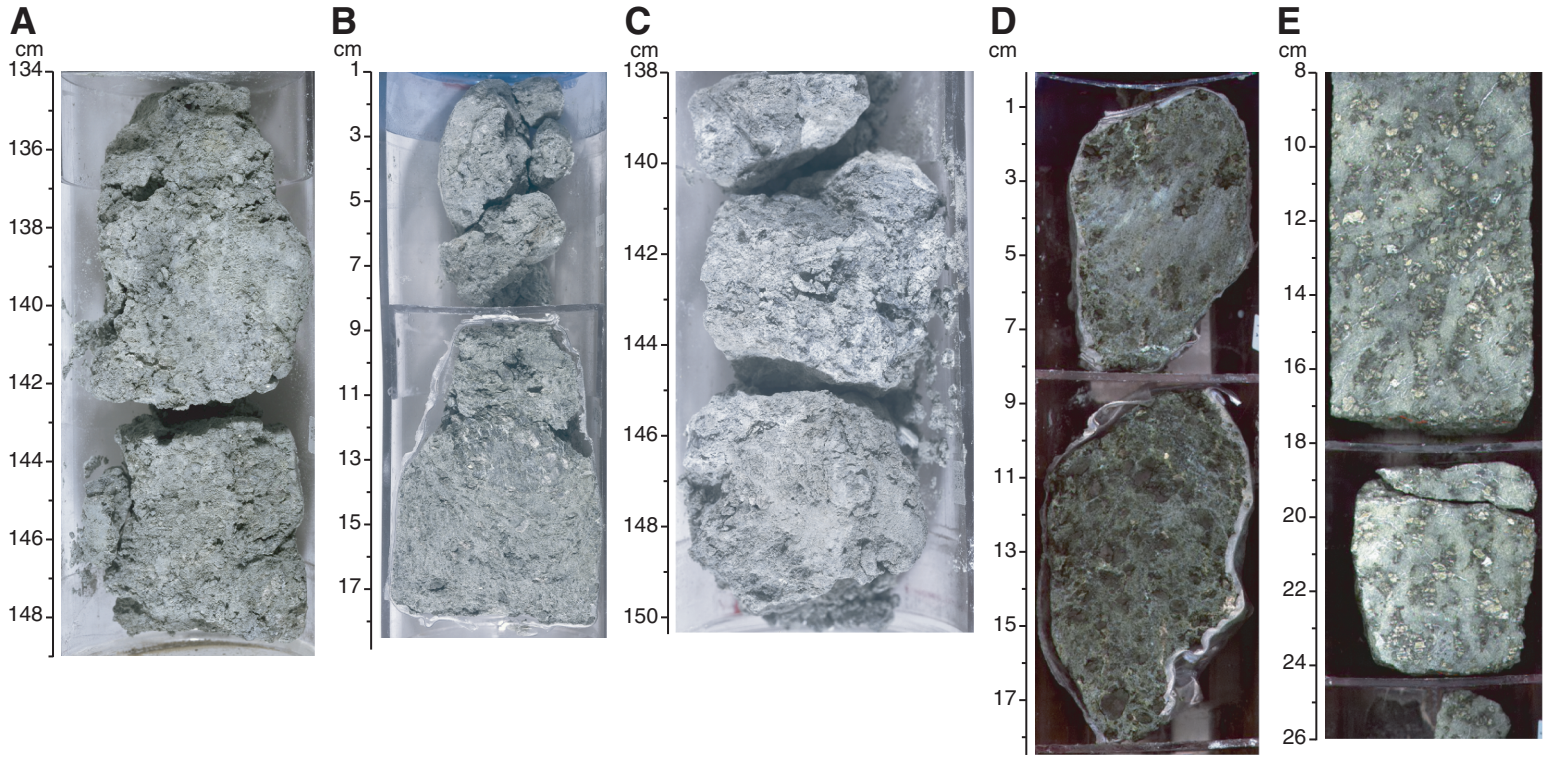
A
cm
134
136
138
140
142
144
146
148
B
cm
1
3
5
7
9
11
13
15
17
C
cm
138
140
142
144
146
148
150
D
cm
1
3
5
7
9
11
13
15
17
E
cm
8
10
12
14
16
18
20
22
24
26

Figure F42

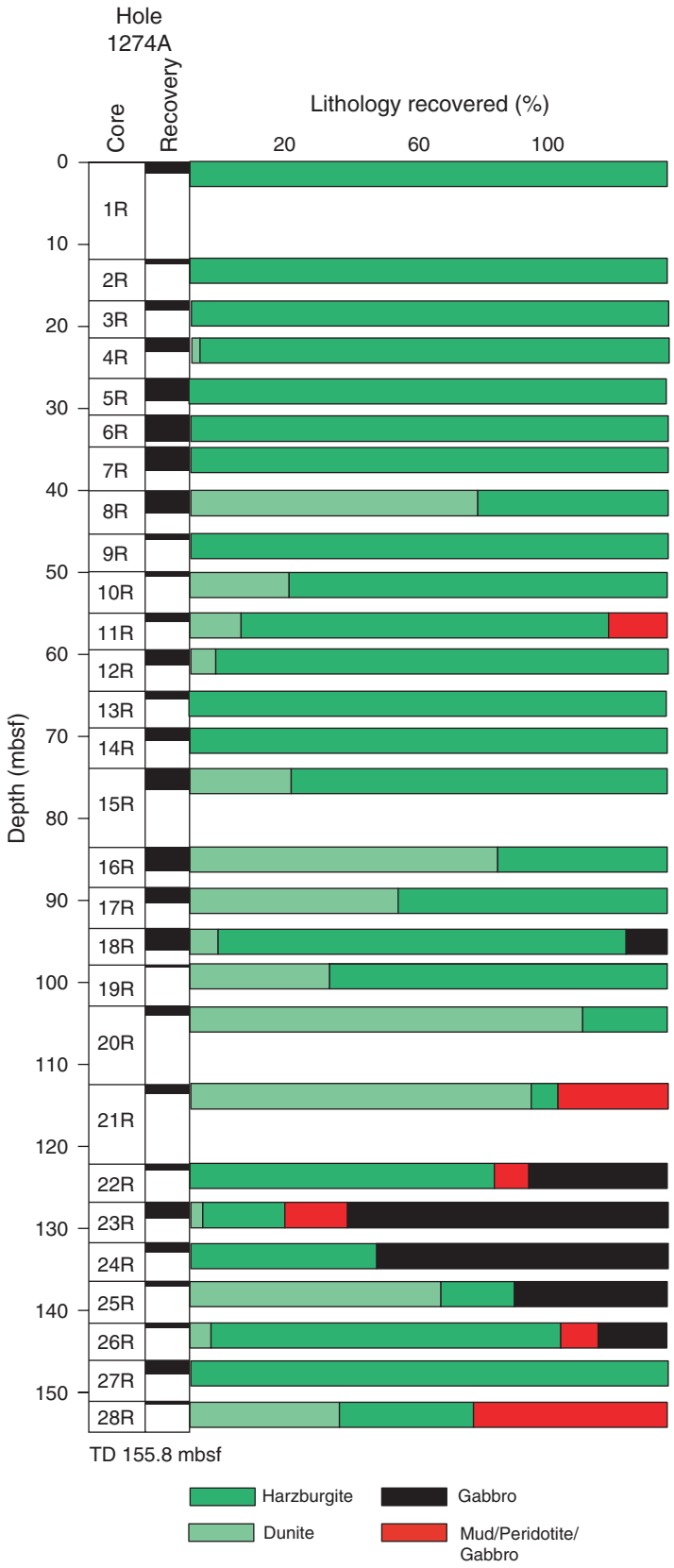
Hole
1274A
Core
Recovery
Lithology recovered (%)
20
60
100
Depth (mbsf)
0
10
20
30
40
50
60
70
80
90
100
110
120
130
140
150
1R
2R
3R
4R
5R
6R
7R
8R
9R
10R
11R
12R
13R
14R
15R
16R
17R
18R
19R
20R
21R
22R
23R
24R
25R
26R
27R
28R
TD 155.8 mbsf
Harzburgite
Gabbro
Dunite
Mud/Peridotite/
Gabbro

Figure F43

A

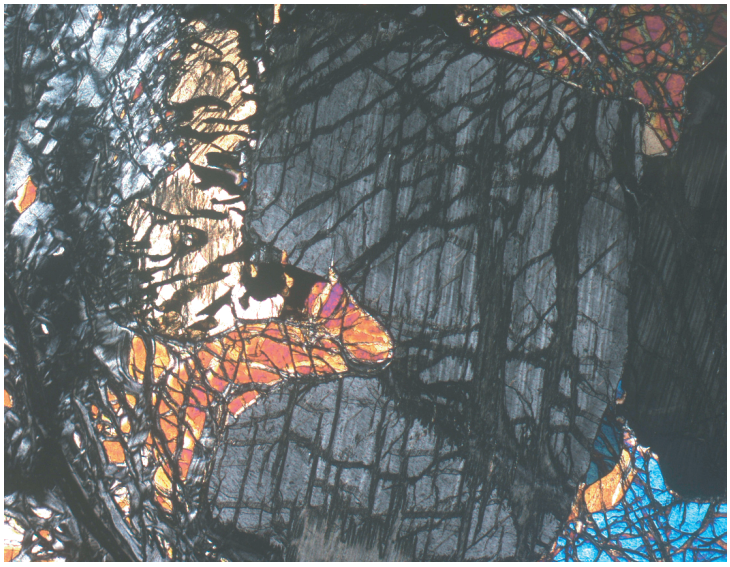

B

Figure F44

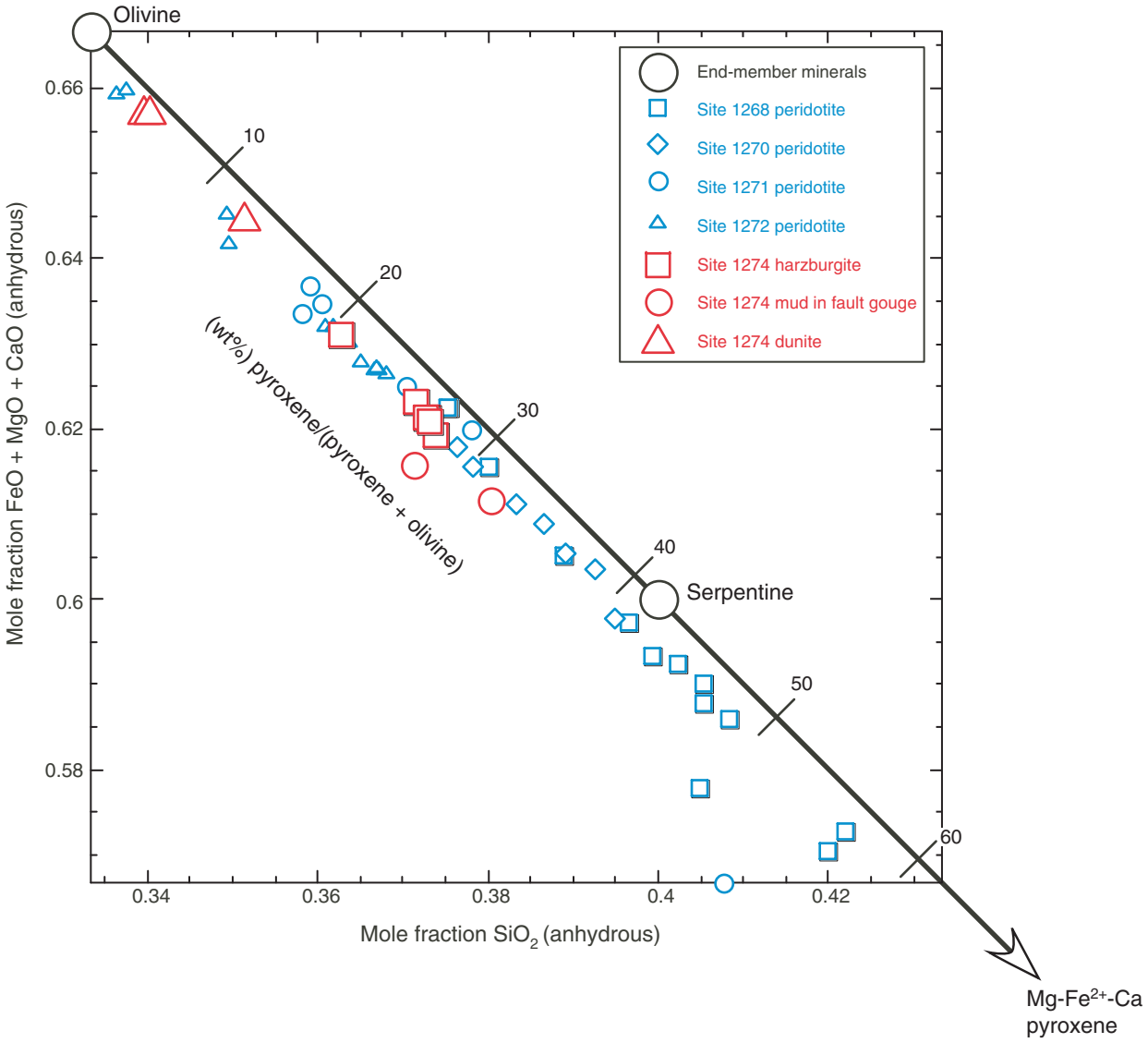
Olivine
Serpentine
Mg-Fe2+-Ca pyroxene
End-member minerals
Site 1268 peridotite
Site 1270 peridotite
Site 1271 peridotite
Site 1272 peridotite
Site 1274 harzburgite
Site 1274 mud in fault gouge
Site 1274 dunite
(wt%) pyroxene/(pyroxene + olivine)
10
20
30
40
50
60
0.66
0.64
0.62
0.6
0.58
0.34
0.36
0.38
0.4
0.42
Mole fraction FeO + MgO + CaO (anhydrous)
Mole fraction SiO2 (anhydrous)

Figure F45

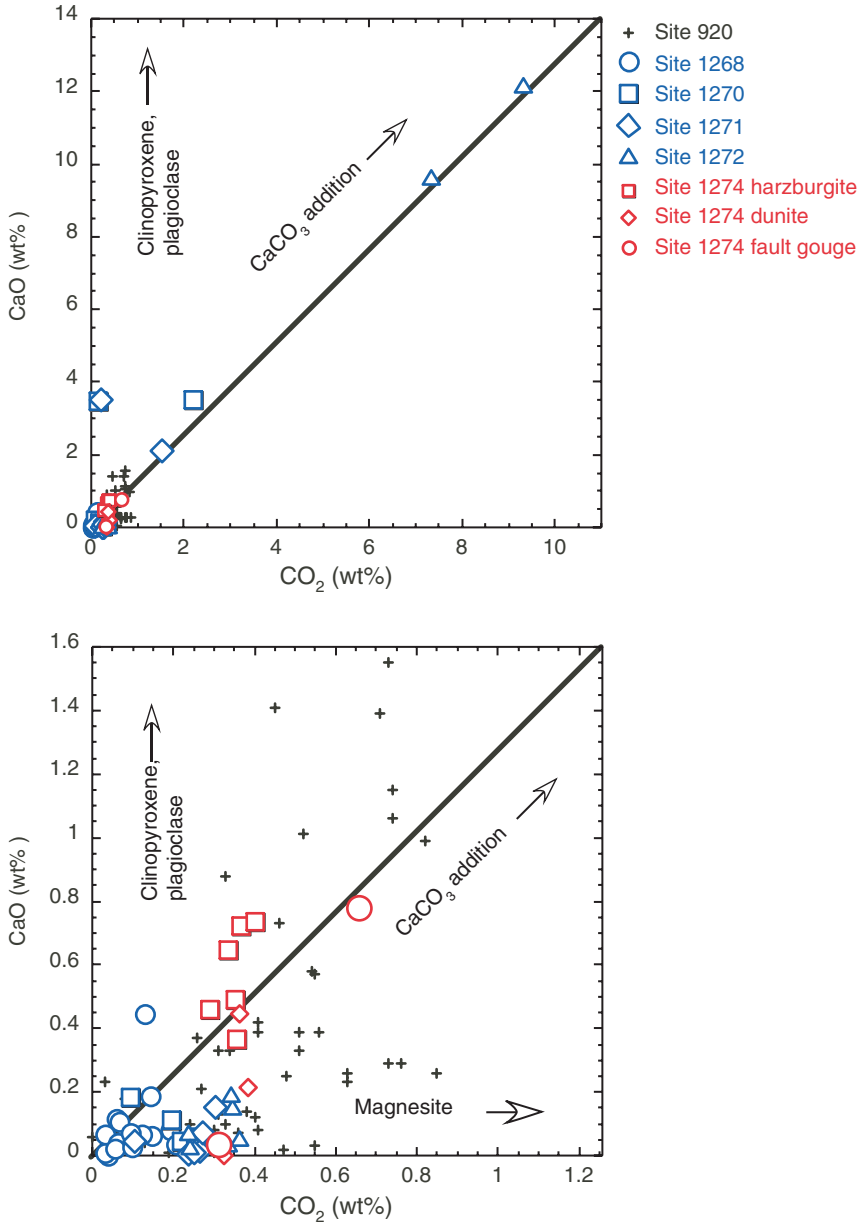
Site 920
Site 1268
Site 1270
Site 1271
Site 1272
Site 1274 harzburgite
Site 1274 dunite
Site 1274 fault gouge
CaO (wt%)
CO2 (wt%)
Clinopyroxene, plagioclase
CaCO3 addition
Magnesite

Figure F46

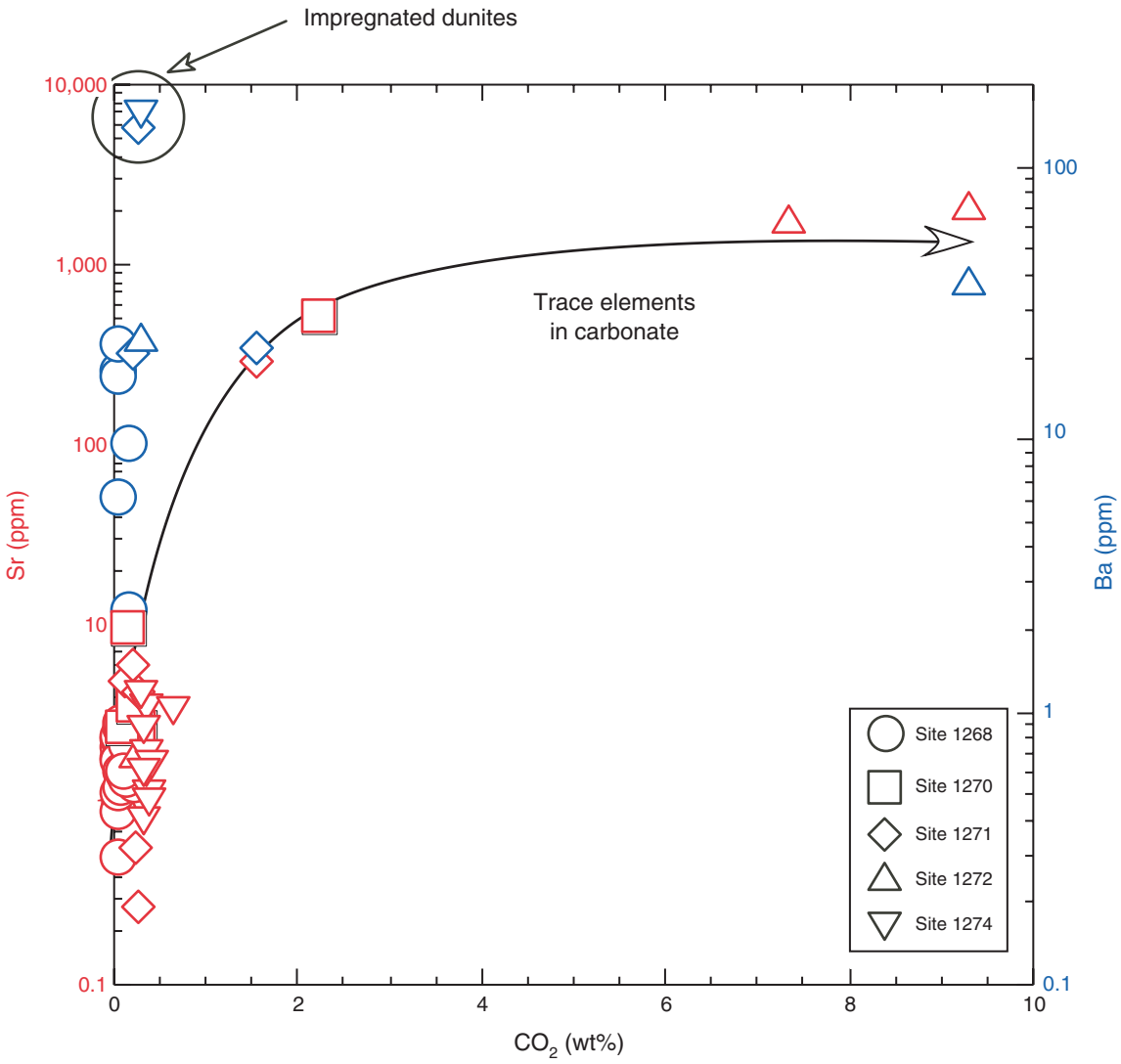
Impregnated dunites
10,000
1,000
100
10
0.1
Sr (ppm)
100
10
1
0.1
Ba (ppm)
Trace elements
in carbonate
Site 1268
Site 1270
Site 1271
Site 1272
Site 1274
0
2
4
6
8
10
CO2 (wt%)

Figure F47

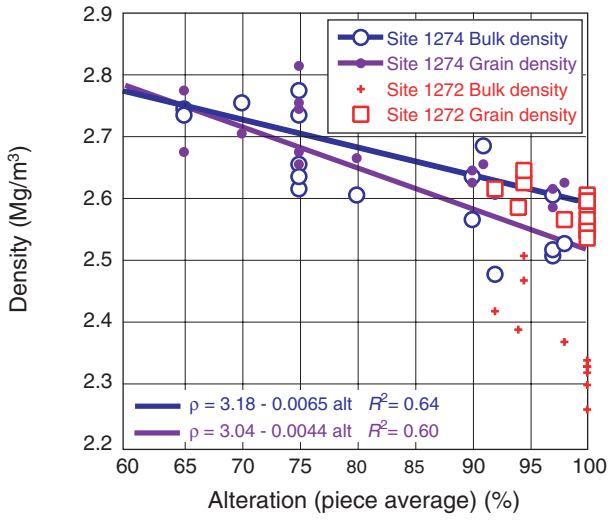
Site 1274 Bulk density
Site 1274 Grain density
Site 1272 Bulk density
Site 1272 Grain density
ρ = 3.18 - 0.0065 alt R^2= 0.64
ρ = 3.04 - 0.0044 alt R^2= 0.60
Density (Mg/m^3)
Alteration (piece average) (%)

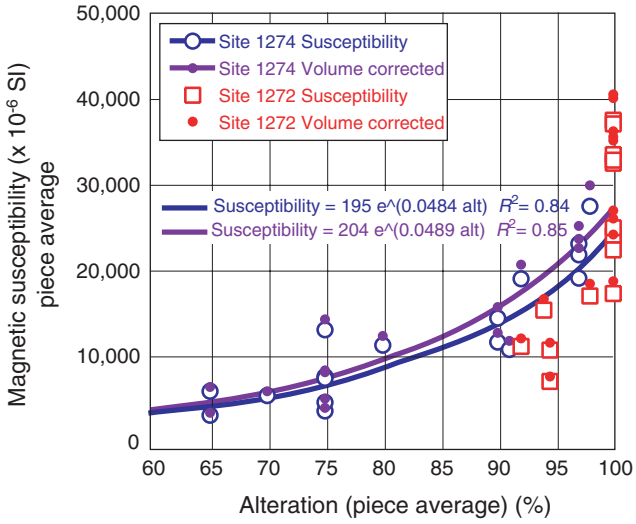
Site 1274 Susceptibility
Site 1274 Volume corrected
Site 1272 Susceptibility
Site 1272 Volume corrected
Susceptibility = 195 e^(0.0484 alt) R^2= 0.84
Susceptibility = 204 e^(0.0489 alt) R^2= 0.85
Magnetic susceptibility (x 10^{-6} SI) piece average
Alteration (piece average) (%)

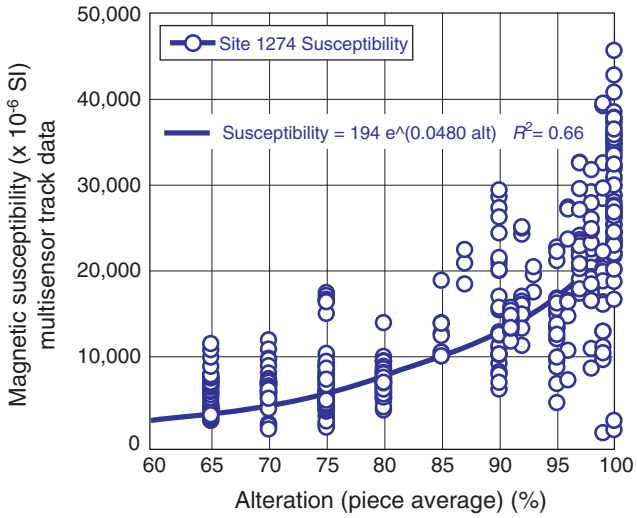
Site 1274 Susceptibility
Susceptibility = 194 e^(0.0480 alt) R^2= 0.66
Magnetic susceptibility (x 10^{-6} SI) multisensor track data
Alteration (piece average) (%)

Figure F48

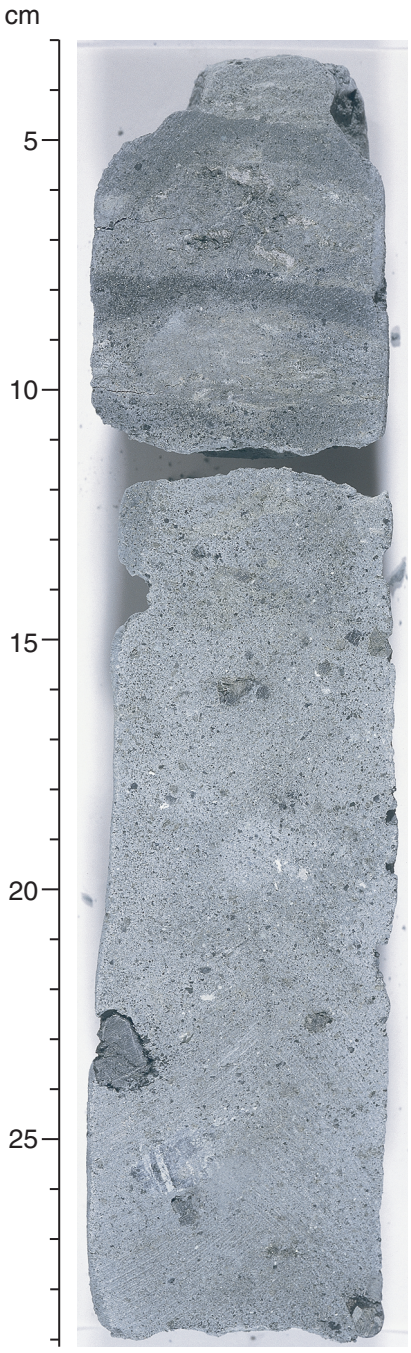

Figure F49

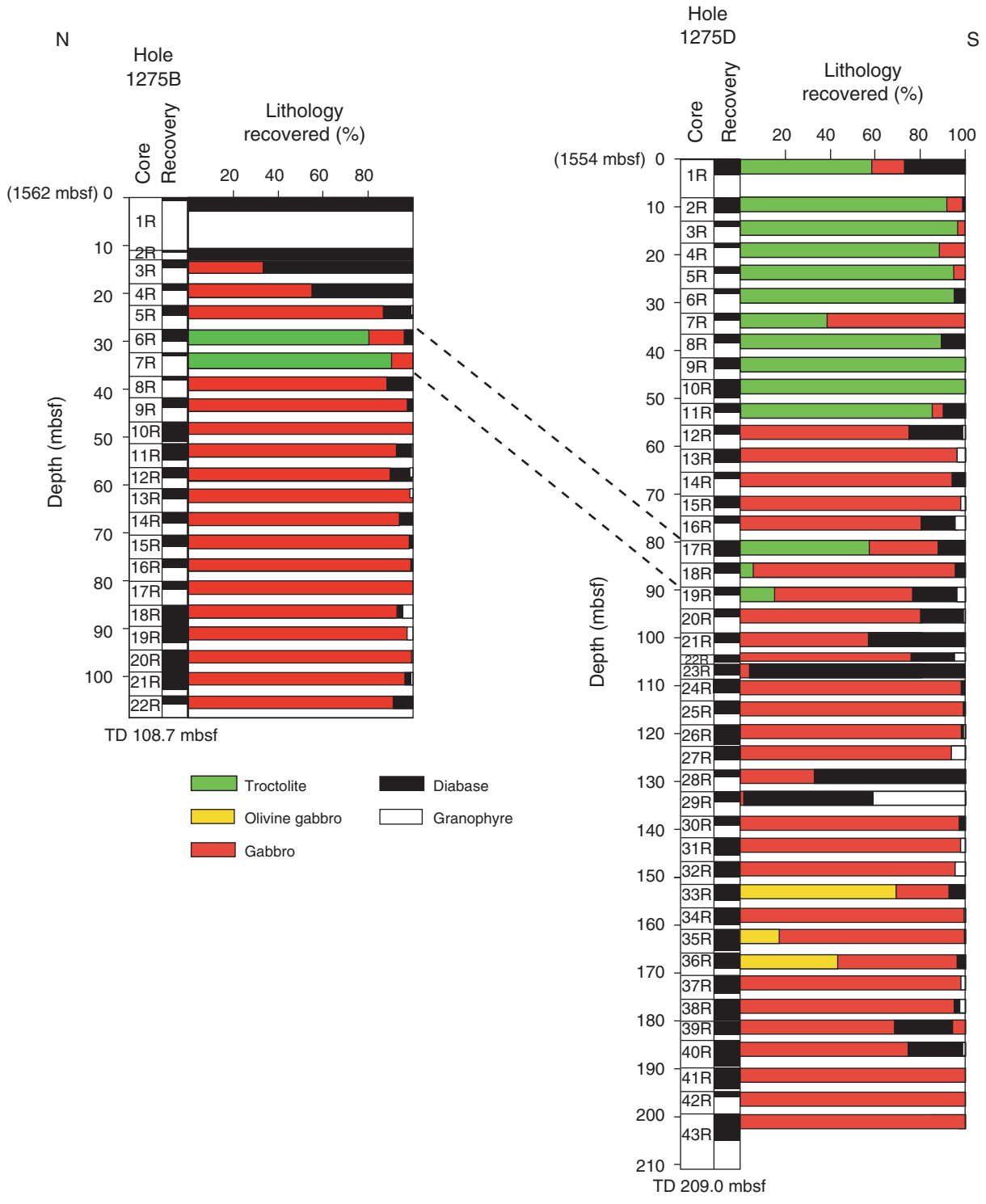
N
Hole 1275B
Core
Recovery
Lithology recovered (%)
20 40 60 80
(1562 mbsf) 0
Depth (mbsf)
1R
2R
3R
4R
5R
6R
7R
8R
9R
10R
11R
12R
13R
14R
15R
16R
17R
18R
19R
20R
21R
22R
TD 108.7 mbsf
Hole 1275D
S
Lithology recovered (%)
20 40 60 80 100
(1554 mbsf) 0
23R
24R
25R
26R
27R
28R
29R
30R
31R
32R
33R
34R
35R
36R
37R
38R
39R
40R
41R
42R
43R
TD 209.0 mbsf
Troctolite
Diabase
Olivine gabbro
Granophyre
Gabbro

Figure F50

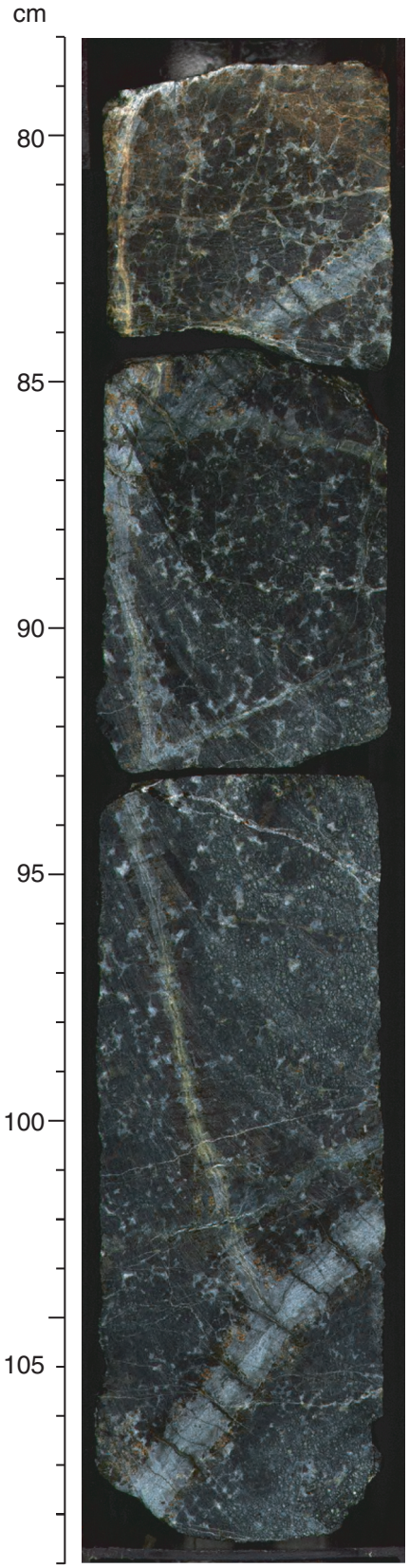

Figure F51

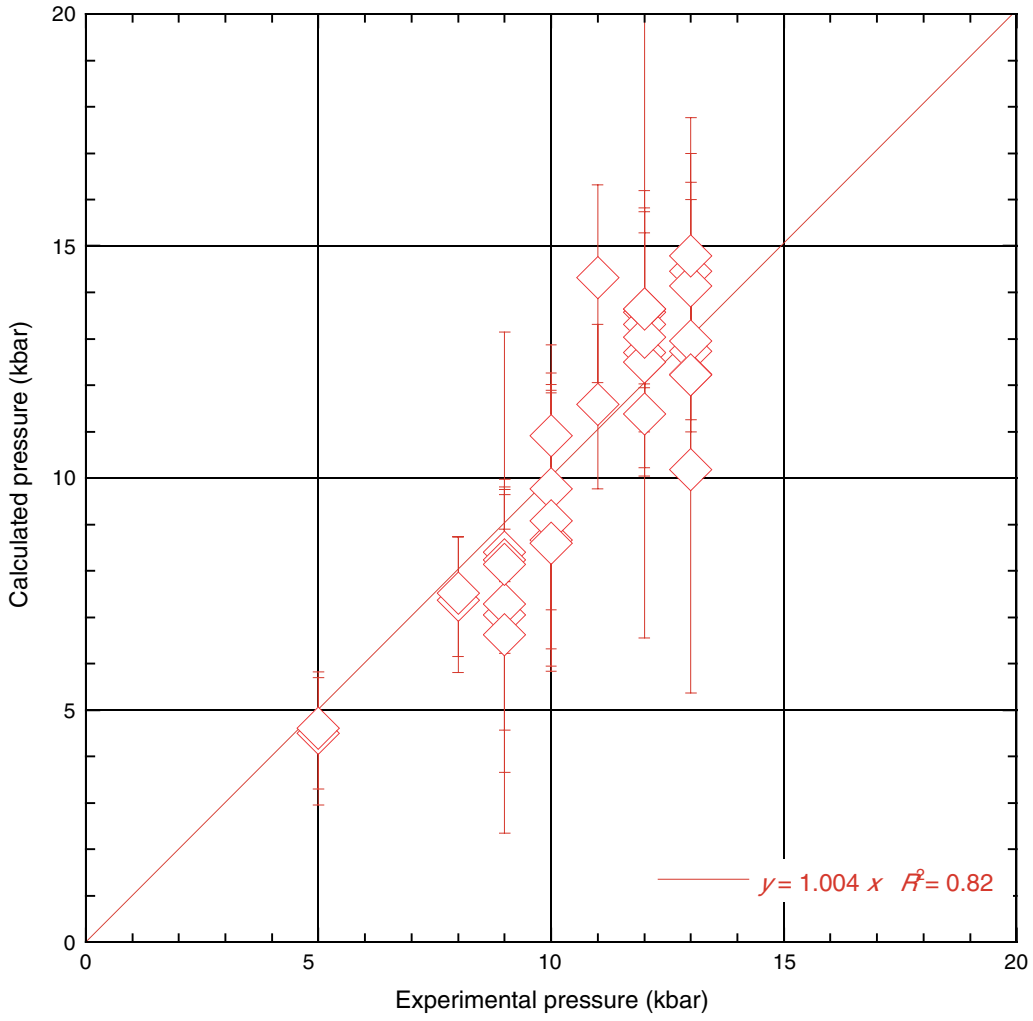
20
15
10
5
0
0
5
10
15
20
Calculated pressure (kbar)
Experimental pressure (kbar)
y = 1.004 x R² = 0.82

Figure F52

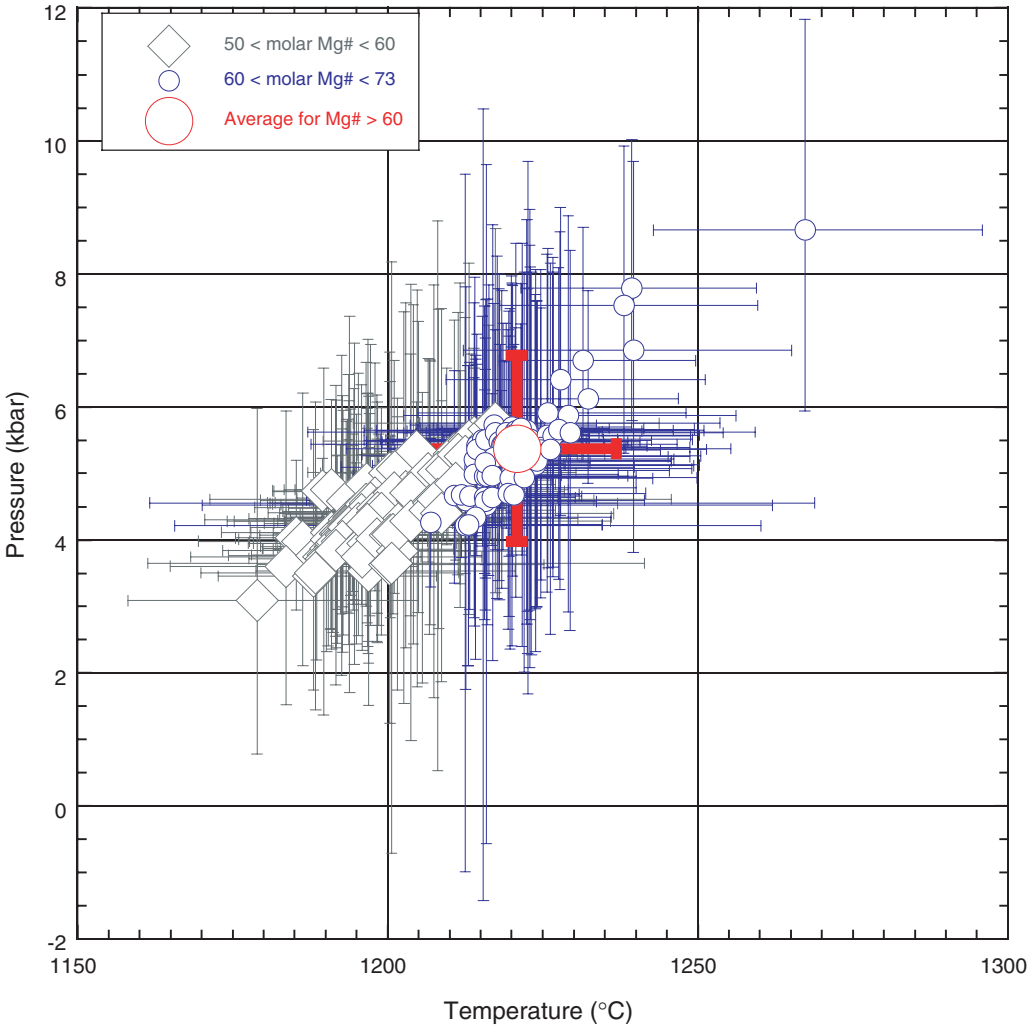
50 < molar Mg# < 60
60 < molar Mg# < 73
Average for Mg# > 60
Pressure (kbar)
Temperature (°C)
12
10
8
6
4
2
0
-2
1150
1200
1250
1300

Figure F53

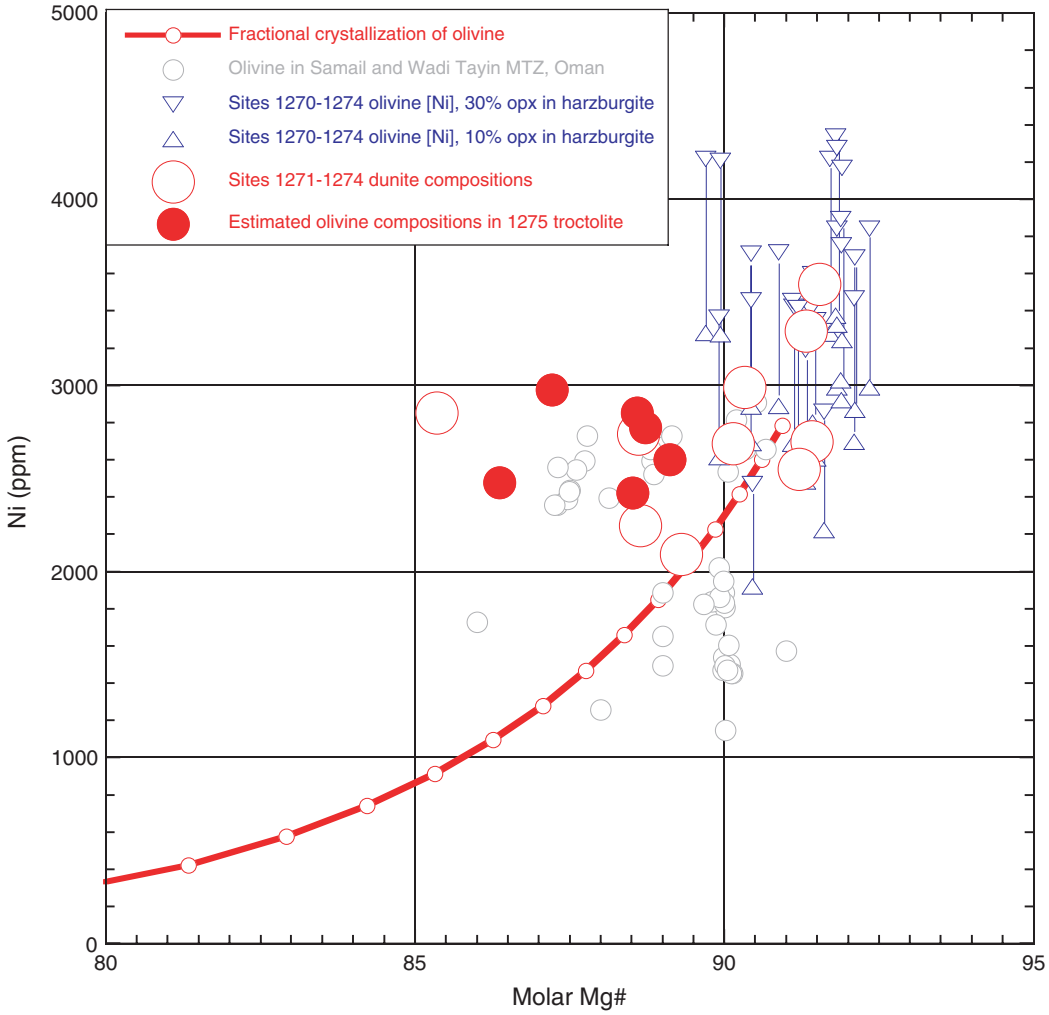
Fractional crystallization of olivine
Olivine in Samail and Wadi Tayin MTZ, Oman
Sites 1270-1274 olivine [Ni], 30% opx in harzburgite
Sites 1270-1274 olivine [Ni], 10% opx in harzburgite
Sites 1271-1274 dunite compositions
Estimated olivine compositions in 1275 troctolite
Ni (ppm)
Molar Mg#
5000
4000
3000
2000
1000
0
80
85
90
95

Figure F54

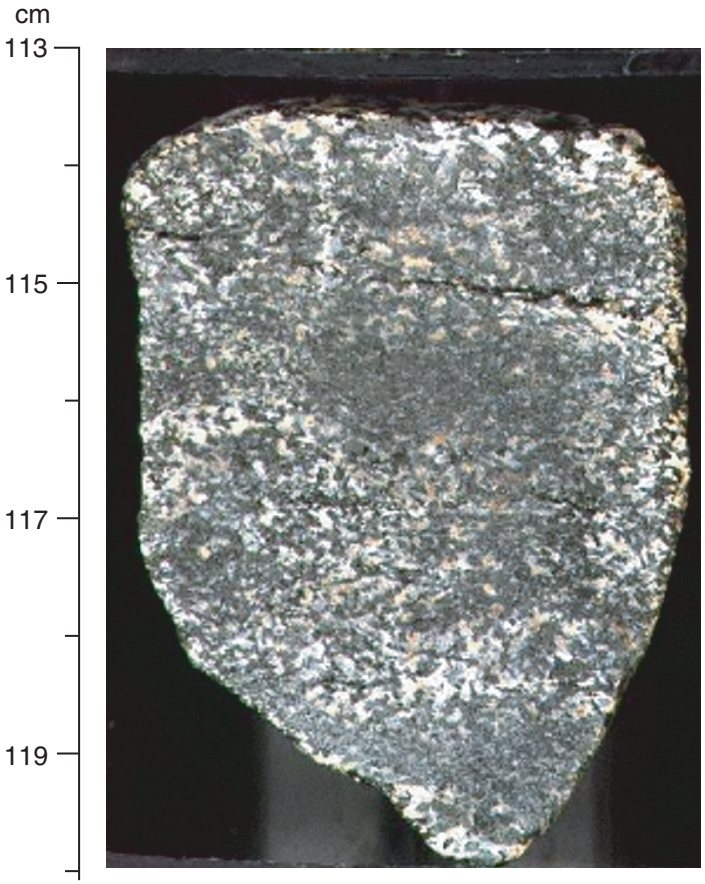

Figure F55

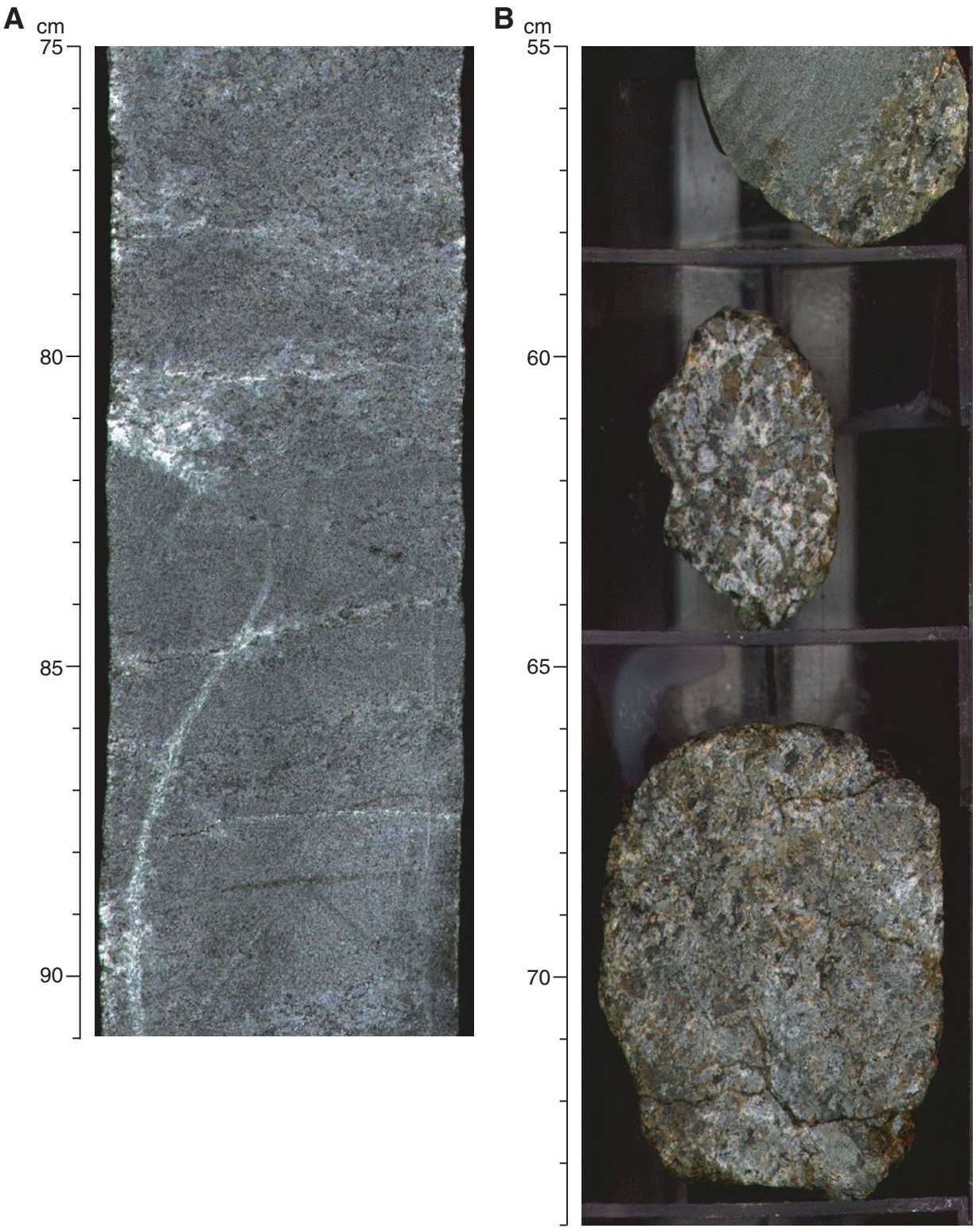

Figure F56

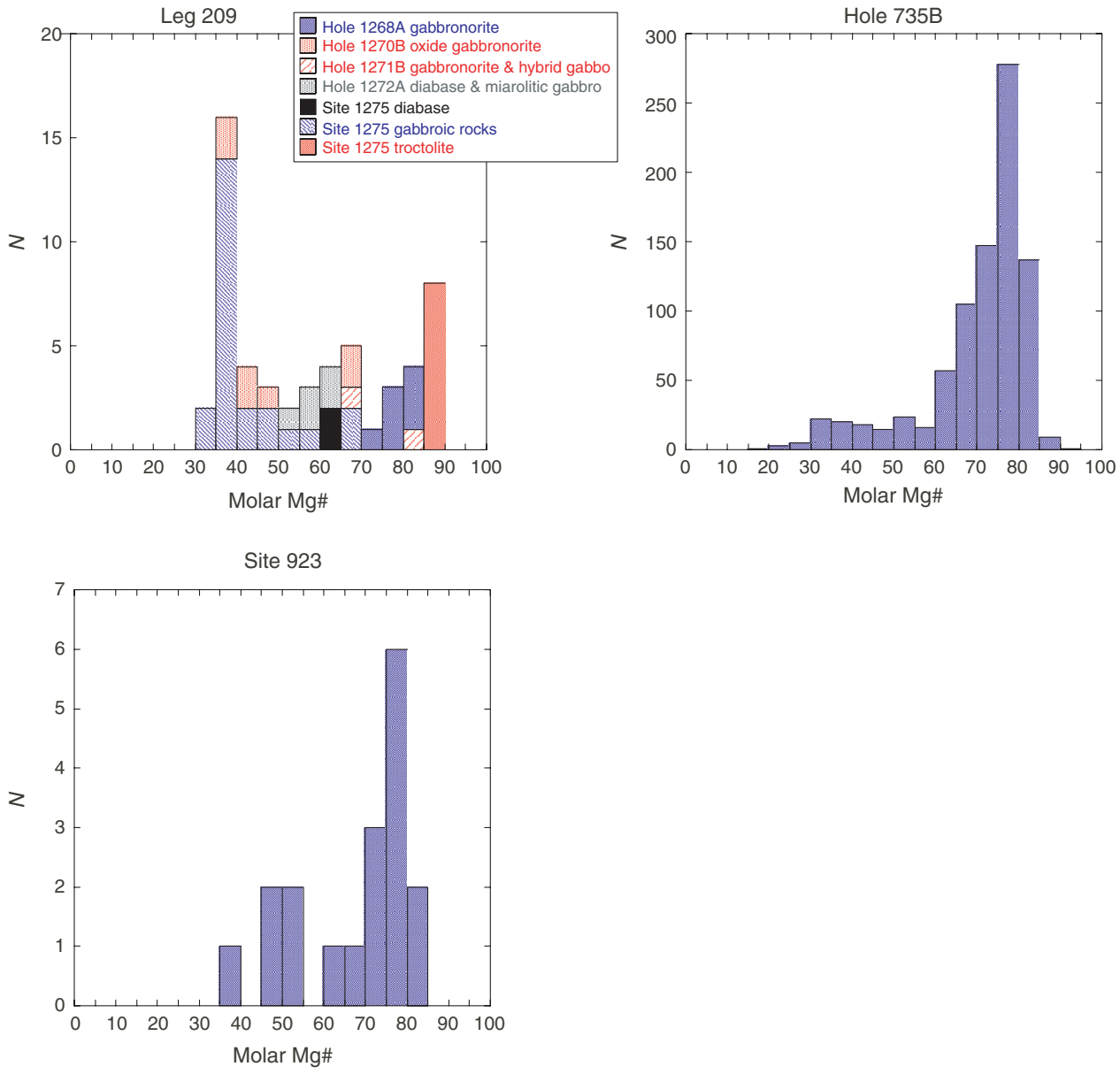
Leg 209
Hole 1268A gabbronorite
Hole 1270B oxide gabbronorite
Hole 1271B gabbronorite & hybrid gabbo
Hole 1272A diabase & miarolitic gabbro
Site 1275 diabase
Site 1275 gabbroic rocks
Site 1275 troctolite
N
Molar Mg#
Hole 735B
N
Molar Mg#
Site 923
N
Molar Mg#

Figure F57

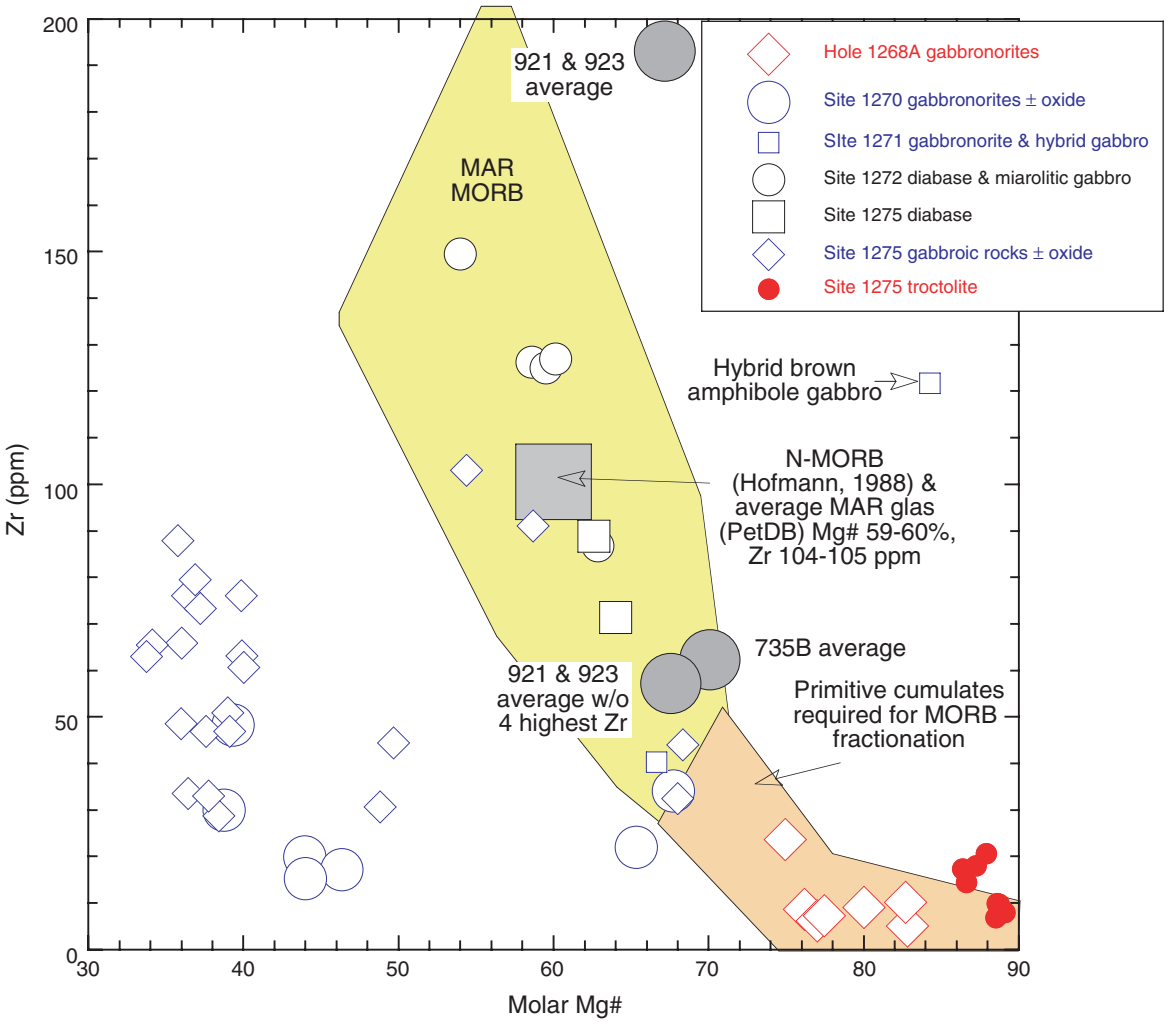
Hole 1268A gabbronorites
Site 1270 gabbronorites ± oxide
SIte 1271 gabbronorite & hybrid gabbro
Site 1272 diabase & miarolitic gabbro
Site 1275 diabase
Site 1275 gabbroic rocks ± oxide
Site 1275 troctolite
921 & 923 average
MAR MORB
Hybrid brown amphibole gabbro
N-MORB (Hofmann, 1988) & average MAR glas (PetDB) Mg# 59-60%, Zr 104-105 ppm
735B average
921 & 923 average w/o 4 highest Zr
Primitive cumulates required for MORB fractionation
Zr (ppm)
Molar Mg#
0
50
100
150
200
30
40
50
60
70
80
90

Figure F58

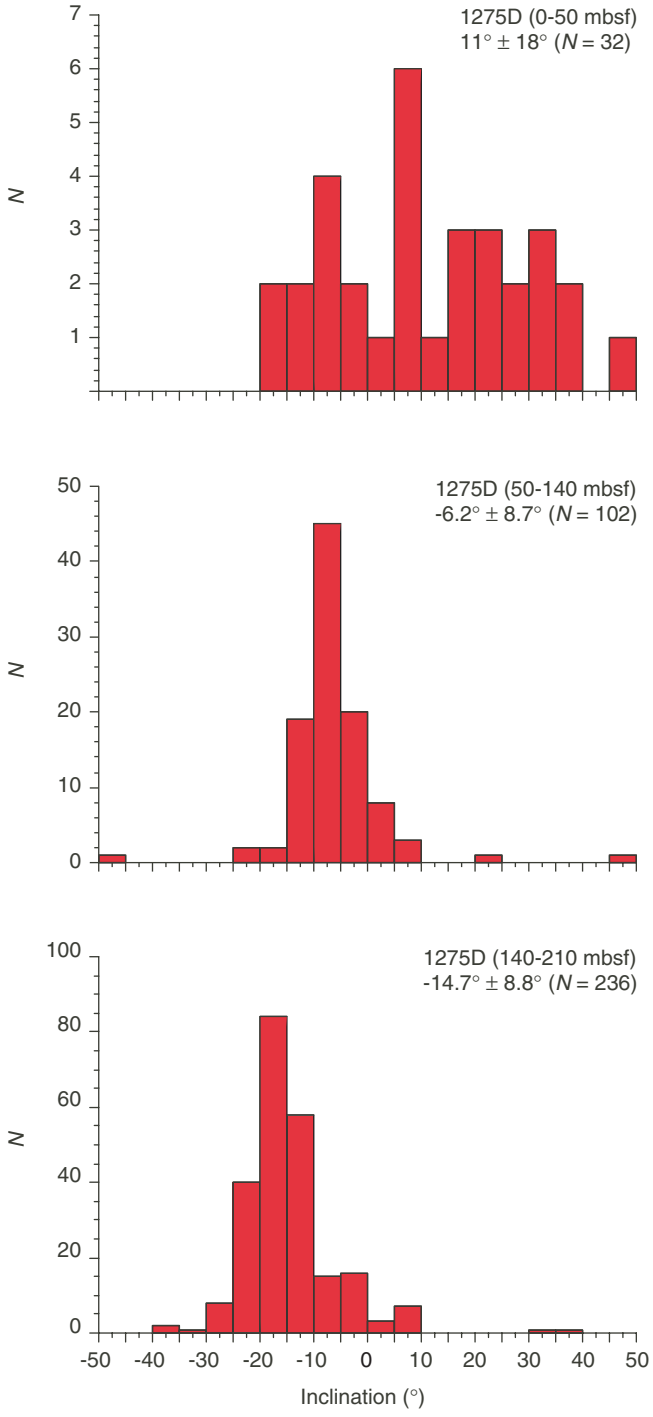
1275D (0-50 mbsf)
11° ± 18° (N = 32)
1275D (50-140 mbsf)
-6.2° ± 8.7° (N = 102)
1275D (140-210 mbsf)
-14.7° ± 8.8° (N = 236)
N
Inclination (°)

Figure F59

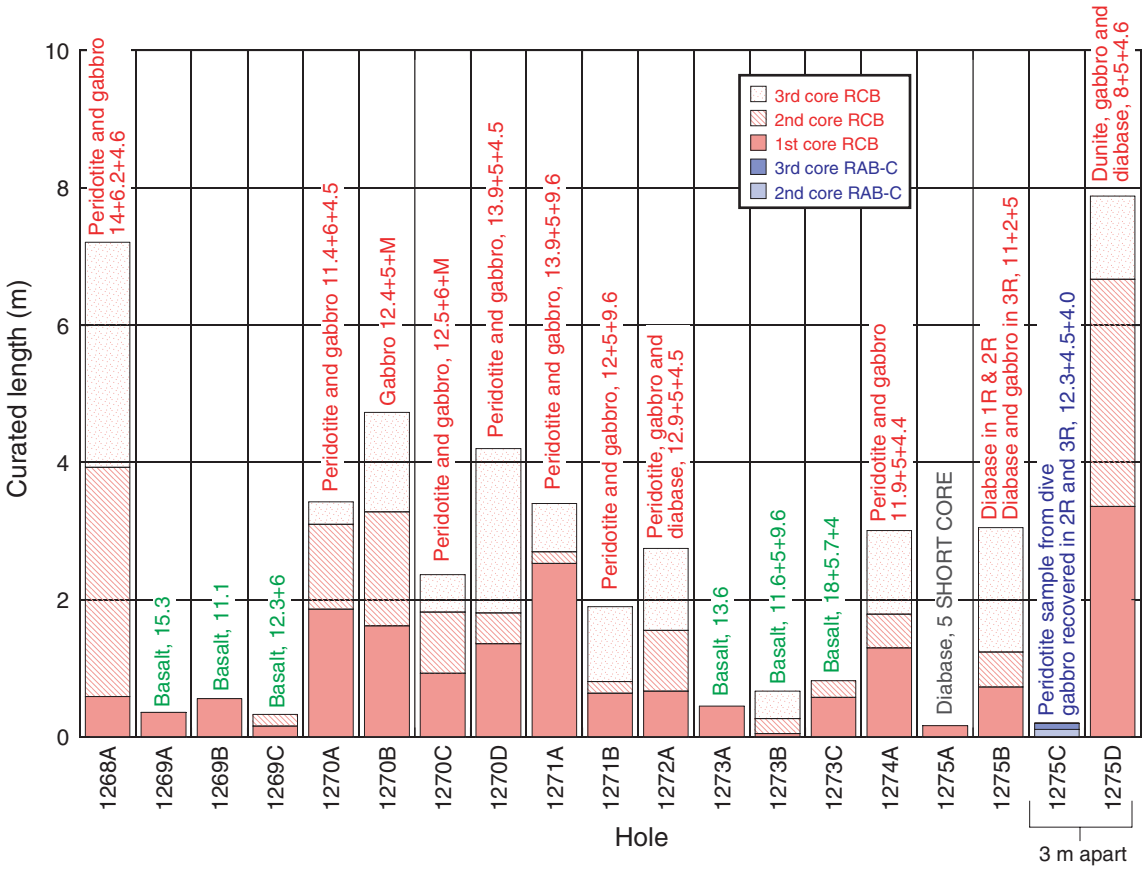
Curated length (m)
0
2
4
6
8
10
3rd core RCB
2nd core RCB
1st core RCB
3rd core RAB-C
2nd core RAB-C
Peridotite and gabbro 14+6.2+4.6
Basalt, 15.3
Basalt, 11.1
Basalt, 12.3+6
Peridotite and gabbro 11.4+6+4.5
Gabbro 12.4+5+M
Peridotite and gabbro, 12.5+6+M
Peridotite and gabbro, 13.9+5+4.5
Peridotite and gabbro, 13.9+5+9.6
Peridotite and gabbro, 12+5+9.6
Peridotite, gabbro and diabase, 12.9+5+4.5
Basalt, 13.6
Basalt, 11.6+5+9.6
Basalt, 18+5.7+4
Peridotite and gabbro 11.9+5+4.4
Diabase, 5 SHORT CORE
Diabase in 1R & 2R
Diabase and gabbro in 3R, 11+2+5
Peridotite sample from dive
gabbro recovered in 2R and 3R, 12.3+4.5+4.0
Dunite, gabbro and diabase, 8+5+4.6
1268A
1269A
1269B
1269C
1270A
1270B
1270C
1270D
1271A
1271B
1272A
1273A
1273B
1273C
1274A
1275A
1275B
1275C
1275D
Hole
3 m apart

Figure F60